SEISMIC WAVE PROPAGATION EFFECTS ON STRAIGHT JOINTED BURIED PIPELINES

by

K. Elhmadi[1] and M.J. O'Rourke[2]

August 24, 1989

Technical Report NCEER-89-0022

NCEER Contract Number 88-3005

NSF Master Contract Number ECE 86-07591

1 Research Assistant, Department of Civil Engineering, Rensselaer Polytechnic Institute
2 Professor, Department of Civil Engineering, Rensselaer Polytechnic Institute

NATIONAL CENTER FOR EARTHQUAKE ENGINEERING RESEARCH
State University of New York at Buffalo
Red Jacket Quadrangle, Buffalo, NY 14261

PREFACE

The National Center for Earthquake Engineering Research (NCEER) is devoted to the expansion and dissemination of knowledge about earthquakes, the improvement of earthquake-resistant design, and the implementation of seismic hazard mitigation procedures to minimize loss of lives and property. The emphasis is on structures and lifelines that are found in zones of moderate to high seismicity throughout the United States.

NCEER's research is being carried out in an integrated and coordinated manner following a structured program. The current research program comprises four main areas:

- Existing and New Structures
- Secondary and Protective Systems
- Lifeline Systems
- Disaster Research and Planning

This technical report pertains to Program 3, Lifeline Systems, and more specifically to water delivery systems.

The safe and serviceable operation of lifeline systems such as gas, electricity, oil, water, communication and transportation networks, immediately after a severe earthquake, is of crucial importance to the welfare of the general public, and to the mitigation of seismic hazards upon society at large. The long-term goals of the lifeline study are to evaluate the seismic performance of lifeline systems in general, and to recommend measures for mitigating the societal risk arising from their failures.

From this point of view, Center researchers are concentrating on the study of specific existing lifeline systems, such as water delivery and crude oil transmission systems. The water delivery system study consists of two parts. The first studies the seismic performance of water delivery systems on the west coast, while the second addresses itself to the seismic performance of the water delivery system in Memphis, Tennessee. For both systems, post-earthquake fire fighting capabilities will be considered as a measure of seismic performance.

The components of the water delivery system study are shown in the accompanying figure.

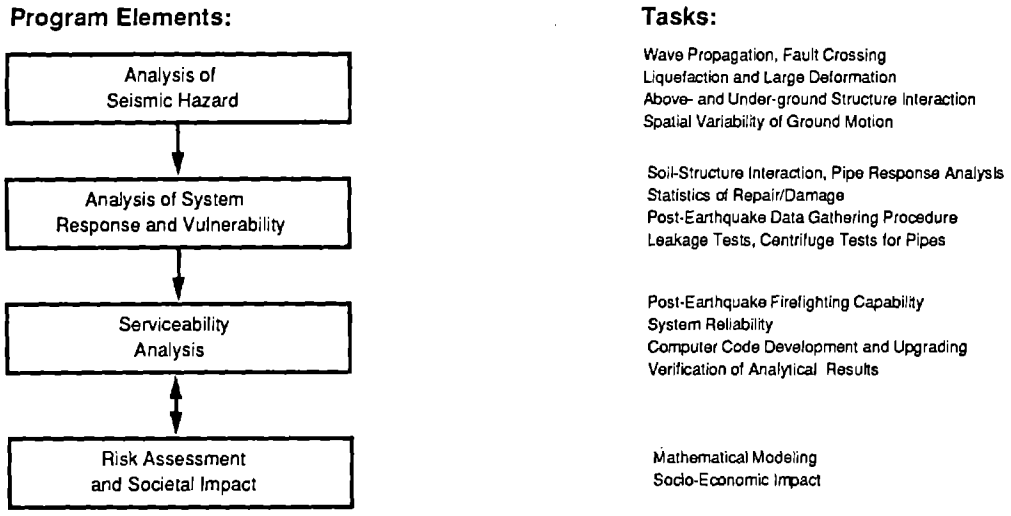

In this report, a realistic model is developed for the seismic response analysis of straight jointed buried cast-iron pipes with lead-caulked joints and ductile iron pipes with rubber-gasketed joints. This model takes into consideration the nonlinearity as well as variability of the pipeline and ground characteristics. The results of the analysis under seismic wave propagation indicate that variability can have a significant influence upon response parameters. The seismic vulnerability of these pipes is examined as a function of the seismically induced ground strain. The effects of ground rotation are found to be negligible. Such a vulnerability analysis made it possible to develop estimation of damage ratios due to a joint pull-out failure mode. These estimates are benchmarked against observed damage to water systems and are found to yield reasonable results.

ABSTRACT

The behavior of *straight jointed buried pipelines* subjected to seismic wave propagation is investigated in this study. A realistic model which takes into account the *nonlinearity* as well as the *variability* of the system characteristics is developed and used to analyze this type of pipeline. First, the seismic environment is quantified in terms of the seismic ground strain and ground rotation. Second, the axial and flexural behavior of pipelines is presented. The pipeline systems considered herein are *Cast Iron Pipes with Lead Caulked Joints* and *Ductile Iron Pipes with Rubber Gasketed Joints*. In the first part, well established stress/strain relationships for the pipe segment materials are presented. The second part involves the quantification of the mechanical properties of the joints, which show nonlinear behavior and pronounced variability. Third, the soil resistance to axial and lateral movements of the pipeline is studied.

Then, an analytical model is constructed to evaluate the response of straight jointed buried pipelines. For this purpose, a nonlinear static formulation is used. The variability of the system characteristics is accounted for by a *simplified Monte Carlo simulation technique*. The model consists of a number of straight pipe segments surrounded by axial and lateral soil spring-sliders and jointed by axial and rotational nonlinear springs.

Results for the response of straight jointed buried pipelines to seismic wave propagation indicate that the variability of system characteristics can have a significant influence upon the response parameters. This influence is stronger for cast iron pipes with lead caulked joints than for ductile iron pipes with rubber gasketed joints. Vulnerability graphs giving the probability of exceedence for selected response parameters as a function of the ground strain, are established for the cast iron system. For the ductile iron system, graphs giving values of selected response parameters as a function of the ground strain, are proposed. Of particular interest are the joint displacement and force since damage occurs more frequently at the joints. The effects of ground rotation are found to be negligible.

The vulnerability graphs proposed are combined with available information on leakage of lead caulked joints in cast iron systems to develop estimates of *damage ratios* due to a joint pull-out failure mode. These estimates are benchmarked against observed damage to water systems and are found to yield reasonable results. The proposed procedure could be extended to include a bell crushing failure mode.

TABLE OF CONTENTS

TABLE OF CONTENTS (Continued)

LIST OF ILLUSTRATIONS

LIST OF ILLUSTRATIONS (Continued)

LIST OF ILLUSTRATIONS (Continued)

LIST OF TABLES

LIST OF TABLES (Continued)

LIST OF TABLES (Continued)

1. INTRODUCTION

1.1 Background

Buried pipeline systems are commonly used to transport water, sewage, oil, natural gas and other chemicals. They are referred to as "Lifelines" as they carry materials essential to the support of life and maintenance of property. These systems are categorized by usage, material, configuration, type of joints and soil conditions. Figure 1-1 summarizes the different characteristics of buried pipelines.

Records of damage during previous earthquakes have established that buried pipelines are seismically very vulnerable. This vulnerability, coupled with the vital role that these systems play, often causes very serious problems after earthquakes. During the 1906 San Francisco earthquake, water mains were severely damaged. Lack of water resulted in the destruction of much of the city after the earthquake [1,2]. Similarly, 35% of the city of Tokyo was ravaged by fire after the 1923 Kanto earthquake [3]. Buried pipelines suffered extensive damage during other earthquakes such as the 1971 San Fernando [4], the 1978 Miyagi-Oki [5] and more recently during the 1985 Mexico City [6].

In spite of its considerable importance, "Lifeline Earthquake Engineering" did not receive the attention of researchers and designers until about fifteen years ago. Available reports on the performance of buried pipelines during past earthquakes were the first tool at hand to understand the problem. Later, these reports provided statistical data on the damage and the ability to benchmark developed analytical models.

The seismic response of buried pipelines is substantially different from most above ground structures. First of all, they are part of long and complex networks composed of a variety of components which include joints, junctions (tees and elbows), hard points (thrust blocks, manholes and terminal structures) and others. In addition, they extend over large areas and are, therefore, subjected to out-of-phase ground motion along their length. Effects of this ground motion on buried pipelines are classified into two groups:

1. Permanent ground movements
2. Wave propagation effects

Permanent ground movements include fault movements, soil liquefaction and landsliding. They all can occur during and after earthquakes, and their effects are usually limited to recognizable areas. Their potential for damage, however, is very high since they subject pipelines to large displacements. Major pipeline breaks during the 1906 San Francisco earthquake occurred in areas of lateral spreading, and 25 to 50% of the pipeline damage during the 1971 San Fernando earthquake was attributed to fault movements [7]. Areas where there is a high risk of these

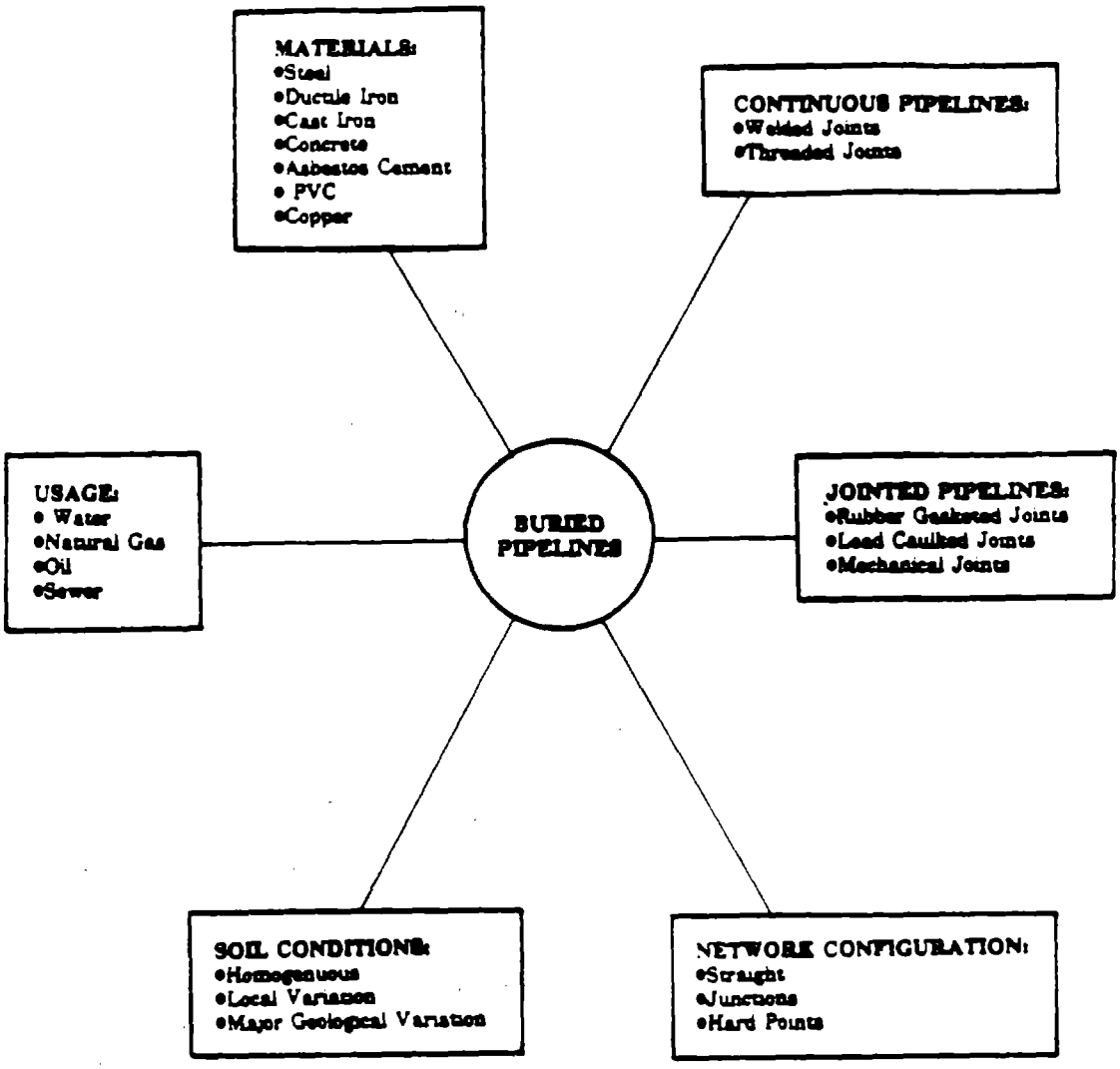

Figure 1-1. Characteristics of Buried Pipelines

permanent ground movements are avoided whenever possible.

On the other hand, wave propagation effects occur during the earthquake itself and can affect a large area around the epicenter. Damage which occurred to pipelines during the 1985 Mexico City earthquake was attributed exclusively to wave propagation effects. This earthquake caused severe damage to the water supply system of Mexico City. Nearly two weeks after the principal earthquake shock, about 3.5 million inhabitants were without running water [6,8].

The state of the art in buried pipeline seismic design has been advanced during the last decade. Newmark and Hall[9] developed an approximate method to estimate the response of continuous steel buried pipelines to fault movements. The same method was later improved by Kennedy et al.[10]. O'Rourke and Trautmann[11] proposed a simplified analytical method for the design of jointed buried pipelines to fault movements. For the design of buried pipelines for wave propagation effects, various methods have also been proposed. The simplest methods assume that the maximum axial strain and curvature in continuous buried pipelines is approximately equal to the maximum ground strain and ground curvature [12,13]. Shah and Chu[14] developed approximate analytical expressions for the response of tees and elbows in continuous systems under seismic wave propagation. Wang et al.[15] studied the behavior of jointed buried pipelines and proposed design procedures for wave propagation effects. Other studies were performed to investigate the problem for permanent ground movements [16,17,18], or for wave propagation effects [19,20,21,22]

This study concentrates on the problem of analysis of straight jointed buried pipelines for seismic wave propagation effects. Information on the performance of this specific type of pipeline during previous earthquakes indicates that damage most often occurs at the pipeline joints [4,6,23,24]. In particular, extension in the longitudinal direction is a major mode of failure. Other modes of failure such as crushing of the pipe bells, or opening of the joints after a combination of extension and rotation, have also been observed.

Currently, two types of procedures are used for the analysis of straight jointed buried pipelines. The first is based on a static solution which gives upper bounds for the axial strain in the pipe segments and axial displacements and rotations in the joints [15]. In the second procedure, an analytical model is developed. The pipe segments are represented by linearly elastic axial elements while the joints and soil are modeled by elasto-plastic springs. Inertia and damping terms are neglected. The seismic excitation is characterized by a non-dispersive wave propagating in time along the pipeline. This procedure is referred to as the quasi-static method [15,25]. These two procedures yield reasonable estimates for "average" response parameter values but fail to identify the range or distribution of these valuese. Note that the average values are of limited use for systems where 1 in 500 or 1 in 1000 joints leaks or fails due to wave

propagation. Neither procedures take into account the non-uniformity of the system parameters along the longitudinal direction.

In the present work, available information on the mechanical properties of pipe segments and joints as well as information on the soil/pipeline interaction are combined to establish a more realistic model. The formulation incorporates both the nonlinearity and the variability of the system parameters.

1.2 Objectives

The objective of this research is the development of new information which will facilitate the design of straight jointed buried pipelines for seismic wave propagation effects. Specifically, procedures to determine the system response as a function of the seismic input intensity will be given. Emphasis is placed on the joint behavior since damage occurs more frequently at the joints.

In the past, results were obtained from computer models in which the system properties are fixed along the pipeline. Experimental results however, show a pronounced variability for the joint properties. Also, the soil properties are expected to vary along the pipeline.

In the present research, two principal objectives are identified. These objectives are:

1. Development of an analytical model which takes into account the variability as well as the nonlinearity of the system properties. This involves the review, synthesis and integration of available information on the seismic environment, the pipeline properties and soil/pipeline interaction.

2. Use of the developed model to estimate the response of typical pipelines under seismic wave effects. First, a sensitivity analysis will be performed to evaluate the effects of the different properties and of their variability on the behavior of the pipeline. Then, a simplified Monte Carlo simulation technique is applied to the model. The response parameters and measures of their variability as a function of the seismic input, are obtained. Results in this form can be used, first, to assess the vulnerability of the different components constituting the system and secondly, to evaluate the performance of the system after the earthquake.

1.3 Format

In this first chapter, information on the seismic design of buried pipelines was presented. Following, the objectives of this research were stated. The rest of this report is composed of seven chapters.

Chapter 2 introduces and defines the problem of design of straight jointed buried pipelines for seismic wave propagation environment effects, with its assumptions and limitations. The

different tasks which have to be accomplished in this research are subsequently identified. In Chapter 3, the seismic environment due to wave propagation effects is quantified. The pipeline properties are presented in Chapter 4. For each of the pipeline systems considered, the mechanical characteristics of the pipe segments and joints are given. Chapter 5 is devoted to the evaluation of the soil properties. This includes the estimation of the characteristics of the soil spring-sliders used to model the axial and lateral soil/pipeline interaction. Chapter 6 explains the model constructed to represent the problem and gives the numerical procedures used for the analysis. This model is then used in Chapter 7 to evaluate the seismic response of specific types of jointed buried pipelines. A discussion of the results obtained is also presented. In addition, Chapter 7 includes a procedure to estimate the damage ratio due to a joint pull-out failure mode for cast iron systems with lead caulked joints. Conclusions and suggestions for future work are presented in Chapter 8.

2. PROBLEM DEFINITION

2.1 Introduction

Seismic wave propagation has caused damage to jointed buried pipelines in the past. The most severe damage usually occurs at the joints, tees and elbows. In order to assess the seismic vulnerability of a buried pipeline system, one needs to analyse first of all, the different components for wave propagation effects. Among these components are straight segments of pipelines, tee junctions and elbow junctions. Based on the performance of each of the components, the response of the whole system can then be evaluated.

In this study, the problem of *straight jointed buried pipelines* subjected to seismic wave propagation effects is investigated. A typical application of this problem would be a large diameter water main which conveys water over a distance of several city blocks before branching at elbows and tees. A schematic of a straight jointed buried pipeline with its details is shown in Figure 2-1.

2.2 Assumptions and Limitations

The main assumptions of the present study are:

1. A static formulation is appropriate to evaluate the pipeline response
2. The pipeline is initially strain free in the longitudinal direction
3. There are no permanent displacements of the soil surrounding the pipeline such as faulting, liquefaction or landsliding

The justifications for the above stated assumptions are outlined below.

1. Static formulation:

Results of several studies show that inertia effects can be neglected [20,26,27]. This is due to the presence of high radiation damping of the surrounding soil and to the fact that the mass of a fluid filled pipe is smaller than the mass of the insitu soil it replaces. Thus, the problem is usually reduced to solving the static equations at different times since the seismic input is a function of time. In this study, it is assumed that a static displacement approach in which the static equations are solved only once, under maximum seismic ground strain and ground rotation, yields good estimates of the response parameters. This is true if the seismic input, that is the ground strain and ground rotation, is not high enough to take the response parameters into the nonlinear range. In this case, the pipeline and soil deformations remain elastic and the seismic cycling does not produce any residual deformations. The static formulation is also a good approximation when the seismic input reaches high values and the system goes into the nonlinear range. A known feature of seismic excitation, is that the ground displacement varies

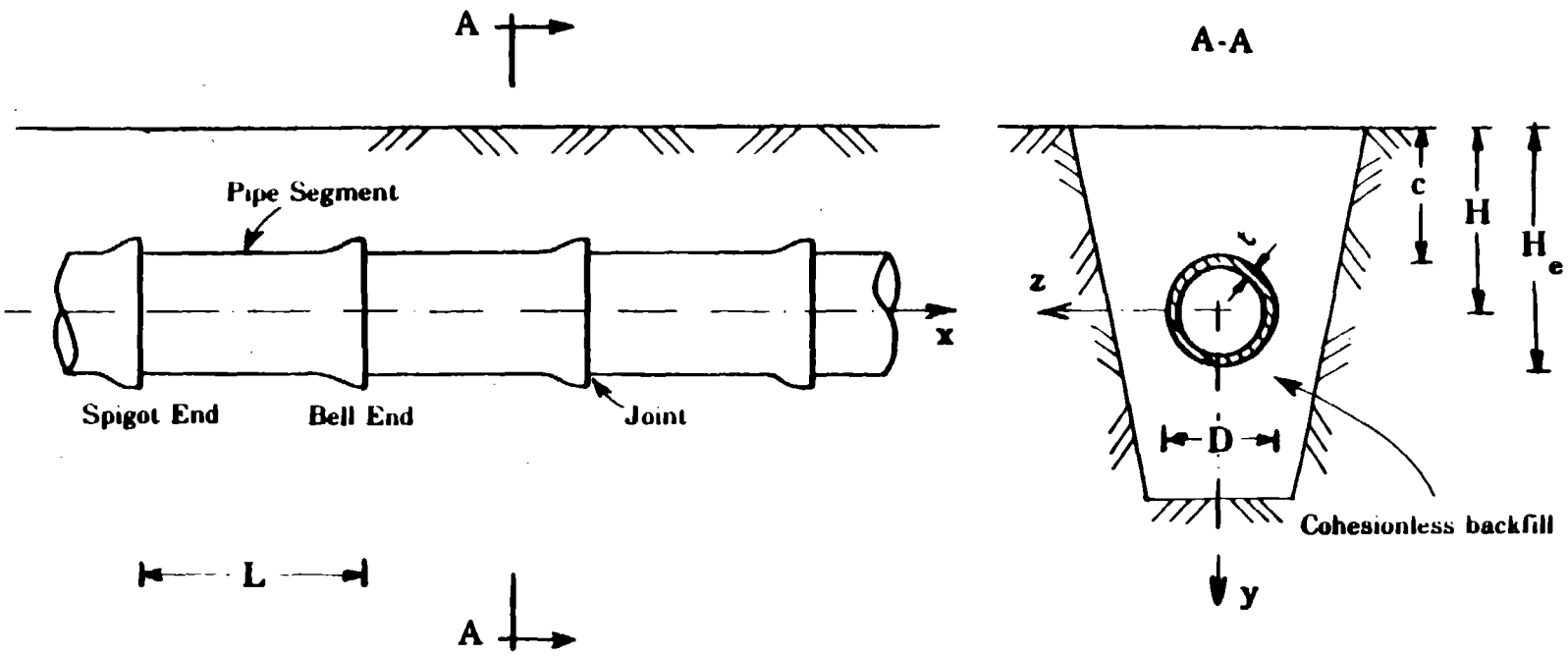

Figure 2-1. Schematic of a Straight Jointed Buried Pipeline

significantly with time. Thus, a cycle of maximum ground strain and ground rotation are often followed in time by a cycle with smaller values of ground strain and ground rotation. This latter cycle may not greatly affect the value of the response parameters. Other reasons for using this static displacement approach are that, first of all, experimental results for cycling of the joints are not available, secondly, a simplified Monte Carlo simulation technique to account for the variability of the system parameters can be easily incorporated into the model and lastly, it is much cheaper in terms of computer money than the true time history approach .

2. Zero initial strain in the longitudinal direction:

Buried pipelines are normally designed to withstand internal pressure, earth loads, and live loads. Because of axisymmetry, the first two loads mainly affect the hoop strain. On the other hand, live loads affect both the axial and hoop strain. Only the hoop strain, however, is considered in the design process since the support provided by the soil prevents the pipeline from deforming appreciably in the longitudinal direction.

3. Effects of permanent ground displacements not included:

It is assumed that the pipeline is located in areas not subjected to faulting, liquefaction or landsliding. That is, this study is limited to wave propagation effects. Although it is recognized that faulting, liquefaction and landsliding are potential causes of damage to pipelines, there are certain cases such as the 1985 Mexico City earthquake where damage was exclusively due to wave propagation effects.

More specific assumptions will be made in this study, when applicable.

Based on observations of damage during past earthquakes, three failure modes are identified. These failure modes are the following:

1. Pull-out of the joints
2. Crushing of the pipe segment bell
3. Opening of the joints by a combination of axial extension and bending rotation

The first and second failure modes are much more frequent than the third one. This is due to the fact that the joints constitute, in general, weak points along the pipeline. In addition, the axial ground strain is usually predominant over the bending ground strain [13,28,29,30].

Two types of pipeline systems are considered in the course of this research. They are:

1. Cast Iron Pipes with Lead Caulked Joints
2. Ductile Iron Pipes with Rubber Gasketed Joints

The first type is quite common in older water supply systems, while the second is more common in newer ones and is often used as replacements. Both systems are also used in gas distribution systems.

2.3 Tasks

The specific goal of this research is to develop analytical procedures for *straight jointed buried pipelines* subjected to seismic waves. Available information on the mechanical properties of pipe segments and joints as well as information on the soil resistance to pipe movements are combined to establish a realistic model. The formulation will incorporate the *nonlinear* behavior as well as the *variability* of the system characteristics. The inclusion of *variability* is considered important first of all, because it allows more accurate modelling of actual conditions and secondly, because neglecting variability would likely result in an unconservative estimate of damage. If all the joints were essentially the same, a fairly uniform distribution of joint displacements would result. For this case, leakage or damage would occur at all joints almost simultaneously at a relatively high level of ground strain. If on the other hand, the characteristics are different from one joint to another, one would also expect that the displacements at the joints would also be different. For this second case, damage would first occur only at the weakest joints, at an overall level of ground strain less than that causing damage to the "uniform" system.

For this purpose, a *simplified Monte Carlo simulation technique* will be used. First, the system characteristics, such as the stiffness for each joint, is determined by random selection from established histograms. The system is then analyzed for seismic waves. These two steps are repeated several times, and results serve to develop histograms of the response parameters. These response parameters include the joint axial displacements and rotations, pipe segment axial strains, and axial and lateral relative displacements between the soil and the pipeline.

In order to accomplish the goal stated above, five tasks are identified. These five tasks are:

- Task 1, Seismic Environment:

Quantify the ground strain and ground rotation due to the propagation of both body and surface waves.

- Task 2, Pipeline Properties:

Quantify the mechanical behavior of pipe segments and joints subjected to axial (longitudinal) and flexural (lateral) loadings. Both the average properties and the variability about the average values are to be determined.

- Task 3, Soil Properties:

Quantify the soil nonlinear resistance to axial and lateral movements of pipes. Both the average resistance and variability about the average values are to be determined.

- Task 4, Analytical Model:

Construct a model for straight jointed buried pipelines and develop the numerical procedures needed for the analysis.

• Task 5, Results:

Subject the model to the seismic environment and evaluate the pipe segment, joint and soil responses. Results are then combined with information on failure to predict the seismic damage.

3. SEISMIC ENVIRONMENT

3.1 Introduction

In order to evaluate seismic wave propagation effects on buried pipelines, one begins by quantifying the seismic ground strain and ground rotation. The ground strain is assumed to act along the pipeline axis, x. Under this assumption, the pipeline is expected to experience the most severe differential axial movements. The ground rotation, on the other hand, is assumed to be in the horizontal plane (x,z). It produces bending strain in the pipeline. For simplicity, rotation in the vertical plane (x,y) is not considered.

Simplified models are proposed to estimate the maximum ground strain, ϵ_g, and the maximum ground rotation, θ_g. A range of realistic values is proposed for the two parameters, ϵ_g and θ_g. These values are used to determine the axial ground displacement, $u_g(x)$, and the lateral ground displacement, $w_g(x)$.

3.2 Ground Strain

If one models the seismic excitation as a single plane traveling wave, Newmark[12] has shown that the maximum ground strain, ϵ_g, in the direction parallel to the traveling wave, is given by:

$$\epsilon_g = \frac{\dot{u}_g^{max}}{C} \tag{3.1}$$

where $\dot{u}_g^{max}$ is the maximum particle velocity parallel to the direction of the wave travel and C is the apparent propagation velocity of the seismic wave with respect to the ground surface.

If a site specific seismic hazard analysis is available, both the peak ground acceleration, $\ddot{u}_g^{max}$, and the peak ground velocity, $\dot{u}_g^{max}$, for a particular return period would likely be available. However, for less critical facilities the seismic hazard may be characterized only by $\ddot{u}_g^{max}$ for the general region in question. In these cases, $\dot{u}_g^{max}$ may be estimated through the use of available values for the ratio $\dot{u}_g^{max}/\ddot{u}_g^{max}$ as proposed by Newmark[31], Seed et al.[32] or Ayala and Rascon[33]. These $\dot{u}_g^{max}/\ddot{u}_g^{max}$ ratios are presented in Table 3-I. They are functions of the local soil conditions. The high value for Mexico City clay is due to the predominate 2 second period for ground motions in the Valley of Mexico. The Newmark and Seed et al. values do not take into consideration the distance from the causative fault to the site. As pointed out by Idriss[34], the ratio $\dot{u}_g^{max}/\ddot{u}_g^{max}$ increases with increasing epicentral distance due to differences in the attenuation of high frequency (acceleration) and moderate frequency (velocity) ground motions.

For a soil site subjected to body waves only (P, SV and SH waves), the apparent propagation velocity with respect to the ground surface, C, is many times larger than the shear wave velocity

Table 3-I

$\dot{u}_g^{max}/\ddot{u}_g^{max}$ Ratios

Material	$\dot{u}_g^{max}/\ddot{u}_g^{max}$ $\frac{\text{inch/sec}}{g}$ ($\frac{\text{cm/sec}}{g}$)		
	Newmark[31]	Seed et al.[32]	Ayala and Rascon[33]
Rock	24 (61)	26 (66)	-
Stiff Soil	-	45 (114)	-
Deep Cohesionless	-	55 (140)	-
Alluvium	48 (122)	-	-
Mexico City Clay	-	-	119 (304)

of the near surface material. Seismic energy originating at depth passes through increasing softer materials and refraction causes a concave travel path. The net result being body waves which arrive at the gound surface with a small angle of incidence with respect to the vertical. If the angle of incidence at the ground surface is γ_i and the shear wave velocity of the top layer is C_s, then as shown in Figure 3-1, the apparent propagation velocity of SV or SH waves with respect to the ground surface is:

$$C = \frac{C_s}{\sin\gamma_i} \tag{3.2}$$

If the body waves were vertically incident (i.e. $\gamma_i = 0$), as is assumed in one-dimensional soil amplification studies, the propagation velocity with respect to the ground surface would be infinite. That is, the motion at the ground surface would be in-phase.

O'Rourke et al.[35] studied the apparent horizontal propagation velocity and calculated values of 2.1 Km/sec and 3.8 Km/sec for the 1971 San Fernando earthquake and the 1979 Imperial Valley earthquake, respectively. These fall in the general range of values for earthquakes in Japan as calculated by Tamura et al.[36] and Tsuchida and Kurata[37]. Table 3-II presents a summary of information on the apparent propagation velocity of body waves.

In summary, for a site subjected to body wave propagation only, the maximum ground strain, ϵ_g, may be evaluated using Eqn.(3.1) in which the apparent propagation velocity with respect to the ground surface is somewhere in the range of 2 to 5 Km/sec. Using this procedure with a peak ground acceleration, $\ddot{u}_g^{max} = 0.60$ g, and a ratio $\dot{u}_g^{max}/\ddot{u}_g^{max} = 48 \frac{\text{inch/sec}}{g}$ ($122 \frac{\text{cm/sec}}{g}$) (i.e. alluvium soil), the value of ϵ_g ranges between 1.50×10^{-4} and 3.70×10^{-4}.

The situation for surface waves is somewhat more complex. Love waves and Rayleigh waves are the two main types of surface waves generated by earthquakes. For Love waves (L-waves), the particle motion is along a horizontal line perpendicular to the direction of propagation and the amplitude decreases with depth below the ground surface. For Rayleigh waves (R-waves), the particle motion traces an ellipse in a vertical plane, the size of the ellipse decreasing with depth below the ground surface. The horizontal component of motion for R-waves is parallel to the direction of propagation.

Consider both an L-wave and an R-wave propagating along the radial line from the epicenter. The L-wave would cause out-of-phase transverse motions at two points along such a line and produce bending in a straight pipeline connecting these two points. On the other hand, the horizontal component of particle motion due to the R-wave would produce axial strain between the two points. It can be shown that the axial strain due to seismic wave propagation is

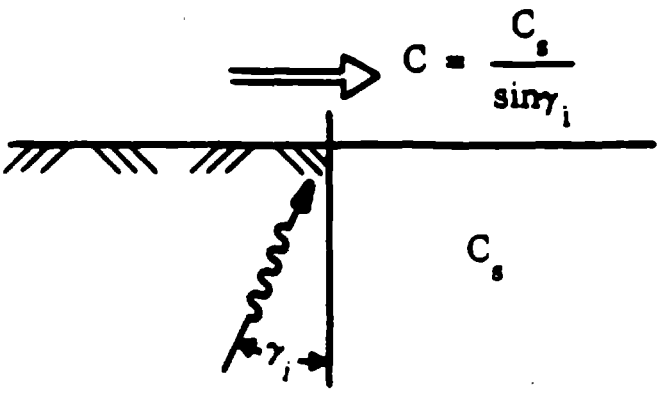

Figure 3-1. Apparent Propagation Velocity of Body Waves

Table 3-II

Apparent Horizontal Propagation Velocity of Body Waves

Event	Site Conditions	Focal Depth (Km)	Epicentral Distance (Km)	Apparent Propagation Velocity (Km/sec)	Reference
Japan 1/23/68	60 m soft alluvium	80	54	2.9	Tamura et al.[36]
Japan 7/1/68	60 m soft alluvium	50	30	2.6	Tamura et al.[36]
San Fernando 2/9/71	Variable	13	29 to 44	2.1	O'Rourke et al.[35]
Japan 5/9/74	70 m of silty clay, sand and silty sand	10	140	5.3	Tsuchida and Kurata[37]
Japan 8/4/74	70 m of silty clay, sand and silty sand	50	54	4.4	Tsuchida and Kurata[37]
Imperial Valley 10/15/79	less than 300 m of alluvium	Shallow	6 to 57	3.8	O'Rourke et al.[35]

generally more important for the design of straight buried pipelines than the bending strain due to wave propagation. Hence, considerations of surface waves will be restricted herein to R-waves. For the idealized case of a uniform halfspace, the propagation velocity of an R-wave along the ground surface is slightly smaller than the shear wave velocity of the medium. For the more typical case of a soil profile in which material stiffness increases with depth, the R-wave propagation velocity is a function of frequency or wave length. That is, the wave is dispersive with long wavelength (low frequency) R-wave traveling faster than short wavelength (high frequency) R-wave. The wavelength, λ, frequency, f, and phase velocity, C_{ph}, are interrelated by:

$$C_{ph} = \lambda \cdot f \tag{3.3}$$

A dispersion curve plots the phase or propagation velocity as a function of frequency. O'Rourke et al.[22] presented an approximate R-wave dispersion curve for a uniform layer of thickness h and shear wave velocity C_L, located over a stiffer uniform halfspace with shear wave velocity C_H. This approximate dispersion curve is shown in Figure 3-2. For short wavelengths (i.e. normalized frequency: $h \cdot f/C_L \geq 0.5$), the layer seems "thick" and the R-wave phase velocity is governed by material properties of the layer. Conversely, for large wavelengths (i.e. normalized frequency: $h \cdot f/C_L \leq 0.25$), the layer seems "thin" and the R-wave phase velocity is governed by material properties of the halfspace. Between these two limits, a straight line variation of phase velocity with frequency is appropriate.

The approximate dispersion curve shown in Figure 3-2 is in general agreement with bounds for the layer over halfspace case as presented by Achenbach and Epstein[38], Mooney and Bolt[39] and Shinozuka et al.[40]. As discussed by O'Rourke et al.[22], an approximate dispersion curve for multiple layers over a halfspace can be determined by extending the concept illustrated in Figure 3-2.

For a site subjected to R-wave propagation, with material properties increasing with depth, the R-wave propagation velocity is an increasing function of wavelength and a decreasing function of frequency. The question then arises as to the appropriate propagation velocity to use in Eqn.(3.1) in order to evaluate the ground strain. O'Rourke et al.[22] studied ground motions recorded during the 1971 San Fernando earthquake in an area of Los Angeles in which, according to Hanks[41,42], the ground displacement waveforms are dominated by the presence of R-wave. Using data from this earthquake, O'Rourke et al.[22] found that the ground strain between two stations separated by less than about 0.6 mile (1 Km), along the same epicentral line, could be

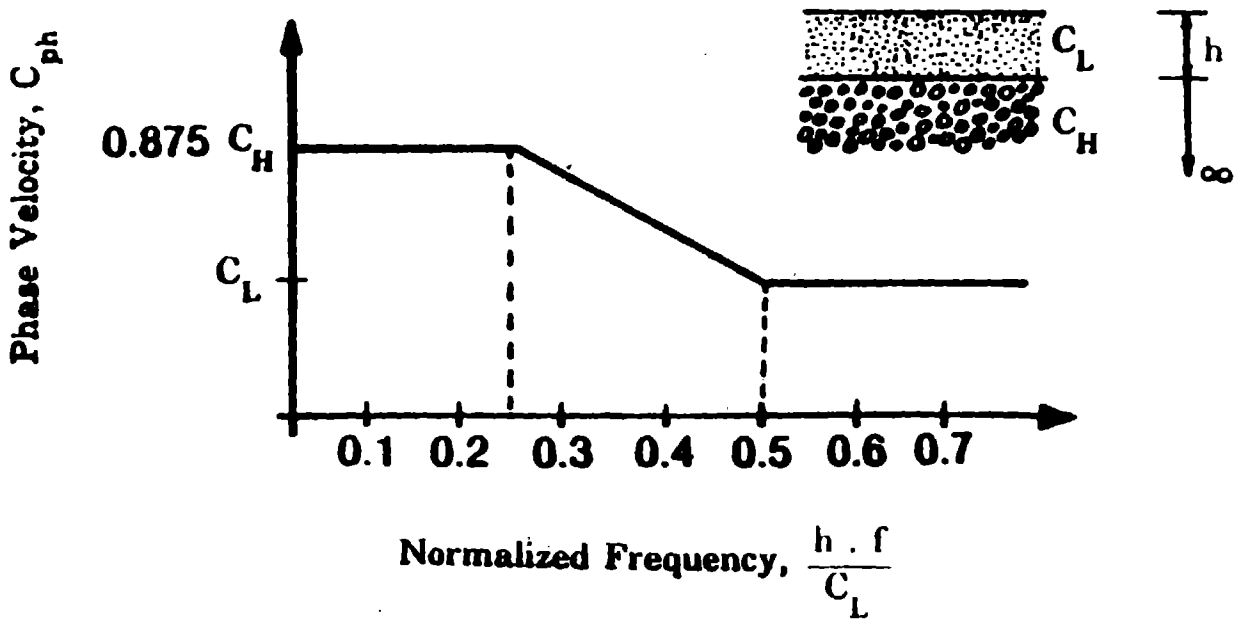

Figure 3-2. Approximate R-Wave Dispersion Curve

reasonably estimated by using a phase velocity corresponding to a wavelength λ equal to four times the separation distance, L_s, between the stations, that is:

$$\lambda = 4 \cdot L_s \tag{3.4}$$

Since R-wave phase or propagation velocities are increasing functions of wavelength, ground strain given by Eqn.(3.1) is a decreasing function of separation distance. Note that a decrease in ground strain with increasing separation distance has also been noticed by Wright and Takada[43].

Hence, for a site subjected to R-wave propagation only, the maximum ground strain, ϵ_g, can be obtained as a function of the separation distance, $L_s = \lambda/4$, using Eqn.(3.1) in conjunction with the approximate dispersion curve in Figure 3-2 and Eqn.(3.3). This method yields a range of values for ϵ_g. Note that the value of ϵ_g obtained when only body waves are assumed to be present, is usually much smaller than the range of values obtained when only R-wave are assumed to be present. For a moderately strong earthquake, the R-wave ground strain could reach values on the order of 1.5×10^{-3} [44].

The seismic exitation for the pipeline model proposed in this study, is given in terms of the axial and lateral ground displacements. The axial ground displacement along the pipeline model, $u_g(x)$, is assumed to be a linear function of x. This assumption is justified by the fact that the value of the seismic wavelength, λ, is typically much larger than the pipeline model length, L_{pm}. The pipeline model length is chosen equal to L_{pm} = 200 feet (60 m), while values of the seismic wavelength, λ, are expected to be substantially larger. Thus, $u_g(x)$ can be expressed as:

$$u_g(x) = \pm \epsilon_g \cdot (x - \frac{L_{pm}}{2}) \tag{3.5}$$

The (+) sign corresponds to a tensile ground strain and the (−) sign corresponds to a compressive ground strain. In this study, values of ϵ_g are taken in the range: $1.0\times10^{-4} \leq \epsilon_g \leq 7.0\times10^{-3}$. These values are believed to cover a wide range of earthquake intensities. Note that during the 1971 San Fernando earthquake, ϵ_g ranged between 0.6×10^{-4} and 6.4×10^{-4} [22] and that during the 1985 Mexico City earthquake, ϵ_g was on the order of 2.0×10^{-3} [6].

3.3 Ground Rotation

O'Rourke et al. [45] have shown that the maximum angle of rotation of the ground about a vertical axis, θ_g, due to a single plane traveling wave, is given by:

$$\theta_g = \frac{\dot{w}_g^{max}}{C} \tag{3.6}$$

where $\dot{w}_g^{max}$ is the maximum particle velocity in the lateral direction, z, and C is the apparent propagation velocity of the seismic wave with respect to the ground surface. The expression for θ_g [i.e. Eqn.(3.6)] is similar to that for ϵ_g [i.e. Eqn.(3.1)], except that $\dot{u}_g^{max}$ is replaced by $\dot{w}_g^{max}$. During earthquakes, values of $\dot{u}_g^{max}$ and $\dot{w}_g^{max}$ are of the same order of magnitude. Hence, values of θ_g can be taken as roughly equal to those of ϵ_g.

As with the axial case, the ground rotation is assumed to be uniform over the extent of the pipeline model. Knowing that: $\theta_g = -\frac{dw(x)}{dx}$, one can obtain the lateral ground displacement, $w_g(x)$, from the following equation:

$$w_g(x) = \theta_g \cdot \left(\frac{L_{pm}}{2} - x\right) \tag{3.7}$$

The range of values for the maximum ground rotation, is taken as $1.0\times10^{-4} \leq \theta_g \leq 7.0\times10^{-3}$ rad. This range corresponds to that chosen for the maximum ground strain.

3.4 Summary

As mentioned previously, three failure modes are considered in this study. The first is *pull-out* of the joints. Accordingly, the corresponding loading consists of subjecting the pipeline model only to the axial ground displacement, $u_g(x)$, given by Eqn.(3.5), with the (+) sign (i.e. a tensile ground strain ϵ_g and $\theta_g = 0$). The loading for the second failure mode which is *crushing* of the pipe segment bell, corresponds to applying a uniform compressive ground strain to the pipeline model. That is, the axial ground displacement, $u_g(x)$, given by Eqn.(3.5) with the (−) sign. As with the first failure mode, $\theta_g = 0$. Since the third failure mode is *opening* of the joints by a combination of axial and bending rotation, the corresponding loading is made up of the axial ground displacement, $u_g(x)$, and the lateral ground displacement, $w_g(x)$, given respectively by Eqn.(3.5) with the (+) sign and Eqn.(3.7).

The range of values used of the parameter ϵ_g, for the three failure modes, is given by:

$$1.0\times10^{-4} \leq \epsilon_g \leq 7.0\times10^{-3} \tag{3.8}$$

and the range of values used for the parameter θ_g, for the third failure mode, is given by:

$$1.0\times10^{-4} \leq \theta_g \leq 7.0\times10^{-3} \text{ rad.}$$

4. PIPELINE PROPERTIES

4.1 Introduction

Straight jointed buried pipelines are composed of two types of elements, namely the pipe segments and the joints. Information about the axial and flexural behavior of these elements is necessary to establish analytical models for such pipelines.

As mentioned previously, two types of pipeline systems are considered in this research. They are:

1. Cast Iron Pipes with Lead Caulked Joints
2. Ductile Iron Pipes with Rubber Gasketed Joints

The first type is very common in older water supply systems. It composes approximately 85% of the water distribution network in the United States [46]. The second type, on the other hand, is common in newer water supply systems and as replacements of the first type. Both types are mainly used in water distribution lines [defined to have roughly a diameter comprised between 4 and 20 inches (10.16 and 50.8 cm)], and to a lesser extent in water transmission lines [defined to have roughly a diameter larger than 20 inches (50.8 cm)]. Note that these two types were also used in gas distribution systems.

The pipeline properties for each of these two systems, are determined after review, synthesis and integration of the existing literature. Emphasis is placed on the properties of pipelines with diameter larger than 12 inches (30.48 cm). These larger diameter pipelines are somewhat more important because if they are damaged by earthquakes, more users would be affected. First, the mechanical behavior of the pipe segment material is characterized by established stress/strain relationships. It should be mentioned that stresses in pipe segments under wave propagation effects are expected to be in the elastic range since damage occurs usually at the joints. In addition to the stress/strain relationship, one needs the dimensions of the cross-section as well as the pipe segment length, L. The dimensions of the cross-section include mainly the outside diameter, D, and the wall thickness, t. These two parameters are function of the depth of cover, c, laying conditions, internal pressure and traffic loads. Their values along with that of the pipe segment length can be obtained from manufacturer's or standard tables. Second, a description of each of the two types of joints is presented. The mechanical properties of the joints are described in terms of the axial force/displacement and bending moment/rotation relationships. The joint behavior is characterized by a wide scatter in test results for both pipeline systems. For this reason, the parameters defining the axial force/displacement and bending moment/rotation relationships are assumed to be random variables. Based on available experimental results, analytical and empirical expressions for the mean values of these parameters and estimates of

their variability are presented. Note that, because of lack of experimental results, it is assumed that there is no interaction between the axial force/displacement and bending moment/rotation relationships.

The last section of this chapter includes a procedure to select the pipeline properties for each of the two pipeline systems considered.

4.2 Cast Iron Pipes with Lead Caulked Joints

4.2.1 Pipe Segment Properties

The use of cast iron pipes in the United States began in the early 1800's. During the hundred and fifty years that followed, cast iron emerged as the only affordable piping material with reliable strength and durability. Cast iron pipes were used especially in water supply systems and to a lesser extent, in gas distribution systems. Approximately 85% of the water distribution network in the United States is composed of cast iron pipes. Cast iron pipes installed before 1920 were manufactured by pit casting methods. They are referred to as pit cast iron pipes. In 1920, centrifugal casting method was introduced and has become, since then, the main manufacturing process. Pipes manufactured by this latter method have better mechanical and physical characteristics. Since centrifugal casting was adopted on a large scale by the pipe industry after 1930, only cast iron pipes centrifugally cast, are considered in this study. Note that manufacturing of cast iron pipes has almost ceased. It has been replaced by ductile iron pipes.

Cast iron exhibits nonlinear behavior even at low levels of strain. In addition, it has different characteristics in tension and in compression. Compressive strength is substantially larger than tension strength. Figure 4-1 shows in solid line a typical stress/strain curve for cast iron [47]. Mechanical properties of standard cast iron are classified in terms of their tensile strength by ASTM [48]. ASTM Class 20, however, was often used in cast iron pipes. This class has an initial tangent modulus (Young's modulus), E_p, equal to 14×10^6 psi (1.0×10^6 Kgf/cm^2), a tensile strength, σ^u, of 22×10^3 psi (1.5×10^3 Kgf/cm^2) and a compressive strength, σ^c, of 83×10^3 psi (5.80×10^3 Kgf/cm^2). The actual relationship between the stress, σ, and the strain, ϵ, in ASTM Class 20 cast iron is approximated by a bilinear model as shown by the dashed line in Figure 4-1. Taki and O'Rourke [49] noticed that the slope of the stress/strain curve in tension starts decreasing rapidly at strains larger than 0.1%. In compression, this slope decreases at a considerably slow rate. With this in mind, a bilinear model was chosen to approximate the (σ,ϵ) relationship. The approximation has a constant slope equal to E_p for strains between -0.3% and 0.1%. For strains outside this range, a constant modulus in tension, $E_p^{(2)}$, and a constant modulus in compression $E_p^{(3)}$, are used. The failure point in tension corresponds to a stress equal to:

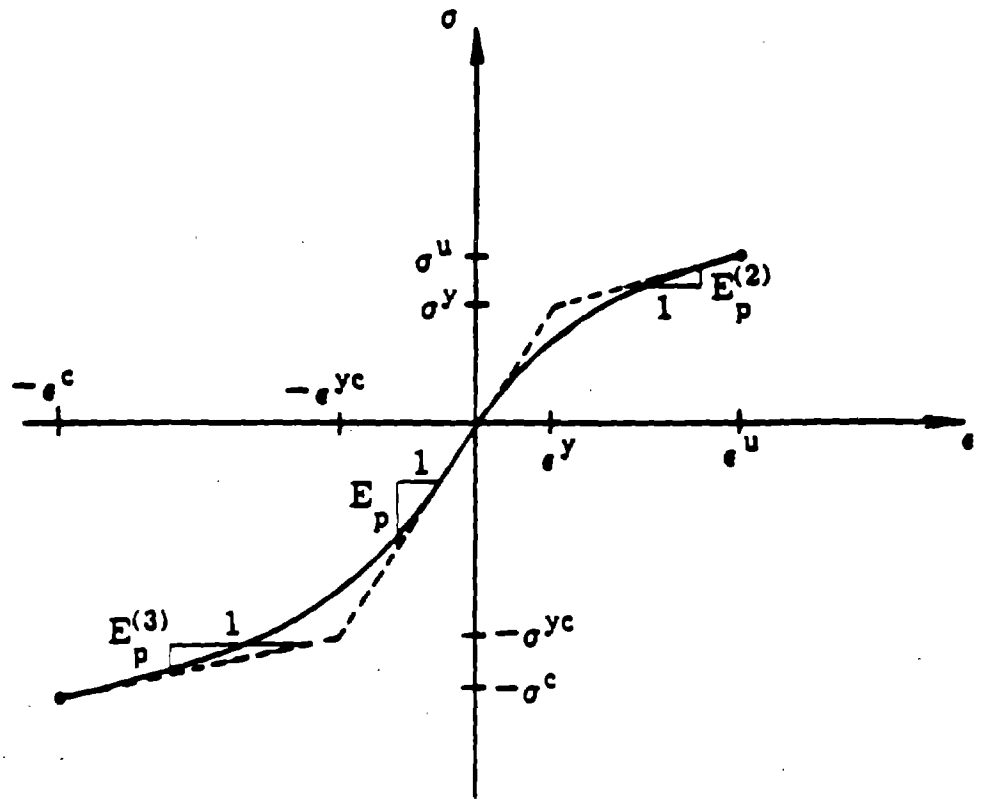

Figure 4-1. Stress/Strain Curve for Cast Iron

$\sigma^u = 22\times10^3$ psi (1.50×10^3 Kgf/cm^2) and a strain equal to: $\epsilon^u = 0.5\%$, while the failure point in compression corresponds to a stress equal to: $\sigma^c = 83\times10^3$ psi (5.80×10^3 Kgf/cm^2) and a strain equal to $\epsilon^c = 4\%$ [50]. That is, the stress/strain relationship for Class 20 cast iron is approximated by the following equations:

$$\sigma = \begin{cases} -\sigma^{yc} + E_p^{(3)} \cdot (\epsilon + 3\times10^{-3}) & ; \epsilon < -3\times10^{-3} \\ E_p \cdot \epsilon & ; -3\times10^{-3} \le \epsilon \le 10^{-3} \\ \sigma^y + E_p^{(2)} \cdot (\epsilon - 10^{-3}) & ; \epsilon > 10^{-3} \end{cases} \quad (4.1)$$

in which $E_p^{(2)} = 2\times10^6$ psi (1.4×10^5 Kgf/cm^2) and $E_p^{(3)} = 10^6$ psi (0.7×10^5 Kgf/cm^2).

The design of cast iron pipe is based on rigid-pipe principles. The pipe wall thickness is computed based on two alternative load combinations. The first load combination includes the working pressure, earth load and pressure surge, while the second one includes the working pressure, earth load and traffic load [51]. Dimensions of cast iron pipes which include the pipe segment length, L, the outside diameter, D, and the wall thickness, t, are taken in this study from "Handbook of Ductile Iron Pipe" [52]. The length L is typically equal to 20 feet (6 m). Values of D and t are given in tables for different values of working pressure, depth of cover and different laying conditions. The depth of cover, c, is a factor in choosing the value of t as a function of D and will be discussed in section 5.2.1 of this report.

4.2.2 Joint Properties

Lead caulked joints are relatively rigid connections. They exist mainly in old cast iron pipeline systems. A typical cross-section of this joint is shown in Figure 4-2. During construction of the joint, the spigot end of each pipe segment is brought to a uniform contact all around the bell end of the adjoining pipe segment. Oakum, which is a hemp yarn, is then packed into the annular space between the spigot and the bell. Following, molten lead is poured on the oakum. The last phase involves the ramming and tamping of the lead, after it has cooled, with a caulking tool. Note that the spigot end has a bead which prevents the oakum packing from sliding past the spigot. The oakum packing serves as a first shield against leakage and also prevents the lead from coming into contact with the material transported by the pipeline. The lead, on the other hand, gives rigidity to the joint and makes the joint tight against leakage by sealing. Note that, since the oakum packing is made of a coarse loose hemp fiber, it is expected that its contribution to the overall stiffness of the joint be negligible compared to that of the lead.

The behavior of lead caulked joints is complicated by the fact that lead is a highly nonlinear

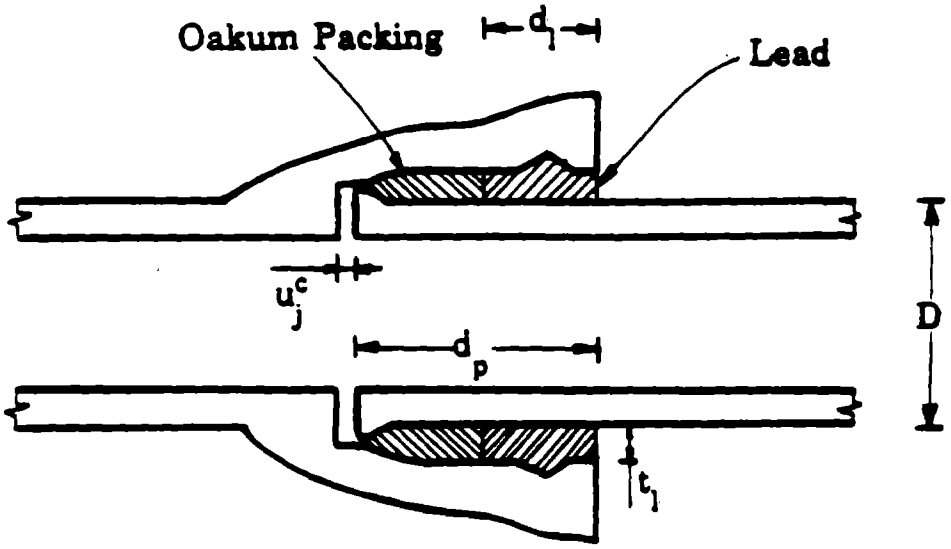

Figure 4-2. Cross-Sectional View of Lead Caulked Joint

material. Moreover, lead is strain dependent and exhibits large amount of creep at ordinary temperatures. Salvadori and Singhal[50] presented some of the mechanical properties of lead. Of interest in this study is the shear modulus, $G_l \simeq 78.0\times10^4$ psi (5.50×10^4 Kgf/cm^2).

Prior[53] performed pull-out (tension) and bending tests on lead caulked joints in cast iron pipes, while Harris and O'Rourke[54] carried out bending tests on the same type of joint. Results from these tests are used herein, to characterize the axial force/displacement and bending moment/rotation relationships for lead caulked joints in cast iron pipes.

4.2.2.1 Axial Force/Displacement Relationship

In the early 1930's, Prior[53] performed a series of laboratory tests to investigate the pull-out strength of lead caulked joints in cast iron water pipes. These tests consisted of two jointed pipes capped at the ends. The two pipes were pulled apart from each other by increasing the internal pipe pressure. The pipes tested had a nominal diameter, D_n, between 6 and 60 inches (15.24 and 152.40 cm). Prior measured the axial force/displacement characteristics of the lead caulked joints as well as the onset of significant leakage.

Figure 4-3 shows a typical graph obtained by Prior. This graph plots the axial force at the joint, F_j, and the corresponding axial displacement, u_j, as a function of time. Results from Prior's tests indicate that the relationship between F_j and u_j is initially very rigid. It is believed that axial forces at the joint are initially resisted by elastic shear forces in the lead. The abrupt drop in stiffness corresponds to the point where these shear forces reach the adhesive strength at the pipe/lead interface. After that, axial forces at the joint are resisted by friction at the pipe/lead interface. Failure is reached when the lead is forced far enough out of the joint.

The axial force/displacement relationship of a lead caulked joint is represented herein by a bilinear model. A sketch of this model is given in Figure 4-4. Note that the push-in (compression) behavior of the joint is assumed to be similar to the pull-out behavior up to the point where the two adjacent pipe segments come into contact with each other, after which the joint becomes very rigid and behaves as if it was not present and the pipe was continuous.

In order to fully define the bilinear model proposed for the (F_j,u_j) relationship, one needs to evaluate the initial axial stiffness, AK_j, the axial force at slippage, F_j^s, the ultimate pull-out force, F_j^u, the axial tensile displacement at failure (displacement corresponding to significant leakage), u_j^u, the axial compressive displacement when contact between the two adjacent pipe segments occurs, u_j^c, (see Figure 4-2), the axial stiffness after contact, $AK_j^{(3)}$, and the ultimate compressive force, F_j^c.

Under the assumption that axial forces at the joint are initially resisted by elastic shear forces in

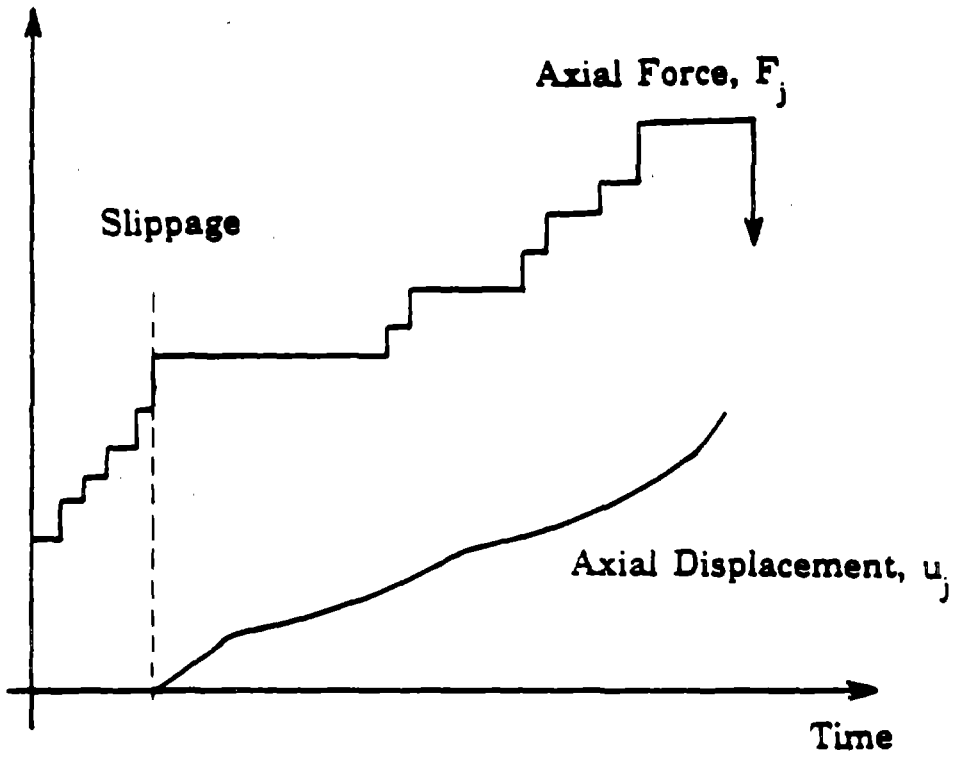

Figure 4-3. Axial Force and Axial Displacement of Lead Caulked Joint versus Time (after Prior [53])

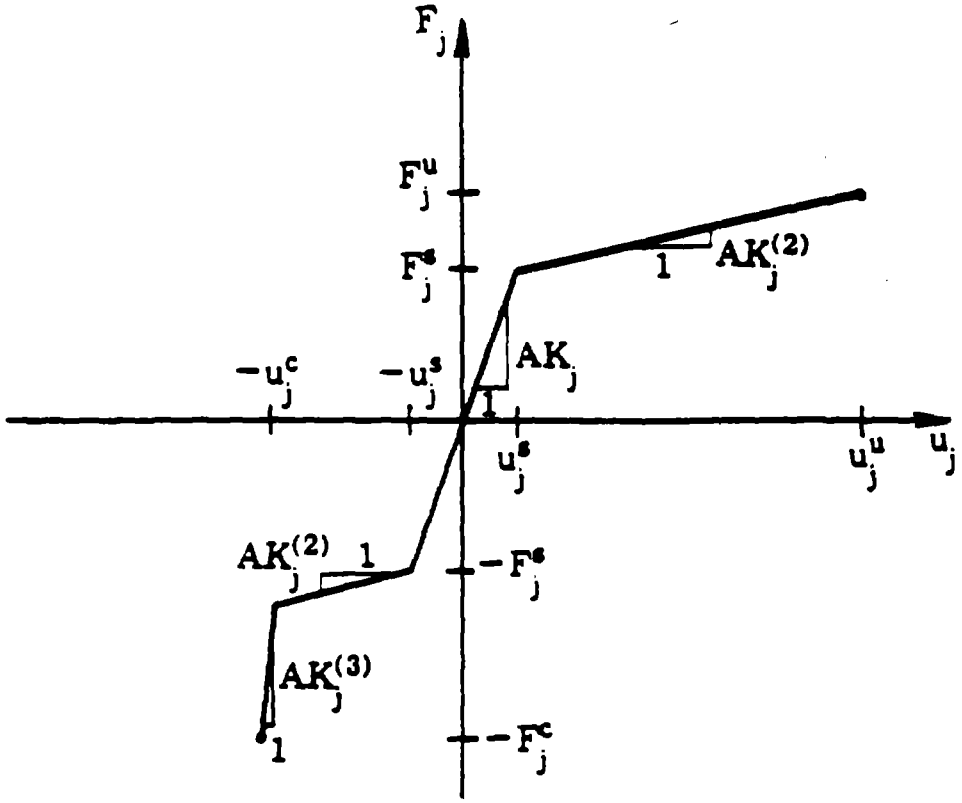

Figure 4-4. Axial Force/Displacement Curve for Lead Caulked Joints

the lead, the initial axial stiffness can be evaluated by:

$$AK_j = G_l \cdot \frac{1}{t_l} \cdot \pi D \cdot d_l \tag{4.2}$$

where G_l is as defined before, the shear modulus of lead [$G_l \simeq 78.0\times10^4$ psi (5.50×10^4 Kgf/cm^2)], πD represents the outer circumference of the pipe, and t_l and d_l are respectively the thickness and the depth of the caulked lead as shown in Figure 4-2.

It is easy to see that AK_j as given by Eqn.(4.2), represents the axial force causing a unit displacement of the joint since the product $(G_l \cdot \frac{1}{t_l})$ is the resulting shear stress in the caulked lead and the product $(\pi D \cdot d_l)$ is the sheared area. Values of AK_j given by Eqn.(4.2) are very high and thus, consistent with the observed initial stiff behavior. However, verification of these values with Prior's test results is not possible because the axial diplacement of the joint before or at slippage are very small and could not be measured by Prior[53].

The thickness of caulked lead, t_l, can be obtained from manufacturer's or standard tables. The American Water Work Association(AWWA) gives the following standard values [52]:

$$t_l = \begin{cases} 0.4 \text{ inch } (1.02 \text{ cm}) & ; 3\ (7.62) \le D_n \le 14 \text{ inches } (35.56 \text{ cm}) \\ 0.5 \text{ inch } (1.27 \text{ cm}) & ; 16\ (40.64) \le D_n \le 60 \text{ inches } (152.40 \text{ cm}) \\ 0.63 \text{ inch } (1.60 \text{ cm}) & ; 72\ (182.80) \le D_n \le 84 \text{ inches } (213.36 \text{ cm}) \end{cases} \tag{4.3}$$

As for the depth of caulked lead, d_l, Prior[53] reported that it is typically equal to 2.25 inches (5.72 cm).

For the axial force at slippage, F_j^s, O'Rourke and Trautmann[55] proposed the following relationship:

$$F_j^s = C_a \cdot \pi D \cdot d_l \tag{4.4}$$

where C_a is the adhesive strength at the pipe/lead interface. After analysis of Prior's pull-out test results, O'Rourke and Trautmann[55] back-calculated the value of C_a. It was found that this value is quite variable and appears to be independent of the pipe diameter. The analysis yielded a mean value C_a = 252 psi (17.70 Kgf/cm^2) and a coefficient of variation μ_{C_a} = 32%.

In order to quantify the ultimate pull-out force, F_j^u, Prior's results are synthesized. It is found

that the ratio F_j^u/F_j^s has a mean value equal to 2.0 and a coefficient of variation equal to 34%. Hence, it is proposed that the mean value of F_j^u be given by:

$$F_j^u = 2 \cdot C_a \cdot \pi D \cdot d_l \tag{4.5}$$

The authors' analysis of Prior's results indicates that the joint tensile displacement at failure (displacement corresponding to significant leakage), u_j^u, is a function of the parameter d_p which represents the depth of the joint (see Figure 4-2). It should be mentioned that values of u_j^u have a poor correlation with the outside diameter of the pipe, D (correlation coefficient = 0.02). Using Prior's data, a cumulative distribution function $P[u_j^u/d_p]$ for the normalized joint axial displacement u_j^u/d_p is established. This cumulative distribution function is shown in Figure 4-5. The ratio u_j^u/d_p ranges roughly between 0.25 to 0.75 with a mean value equal to 0.52 and a coefficient of variation of 10%. That is, the mean value of u_j^u can be evaluated from:

$$u_j^u = 0.52\, d_p \tag{4.6}$$

in which the value of d_p is given by [52]:

$$d_p = \begin{cases} 4.0 \text{ inches (10.16 cm)} ; 8\ (20.32) \le D_n \le 24 \text{ inches (60.96 cm)} \\ 4.5 \text{ inches (11.43 cm)} ; 30\ (76.20) \le D_n \le 36 \text{ inches (91.44 cm)} \\ 5.0 \text{ inches (12.70 cm)} ; 42\ (106.68) \le D_n \le 48 \text{ inches (121.92 cm)} \\ 5.5 \text{ inch (13.97 cm)} ; 54\ (137.16) \le D_n \le 84 \text{ inches (213.36 cm)} \end{cases} \tag{4.7}$$

Note that since u_j^u corresponds to a joint displacement which leads to significant leakage, $P[u_j^u/d_p]$ represents also *the conditional cumulative distribution function* $P[\,| \, u_j/d_p]$ for the probability of leakage as a function of the normalized joint axial displacement u_j/d_p (i.e. $P[u_j^u/d_p] = P[\,| \, u_j/d_p]$). The slope of the (F_j,u_j) curve after slippage, $AK_j^{(2)}$, is a function of AK_j, F_j^s, F_j^u and u_j^u. Combining Eqns.(4.4) and (4.5), it can be shown that:

$$AK_j^{(2)} = \left(\frac{u_j^s}{u_j^u - u_j^s}\right) \cdot AK_j \tag{4.8}$$

No data is presently available to estimate the value of the axial compressive displacement at

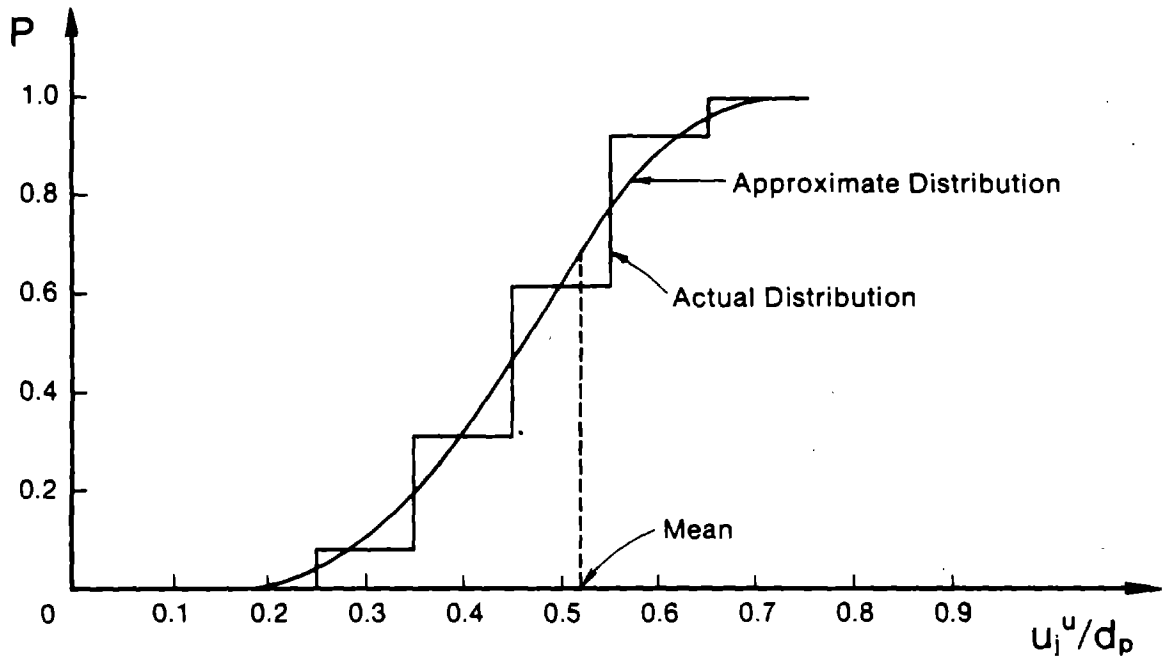

Figure 4-5. Cumulative Distribution Function for Leakage of Lead Caulked Joints

which contact between the two adjacent pipe segments occurs, u_j^c. This parameter represents the clearance before metal to metal contact takes place during axial compression. Values of u_j^c are expected to be quite variable and ranging between 3/32 and 5/32 inch (0.24 to 0.40 cm).

The axial stiffness after contact, $AK_j^{(3)}$, and the ultimate compressive force, F_j^c, depends mainly on the strength of cast iron, the geometry of the bell and the internal pressure. Experimental results are needed to evaluate these two parameters. Under compressive ground strain, the joint is locked in between the spigot and bell ends, and is expected to become very rigid. For the purpose of analysis, a very high value is assumed for the parameter $AK_j^{(3)}$. In order to study the crushing of the pipe segment bell mode failure, forces at the joint will be first converted into stresses at the bell and then compared to the compressive strength of cast iron.

4.2.2.2 Bending Moment/Rotation Relationship

Information on the bending behavior of lead caulked joints is limited to test results obtained by Prior[53] for a 20 inch (50.80 cm) diameter cast iron water pipe and test results obtained by Harris and O'Rourke[54] for 4, 6 and 8 inch (10.16, 15.24 and 20.32 cm) diameter cast iron gas pipes.

Prior[53] performed three deflection tests to investigate the strength of the bell in a 20 inch (50.80 cm) diameter cast iron water pipe. Results from these tests, however, can be used to study the relationship between the bending moment, M_j, and the corresponding rotation of the joint, θ_j. The diagram of the first two tests is shown in Figure 4-6(a), while that of the third test is shown in Figure 4-6(b). Prior measured the deflection of the joint, v_j, as a function of the applied load, Q. Graphs of Q versus v_j were presented for the three tests. Using statics and geometry, one can deduce the graphs of M_j versus θ_j. The bending moment for the first two tests [see Figure 4-6(a)] is given by:

$$M_j = \frac{Q}{2} \cdot a + W \cdot \frac{l_1 + l_2}{8} \tag{4.9}$$

in which a is the distance between the left support and the point of application of the load Q/2, W is the total weight of two pipe segments, and l_1 is the distance between the left support and the joint and l_2 is the distance between the right support and the joint.

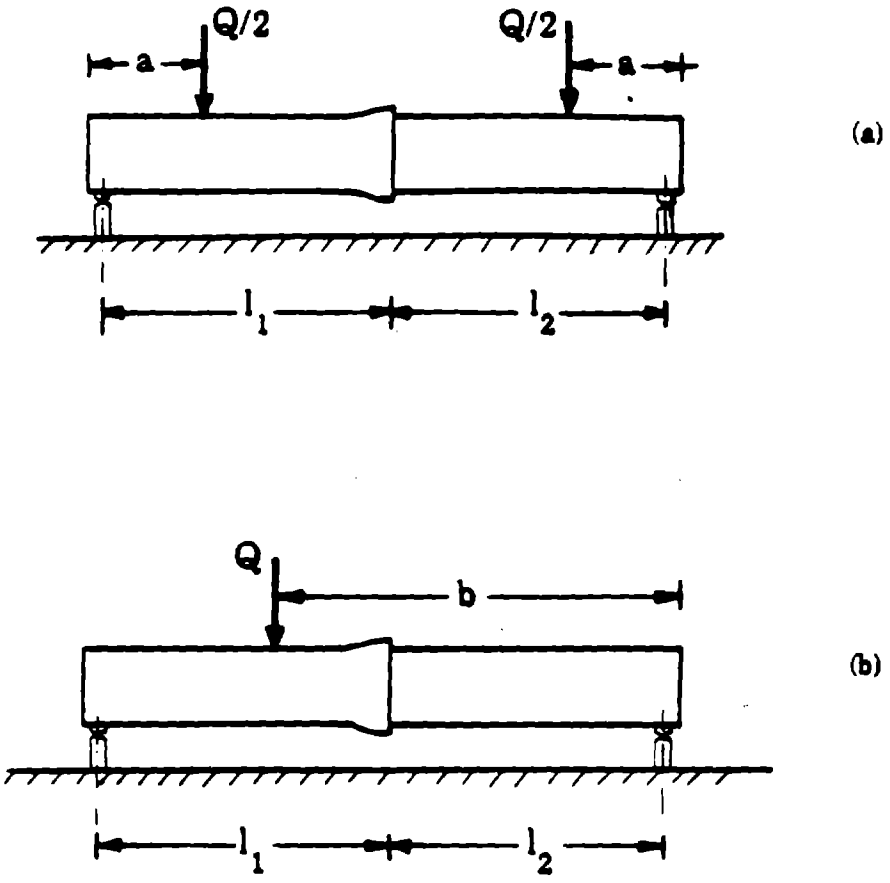

Figure 4-6. Diagram of Deflection Tests (after Prior [53])

For the third test [see Figure 4-6(b)], the bending moment is equal to:

$$M_j = Q \cdot \frac{b \cdot l_1}{l_1 + l_2} + W \cdot \frac{l_1 + l_2}{8} \tag{4.10}$$

in which b is the distance between the right support and the point of application of the load Q.
If one assumes that the flexural rigidity of the pipe segments is very large compared to that of the joint, it is easy to relate v_j to θ_j. The relation is given by:

$$\theta_j = v_j \cdot \left(\frac{1}{l_1} + \frac{1}{l_2}\right) \tag{4.11}$$

Figure 4-7 shows the (M_j, θ_j) curves obtained from Prior's test results.
Harris and O'Rourke[54], on the other hand, presented bending moment/rotation curves for 4, 6 and 8 inch (10.16, 15.24 and 20.32 cm) diameter cast iron gas pipes. They proposed a range of values for the initial rotational stiffness, RK_j, of each of the pipe diameters considered.
Based on the available test results [53,54], the relationship between the bending moment, M_j, and the corresponding rotation of the joint, θ_j, is approximated by a bilinear model. As shown in Figure 4-8, the bilinear model is characterized by an initial stiffness, RK_j, a rotation at slippage, θ_j^s, a second stiffness, $RK_j^{(2)}$, and an ultimate rotation, θ_j^u. Table 4-I presents the mean values and the coefficients of variation of the approximate bilinear model characteristics obtained from the test results.
Attempts to develop an analytical expression for the mean value of RK_j as a function of pipe diameter were unsuccessful. For this reason, a regression analysis on the available test results is performed. The resulting equation estimates RK_j as a function of the outside diameter, D. That is:

$$RK_j = 1405 \times 10^3 \, (D)^{1.37} \tag{4.12}$$

in which D is in inches and RK_j is in lb.inch/rad. If D is expressed in cm and RK_j in Kgf.cm/rad, Eqn.(4.12) becomes: $RK_j = 451.40 \times 10^3 \, (D)^{1.37}$. Figure 4-9 is a graph of the measured initial rotational stiffness against the predicted value by Eqn.(4.12). The correlation coefficient between the measured and the predicted values is equal to 0.88. Table 4-II compares the experimental mean values of RK_j with those obtained by Eqn.(4.12). The percent error is between 15 and 36%.

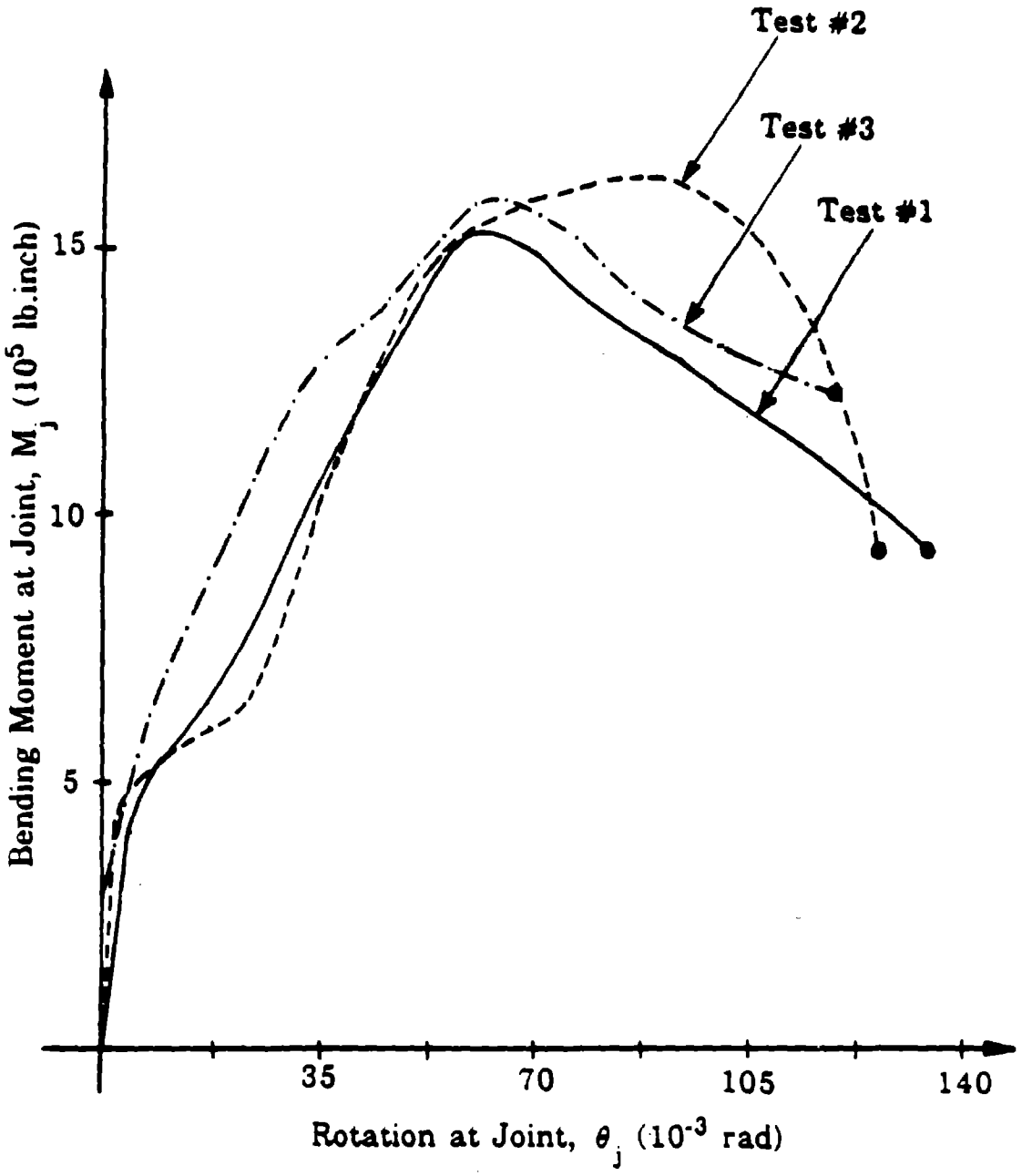

Figure 4-7. Bending Moment/Rotation Curves Obtained from Prior's Test Results

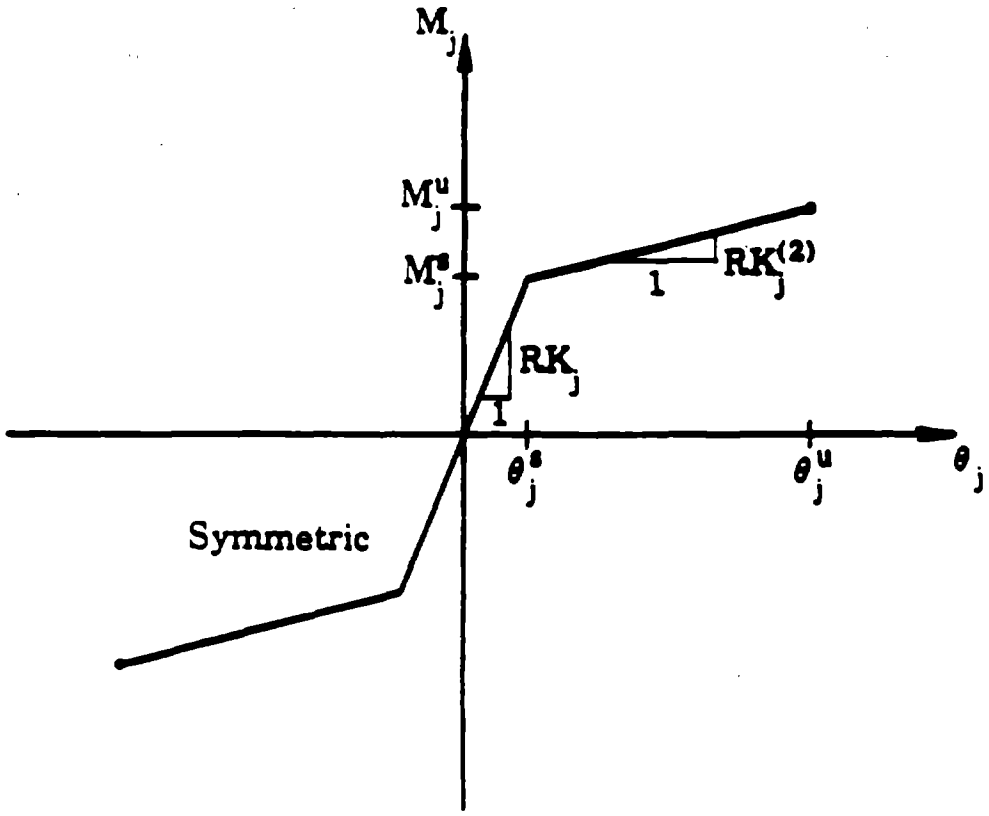

Figure 4-8. Bending Moment/Rotation Curve for Lead Caulked Joints or for Rubber Gasketed Joints

Table 4-I

Experimental Values of the Bending Moment/Rotation Curve Characteristics for Lead Caulked Joints

D_n	D	RK_j		θ_j^s	
		Mean Value	Coef. Var.	Mean Value	Coef. Var.
inch(cm)	inch(cm)	lb.inch/rad (kgf.cm/rad)	%	rad	%
4 (10.16)	4.80 (12.19)	1.463×10^7 (1.685×10^7)	62	4.40×10^{-3}	46
6 (15.24)	6.86 (17.42)	2.650×10^7 (3.053×10^7)	40	3.50×10^{-3}	75
8 (20.32)	8.90 (22.61)	1.700×10^7 (1.958×10^7)	31	11.70×10^{-3}	30
20 (50.80)	22.10 (56.13)	11.540×10^7 (13.300×10^7)	32	4.90×10^{-3}	53

D_n	$RK_j/RK_j^{(2)}$		θ_j^u	
	Mean Value	Coef. Var.	Mean Value	Coef. Var.
inch(cm)		%	rad	%
4 (10.16)	4.40	62	15.00×10^{-3}	20
6 (15.24)	9.70	146	22.80×10^{-3}	61
8 (20.32)	5.40	54	39.30×10^{-3}	25
20 (50.80)	7.20	66	69.70×10^{-3}	26

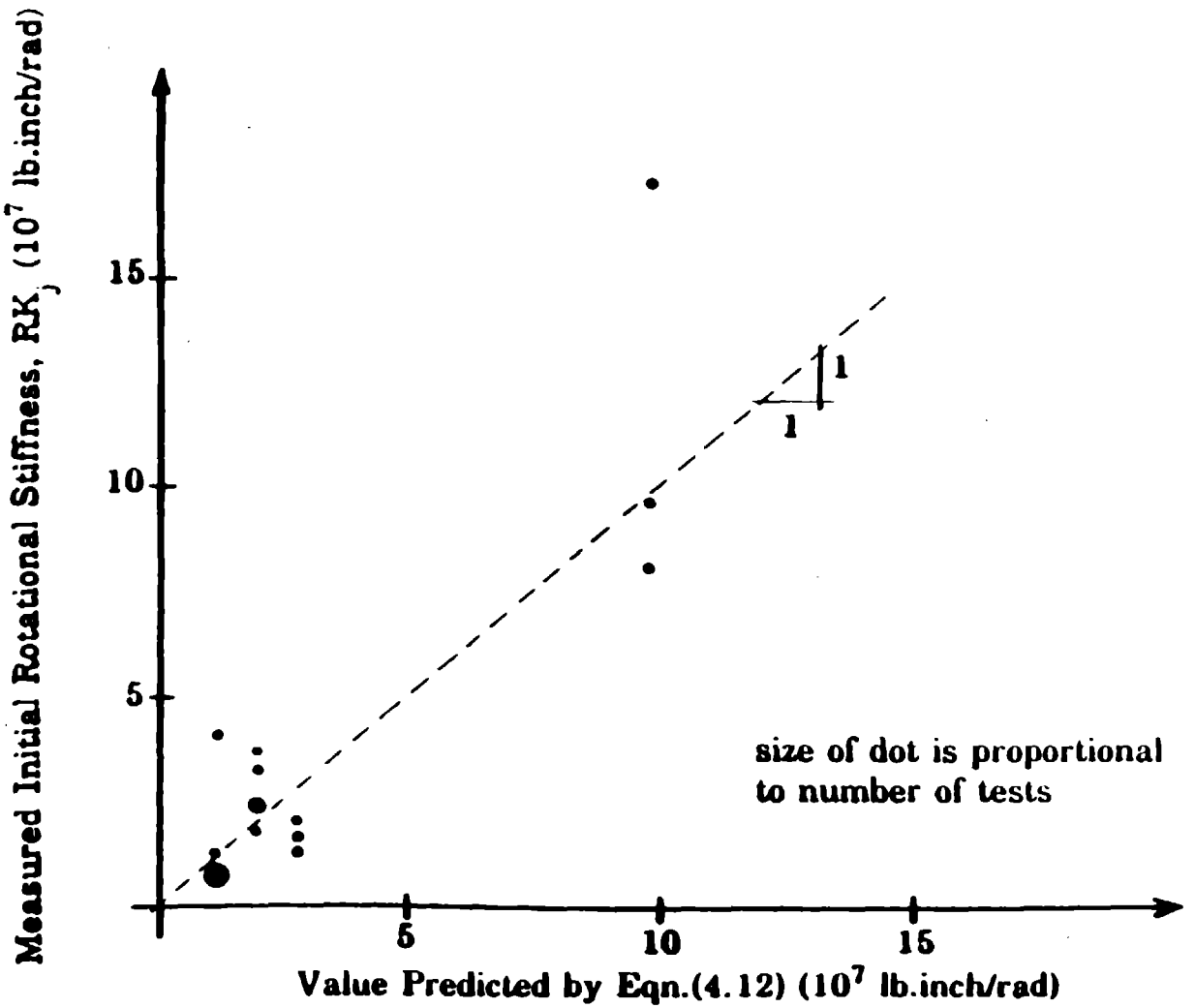

Figure 4-9. Measured Initial Rotational Stiffness, RK_j, versus Value Predicted by Eqn.(4.12)

Values of the rotation at slippage, θ_j^s, are poorly correlated with the pipe diameter (correlation coefficient = 0.08). The mean value of θ_j^s for each pipe diameter varies between 3.50×10^{-3} and 11.70×10^{-3} rad. It is proposed, herein, that the mean value of θ_j^s be approximated by the global mean value calculated for all pipe diameters. This global mean value is equal to: $\theta_j^s = 5.50\times10^{-3}$ rad.

The ratio $RK_j/RK_j^{(2)}$ has a global mean value equal to 6.60. It is poorly correlated with the outside diameter, D (correlation coefficient = 0.06). In this study, the parameter $RK_j^{(2)}$ is estimated by:

$$RK_j^{(2)} = \frac{RK_j}{6.60} \tag{4.13}$$

In order to evaluate the ultimate rotation, θ_j^u, a regression equation as a function of the pipe outside diameter, D, is proposed. This equation is given by:

$$\theta_j^u = 2.90\times10^{-3} (D)^{1.044} \tag{4.14}$$

in which D is in inches and θ_j^u is in radians. If D is expressed in cm, the equation becomes: $\theta_j^u = 1.10\times10^{-3} (D)^{1.044}$. The correlation coefficient of this regression equation is equal to 0.82.

4.3 Ductile Iron Pipes with Rubber Gasketed Joints

4.3.1 Pipe Segment Properties

Ductile iron can be defined as cast iron with primary graphite in the nodular or spheroidal form. This material was invented in 1948 and it was quickly recognized as an excellent piping material. It is as durable as cast iron and has a higher strength. Moreover, it has the capacity to withstand significant plastic deformations. Ductile iron pipes are used to transport water, sewage, gas and other industrial materials.

The stress/strain relationship of ductile iron has a well defined yield point. The value of Young's modulus, E_p, is equal to 24×10^6 psi (1.7×10^6 Kgf/cm^2). Ductile iron is graded by minimum mechanical properties. Grade 60-42-10 is the grade most commonly used in the manufacturing of pipes. It has a minimum tensile strength of 60×10^3 psi (4.2×10^3 Kgf/cm^2), a minimum tensile yield strength of 42×10^3 psi (3.0×10^3 Kgf/cm^2) and a minimum ultimate elongation of 10%. In compression, the behavior of ductile iron is slightly different. Grade 60-42-10 has a compressive

Table 4-II

Comparision of Mean Initial Rotational Stiffness of Lead Caulked Joints RK_j and Value Given by Eqn.(4.12)

D_n inch(cm)	Mean Measured RK_j lb.inch/rad (Kgf.cm/rad)	RK_j by Eqn.(4.12) lb.inch/rad (Kgf.cm/rad)	Percent Error %
4 (10.16)	1.463×10^7 (1.685×10^7)	1.205×10^7 (1.388×10^7)	18
6 (15.24)	2.650×10^7 (3.053×10^7)	1.965×10^7 (2.263×10^7)	26
8 (20.32)	1.700×10^7 (1.958×10^7)	2.808×10^7 (3.236×10^7)	36
20 (50.80)	11.540×10^7 (13.300×10^7)	9.761×10^7 (11.245×10^7)	15

yield strength equal to 52×10^3 psi (3.7×10^3 Kgf/cm^2) [48].

In this study, a bilinear model is adopted for the relationship between the stress, σ, and the strain, ϵ, in ductile iron material. This model is shown in dashed line in Figure 4-10. The solid line, on the same figure, represents the actual (σ,ϵ) curve [56]. The bilinear model is characterized by Young's modulus, E_p, the tensile yield strength, σ^y, the tensile strength, σ^u, the ultimate elongation, ϵ^u and the compressive yield strength, σ^{yc}. Values of these characteristics are given in Table 4-III.

Note that the slope of the (σ,ϵ) curve for compression stresses higher in magnitude than σ^{yc} is assumed to be equal to the slope for tensile stresses larger than σ^y. The ratio between the value of this slope, termed $E_p^{(2)}$, and the Young's modulus E_p is approximately equal to 7.6×10^{-3} [or $E_p^{(2)} = 1.83\times10^5$ psi (0.13×10^5 Kgf/cm^2)]. Hence, the stress/strain relationship for Grade 60-42-10 ductile iron is approximated by the following equations:

$$\sigma = \begin{cases} -\sigma^{yc} + E_p^{(2)}\cdot(\epsilon + 2.17\times10^{-3}) & ;\ \epsilon < -2.17\times10^{-3} \\ E_p\cdot\epsilon & ;\ -2.17\times10^{-3} \le \epsilon \le 1.75\times10^{-3} \\ \sigma^y + E_p^{(2)}\cdot(\epsilon - 1.75\times10^{-3}) & ;\ \epsilon > 1.75\times10^{-3} \end{cases} \qquad (4.15)$$

Because of its ductility, ductile iron pipe is considered a flexible structure. Hence, it is designed according to flexible-pipe principles which are controlled by two load combinations. The first load combination considers the earth and the traffic loads, while the second considers the working pressure and pressure surge [57]. As with cast iron pipes, dimensions of ductile iron pipes are taken in this study from "Handbook of Ductile Iron Pipe" [52]. The pipe segment length, L, is typically equal to 20 feet (6 m). Values of the pipe outside diameter, D, and wall thickness, t, are chosen as a function of the depth of cover, c, laying conditions and working pressure. As mentioned previously, the range of values usually chosen for the depth of cover, c, is discussed in section 5.2.1.

4.3.2 Joint Properties

Rubber gasketed joints are effective in providing a leakproof and flexible connection for jointed buried pipelines. In addition to ductile iron pipes, this type of joint is also used with concrete and asbestos-cement pipes. The information presented herein, however, is mainly for rubber gasketed joints with ductile iron pipes.

Rubber gaskets have roughly the shape of a doughnut. In cross-section, the gasket consists of a circular "main body", and a smaller and stiffer trapezoidal "outer body". A typical gasket

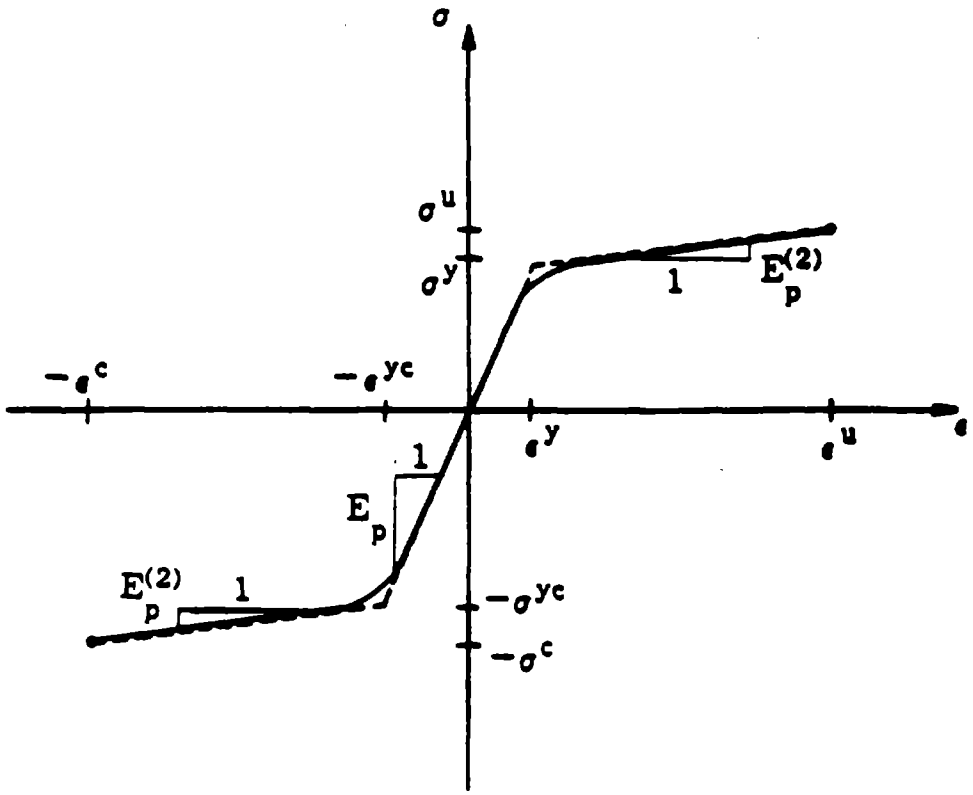

Figure 4-10. Stress/Strain Curve for Ductile Iron

Table 4-III

Stress/Strain Curve Characteristics of Ductile Iron

Characteristic	Value
E_p psi (Kgf/cm²)	24×10^6 (1.7×10^6)
σ^y psi (Kgf/cm²)	42×10^3 (3.0×10^3)
σ^u psi (Kgf/cm²)	60×10^3 (4.2×10^3)
ϵ^u %	10
σ^{yc} psi (Kgf/cm²)	52×10^3 (3.7×10^3)

cross-section is shown in Figure 4-11, while the dimensions for gaskets used in 4, 6, 8 and 10 inch (10.16, 15.24, 20.32 and 25.40 cm) diameter ductile iron pipes are presented in Table 4-IV. During installation, the gasket's circular main body is compressed between the outer surface of the male end of a pipe segment and the inner surface of the female end of the adjacent pipe segment. The rubber gasket before and after installation is shown in Figure 4-12, while the dimensions of the annular space available for the rubber gasket are listed in Table 4-V for 4, 6, 8 and 10 inch (10.16, 15.24, 20.32 and 25.40 cm) diameter ductile iron pipes. As shown in Figure 4-12, the trapezoidal outer body fits in a groove in the female end which prevents movement of the gasket in the longitudinal direction.

Information about the mechanical behavior of rubber gasketed joints is presently limited to results from laboratory tests on small diameter pipes. Singhal[58] performed tests on the pull-out (tension) and bending of rubber gasketed joints for 4, 6, 8 and 10 inch (10.16, 15.24, 20.32 and 25.40 cm) diameter ductile iron pipes. No test data are presently available for larger diameter rubber gasketed joints. In the course of his investigation, Singhal determined some mechanical properties of the vulcanized rubber used in this type of joint. He found that the main body of the gasket has a Poisson's ratio ν_r of 0.5. The stress/strain relationship for the main body of the gasket is nonlinear. However, Young's modulus in tension is essentially constant up to strains on the order of 50%. Singhal found this low strain modulus of elasticity, E_r, to be about 370 psi (26.0 Kgf/cm^2). This value is in general agreement with data published by Lindley[59] for vulcanized rubber with a hardness, IRHD (International Rubber Hardness Degrees) of about 50 to 55. Finally, Singhal determined that the coefficient of friction between a soaped rubber gasket and ductile iron, μ_r was about equal to 0.1. Note that, during installation the rubber gasket is usually soaped for ease of installation.

Based on Singhal's test results, the characteristics of the axial force/displacement and bending moment/rotation relationships are determined. Analytical or empirical expressions are developed for the mean value of each of these characteristics. In addition, estimates of their variability about these mean values are given.

4.3.2.1 Axial Force/Displacement Relationship

The resistance to axial movement at a rubber gasketed joint is provided by friction between the compressed main body of the rubber gasket and the male end of the pipe. Results from Singhal's tests on the pull-out behavior of rubber gasketed joints indicate that the force/displacement is linear up to an ultimate pull-out force, F_j^u. At that point, the pipe segments begin to separate under a constant applied force. That is, the behavior in tension can be modeled as elasto-plastic.

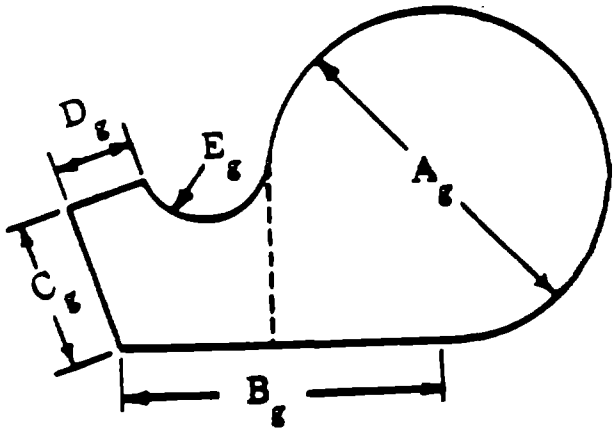

Figure 4-11. Cross-Sectional Geometry of Rubber Gasket before Installation

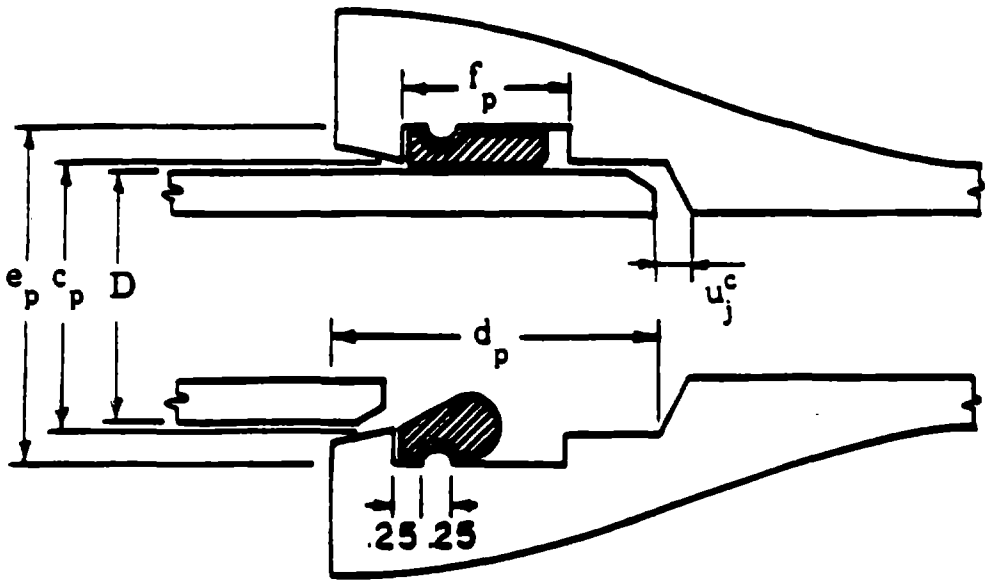

Figure 4-12. Rubber Gasketed Joint before and after Installation

Table 4-IV

Cross-Sectional Geometry of Rubber Gasket

D_n inch(cm)	A_g inch(cm)	B_g inch(cm)	C_g inch(cm)	D_g inch(cm)	E_g inch(cm)
4 (10.16)	0.60 (1.52)	0.71 (1.80)	0.35 (0.89)	0.20 (0.51)	0.13 (0.33)
6 (15.24)	0.60 (1.52)	0.71 (1.80)	0.35 (0.89)	0.20 (0.51)	0.13 (0.33)
8 (20.32)	0.72 (1.83)	0.79 (2.00)	0.39 (1.00)	0.26 (0.66)	0.17 (0.43)
10 (25.40)	0.72 (1.83)	0.98 (2.45)	0.39 (1.00)	0.26 (0.66)	0.17 (0.43)

Table 4-V

Cross-Sectional Geometry of Rubber Gasketed Joint

D_n inch(cm)	D inch(cm)	c_p inch(cm)	d_p inch(cm)	e_p inch(cm)	f_p inch(cm)
4 (10.16)	4.80 (12.20)	4.91 (12.47)	3.15 (8.00)	5.64 (14.33)	1.36 (3.45)
6 (15.24)	6.90 (17.53)	7.10 (17.80)	3.38 (8.58)	7.74 (19.66)	1.36 (3.45)
8 (20.32)	9.05 (23.00)	9.17 (23.30)	3.69 (9.37)	9.98 (25.35)	1.76 (4.47)
10 (25.40)	11.10 (28.20)	11.22 (28.50)	3.75 (9.52)	12.03 (30.56)	1.96 (4.98)

No test results on the push-in (compression) behavior of the joint are available. However, this push-in behavior is likely to be similar to the pull-out behavior except that, when contact between the two adjacent pipe segments occurs, the joint becomes very rigid and behaves as if it was not present and the pipe was continuous. Figure 4-13 illustrates the model adopted for the axial force/displacement for the rubber gasketed joint. The axial force at the joint is denoted by F_j, while the corresponding axial displacement is denoted by u_j. If one assumes that the joint does not reach failure, only four parameters are needed to define this model. They are the ultimate pull-out force, F_j^u, the initial axial stiffness, AK_j, the axial compressive displacement when contact between the two adjacent pipe segments occurs, u_j^c, and the axial stiffness after contact, $AK_j^{(3)}$. The failure parameters which include the ultimate axial tensile displacement, u_j^u, and the ultimate compressive axial force, F_j^c are not presently well defined.

Singhal performed a number of tests for each pipe diameter. He found that the ultimate pull-out force, F_j^u, as well as the axial stiffness, AK_j, varied substantially from test to test. Mean values as well as coefficients of variation for F_j^u and AK_j, as obtained by Singhal and Benavides[60] and Singhal[58], are presented in Table 4-VI. Note that, both F_j^u and AK_j increase with increasing pipe diameter as one might expect intuitively. However, for any particular diameter, there is a poor correlation between experimental values for F_j^u and AK_j. This suggests that for a particular diameter, F_j^u and AK_j are statistically independent.

Singhal[58] presented an analytical expression for the ultimate pull-out force:

$$F_j^u = \frac{5}{24}\,\pi^2 \cdot \mu_r \cdot E_r \cdot A_g \cdot D \cdot \left[\frac{A_g - 0.5(e_p - D)}{e_p - D}\right] \tag{4.16}$$

where μ_r is the coefficient of friction between the rubber gasket and the pipe taken equal to 0.1, E_r is Young's modulus of rubber taken equal to 370 psi (26.0 Kgf/cm^2), A_g is the initial diameter of the gasket's main body which varies with pipe diameter as shown in Table 4-IV, D is the outside pipe diameter as given in Table 4-IV and $(e_p - D)$ quantifies the space occupied by the main body of the rubber gasket after installation.

As will be shown in more details later, Eqn.(4.16) matches reasonably well the mean of laboratory test values for 4 and 6 inch (10.16 and 15.26 cm) diameter pipes. However, for 8 and 10 inch (20.32 and 25.40 cm) diameter pipes, Eqn.(4.16) underestimate the mean value of F_j^u from laboratory tests. Hence, the applicability of Singhal's relationship for F_j^u to pipes of interest, that is, pipes with diameter larger than 12 inches (30.48 cm), is questionable.

If one knows the pressure p_i (force per unit length) between the rubber gasket and the male end of the pipe, the ultimate pull-out force is given by:

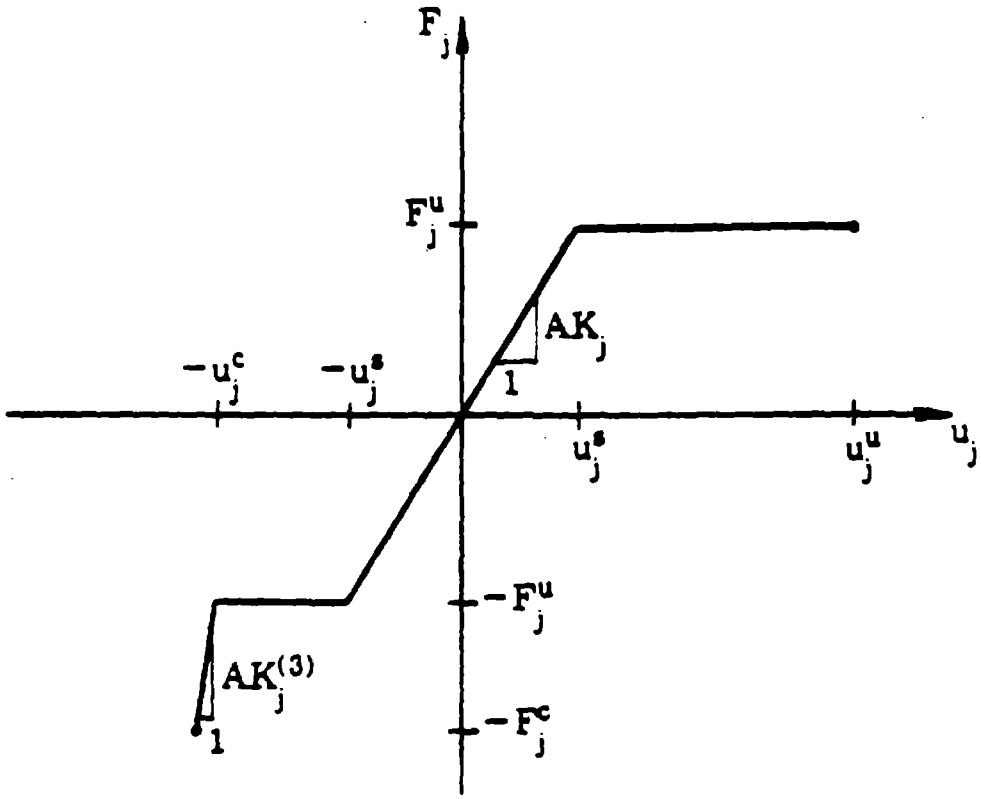

Figure 4-13. Axial Force/Displacement Curve for Rubber Gasketed Joints

Table 4-VI

Experimental Values of the Axial Force/Displacement Curve Characteristics for Rubber Gasketed Joints

D_n	F_j^u		AK_j	
inch(cm)	Mean Value lb(Kgf)	Coef. Var. %	Mean Value lb/inch(Kgf/cm)	Coef. Var. %
4 (10.16)	34 (15.40)	71	515 (92.20)	38
6 (15.24)	69 (31.30)	22	782 (139.70)	50
8 (20.32)	333 (151.20)	19	1558 (278.30)	16
10 (25.40)	386 (175.10)	24	2370 (423.10)	46

$$F_j^u = \mu_r \cdot p_i \cdot \pi D \tag{4.17}$$

where πD represents the outer circumference of the pipe.

Installation of the male end of a pipe segment into the female end of the adjoining segment results in deformation of the main body of the rubber gasket. Because of clearances, the trapezoidal body of the rubber gasket remains essentially undeformed. The presence of the bell at the female end of the pipe prevents the outer circumference of the doughnut shaped gasket from moving. When the male end is inserted, the inner circumference of the doughnut is forced to expand. This imposed deformation results in hoop tension in a ring whose diameter is approximately D, as well as compression across the diameter of the circular main body whose original diameter is A_g. That is, insertion of the male end results in a normal pressure, p_i (force per unit length), between the gasket and the male pipe end. This pressure is balanced by hoop tension as well as a normal pressure, p_o (force per unit length), between the gasket and the female pipe end. In other words, p_i acts at the inner circumference of the gasket, while p_o acts at the outer circumference of the gasket.

Determination of the normal pressure p_i and hence, the ultimate pull-out force by Eqn.(4.17), is complicated by the fact that the force deformation relationship for compression is nonlinear. That is, some of the imposed deformation is due to Poisson's ratio in conjunction with hoop tension, while the remaining imposed deformation results from compression across the diameter A_g due to pressure p_o. However, the force/deformation for p_o involves geometric nonlinearity.

Consider a solid rubber cylinder compressed across its diameter between two rigid plates as sketched in Figure 4-14. When the compressive force is low, the area of contact between the cylinder and the two plates is small, and the stiffness is low. At higher loads and as the plates move towards each other, the contact area becomes larger and the stiffness increases. Hence, the stiffness increases with load due to geometric nonlinearity.

In order to determine the relative contribution of hoop tension and compression across the diagonal, a thick elastic ring with a square cross-section is considered. The outer circumference is restrained from movement and the inner circumference has a specified displacement due to insertion of the male pipe, that is:

$$u_r^{outer} = 0$$

$$u_r^{inner} = X = A_g - \frac{e_p - D}{2} \tag{4.18}$$

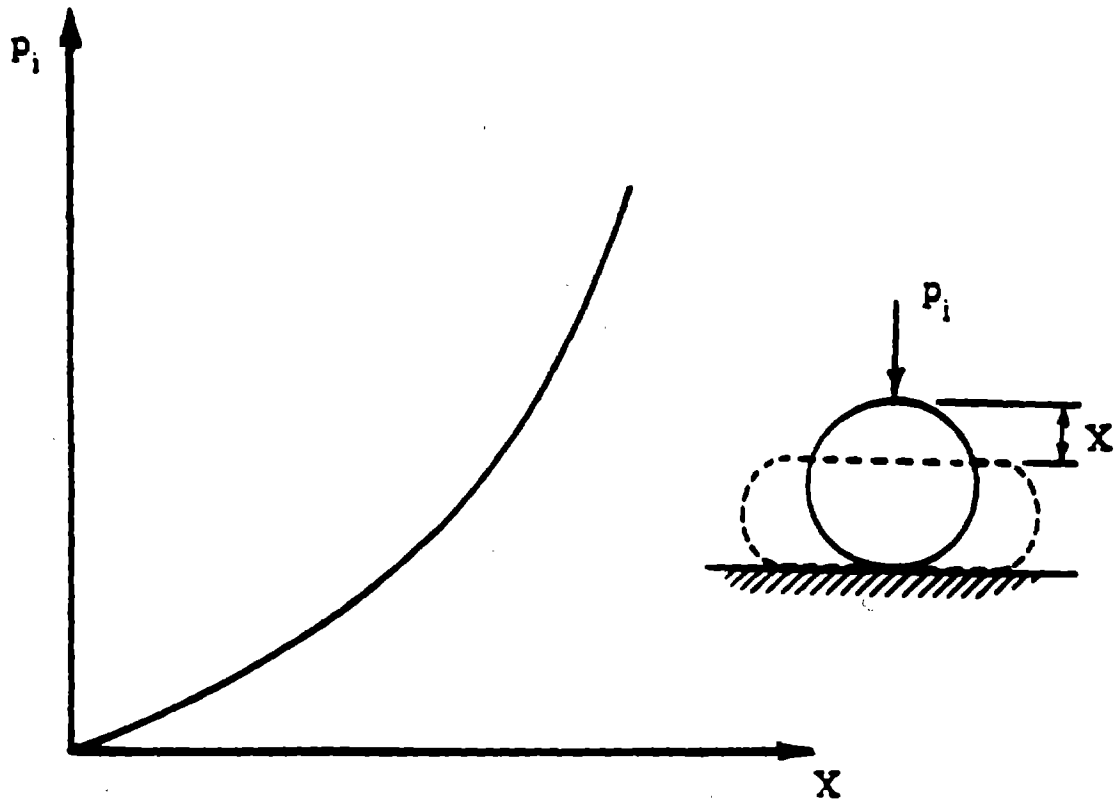

Figure 4-14. Pressure/Deformation Relationship for a Solid Rubber Cylinder

where u_r represents the displacement of the ring along the line of action of the pressures p_i and p_o.

Using the elasticity solution for a thick elastic ring given in Boresi at al.[61], the ratio p_i/p_o becomes:

$$\frac{p_i}{p_o} = \frac{1}{2}\left[(1 - \nu_r)\left(\frac{e_p}{e_p - 2A_g}\right)^2 + (1 + \nu_r)\right] \tag{4.19}$$

The ratio p_i/p_o is presented in Table 4-VII for 4, 6, 8 and 10 inch (10.16, 15.24, 20.32 and 25.40 cm) rubber gasketed ductile iron pipes. Note that the ratios are slightly larger than unity and that they approach unity as the diameter increases. This suggests that the imposed deformation is mainly due to compression across the original diameter A_g, and as a first approximation the hoop tension may be neglected.

Hence, it is proposed herein that the pressure p_i (force per unit length) be taken as that required to cause a compression deformation $X = [A_g - (e_p - D)/2]$, across a solid cylinder with original diameter A_g. Note that values of the rubber gasket relative deformation, X/A_g, for the 4, 6, 8 and 10 inch range between 30 and 35%. The solution for p_i is available in Lindley[59]. It is given by:

$$p_i = E_r \cdot A_g \cdot \left[1.25\left(\frac{X}{A_g}\right)^{1.5} + 50.0\left(\frac{X}{A_g}\right)^6\right] \tag{4.20}$$

Hence, it is proposed herein that the ultimate pull-out force, F_j^u, for rubber gasketed ductile iron joints be calculated using Eqns.(4.17) and (4.20). Results obtained using the proposed method are compared to laboratory test data in Table 4-VIII.

Note that the percent error between the predicted value [i.e. Eqns.(4.17) and (4.20)] and the mean experimental value decreases with increasing diameter. This is likely due to the fact that the hoop tension, which is neglected in the proposed relationship, becomes less important as the nominal pipe diameter increases.

As mentioned previously, for any particular nominal pipe diameter, there was a significant amount of scatter in measured values for F_j^u. Figures 4-15, 4-16, 4-17 and 4-18 are histograms for measured F_j^u values. Also shown in these figures are, Singhal's empirical relationship [i.e. Eqn.(4.16)] as well as the proposed analytical relationship [i.e. Eqns.(4.17) and (4.20)].

Note that for the 4 and 6 inch (10.16 and 15.24 cm) nominal diameters, Singhal's relationship [i.e. Eqn.(4.16)] predicts F_j^u values which are reasonably accurate while the proposed relationship

Table 4-VII

Ratio of Pressures at Inner and Outer Circumference

D_n inch(cm)	p_i/p_o
4 (10.16)	1.15
6 (15.24)	1.10
8 (20.32)	1.09
10 (25.40)	1.07

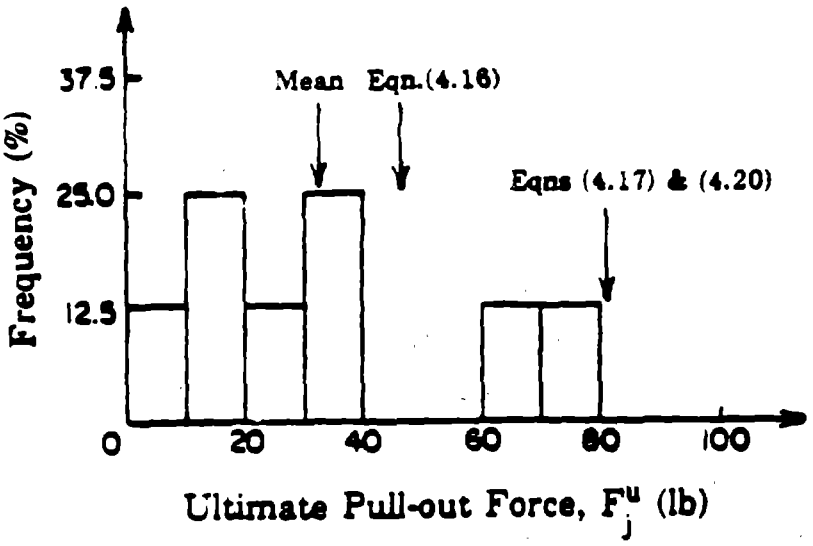

Figure 4-15. Histogram of Measured Ultimate Pull-Out Force F_j^u for Rubber Gasketed Joints in 4 inch (10.16 cm) Nominal Diameter Ductile Iron Pipes

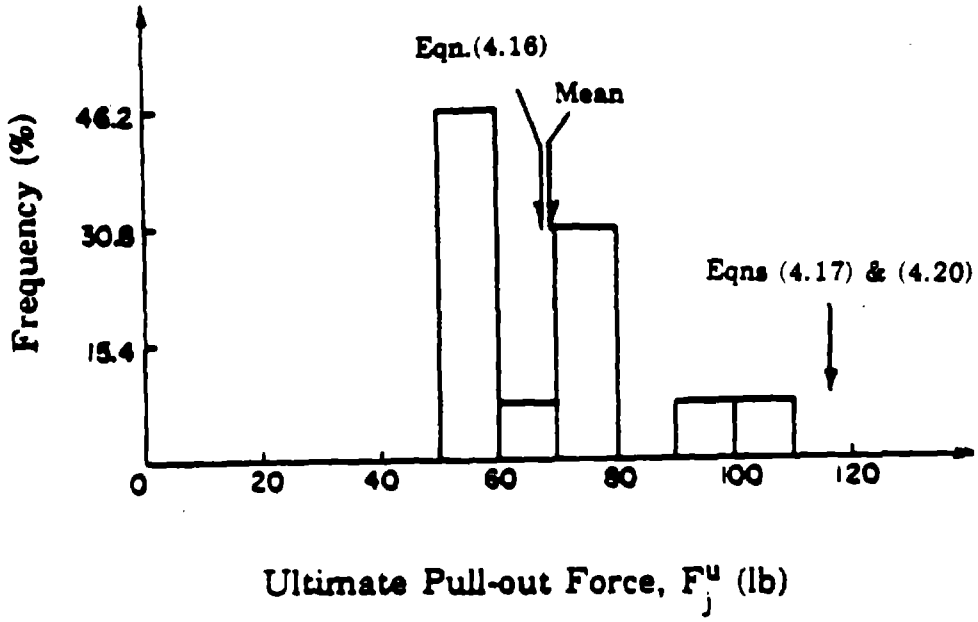

Figure 4-16. Histogram of Measured Ultimate Pull-Out Force F_j^u for Rubber Gasketed Joints in 6 inch (15.24 cm) Nominal Diameter Ductile Iron Pipes

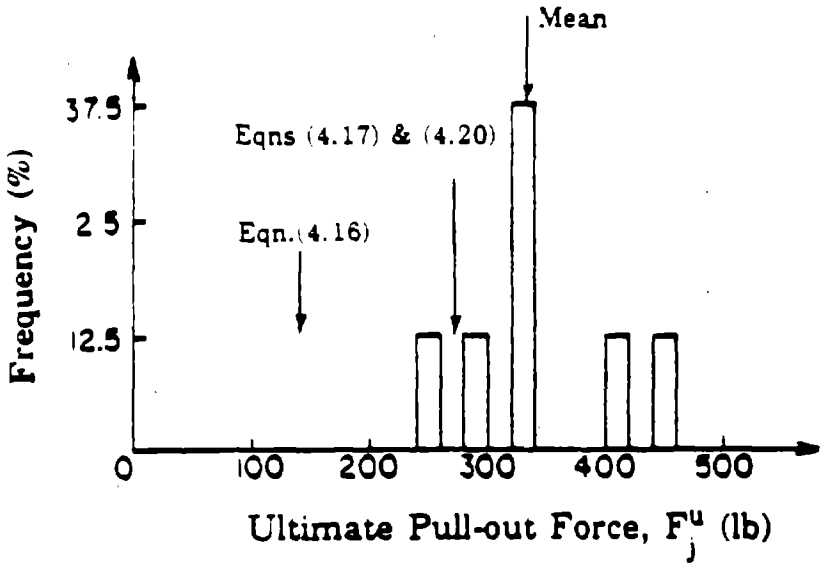

Figure 4-17. Histogram of Measured Ultimate Pull-Out Force F_j^u for Rubber Gasketed Joints in 8 inch (20.32 cm) Nominal Diameter Ductile Iron Pipes

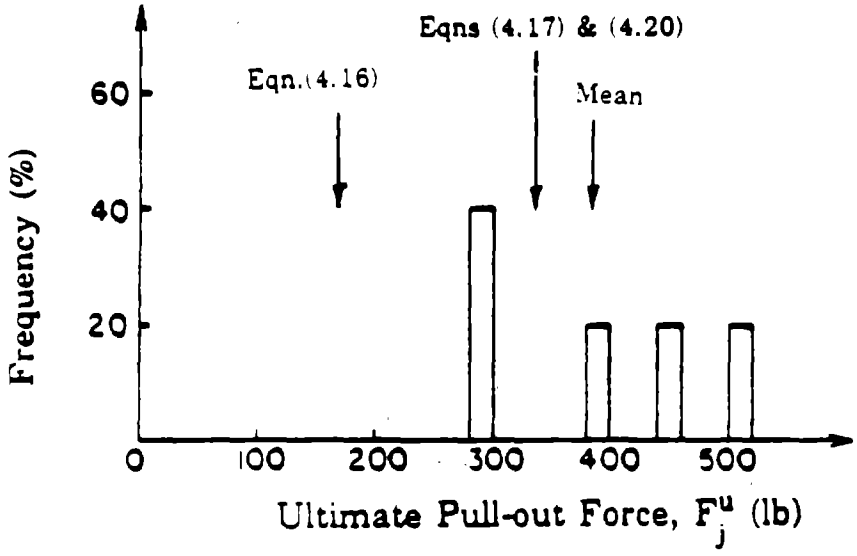

Figure 4-18. Histogram of Measured Ultimate Pull-Out Force F_j^u for Rubber Gasketed Joints in 10 inch (25.40 cm) Nominal Diameter Ductile Iron Pipes

[i.e. Eqns.(4.17) and (4.20)] yield high values. However, for the 8 and 10 inch (20.32 and 25.40 cm) nominal diameters, the proposed method is reasonably close to the mean of the measured values. For these larger diameters, Singhal's relationship yields low values. Since the proposed method neglects the hoop tension and the hoop tension becomes less important for larger diameters (see Table 4-VII), it is expected that this method [i.e. Eqns.(4.17) and (4.20)] will provide reasonable estimates of the ultimate pull-out force for large diameter pipes (12 inch (30.48 cm) nominal diameter and above).

Singhal's test results are also used herein to estimate the initial axial stiffness, AK_j. As with lead caulked joints, it was first assumed that axial forces are initially resisted by elastic shear forces in the rubber gasket. Values of AK_j obtained by this model were much larger than the experimental values. This is due in part to the fact that the shear stiffness of rubber drops significantly under compression. In the literature, this is referred to as "shape" effects. Because of this difficulty, a regression analysis is applied to Singhal's results and an empirical relationship for AK_j as a function of the pipe outside diameter, D, is developed. This relationship is given by:

$$AK_j = 22.4 \, (D)^{1.88} \tag{4.21}$$

where D is in inches and AK_j is in lb/inch. If D is expressed in cm and AK_j in Kgf/cm, Eqn.(4.21) becomes: $AK_j = 0.70 \, (D)^{1.88}$.

Values predicted by Eqn.(4.21) and measured mean values of AK_j are compared in Table 4-IX. The percent error between these two values ranges between 8 and 17%. Note that the correlation coefficient between predicted and measured values of AK_j is found to be equal to 0.84. It is proposed herein that Eqn.(4.21) be used to predict the mean value of AK_j for pipes with nominal diameter D_n larger or equal to 12 inches (30.50 cm).

As mentioned previously, the parameter u_j^c represents the clearance before metal to metal contact takes place between adjacent pipe segments during axial compression. The mean value of u_j^c will be taken equal to 0.3 in (0.76 cm) as suggested by Singhal[58]. Singhal reported also that u_j^u is of the order of 1.2 inches (3.05 cm). However, it is expected that values of u_j^u be higher for large diameter pipes.

As with lead caulked joints, no data is presently available on the axial stiffness after contact, $AK_j^{(3)}$, or on the ultimate compressive force, F_j^c. After contact between the adjacent pipe segments occurs, the joint becomes very rigid. Hence, during the analysis of pipelines under compressive strain, a very high value is assumed for the parameter, $AK_j^{(3)}$. The obtained

Table 4-VIII

Comparision of Mean Ultimate Pull-Out Force for Rubber Gasketed Joints F_j^u and Value Given by Eqns (4.17) & (4.20)

D_n inch(cm)	Mean Measured F_j^u lb(Kgf)	F_j^u by Eqns.(4.17) & (4.20) lb(Kgf)
4 (10.16)	34 (15.20)	81 (36.75)
6 (15.24)	69 (31.30)	118 (53.50)
8 (20.32)	333 (151.20)	274 (124.30)
10 (25.40)	386 (175.10)	336(152.40)

Table 4-IX

Comparision of Mean Initial Axial Stiffness AK_j and Value Given by Eqn.(4.21)

D_n inch(cm)	Mean Measured AK_j lb/inch(Kgf/cm)	AK_j by Eqn.(4.21) lb/inch(Kgf/cm)	Percent Error %
4 (10.16)	515 (92.20)	427 (76.25)	17
6 (15.24)	782 (139.70)	846 (151.05)	8
8 (20.32)	1558 (278.30)	1408 (251.50)	10
10 (25.40)	2370 (423.10)	2068 (369.25)	13

compressive forces at the joints can be converted into stresses at the bell and compared to the compressive strength of ductile iron.

4.3.2.2 Bending Moment/Rotation Relationship

Test results on the bending behavior of rubber gasketed joints are available for 4, 6, 8 and 10 inch (10.16, 15.24, 20.32 and 25.40 cm) diameter ductile iron pipes [58]. These results are analysed and used herein to characterize the bending moment/rotation relationship for larger diameter pipes. Singhal's test results show that the relationship between the bending moment, M_j, and the corresponding rotation of the joint, θ_j can be represented by a bilinear model similar to that proposed for lead caulked joints (see Figure 4-8). The (M_j,θ_j) curve has an initial straight line whose slope is identified as the initial rotational stiffness, RK_j. This line continues up to the point of coordinates (M_j^s,θ_j^s). Beyond this point, the (M_j,θ_j) curve has a smaller slope denoted by $RK_j^{(2)}$. The joint becomes very rigid when metal-to-metal contact between the two adjacent pipe segments occurs. Table 4-X gives the mean values as well as the coefficients of variation for the initial rotational stiffness, RK_j, the rotation at slippage, θ_j^s, and the ratio between the initial and the second rotational stiffnesses, $RK_j/RK_j^{(2)}$, as obtained by Singhal and Benavides[60] and Singhal[58]. The value of the ultimate joint rotation, θ_j^u, was found to be approximately equal to 7×10^{-2} rad, for the different diameters considered.

Singhal and Cheng[62] presented an analytical expression for the initial rotational stiffnesss, RK_j. In developing this expression, it is assumed that the applied bending moment is balanced by shear forces in the rubber gasket main body, and that no slippage occurs between the rubber gasket and the pipe. This expression is given by:

$$RK_j = \frac{\pi^2 G_r \cdot D^3 \cdot A_g^2}{8 (e_p - D)^2} \qquad (4.22)$$

in which G_r is the shear modulus of rubber. In Table 4-XI, the experimental mean values of RK_j and those predicted by Eqn.(4.22) are compared. Note that the percent error between these two values ranges between 2 and 38%. Eqn.(4.22) is used herein to estimate the mean value of RK_j.

Analysis of the values obtained by Singhal for the joint rotation at slippage, θ_j^s, shows that this parameter is poorly correlated with the pipe diameter (correlation coefficient = 0.36). The average of all values obtained for the different pipe diameters, is equal to 5.1×10^{-3} rad and the coefficient of variation is equal to 37%.

Values of the ratio $RK_j/RK_j^{(2)}$ are poorly correlated with the pipe diameter (coefficient of correlation = 0.05). The mean value of this ratio for each pipe diameters ranges between 4.90

Table 4-X

Experimental Values of the Bending Moment/Rotation Curve Characteristics for Rubber Gasketed Joints

D_n	RK_j		θ_j^s		$RK_j/RK_j^{(2)}$	
	Mean Value	Coef. Var.	Mean Value	Coef. Var.	Mean Value	Coef. Var.
inch(cm)	lb.inch/rad (kgf.cm/rad)	%	rad	%		%
4 (10.16)	0.134×10^5 (0.154×10^5)	25	4.90×10^{-3}	19	4.90	42
6 (15.24)	0.305×10^5 (0.351×10^5)	40	4.70×10^{-3}	22	7.80	64
8 (20.32)	1.081×10^5 (1.245×10^5)	31	3.70×10^{-3}	8	7.0	35
10 (25.40)	1.223×10^5 (1.409×10^5)	32	7.60×10^{-3}	32	5.40	41

Table 4-XI

Comparision of Mean Initial Rotational Stiffness RK_j and Value Given by Eqn.(4.22)

D_n	Mean Measured RK_j	RK_j by Eqn.(4.22)	Percent Error
inch(cm)	lb.inch/rad (Kgf.cm/rad)	lb.inch/rad (Kgf.cm/rad)	%
4 (10.16)	0.134×10^5 (0.154×10^5)	0.086×10^5 (0.093×10^5)	36
6 (15.24)	0.305×10^5 (0.351×10^5)	0.254×10^5 (0.293×10^5)	16
8 (20.32)	1.081×10^5 (1.245×10^5)	0.674×10^5 (0.776×10^5)	38
10 (25.40)	1.223×10^5 (1.409×10^5)	1.244×10^5 (1.433×10^5)	2

and 7.80 with a global mean value equal to 6.30. It is proposed herein that $RK_j^{(2)}$ be evaluated as a function of RK_j by:

$$RK_j^{(2)} = \frac{RK_j}{6.30} \tag{4.23}$$

4.4 Selection of Pipeline Properties

4.4.1 Selection of Pipe Segment Properties

First, the stress/strain relationships established in sections 4.2.1 and 4.3.1, are used to characterize the mechanical behavior of the pipe segment material. The dimensions of the cross-section which include the outside diameter, D, and the wall thickness, t, are then obtained from standard tables [52]. Values of D and t correspond to a working pressure ranging between 200 and 250 psi (14.10 and 17.60 Kgf/cm^2). The laying condition for cast iron pipes is a Standard B (pipe laid on flat bottom trench, backfill not tamped). For ductile iron pipes, the laying condition is a Type 3 (pipe bedded in 4 inch minimum loose soil, backfill lightly consolidated to top of pipe). The depth of cover, c, is estimated according to section 5.2.1. As mentioned before, the length of a pipe segment, L, is typically equal to 20 feet (6 m).

The cross-sectional area, A, and the transverse moment of inertia, I, are needed to estimate the axial and bending stiffnesses of the pipe segments. They can be determined from the following equations:

$$A = \frac{\pi [D^2 - (D-2\,t)^2]}{4} \tag{4.24}$$

$$I = \frac{\pi [D^4 - (D-2\,t)^4]}{64} \tag{4.25}$$

4.4.2 Selection of Joint Properties

The joint characteristics for the two pipeline systems considered, show a relatively high variability. Since wave propagation damage to jointed pielines occurs often at the joints, this variability is important and needs to be accounted for properly. These joint characteristics are assumed to vary randomly from one joint to another, along the pipeline model. They are selected according to the procedure outlined below.

The Rayleigh density function is proposed to approximate the probability density function of each

of the parameters representing the axial force/displacement relationship (i.e. F_j^s, u_j^s, u_j^c and u_j^u) as well as each of the parameters representing the bending moment/rotation relationship (i.e. M_j^s, θ_j^s, θ_j^s and $RK_j/RK_j^{(2)}$). For simplicity, the eight parameters defining these two relationships are assumed to be independent. Appendix A presents the Rayleigh probability density function and show how it can be used in conjunction with a random number generator. A set of eight random numbers is generated for each joint along the pipeline model. Each random number is then used to back-calculate one of the parameters defining the (F_j,u_j) and the (M_j,θ_j) relationships.

The procedure outlined above also can be used in the case where the joint properties are assumed to be deterministic but vary along the pipeline model. First, the joint dimensions are evaluated for each joint along the pipeline. Following, the axial force/displacement and the bending moment/rotation relationships are characterized also for each joint along the pipeline model.

5. SOIL PROPERTIES

5.1 Introduction

The response of a buried pipeline to seismic waves is controlled by differential movements along its length. Since the pipeline is totally surrounded by soil, soil/pipeline interaction is an important factor in determining the pipeline response to these seismic waves. The soil properties of interest in this study are those related to the resistance provided by the soil to axial as well as lateral movements of the pipeline.

The soil/pipeline interaction is usually represented by nonlinear springs distributed along the pipeline, as shown in Figure 5-1. Figure 5-2(a) shows the axial force per unit length versus the relative axial displacement, while Figure 5-2(b) shows the lateral force per unit length versus the relative lateral displacement. The axial and lateral forces per unit length transmitted between the soil and pipeline are denoted respectively by f_x and f_z. The corresponding relative displacements are denoted by Δu and Δw.

The American Society of Civil Engineers (ASCE) Committee on Gas and Liquid Fuel Lifelines[63] suggests the use of elasto-plastic or hyperbolic models for the (f_x, Δu) and (f_z, Δw) relationships. For simplicity and numerical purposes, the elasto-plastic model which is equivalent to using spring-sliders, is adopted herein. Characteristics of these spring-sliders are determined after review, synthesis and integration of the existing literature.

The soil properties involved in the definition of the spring-slider characteristics are assumed to be random variables. This is done to model their inherent variability and recognize the fact that they vary somewhat along the pipeline. In the next two sections, ranges for the soil properties, and relationships for the axial and lateral soil restraints characteristics are given. The third section presents the procedure used to select the soil properties in this study.

It should be mentioned that the results presented herein, apply to the typical case where the pipeline is placed in a trench and backfilled with cohesionless soil.

5.2 Axial Restraint Component

The axial movement of the pipeline is restrained by friction-like forces at the soil/pipeline interface. Tests performed by Colton et al.[64] on a full-scale pipe indicate that the axial force/displacement relationship is linear at small displacements. The soil resistant force reaches a "plateau" when slippage of the pipe with respect to the soil occurs. This is illustrated in Figure 5-2(a), which shows in solid line, the relationship between the axial force per unit length at the soil/pipeline interface, f_x, and the relative axial displacement between the soil and the pipeline, Δu. The dashed line represents the elasto-plastic model used to approximate the (f_x, Δu)

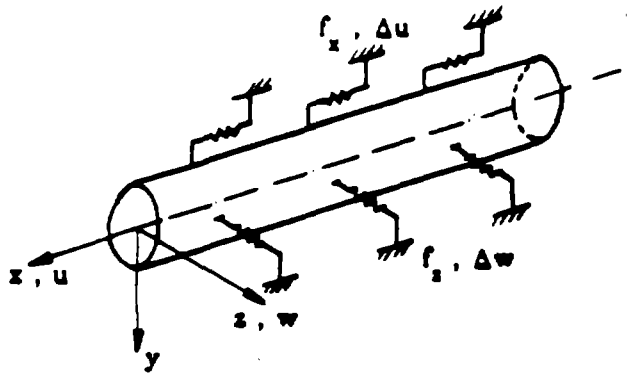

Figure 5-1. Soil/Pipeline Interaction Model

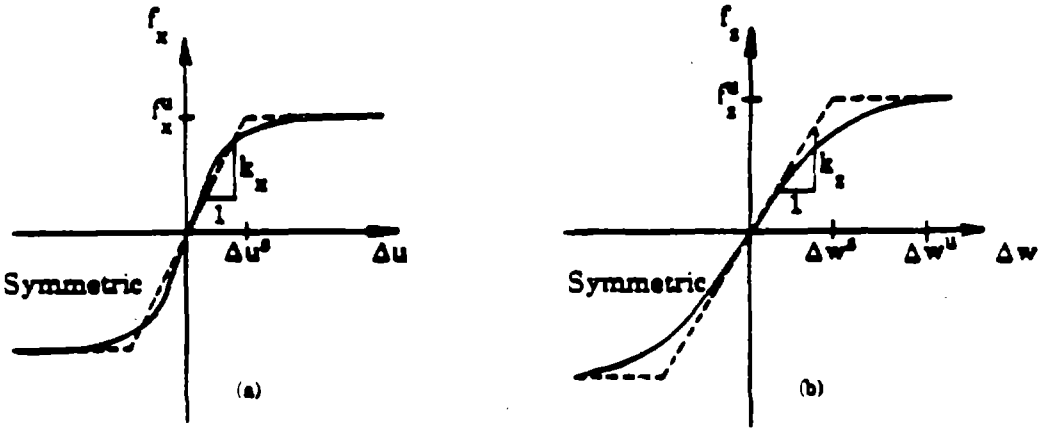

Figure 5-2. Force per Unit Length/Displacement Curve for the (a)Axial and (b)Lateral Soil Springs

curve.

The elasto-plastic model adopted for the axial soil springs is fully defined by two parameters. The first one is the ultimate axial force per unit length at the soil/pipeline interface, f_x^u, and the second is the initial axial stiffness, k_x. In the next subsections, these two parameters are determined.

5.2.1 Ultimate Axial Force per Unit Length

For the case where the pipeline trench is backfilled with cohesionless soil, the ultimate force per unit length at the soil/pipeline interface, f_x^u, is simply the coefficient of friction times the product of the average of the vertical and the horizontal pressure on the pipeline, that is:

$$f_x^u = \mu_s \cdot \gamma H \cdot \frac{(1 + K_o)}{2} \cdot \pi D \tag{5.1}$$

where μ_s is the coefficient of friction at or near the soil/pipeline interface, γ is the unit weight of the soil, H is the depth to the pipe centerline, K_o is the coefficient of lateral earthpressure and $\dot{D}$ is the outside diameter of the pipe.

Experimental studies have shown that the coefficient of friction between the soil and the pipeline, μ_s, depends mainly on the nature of the pipe surface, the angularity of the soil grains and the relative roughness of the pipe surface with respect to the soil grains. Results obtained by Kulhawy and Peterson[65] show that for rough concrete pipe surfaces, slippage occurs in the soil near the interface and that the coefficient of friction, $\mu_s \simeq \tan\phi$, where ϕ is the angle of shearing resistance of the soil. For the case of concrete pipes with smooth surfaces, slippage occurs at the interface with $\mu_s/\tan\phi$ ranging from 0.8 to 1.0, with a mean value of 0.9 ($\mu_s \simeq 0.9 \tan\phi$). Colton et al.[64] noticed that for pipes wrapped with plastic covering, slippage happens in the soil near the pipe rather than, at the interface. The reason is that the soil grains become partially embedded in the plastic cover at the interface. Brumund and Leonards[66] also observed that $\tan\phi$ is an upper bound for μ_s, regardless of the rate at which slippage is initiated. Two types of surfaces were studied: Mortar/Sand and Polished Steel/Sand. The results for the first surface were similar to Kulhawy and Peterson's results for concrete surfaces. For the Polished Steel surface, the mean value of μ_s is equal to $0.5 \tan\phi$.

Based on these experimental results, mean values for μ_s, for different pipe materials, can be determined from the following equations:

$$\mu_s = \begin{cases} \tan\phi & \text{Concrete pipes with rough surface and Steel, Cast iron or Ductile iron pipes with plastic covering} \\ 0.9\tan\phi & \text{Concrete pipes with smooth surface and Steel, Cast iron or Ductile iron normal pipes} \\ 0.5\tan\phi & \text{Steel, Cast iron or Ductile iron polished pipes} \end{cases} \quad (5.2)$$

The value of γ, for cohesionless soils, ranges between about 110 and 140 pcf (1.75×10^{-3} to 2.25×10^{-3} Kgf/cm^3). It is mainly a function of the level of compactness, particle size distribution and moisture content of the soil [67].

The depth to the pipe centerline, H, is equal to the sum of the depth of earth cover, c, and half the outside diameter of the pipe, that is: H = c + D/2. The earth cover serves as a cushion to absorb shocks due to live loads. It is, however, limited by the capacity of the pipe to support the earth load. It is recommended that the value of c range between 4 and 5 feet (1.22 and 1.53 m) for large diameter ductile iron pipes [$D_n \geq 30$ inches (76.20 cm)], and between 2.5 and 4 feet (0.76 and 1.22 m) for smaller diameter pipes. The value of c is much larger in areas of severe frost conditions. In the northern states, it is of the order of 8 feet (2.44 m) [68].

The magnitude of K_o for normally consolidated cohesionless soil has been reported to range from 0.35 to 0.47 [69]. However, because of the backfilling and compaction of the soil around the pipeline, one expects K_o to be somewhat larger. O'Rourke et al.[7] recommend that K_o = 1.0, as a conservative estimate under most conditions of pipeline burial. It is proposed herein, that K_o ranges between 0.5 to 1.5.

5.2.2 Initial Axial Stiffness

The technical literature contains a number of relations for the initial axial stiffness, k_x. For the plane strain case, Novak et al.[70] presented the initial axial stiffness as a function of frequency with values ranging from about 1.50 to 2.75 times the soil shear modulus, G_s ($1.50\ G_s \leq k_x \leq 2.75\ G_s$). O'Leary and Datta[71] calculated k_x at low frequency to be about two times G_s. In their comparision of the observed behavior of a tunnel with a multiple mass-spring model, Shibata et al.[72] have used $k_x = G_s$. In a Japanese design procedure for buried pipelines, Kuboto Ltd.[73] suggests a value of $k_x = 3.0\ G_s$. Based upon analytical studies of piles, O'Rourke and Wang[74] used $k_x = 2.0\ G_s$.

A full-scale experiment on buried pipes was performed by Colton et al.[64] to study the axial soil/pipe interaction. Results from this experiment, are used herein to back-calculate the value of

the initial axial stiffness per unit length of pipe, k_x, as well as the ratio $\alpha = k_x/G_s$. A schematic diagram of the experimental setup is shown in Figure 5-3. It consists of three 12 inch (30.5 cm) nominal diameter steel pipes buried end-to-end in a trench backfilled with sand. The middle pipe is the test pipe, and the two others serve to simulate the end conditions in the field. A low frequency axial force, P, was applied at the right end of the test pipe by a hydraulic actuator located in a pit adjacent to the trench. A displacement gage was placed at the same end to measure the axial displacement. Colton et al. performed both small and large displacement tests. The large displacement test resulted in slippage (i.e. $\Delta u > \Delta u^s$) over a portion of the specimen. Since the axial soil stiffness before slippage is of interest, only results from the small displacement test are used herein.

The pipes used had an outside diameter, D = 12.75 inches (32.40 cm), a wall thickness, t = 0.25 inch (0.64 cm), and a depth to the centerline of the pipes, H = 33.40 inches (84.85 cm). The test pipe had a length, L = 15 feet (4.57 m). The backfill properties are a unit weight, γ = 110 pcf (1.75×10^{-3} Kgf/cm^3) and a void ratio, e = 0.60.

Figure 5-4 shows the axial force/displacement curve obtained for the small displacement test. Note that the response of the soil/pipe system is nearly linear with system stiffness, K_{sy} (the ratio of the force at the pipe end to the corresponding pipe displacement) equaling about 630×10^3 lb/inch (135×10^3 Kgf/cm). The pipe inertia force per unit length for the test considered was more than two orders of magnitude lower than the soil restoring force per unit length. Hence, the pseudo-static model shown in Figure 5-5 is appropriate for back-calculating the soil stiffness per unit length, k_x. For the no-slip condition, the governing differential equation for the pipe axial displacement, u(x), is:

$$\frac{d^2u(x)}{dx^2} - \beta^2 u(x) = 0 \qquad (5.3)$$

where $\beta^2 = k_x/(E_p \cdot A)$, E_p is Young's modulus [$E_p = 30\times10^6$ psi (2.1×10^6 Kgf/cm^2)] and A is the cross-sectional area of the pipe.

The boundary conditions for the test are:

$$\frac{du(0)}{dx} = 0$$

$$\frac{du(L)}{dx} = \frac{P}{E_p \cdot A} \qquad (5.4)$$

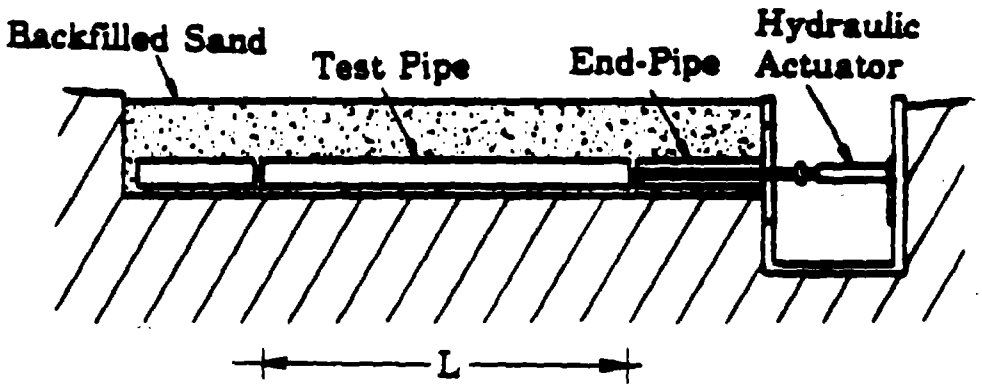

Figure 5-3. Schematic Diagram of Experimental Setup (after Colton et al.[64])

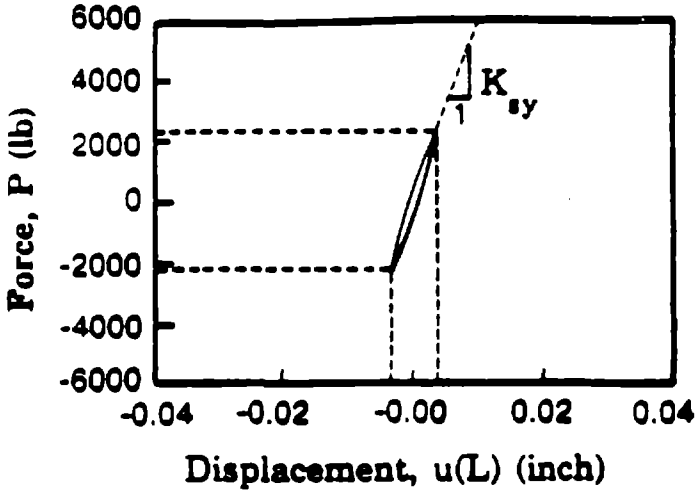

Figure 5-4. Axial Force/Displacement at End of Pipe (after Colton et al.[64])

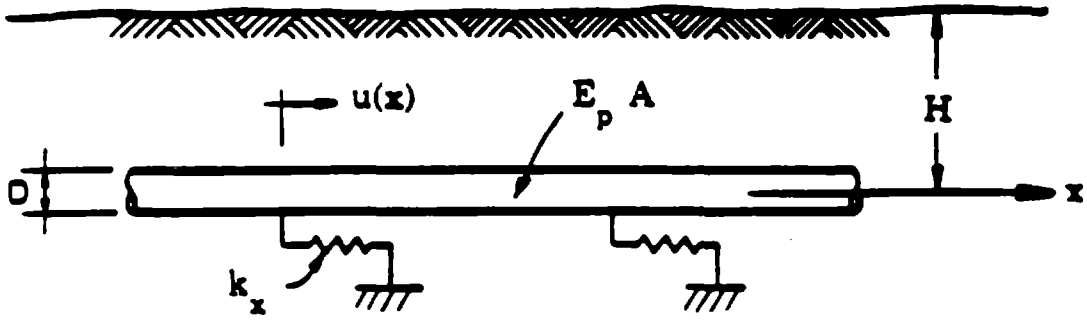

Figure 5-5. Pseudo-Static Model of Buried Pipe and Soil

The solution for the pipe displacement is:

$$u(x) = \frac{P}{\beta \cdot E_p \cdot A} \cdot \frac{\cosh(\beta x)}{\sinh(\beta L)} \tag{5.5}$$

and the system stiffness (ratio of end force to end displacement) is:

$$K_{sy} = \frac{P}{u(L)} = \beta \cdot E_p \cdot A \cdot \tanh(\beta L) \tag{5.6}$$

Knowing the system stiffness, K_{sy}, (i.e. $K_{sy} \simeq 630 \times 10^3$ lb/inch), the axial soil stiffness per unit length of pipe, k_x, can be obtained after back-calculation of the coefficient β. This procedure yields: k_x = 3980 psi (280 Kgf/cm²).

In order to estimate the ratio, $\alpha = k_x/G_s$, a value for the soil shear modulus, G_s, is needed. Seed and Idriss[75] propose the following empirical relationship for G_s:

$$G_s = 1000\, K_2 \sqrt{\gamma H \cdot \frac{(1 + 2\, K_o)}{3}} \tag{5.7}$$

where K_o is the coefficient of lateral earthpressure as defined in the previous section and K_2 is a coefficient which depends upon the relative density of the soil, D_r, and the soil shear strain, Γ_s, as shown in Figure 5-6. Note that, in this empirical relationship, γ is in pcf, H is in feet and G_s is in psf. If γ, H and G_s are expressed respectively in Kgf/cm³, cm and Kgf/cm², Eqn.(5.7) becomes: $G_s = 22.10\, K_2 \sqrt{\gamma H \cdot (1 + 2\, K_o)/3}$.

To determine the soil shear strain, Γ_s, a pipe buried in an infinite elastic medium is considered. If one assumes longitudinal soil displacements which decrease exponentially with distance from the pipe, Wang et al.[15] has shown that the soil shear strain at the soil/pipeline interface is:

$$\Gamma_s(x) \simeq \frac{\Delta u(x)}{D/2} \tag{5.8}$$

The value of Γ_s used in evaluating K_2 for Eqn.(5.7), is taken to be the average of shear strains at both ends of the pipe, that is:

$$\Gamma_s = \frac{\Gamma_s(0) + \Gamma_s(L)}{2} \simeq 5.25 \times 10^{-2}\% \tag{5.9}$$

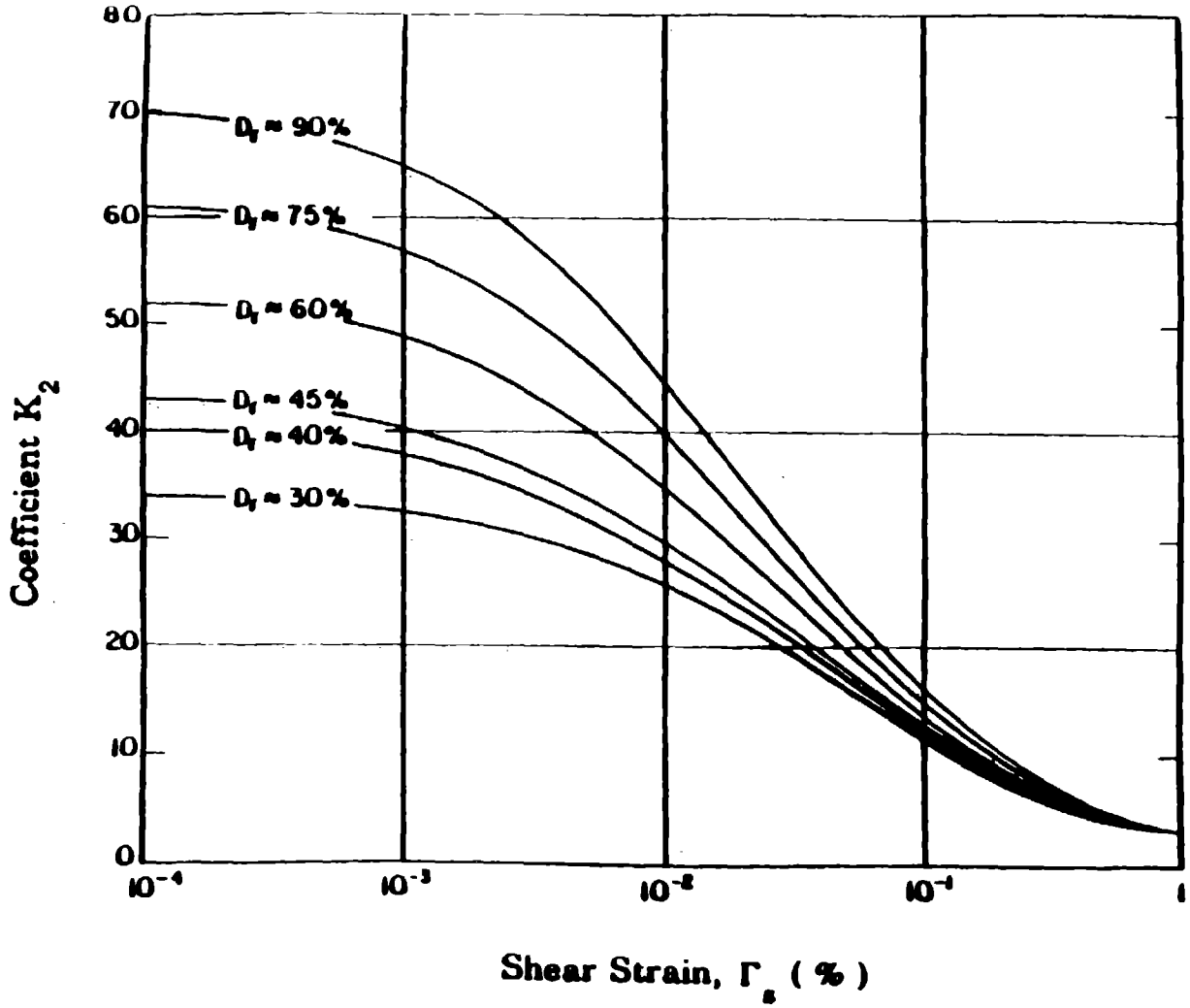

Figure 5-6. Shear Modulus Coefficient for Sands at Different Relative Densities (after Seed and Idriss 1970)

For Colton et al.'s test, the relative density of the backfill, D_r is about 55%, and K_o is expected to be in the range of 0.7 to 0.9 since the backfill was compacted. Using these values in conjunction with the shear strain, $\Gamma_s = 5.25 \times 10^{-2}\%$, and H = 33.40 inches, Eqn (5.7) yields a shear modulus G_s ranging from about 2350 to 2540 psi (165 to 179 Kgf/cm^2). Hence, the ratio a for the tests by Colton et al. ranges from 1.57 to 1.70 ($1.57 \leq a \leq 1.70$). This result falls in the general range of values for k_x, which have previously appeared in the literature. Moreover, it highlights the importance of accounting for the level of shear strain when evaluating G_s. Hence, it appears that the relationship: $k_x = a.G_s$, is appropriate, with values of a ranging between 1.0 and 3.0 ($1.0 \leq a \leq 3.0$). In this study, the coefficient a is taken equal to 2.0, that is:

$$k_x \simeq 2.0\, G_s \tag{5.10}$$

The specific value of Γ_s used to evaluate G_s and then, estimate k_x by Eqn.(5.10), corresponds to a value of the axial relative displacement at which the slope of the (f_x, Δu) curve starts decreasing appreciably. This relative axial displacement is denoted by $\overline{\Delta u}$ and the corresponding soil shear strain is denoted by $\overline{\Gamma_s}$. That is, $\overline{\Gamma_s} = 2\,\overline{\Delta u}/D$. Values of $\overline{\Delta u}$ are inferred from tests on soil/pile interaction performed by Holloway[76]. In these tests, $\overline{\Delta u}$ ranges between 0.01 and 0.04 inch (0.025 and 0.1 cm). Lower values of $\overline{\Delta u}$ correspond to denser soils with higher overburden pressure and vice versa.

5.3 Lateral Restraint Component

The soil resistance to lateral pipeline movements is needed to model the flexural behavior of the pipeline. This resistance is analogous to that offered to laterally loaded vertical anchor plates, piles, or foundation footings. First, available test results on the lateral soil restraint, are synthesized. On the basis of these results, an approximate elasto-plastic model is proposed.

5.3.1 Test Results Synthesis

Tests of pipes embedded in sand by Audibert and Nyman[77], indicate that the relationship between the lateral force per unit length, f_z, and the corresponding relative displacement between the soil and pipeline, Δw, can be represented by a hyperbolic function. This hyperbolic function is given in terms of two parameters, which are, the ultimate lateral force per unit length, f_z^u, and the corresponding ultimate relative lateral displacement, Δw^u. A model originally developed for rigid piles by Hansen[81], is used to estimate f_z^u. A range for Δw^u as a function of the sand density, is also given.

An independent series of tests on dry sand by Trautmann and O'Rourke[78] yield a force/displacement relationship which is quite similar to that obtained by Audibert and Nyman[77]. However, the parameter f_z^u is determined using a different model based on the soil resistance to laterally loaded vertical anchor plates [79,80]. Values of f_z^u predicted by this latter model, are about half those obtained using the model proposed by Hansen[81]. The range of values obtained for Δw^u, is higher than that found by Audibet and Nyman[77].

Based on these two studies, it has been shown that the relationship between f_z and Δw can be approximated by the following hyperbolic function:

$$f_z = \frac{\Delta w}{0.15\ \Delta w^u + 0.85\ \Delta w} \cdot f_z^u \qquad (5.11)$$

This function is plotted as a solid line, in Figure 5-2(b).

The ASCE Committee on Gas and Liquid Fuel Lifelines[63] recommends the following ranges for the ultimate relative lateral displacement:

$$\Delta w^u = \begin{cases} (0.07 \text{ to } 0.10)\ H_e & ; \text{for loose sand} \\ (0.03 \text{ to } 0.05)\ H_e & ; \text{for medium sand} \\ (0.02 \text{ to } 0.03)\ H_e & ; \text{for dense sand} \end{cases} \qquad (5.12)$$

where H_e is the depth of embedment as shown in Figure 2-1 ($H_e = H + D/2$).

The ultimate lateral force per unit length, f_z^u, on the other hand, can be expressed as:

$$f_z^u = \gamma H \cdot D \cdot N_{qh} \qquad (5.13)$$

where N_{qh} is the horizontal bearing capacity coefficient of the soil.

The analytical model proposed by Ovesen[79] to estimate the value of N_{qh}, agrees with the experimental results obtained by Trautmann and O'Rourke[78]. Moreover, Thomas[82] has noticed that Hansen's model[81] is not accurate for large diameter pipes. Based on the model of Ovesen[79], Figure 5-7 gives values of N_{qh} as a function of the ratio H/D for angle of shearing resistance, ϕ, between 30° and 45°. Figure 5-7 is applicable to dry or saturated sands and gravels, and to partially saturated gravels and coarse sands. For partially saturated medium to fine sands, Tawfic and O'Rourke[18] recommends that the value of N_{qh} be taken higher than that given in Figure 5-7, by a factor of 1.5 to 2.0. The reason is that short term loading

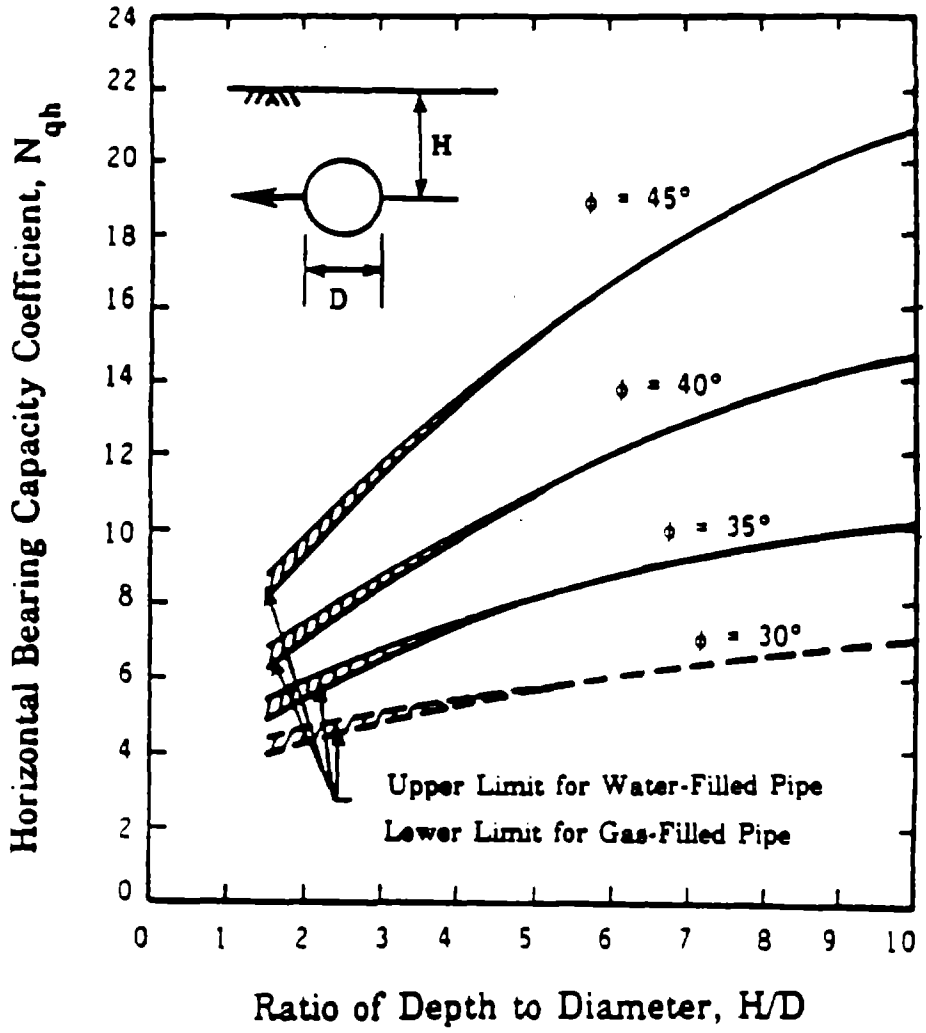

Figure 5-7. Horizontal Bearing Capacity Coefficient for Sands as a Function of Depth to Diameter Ratio of Buried Pipelines (after Trautmann and O'Rourke[78])

increases the shear strength of such sands. The line of 30° is dashed in Figure 5-7 to indicate the need of caution in estimating the coefficient N_{qh} for loose sands. This is due to the fact that loose sands usually compact under lateral loading, resulting in a lateral restraint equivalent to that of a sand initially dense.

5.3.2 Elasto-Plastic Model

The relationship between f_z and Δw is approximated by a simple elasto-plastic model, as shown by the dashed line in Figure 5-2(b). This model is defined by the two parameters f_z^u and k_z. The value of f_z^u is estimated by Eqn.(5.13) in conjunction with Figure 5-7.

The choice of the initial lateral stiffness, k_z, is, however, dictated by the magnitude of lateral displacements to which the soil springs are subjected. For an elasto-plastic model intersecting the hyperbolic (f_z, Δw) curve at a lateral force per unit length $f_z = \alpha_s \cdot f_z^u$, it can be shown that k_z is given by:

$$k_z = \frac{1 - (0.85)\ \alpha_s}{0.15} \cdot \left(\frac{f_z^u}{\Delta w^u}\right) \qquad (5.14)$$

A model with the coefficient $\alpha_s = 0.70$, that is: $k_z = 2.70\ (f_z^u/\Delta w^u)$, has been suggested by Thomas[82] for pipeline analyses involving large lateral soil displacements. Lateral soil displacements caused by wave propagation effects, however, are very small as shown in Chapter 3. In the present study, the coefficient α_s is initially taken equal to zero ($\alpha_s = 0.0$), which corresponds to:

$$k_z = 6.667 \left(\frac{f_z^u}{\Delta w^u}\right) \qquad (5.15)$$

Preliminary results indicate that the value of k_z given by Eqn.(5.15) is appropriate for the level of lateral soil displacements expected.

5.4 Selection of Soil Properties

This section presents the procedure used to select the soil strength parameters in this study. These parameters are assumed to vary randomly along the pipeline model. They, however, are constant over each pipe segment. The procedure includes is outlined below.

Depending on the actual site conditions, assign a coefficient of variation to each of the five parameters: γ, μ_s, K_o, K_2 and N_{qh}. It is expected that the coefficients of variation for these parameters, range between 20 to 40%. Note that these five parameters are strongly correlated

between one another. A linear correlation between one another is assumed herein. After that, choose an approximate probability density function to model the variability of each of these five parameters. In this study, a Rayleigh density function is chosen. This density can be easily used in conjunction with a random number generator as shown in Apendix A.

Using a random number generator in conjunction with the approximate probability density function, generate values of the parameters γ, μ_s, K_o, K_2 and N_{qh} for each pipe segment along the pipeline model. Since values of these five parameters are assumed to be linearly correlated, the same random number is used to generate their values. The characteristics of the (f_x,Δu) and (f_z, Δw) curves for each pipe segment are subsequently computed. This involves computing the value of f_x^u by Eqn.(5.1), the value of k_x by Eqn.(5.10) the value of f_z^u by Eqn.(5.13) and finally the value of k_z by Eqn.(5.15).

6. ANALYTICAL MODEL

6.1 Introduction

The pipeline properties established in Chapter 4 and the soil restraint properties established in Chapter 5 are used to construct an analytical model for the analysis of straight jointed buried pipelines. The model takes into account the variability as well as the nonlinearity of the system characteristics. In this chapter, the proposed model and the formulation of the problem are introduced. Finally, the algorithm and numerical procedures used to solve the problem, are presented.

6.2 Model Description

The proposed model is shown in Figure 6-1. It consists of a number of pipe segments surrounded by axial and lateral soil spring-sliders. It should be mentioned that these spring-sliders are treated as continuous rather than discrete. The number of pipe segments in the model is denoted by n_s. Each pipe segment is discretized into a number, n_e, of truss and beam elements, as shown in Figure 6-2. Each of these elements has two nodes, one at each end. The length of each element is indicated by l (i.e. $l = L/n_e$, with L being the pipe segment length). Joints exist between the pipe segments and are represented by axial and rotational nonlinear springs. These nonlinear springs are assumed to have a negligible length. Hence, the total length of the model is equal to: $L_{pm} = n_s \cdot L$. The strength characteristics of the pipe segments, the joint springs and the soil spring-sliders are denoted as in Chapters 4 and 5. The axial and lateral directions are respectively indicated by x and z. The ground nodes of the soil spring-sliders as well as the two end supports of the model follow specified axial and lateral displacement functions, as defined in Chapter 3, thus providing the input excitation for the system. The axial and lateral displacements of the pipeline are denoted respectively by u and w, while the axial and lateral displacements of the ground are denoted by u_g and w_g. Hence, the axial and lateral deformations of the soil spring-sliders along the pipeline, Δu and Δw, are respectively given by:

$$\Delta u(x) = u(x) - u_g(x) \tag{6.1}$$

$$\Delta w(x) = w(x) - w_g(x) \tag{6.2}$$

A finite element formulation is used to develop the governing algebraic equations. This formulation includes the case where the system characteristics are deterministic as well as the

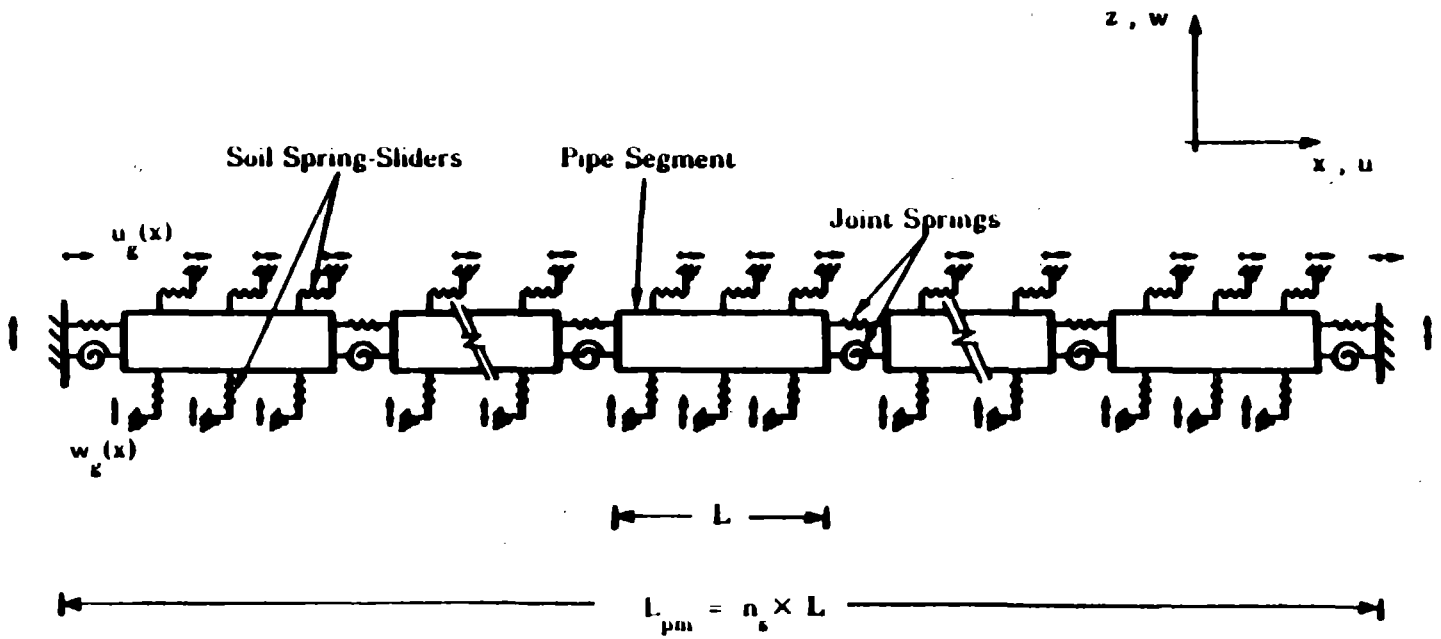

Figure 6-1. Plan View of Model for Straight Jointed Buried Pipelines

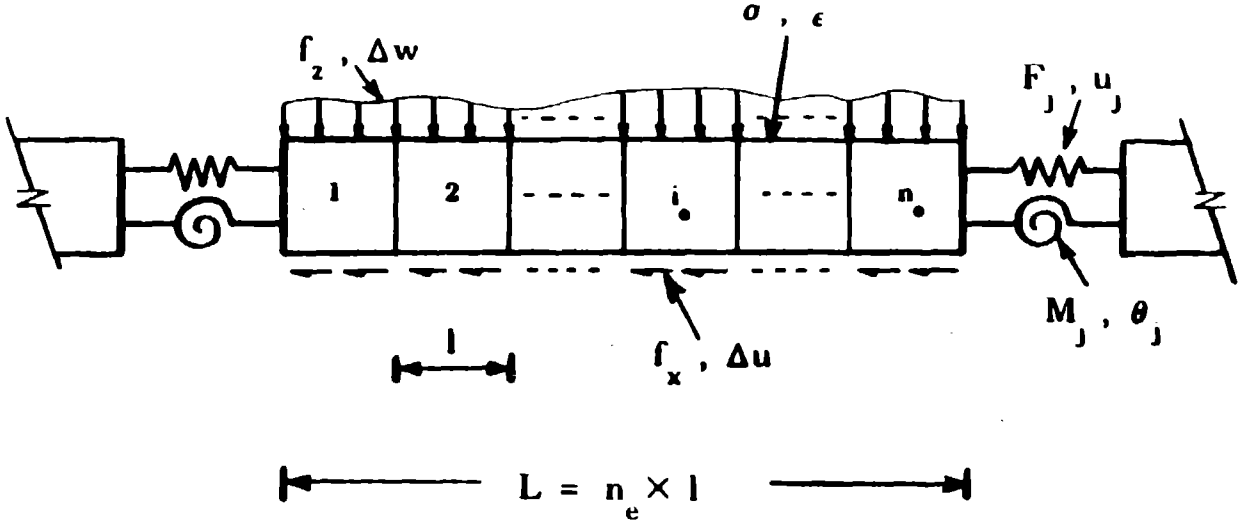

Figure 6-2. Pipe Segment Detail

case where they are random. In both cases, the pipe segment properties are constant along the model, while the joint properties can vary from joint to another. On the other hand, the soil properties can vary along the model but need to be constant over each pipe segment. In the case where the system characteristics are assumed to be random, a simplified Monte Carlo simulation technique is incorporated into the model. This simplified Monte Carlo simulation technique is described in Appendix A.

6.3 Mathematical Formulation

First, the method of weighted residuals with "Galerkin" criterion [83] is used to discretize the governing elastic (linear) differential equations, and obtain the element stiffness matrix and the element load vector for the pipe segment and soil system. Then, the element stiffness matrix for the joint in the elastic (linear) range is presented. The global stiffness matrix and global load vector are then assembled. The resulting algebraic equations are applicable only in the elastic (linear) range. However, when solved incrementally, these algebraic equations can be extended to the nonlinear range.

6.3.1 Pipe Segment Element Formulation

The governing differential equations for the axial and lateral pipeline displacements, u(x) and w(x), in the elastic range, are respectively given by:

$$E_p \cdot A \cdot \frac{d^2u(x)}{dx^2} - k_x \cdot [u(x) - u_g(x)] = 0 \tag{6.3}$$

$$E_p \cdot I \cdot \frac{d^4w(x)}{dx^4} + k_z \cdot [w(x) - w_g(x)] = 0 \tag{6.4}$$

where E_p is Young's modulus, A is the cross-sectional area and I is the transverse moment of inertia of the pipe. On the other hand, k_x and k_z represent respectively the initial axial and lateral stiffnesses of the soil springs. As shown in Figure 6-3, the products $k_x \cdot [u(x) - u_g(x)]$ and $k_z \cdot [w(x) - w_g(x)]$ represent respectively the soil spring restoring forces in the axial and lateral directions. Note that the development of Eqn.(6.4) is based on the "Beam on Elastic Foundation" approach [61].

A diagram of a pipe segment element and the surrounding soil springs is shown in Figure 6-4. Two coordinate schemes are used in the element formulation. The first one is the global coordinate system, x, and the second one is the natural coordinate system, ξ. The relation between these two coordinate systems is given by:

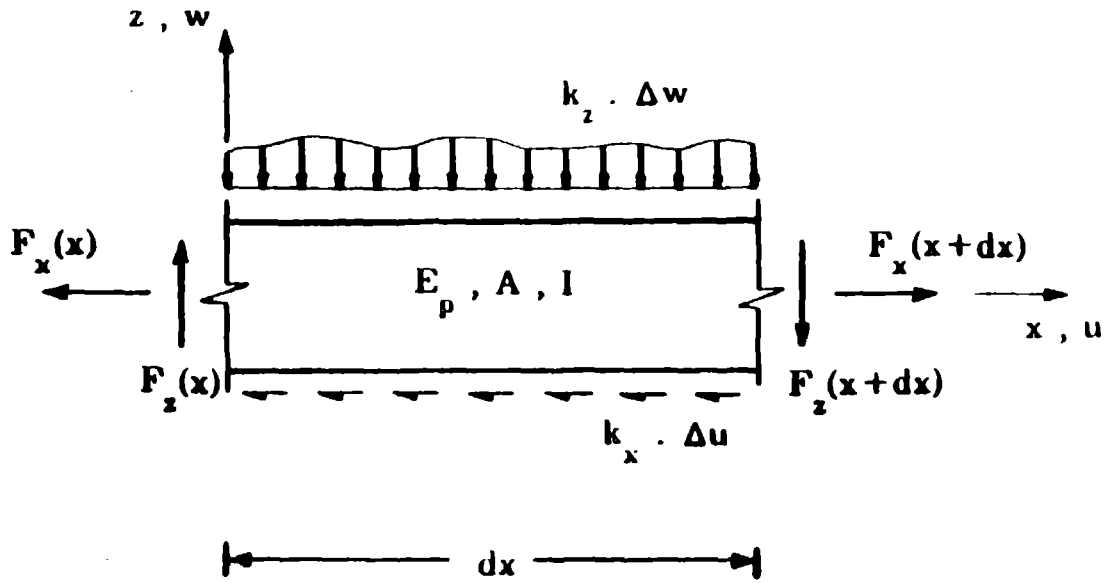

Figure 6-3. Elastic Equilibrium Diagram of a Buried Pipe, in the Axial and Lateral Directions

$$\xi = \frac{2 \cdot (x - x_1)}{l} - 1 \tag{6.5}$$

where x_1 is the global axial coordinate of node 1 (see Figure 6-1).

Eqns.(6.3) and (6.4) can be expressed in terms of the natural coordinate ξ. Using chain rule, they become:

$$E_p \cdot A \cdot (\frac{2}{l})^2 \cdot \frac{d^2u(\xi)}{d\xi^2} - k_x \cdot [u(\xi) - u_g(\xi)] = 0 \tag{6.6}$$

$$E_p \cdot I \cdot (\frac{2}{l})^4 \cdot \frac{d^4w(\xi)}{d\xi^4} + k_z \cdot [w(\xi) - w_g(\xi)] = 0 \tag{6.7}$$

Each pipeline node i_n has three degrees of freedom associated with it. They are the axial displacement, u_{i_n}, the lateral displacement, w_{i_n} and the angle of rotation in the (x,z) plane, θ_{i_n}

Thus, the pipe segment element displacements may be listed in the following vector:

$$\left\{\Delta^e\right\} = \left[u_1, w_1, \theta_1, u_2, w_2, \theta_2\right]^T \tag{6.8}$$

and the corresponding pipe segment element force vector is:

$$\left\{F^e\right\} = \left[F_{x,1}, F_{z,1}, M_1, F_{x,2}, F_{z,2}, M_2\right]^T \tag{6.9}$$

The shape functions associated with the axial degrees of freedom u_1 and u_2 are respectively equal to:

$$N_1^{(a)}(\xi) = \frac{1}{2}(1 - \xi)$$

$$N_2^{(a)}(\xi) = \frac{1}{2}(1 + \xi) \tag{6.10}$$

Thus, the axial pipeline displacement, $u(\xi)$, at any point within the element can be approximated by:

$$u(\xi) = N_1^{(a)}(\xi) \cdot u_1 + N_2^{(a)}(\xi) \cdot u_2 \tag{6.11}$$

For the bending degrees of freedom w_1, θ_1, w_2 and θ_2, the associated shape functions are respectively:

$$N_1^{(b)}(\xi) = \frac{1}{4}(\xi^3 - 3\xi + 2)$$

$$N_2^{(b)}(\xi) = -\frac{1}{8}(\xi^2 - 1) \cdot (\xi - 1) \cdot l$$

$$N_3^{(b)}(\xi) = -\frac{1}{4}(\xi^3 - 3\xi - 2)$$

$$N_4^{(b)}(\xi) = -\frac{1}{8}(\xi^2 - 1) \cdot (\xi + 1) \cdot l \tag{6.12}$$

and the lateral pipeline displacement $w(\xi)$ at any point within the element is approximated by:

$$w(\xi) = N_1^{(b)}(\xi) \cdot w_1 + N_2^{(b)}(\xi) \cdot \theta_1 + N_3^{(b)}(\xi) \cdot w_2 + N_4^{(b)}(\xi) \cdot \theta_2 \tag{6.13}$$

The same representation is adopted for the axial and lateral ground displacements $u_g(\xi)$ and $w_g(\xi)$. That is:

$$u_g(\xi) = N_1^{(a)}(\xi) \cdot u_{g,1} + N_2^{(a)}(\xi) \cdot u_{g,2} \tag{6.14}$$

$$w_g(\xi) = N_1^{(b)}(\xi) \cdot w_{g,1} + N_2^{(b)}(\xi) \cdot \theta_{g,1} + N_3^{(b)}(\xi) \cdot w_{g,2} + N_4^{(b)}(\xi) \cdot \theta_{g,2} \tag{6.15}$$

where $u_{g,1}$, $w_{g,1}$ and $\theta_{g,1}$ are respectively the axial displacement, lateral displacement and rotation of the ground at node 1, and similarly $u_{g,2}$, $w_{g,2}$ and $\theta_{g,2}$ are respectively the axial displacement, lateral displacement and rotation of the ground at node 2. Eqn.(6.14) is a linear interpolation of the axial ground displacement along the pipe segment element and hence, is equivalent to Eqn.(3.5). On the other hand, Eqn.(6.15) gives the lateral ground dislacement as a function of four parameters (i.e. $w_{g,1}$, $\theta_{g,1}$, $w_{g,2}$ and $\theta_{g,2}$). Therefore, Eqn.(6.15) is equivalent to Eqn.(3.7).

A ground displacement vector, $\left\{\Delta_g^e\right\}$, and a ground force vector, $\left\{F_g^e\right\}$ are assigned to each pipe segment element. They are respectively given by:

$$\left\{\Delta_g^e\right\} = \left[u_{g,1},\ w_{g,1},\ \theta_{g,1},\ u_{g,2},\ w_{g,2},\ \theta_{g,2}\right]^T \tag{6.16}$$

$$\left\{F_g^e\right\} = \left[F_{gx,1},\ F_{gz,1},\ M_{g,1},\ F_{gx,2},\ F_{gz,2},\ M_{g,2}\right]^T \tag{6.17}$$

In accordance with the method of weighted residuals with "Galerkin" criterion, the element stiffness matrix and the element load vector for the pipe segment and soil system can be obtained from the following equations:

$$\int_{-1}^{1} N_i^{(a)}(\xi)\left\{E_p \cdot A \cdot (\frac{2}{l})^2 \cdot \frac{d^2u(\xi)}{d\xi^2} - k_x \cdot [u(\xi) - u_g(\xi)]\right\}(\frac{l}{2}) \cdot d\xi = 0 \qquad i = 1,2 \tag{6.18}$$

$$\int_{-1}^{1} N_i^{(b)}(\xi)\left\{E_p \cdot I \cdot (\frac{2}{l})^4 \cdot \frac{d^4w(\xi)}{d\xi^4} + k_z \cdot [w(\xi) - w_g(\xi)]\right\}(\frac{l}{2}) \cdot d\xi = 0 \qquad i = 1,2,3,4 \tag{6.19}$$

Applying integration by parts to Eqn.(6.18) once and to Eqn.(6.19) twice, yields:

$$\int_{-1}^{1} E_p \cdot A \cdot (\frac{2}{l}) \cdot \frac{dN_i^{(a)}(\xi)}{d\xi} \cdot \frac{du(\xi)}{d\xi} \cdot d\xi + \int_{-1}^{1} k_x \cdot N_i^{(a)}(\xi) \cdot u(\xi) \cdot (\frac{l}{2}) \cdot d\xi =$$

$$\left[E_p \cdot A \cdot (\frac{2}{l}) \cdot N_i^{(a)}(\xi) \cdot \frac{du(\xi)}{d\xi}\right]_{-1}^{1} + \int_{-1}^{1} k_x \cdot N_i^{(a)}(\xi) \cdot u_g(\xi) \cdot (\frac{l}{2}) \cdot d\xi \qquad i=1,2 \tag{6.20}$$

$$\int_{-1}^{1} E_p \cdot I \cdot (\frac{2}{l})^3 \cdot \frac{d^2N_i^{(b)}(\xi)}{d\xi^2} \cdot \frac{d^2w(\xi)}{d\xi^2} \cdot d\xi + \int_{-1}^{1} k_z \cdot N_i^{(b)}(\xi) \cdot w(\xi) \cdot (\frac{l}{2}) \cdot d\xi =$$

$$- \left[E_p \cdot I \cdot (\frac{2}{l})^3 \cdot N_i^{(b)}(\xi) \cdot \frac{d^3w(\xi)}{d\xi^3}\right]_{-1}^{1} + \left[E_p \cdot I \cdot (\frac{2}{l})^3 \cdot \frac{dN_i^{(b)}(\xi)}{d\xi} \cdot \frac{d^2w(\xi)}{d\xi^2}\right]_{-1}^{1}$$

$$+ \int_{-1}^{1} k_z \cdot N_i^{(b)}(\xi) \cdot w_g(\xi) \cdot \frac{l}{2} \cdot d\xi \qquad i=1,2,3,4 \tag{6.21}$$

Knowing that the axial force, F_x, the lateral shear force, F_z, and the bending moment in the pipe segment, M, are respectively given by:

$$E_p \cdot A \cdot (\frac{2}{l}) \cdot \frac{du(\xi)}{d\xi} = F_x \,, \tag{6.22}$$

$$E_p \cdot I \cdot (\frac{2}{l})^3 \cdot \frac{d^3w(\xi)}{d\xi^3} = F_z \,, \tag{6.23}$$

and

$$E_p \cdot I \cdot (\frac{2}{l})^2 \cdot \frac{d^2w(\xi)}{d\xi^2} = M \,, \tag{6.24}$$

it is easy to show that the boundary terms of Eqns.(6.20) and (6.21) yield the pipe segment element vector $\left\{F_e\right\}$. Note that Eqns.(6.22), (6.23) and (6.24) correspond to a sign convention which gives positive values to a tensile force, F_x, a downward shear force, F_z, on the right hand side of an element, and a bending moment, M, causing tensile stresses in the negative fibers (i.e. fibers with $z \leq 0$).

From Eqns.(6.11) and (6.13), one can write:

$$\frac{du(\xi)}{d\xi} = \frac{dN_1^{(a)}(\xi)}{d\xi} \cdot u_1 + \frac{dN_2^{(a)}(\xi)}{d\xi} \cdot u_2 \tag{6.25}$$

$$\frac{d^2w(\xi)}{d\xi^2} = \frac{d^2N_1^{(b)}(\xi)}{d\xi^2} \cdot w_1 + \frac{d^2N_2^{(b)}(\xi)}{d\xi^2} \cdot \theta_1 + \frac{d^2N_3^{(b)}(\xi)}{d\xi^2} \cdot w_2 + \frac{d^2N_4^{(b)}(\xi)}{d\xi^2} \cdot \theta_2 \tag{6.26}$$

Note that the axial strain in the outer fibers of the pipe segment cross-section, $\epsilon(\xi)$, can be determined from Eqns.(6.25) and (6.26) using:

$$\epsilon(\xi) = \frac{du(\xi)}{d\xi} \cdot (\frac{2}{l}) \pm \frac{D}{2} \cdot \frac{d^2w(\xi)}{d\xi^2} \cdot (\frac{2}{l})^2 \tag{6.27}$$

The first term in Eqn.(6.27) represents the strain due to axial deformations, while the second represents the maximum bending strain due to lateral deformations. The (+) sign between these two terms gives $\epsilon(\xi)$ at $z = -D/2$ and the (−) sign gives $\epsilon(\xi)$ at $z = D/2$. In the remainder of this report, $\epsilon(\xi)$ will denote the higher value of the two pipe segment strains given by Eqn.(6.27)

at a cross-section.

Replacing the boundary terms by the pipe segment element vector, substituting Eqns.(6.11) and (6.25) into Eqn.(6.20), and substituting Eqns.(6.13) and (6.26) into Eqn.(6.21), results in an equation of the form:

$$\left(\left[K_p^e \right] + \left[K_s^e \right] \right) \cdot \left\{ \Delta^e \right\} = \left\{ F^e \right\} + \left[K_s^e \right] \cdot \left\{ \Delta_g^e \right\} \tag{6.28}$$

where $\left[K_p^e \right]$ is a (6×6) matrix representing the element stiffness of the pipe segment and $\left[K_s^e \right]$ is a (6×6) matrix representing the element stiffness of the soil restraint, characterized by the distributed springs. The sum of these two matrices is equal to the element stiffness of the pipe segment and soil system, $\left[K^e \right]$. That is:

$$\left[K^e \right] = \left[K_p^e \right] + \left[K_s^e \right] \tag{6.29}$$

Since $\left[K_p^e \right]$ and $\left[K_s^e \right]$ are symmetric matrices, it is sufficient to just evaluate the diagonal and upper-diagonal terms. The terms of $\left[K_p^e \right]$ are determined by evaluating the first integral expression in the left hand side of each of Eqns.(6.20) and (6.21). That is:

$$K_p^e(1,1) = \int_{-1}^{1} E_p \cdot A \cdot \left(\frac{2}{l}\right) \cdot \left[\frac{dN_1^{(a)}(\xi)}{d\xi}\right]^2 \cdot d\xi = \frac{E_p \cdot A}{l}$$

$$K_p^e(1,4) = \int_{-1}^{1} E_p \cdot A \cdot \left(\frac{2}{l}\right) \cdot \frac{dN_1^{(a)}(\xi)}{d\xi} \cdot \frac{dN_2^{(a)}(\xi)}{d\xi} \cdot d\xi = -\frac{E_p \cdot A}{l}$$

$$K_p^e(4,4) = \int_{-1}^{1} E_p \cdot A \cdot \left(\frac{2}{l}\right) \cdot \left[\frac{dN_2^{(a)}(\xi)}{d\xi}\right]^2 \cdot d\xi = \frac{E_p \cdot A}{l}$$

$$K_p^e(2,2) = \int_{-1}^{1} E_p \cdot I \cdot \left(\frac{2}{l}\right)^3 \cdot \left[\frac{d^2N_1^{(b)}(\xi)}{d\xi^2}\right]^2 \cdot d\xi = 12\,\frac{E_p \cdot I}{l^3}$$

$$K_p^e(2,3) = \int_{-1}^{1} E_p \cdot I \cdot \left(\frac{2}{l}\right)^3 \cdot \frac{d^2N_1^{(b)}(\xi)}{d\xi^2} \cdot \frac{d^2N_2^{(b)}(\xi)}{d\xi^2} \cdot d\xi = -6\,\frac{E_p \cdot I}{l^2}$$

$$K_p^e(2,5) = \int_{-1}^{1} E_p \cdot I \cdot \left(\frac{2}{l}\right)^3 \cdot \frac{d^2N_1^{(b)}(\xi)}{d\xi^2} \cdot \frac{d^2N_3^{(b)}(\xi)}{d\xi^2} \cdot d\xi = -12\,\frac{E_p \cdot I}{l^3}$$

$$K_p^e(2,6) = \int_{-1}^{1} E_p \cdot I \cdot \left(\frac{2}{l}\right)^3 \cdot \frac{d^2N_1^{(b)}(\xi)}{d\xi^2} \cdot \frac{d^2N_4^{(b)}(\xi)}{d\xi^2} \cdot d\xi = -6\,\frac{E_p \cdot I}{l^2}$$

$$K_p^e(3,3) = \int_{-1}^{1} E_p \cdot I \cdot (\frac{2}{l})^3 \cdot \left[\frac{d2N_2^{(b)}(\xi)}{d\xi^2}\right]^2 \cdot d\xi = 4\,\frac{E_p \cdot I}{l}$$

$$K_p^e(3,5) = \int_{-1}^{1} E_p \cdot I \cdot (\frac{2}{l})^3 \cdot \frac{d^2N_2^{(b)}(\xi)}{d\xi^2} \cdot \frac{d^2N_3^{(b)}(\xi)}{d\xi^2} \cdot d\xi = 6\,\frac{E_p \cdot I}{l^2}$$

$$K_p^e(3,6) = \int_{-1}^{1} E_p \cdot I \cdot (\frac{2}{l})^3 \cdot \frac{d^2N_2^{(b)}(\xi)}{d\xi^2} \cdot \frac{d^2N_4^{(b)}(\xi)}{d\xi^2} \cdot d\xi = 2\,\frac{E_p \cdot I}{l}$$

$$K_p^e(5,5) = \int_{-1}^{1} E_p \cdot I \cdot (\frac{2}{l})^3 \cdot \left[\frac{d^2N_3^{(b)}(\xi)}{d\xi^2}\right]^2 \cdot d\xi = 12\,\frac{E_p \cdot I}{l^3}$$

$$K_p^e(5,6) = \int_{-1}^{1} E_p \cdot I \cdot (\frac{2}{l})^3 \cdot \frac{d^2N_3^{(b)}(\xi)}{d\xi^2} \cdot \frac{d^2N_4^{(b)}(\xi)}{d\xi^2} \cdot d\xi = 6\,\frac{E_p \cdot I}{l^2}$$

$$K_p^e(6,6) = \int_{-1}^{1} E_p \cdot I \cdot (\frac{2}{l})^3 \cdot \left[\frac{d^2N_4^{(b)}(\xi)}{d\xi^2}\right]^2 \cdot d\xi = 4\,\frac{E_p \cdot I}{l}$$

and

$$K_p^e(1,2) = K_p^e(1,3) = K_p^e(1,5) = K_p^e(1,6) = K_p^e(2,4) = K_p^e(3,4) = K_p^e(4,5) = K_p^e(4,6) = 0 \qquad (6.30)$$

with $K_p^e(i,k)$ denoting the term in the i^{th} row and k^{th} column of $\left[K_p^e \right]$. A similar notation is used for all matrices in this report. The terms of $\left[K_s^e \right]$ are determined from the second integral expression in the left hand side of each of Eqns.(6.20) and (6.21). These terms are equal to:

$$K_s^e(1,1) = \int_{-1}^{1} k_x \cdot \left(N_1^{(a)}(\xi)\right)^2 \cdot (\frac{l}{2}) \cdot d\xi = \frac{k_x \cdot l}{3}$$

$$K_s^e(1,4) = \int_{-1}^{1} k_x \cdot N_1^{(a)}(\xi) \cdot N_2^{(a)}(\xi) \cdot (\frac{l}{2}) \cdot d\xi = \frac{k_x \cdot l}{6}$$

$$K_s^e(4,4) = \int_{-1}^{1} k_x \cdot \left(N_2^{(a)}(\xi)\right)^2 \cdot (\frac{l}{2}) \cdot d\xi = \frac{k_x \cdot l}{3}$$

$$K_s^e(2,2) = \int_{-1}^{1} k_z \cdot \left(N_1^{(b)}(\xi)\right)^2 \cdot (\frac{l}{2}) \cdot d\xi = \frac{156}{420}\,k_z \cdot l$$

$$K_s^e(2,3) = \int_{-1}^{1} k_z \cdot N_1^{(b)}(\xi) \cdot N_2^{(b)}(\xi) \cdot (\frac{l}{2}) \cdot d\xi = -\frac{22}{420}\,k_z \cdot l^2$$

$$K_s^e(2,5) = \int_{-1}^{1} k_z \cdot N_1^{(b)}(\xi) \cdot N_3^{(b)}(\xi) \cdot (\frac{l}{2}) \cdot d\xi = \frac{54}{420} k_z \cdot l$$

$$K_s^e(2,6) = \int_{-1}^{1} k_z \cdot N_1^{(b)}(\xi) \cdot N_4^{(b)}(\xi) \cdot (\frac{l}{2}) \cdot d\xi = \frac{13}{420} k_z \cdot l^2$$

$$K_s^e(3,3) = \int_{-1}^{1} k_z \cdot \left(N_2^{(b)}(\xi)\right)^2 \cdot (\frac{l}{2}) \cdot d\xi = \frac{4}{420} k_z \cdot l^3$$

$$K_s^e(3,5) = \int_{-1}^{1} k_z \cdot N_2^{(b)}(\xi) \cdot N_3^{(b)}(\xi) \cdot (\frac{l}{2}) \cdot d\xi = -\frac{13}{420} k_z \cdot l^2$$

$$K_s^e(3,6) = \int_{-1}^{1} k_z \cdot N_2^{(b)}(\xi) \cdot N_4^{(b)}(\xi) \cdot (\frac{l}{2}) \cdot d\xi = -\frac{3}{420} k_z \cdot l^3$$

$$K_s^e(5,5) = \int_{-1}^{1} k_z \cdot \left(N_3^{(b)}(\xi)\right)^2 \cdot (\frac{l}{2}) \cdot d\xi = \frac{156}{420} k_z \cdot l$$

$$K_s^e(5,6) = \int_{-1}^{1} k_z \cdot N_3^{(b)}(\xi) \cdot N_4^{(b)}(\xi) \cdot (\frac{l}{2}) \cdot d\xi = \frac{22}{420} k_z \cdot l^2$$

$$K_s^e(6,6) = \int_{-1}^{1} k_z \cdot \left(N_4^{(b)}(\xi)\right)^2 \cdot (\frac{l}{2}) \cdot d\xi = \frac{4}{420} k_z \cdot l^3$$

and

$$K_s^e(1,2) = K_s^e(1,3) = K_s^e(1,5) = K_s^e(1,6) = K_s^e(2,4) = K_s^e(3,4) = K_s^e(4,5) = K_s^e(4,6) = 0 \qquad (6.31)$$

The product $\left[K_s^e \right] \cdot \left\{ \Delta_g^e \right\}$ in Eqn.(6.28), represents the element load vector which is equal to the element ground force vector. That is:

$$\left\{ F_g^e \right\} = \left[K_s^e \right] \cdot \left\{ \Delta_g^e \right\} \qquad (6.32)$$

Substitution of Eqns.(6.29) and (6.32) into (6.28) gives the stiffness equations for a pipe segment and soil element. That is:

$$\left[K^e \right] \cdot \left\{ \Delta^e \right\} = \left\{ F^e \right\} + \left\{ F_g^e \right\} \tag{6.33}$$

6.3.2 Joint Element Formulation

The joint element stiffness in the elastic range, can be obtained from equilibrium considerations. Figure 6-5 shows a joint element with its degrees of freedom. Note that since the joint is contained between the spigot end of a pipe segment and the bell end of the adjacent pipe segment, it moves as a rigid body in the lateral direction. That is, there is no relative lateral displacement between the two end nodes (i.e. $w_1 = w_2$). The joint element displacement vector, $\left\{ \Delta_j^e \right\}$, and the joint element force vector, $\left\{ F_j^e \right\}$, can be defined as:

$$\left\{ \Delta_j^e \right\} = \left[u_1,\ \theta_1,\ u_2,\ \theta_2 \right]^T \tag{6.34}$$

$$\left\{ F_j^e \right\} = \left[F_{x,1},\ M_1,\ F_{x,2},\ M_2 \right]^T \tag{6.35}$$

Referring to Figure 6-5, the joint elongation, u_j, and the joint rotation, θ_j, are respectively equal to:

$$u_j = u_2 - u_1 \tag{6.36}$$

$$\theta_j = \theta_2 - \theta_1 \tag{6.37}$$

The joint element force vector is related to the displacement vector by:

$$\left[K_j^e \right] \cdot \left\{ \Delta_j^e \right\} = \left\{ F_j^e \right\} \tag{6.38}$$

where $\left[K_j^e \right]$ is a (4×4) symmetric matrix representing the joint element stiffness. The diagonal

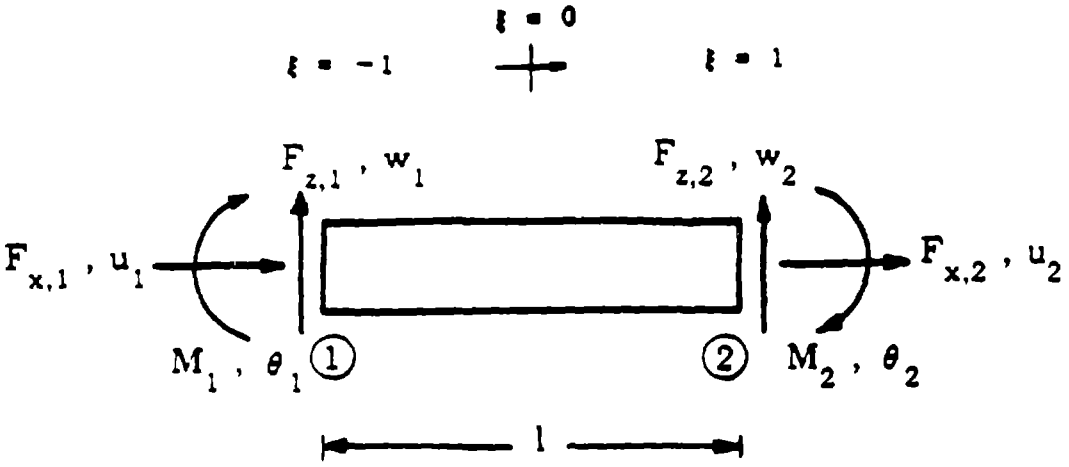

Figure 6-4. Pipe Segment Element with Nodal Forces and Displacements

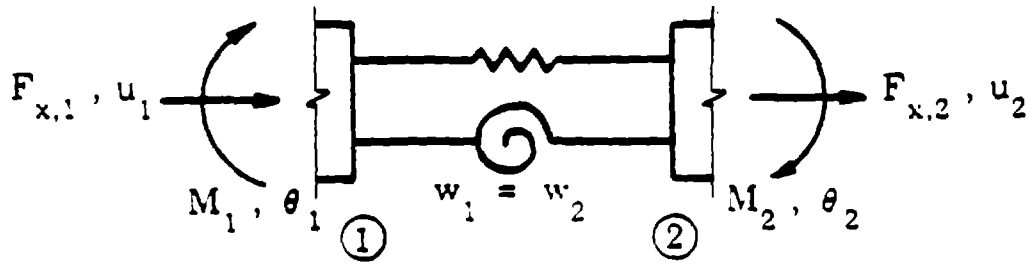

Figure 6-5. Joint Element with Nodal Forces and Displacements

and upper-diagonal terms of this matrix are given by:

$$K_j^e(1,1) = -K_j^e(1,3) = K_j^e(3,3) = AK_j$$

$$K_j^e(2,2) = -K_j^e(2,4) = K_j^e(4,4) = RK_j$$

$$K_j^e(1,2) = K_j^e(1,4) = K_j^e(2,3) = K_j^e(3,4) = 0 \qquad (6.39)$$

in which AK_j is the initial axial joint stiffness and RK_j is the initial rotational joint stiffness.

6.3.3 Global Formulation

The force/displacement relationships established for each element of the pipeline model, are assembled to form the global algebraic equations. A direct stiffness method is used for this purpose. This method consists of combining the pipe segment element and the joint element force/displacement relationships [i.e. Eqns.(6.33) and (6.38)] in a manner dictated by the requirements of node equilibrium and displacement continuity.

First, the nodes in the model are numbered. The total number of nodes, including the two end supports, n_n, is equal to:

$$n_n = n_s \cdot (n_e + 1) + 2 \qquad (6.40)$$

where n_s is, as mentioned before, the number of pipe segments in the model and n_e is the number of elements per pipe segment.

Second the degrees of freedom associated with these nodes are numbered. Since the joint element has a negligible length and the lateral direction is a rigid body mode, the two lateral displacements, one at each end of the joint element, are treated just as one lateral degree of freedom. Thus, five degrees of freedom are associated with each interior joint (i.e. joints connecting two pipe segments). Except for the interior joint nodes and the two end supports, each of the other nodes in the model has an axial, a lateral and a rotation degrees of freedom. As mentioned before, the axial, lateral and rotational movements of the middle of the two end joints are assumed to follow the ground movements (i.e. u_g, w_g and θ_g), and are ,therefore, not counted as degrees of freedom. The total number of degrees of freedom of the model is hence, equal to:

$$n_{dof} = 5 \cdot (n_s - 1) + 3 \cdot n_s \cdot (n_e - 1) + 6 \tag{6.41}$$

Figure 6-6 shows the model with the pipe segments, joints and nodes numbered, as well as the degrees of freedom associated with each node.

Third, the boundary conditions used for the model, are specified. These boundary conditions are chosen such that they duplicate the model, to a certain degree, beyond the length considered. Consider an infinitely long pipeline model. Let us truncate this model right in the middle of two different joints and assume that the portion between the two truncation points constitutes the proposed model. The infinitely long model and the truncated model are shown in Figure 6-7. In the case where the pipe segment, joint and soil properties are constant along the infinitely long model, one would expect that, under a uniform axial ground strain and a linearly varying ground rotation, the joint displacements as well as the joint rotations be constant at any joint. Under the same type of conditions (i.e. constant properties and similar loading), these results are duplicated in the truncated model if the axial and rotational initial stiffnesses of the two end joints are taken equal to twice their respective actual values. That is, the axial and rotational initial joint stiffnesses at both ends of the truncated model are respectively taken equal to: $2(AK_j)$ and $2(RK_j)$, where AK_j and RK_j are respectively the actual axial and rotational initial joint stiffnesses of the other joints. Note that in order to evaluate the end joint displacements and rotations from the proposed model (i.e. truncated model), one should take into account that these joints have been cut in the middle. Consequently, it seems appropriate to evaluate the joint axial displacement and rotation at the left end, $u_{j,1}$ and $\theta_{j,1}$, and the joint axial displacement and rotation at the right end, u_{j,n_s+1} and θ_{j,n_s+1}, by the following equations:

$$u_{j,1} = 2 \cdot (u_2 - u_{g,1}) \tag{6.42}$$

$$\theta_{j,1} = 2 \cdot (\theta_2 - \theta_{g,1}) \tag{6.43}$$

$$u_{j,n_s+1} = 2 \cdot (u_{g,n_n} - u_{n_n-1}) \tag{6.44}$$

$$\theta_{j,n_s+1} = 2 \cdot (\theta_{g,n_n} - \theta_{n_n-1}) \tag{6.45}$$

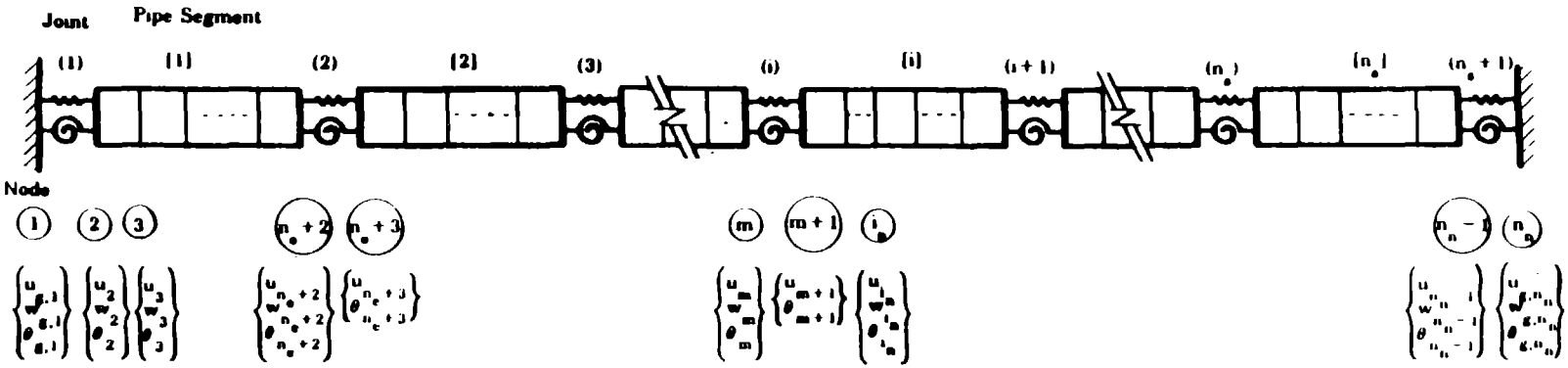

Figure 6-6. Pipeline Model with Numbered Pipe Segments, Joints and Nodes

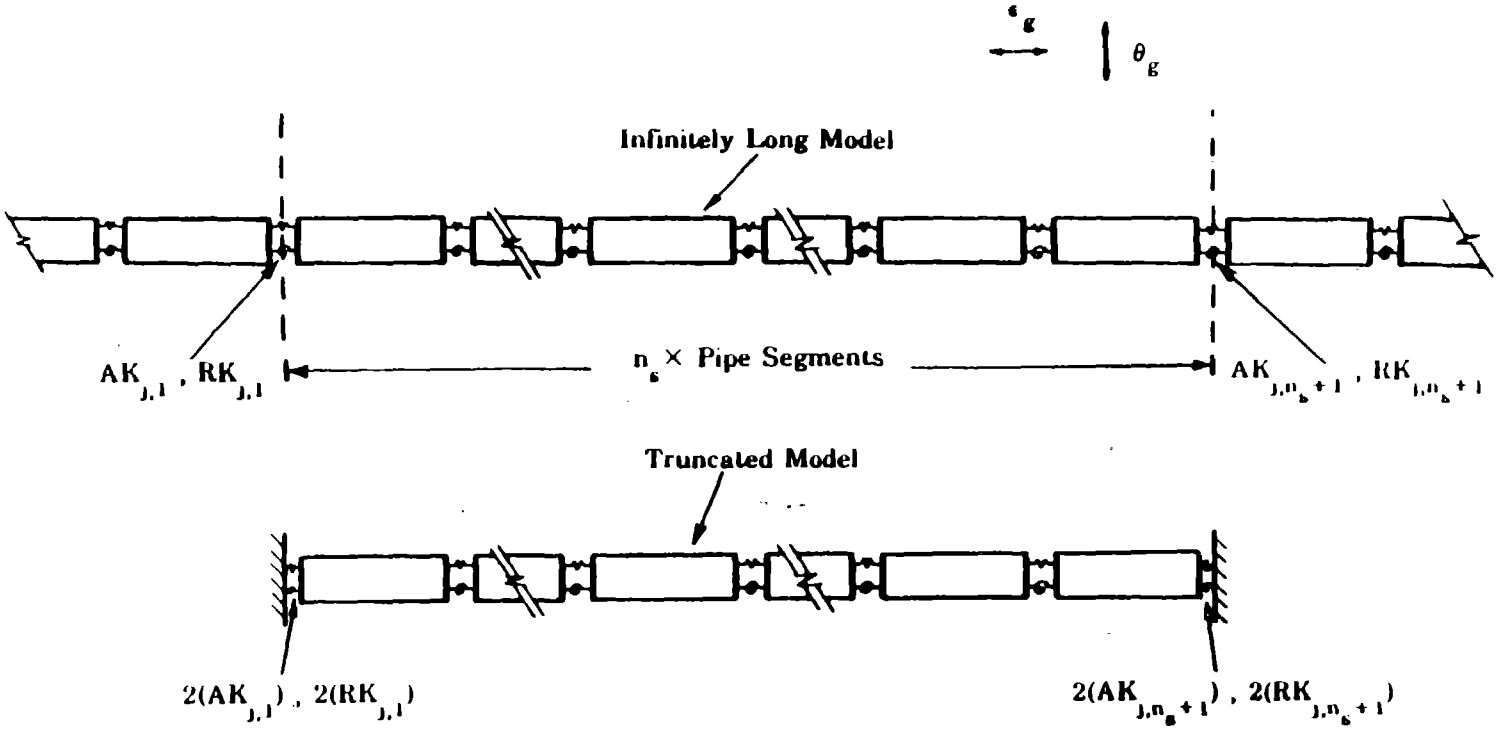

Figure 6-7. Infinitely Long and Truncated Models

where u_2 and θ_2 are respectively the axial displacement and rotation of node 2, while u_{n_n-1} and θ_{n_n-1} are respectively the axial displacement and rotation of node n_n-1. On the other hand, $u_{g,1}$ and $\theta_{g,1}$ represent respectively the ground axial displacement and rotation of node 1, while u_{g,n_n} and θ_{g,n_n} represent the ground axial displacement and rotation of node n_n (see Figure 6-6). Hence, the initial stiffnesses of the two end joints, for the proposed model, are doubled to account for the presence of the actual system beyond the length of the model considered. That is, if joint 1 (i.e. left end joint) has an axial and a rotational initial stiffnesses equal to $AK_{j,1}$ and $RK_{j,1}$, and joint n_s+1 (i.e. right end joint) has an axial and rotational initial stiffnesses equal to AK_{j,n_s+1} and RK_{j,n_s+1}, the corresponding values used in the model formulation are respectively equal to: $2(AK_{j,1})$, $2(RK_{j,1})$, $2(AK_{j,n_s+1})$ and $2(RK_{j,n_s+1})$.

After definition of the boundary conditions, a $(n_{dof} \times n_{dof})$ matrix and a vector with n_{dof} components, are used to construct respectively the global stiffness matrix, $\left[K \right]$, and the global load vector, $\left\{F_g\right\}$. For each pipe segment or joint element in the model, the terms in the corresponding element stiffness matrix are placed in the global stiffness matrix. A term at the i^{th} row and k^{th} column of the element stiffness of the pipe segment and soil system, $K^e(i,k)$ [i.e. $(1,1) \leq (i,k) \leq (6,6)$], is placed at the i'^{th} row and k'^{th} of $\left[K \right]$, with the index i' being the global number of the local i^{th} degree of freedom and similarly, the index k' being the global number of the k^{th} local degree of freedom. The same procedure is applied for the terms in each joint element stiffness, $K_j^e(i,k)$, with the difference being: $(1,1) \leq (i,k) \leq (4,4)$. Each time a term is placed in a location where a value has been already been placed, it is added to the latter. The process is repeated for all pipe segment and joint elements. The global load vector is assembled in the same way. That is, for each pipe segment, the i^{th} term in $\left\{F_g^e\right\}$, with i ranging between 1 and 6, is placed in the position i' of $\left\{F_g\right\}$. The index i' is the global number of the i^{th} local degree of freedom. The process of constructing $\left\{F_g\right\}$ includes only the pipe segment elements. The resulting global stiffness equations are given by:

$$\left[K \right] \cdot \left\{\Delta\right\} = \left\{F_g\right\} + \left\{F_g^{b.c.}\right\} \tag{6.46}$$

where $\left\{\Delta\right\}$ is the global displacement vector, and $\left\{F_g^{b.c.}\right\}$ represents a boundary load vector resulting from the contribution of the element stiffness matrices of joint 1 and joint n_s+1 to the global stiffness matrix.

The global stiffness matrix, $\left[K \right]$ can be written as:

$$\left[K \right] = \left[K_p \right] + \left[K_s \right] + \left[K_j \right] \tag{6.47}$$

where $\left[K_p \right]$ is the global stiffness of the pipe segments, $\left[K_s \right]$ is the global stiffness of the soil restraint and $\left[K_j \right]$ is the global stiffness of the joints. The matrices $\left[K_p \right]$ and $\left[K_s \right]$ can be obtained by assembling respectively the matrices $\left[K_p^e \right]$ and $\left[K_s^e \right]$ for all pipe segment elements. Similarly, $\left[K_j \right]$ can be constructed by assembling the matrices $\left[K_j^e \right]$ for all joints. The global displacement vector, $\left\{ \Delta \right\}$, list all the degrees of freedom. Referring to Figure 6-6, this vector is given by:

$$\left\{ \Delta \right\} = \Big[u_2, w_2, \theta_2, u_3, w_3, \theta_3, \cdots, u_{n_e+2}, w_{n_e+2}, \theta_{n_e+2}, u_{n_e+3}, \theta_{n_e+3}, \cdots,$$

$$u_m, w_m, \theta_m, u_{m+1}, \theta_{m+1}, \cdots, u_{i_n}, w_{i_n}, \theta_{i_n}, \cdots, u_{n_n-1}, w_{n_n-1}, \theta_{n_n-1} \Big]^T \tag{6.48}$$

where u_{i_n}, w_{i_n} and θ_{i_n} are respectively the axial displacement, lateral displacement and rotation of node i_n. Note that an interior joint i has five degrees of freedom which are: u_m, w_m, θ_m, u_{m+1}, θ_{m+1}. The index m denoting the number of the left node of joint i, is equal to: $m = (i-1) \cdot (n_e+1) + 1$.

From Eqn.(6.32), it is easy to see that $\left\{ F_g \right\}$ is equal to:

$$\left\{ F_g \right\} = \left[K_s \right] \cdot \left\{ \Delta_g \right\} \tag{6.49}$$

where $\left\{ \Delta_g \right\}$ is the global ground displacement vector. This vector lists the ground movements in the same order as that of the corresponding degrees of freedom. Values of these ground movements are obtained by computing $u_g(x)$, $w_g(x)$ or $\theta(x)$ at the corresponding node.

The vector $\left\{ F_g^{b.c.} \right\}$ can be determined from the stiffness equations of the two end joints. The axial force and moment at node 2, due to joint 1 deformations, $F_{x,2}$ and M_2, are respectively given by:

$$F_{x,2} = -2 \cdot AK_{j,1} \cdot u_{g,1} + 2 \cdot AK_{j,1} \cdot u_2 \tag{6.50}$$

$$M_2 = -2 \cdot RK_{j,1} \cdot \theta_{g,1} + 2 \cdot RK_{j,1} \cdot \theta_2 \tag{6.51}$$

and the axial force and moment at node $n_n - 1$, due to joint $n_s + 1$ deformations, F_{x,n_n-1} and M_{n_n-1}, are respectively given by:

$$F_{x,n_n-1} = 2 \cdot AK_{j,n_s+1} \cdot u_{n_n-1} - 2 \cdot AK_{j,n_s+1} \cdot u_{g,n_n} \tag{6.52}$$

$$M_{n_n-1} = 2 \cdot RK_{j,n_s+1} \cdot \theta_{n_n-1} - 2 \cdot RK_{j,n_s+1} \cdot \theta_{g,n_n} \tag{6.53}$$

The terms containing degrees of freedom (i.e. u_2, θ_2, u_{n_n-1} and θ_{n_n-1}) in Eqns.(6.50), (6.51), (6.52) and (6.53), are included in the right hand side of Eqn.(6.46). This is done when the element stiffnesses of joint 1 and joint n_s+1 are added to the global stiffness. On the other hand, the terms containing ground axial displacement or rotation (i.e. $u_{g,1}$, $\theta_{g,1}$, u_{g,n_n} and θ_{g,n_n}), result in the boundary load vector, $\left\{F_g^{b.c.}\right\}$. From Eqns.(6.50), (6.51), (6.52) and (6.53), the components of $\left\{F_g^{b.c.}\right\}$ can be derived. These components are given by:

$$F_g^{b.c.}(1) = 2 \cdot AK_{j,1} \cdot u_{g,1}$$

$$F_g^{b.c.}(2) = 0$$

$$F_g^{b.c.}(3) = 2 \cdot RK_{j,1} \cdot \theta_{g,1}$$

$$F_g^{b.c.}(i) = 0 \qquad \text{for: } 4 \le i \le n_{dof}-3$$

$$F_g^{b.c.}(n_{dof}-2) = 2 \cdot AK_{j,n_s+1} \cdot u_{g,n_n}$$

$$F_g^{b.c.}(n_{dof}-1) = 0$$

$$F_g^{b.c.}(n_{dof}) = 2 \cdot RK_{j,n_s+1} \cdot \theta_{g,n_n} \tag{6.54}$$

The sum of $\left\{F_g\right\}$ and $\left\{F_g^{b.c.}\right\}$ represents the total global load vector and is denoted by $\left\{\bar{F}_g\right\}$. That is:

$$\left\{\bar{F}_g\right\} = \left\{F_g\right\} + \left\{F_g^{b.c.}\right\} \tag{6.55}$$

Hence, the global algebraic equation becomes:

$$\left[K \right] \cdot \left\{ \Delta \right\} = \left\{ \bar{F}_g \right\} \tag{6.56}$$

Note that substitution of Eqns.(6.49) and (6.54) into Eqn.(6.55), and arranging terms, yield the following relation:

$$\left\{ \bar{F}_g \right\} = \left[\bar{K}_s \right] \cdot \left\{ \Delta_g \right\} \tag{6.57}$$

where $\left[\bar{K}_s \right]$ represents a modified global stiffness of the soil restraint. The terms in $\left[\bar{K}_s \right]$ are equal to:

$$\begin{aligned}
&\bar{K}_s(i,k) = K_s(i,k) \qquad ;(1,1) \le (i,k) \le (n_{dof}, n_{dof}) \text{ and} \\
&\qquad\qquad\qquad\qquad (i,k) \ne (1,1);\ (3,3);\ (n_{dof}-2, n_{dof}-2);\ (n_{dof}, n_{dof}) \\
&\bar{K}_s(1,1) = K_s(1,1) + 2 \cdot AK_{j,1} \\
&\bar{K}_s(3,3) = K_s(3,3) + 2 \cdot RK_{j,1} \\
&\bar{K}_s(n_{dof}-2, n_{dof}-2) = K_s(n_{dof}-2, n_{dof}-2) + 2 \cdot AK_{j,n_s+1} \\
&\bar{K}_s(n_{dof}, n_{dof}) = K_s(n_{dof}, n_{dof}) + 2 \cdot RK_{j,n_s+1}
\end{aligned} \tag{6.58}$$

Eqn.(6.56) represents the global algebraic equations for the pipeline model when the pipe segment axial strain along the model, $\epsilon(x)$, the axial and lateral relative displacements between the soil and the pipeline, $\Delta u(x)$ and $\Delta w(x)$, as well as the axial displacement and rotation at any joint i, $u_{j,i}$ and $\theta_{j,i}$, are within the elastic limits established in Chapters 4 and 5. These conditions can be summarized in the following inequalities:

$$\begin{aligned}
&-\epsilon^{yc} \le \epsilon(x) \le \epsilon^{y} && ;\ 0 \le x \le L_{pm} \\
&|\Delta u(x)| \le \Delta u^{s} && ;\ 0 \le x \le L_{pm} \\
&|\Delta w(x)| \le \Delta w^{s} && ;\ 0 \le x \le L_{pm} \\
&|u_{j,i}| \le u_j^{s} && ;\ 1 \le i \le n_s+1 \\
&|\theta_{j,i}| \le \theta_j^{s} && ;\ 1 \le i \le n_s+1
\end{aligned} \tag{6.59}$$

Values for the response parameters $\epsilon(x)$, $\Delta u(x)$, $\Delta w(x)$, $u_{j,i}$ and $\theta_{j,i}$ can be obtained from the global displacement vector, $\{\Delta\}$, and the corresponding applied global ground displacement vector, $\{\Delta_g\}$. Note that it is more convenient to evaluate the pipe segment axial strain, the relative axial displacement between the soil and the pipeline, and the relative lateral displacement between the soil and the pipeline, along each pipe segment element first. That is, determine $\epsilon(\xi)$, $\Delta u(\xi)$ and $\Delta w(\xi)$, separately for each pipe segment element along the pipeline model. Using Eqn.(6.5), it is possible to convert the three response parameters, $\epsilon(\xi)$, $\Delta u(\xi)$ and $\Delta w(\xi)$, into functions of the global coordinate x, $\epsilon(x)$, $\Delta u(x)$ and $\Delta w(x)$. The value of $\epsilon(\xi)$ is determined from Eqn.(6.27). The parameters $\Delta u(\xi)$ and $\Delta w(\xi)$ are found using respectively Eqns.(6.1) and (6.2), with $u(\xi)$, $w(\xi)$, $u_g(\xi)$ and $w_g(\xi)$ given respectively by Eqns.(6.11), (6.13), (6.14) and (6.15). The axial displacement and rotation at an internal joint i, $u_{j,i}$ and $\theta_{j,i}$, are evaluated respectively by Eqns.(6.36) and (6.37). For the two end joints (i.e. joints 1 and n_s+1), the axial displacement and rotation, are evaluated by Eqns.(6.42), (6.43), (6.44) and (6.45). On the other hand, values of ϵ^{yc}, ϵ^{y}, u_j^s and θ_j^s for the two pipeline systems considered can be obtained from Chapter 5, while those of Δu^s and Δw^s can be determined from Chapter 4. As mentioned previously, the parameters u_j^s and θ_j^s can vary from joint to joint, while the parameters Δu^s and Δw^s can vary from pipe segment to pipe segment, along the model.

In the case where any of the response parameters, $\epsilon(x)$, $u_{j,i}$, $\theta_{j,i}$, $\Delta u(x)$ or $\Delta w(x)$, enters the plastic range [i.e. one of the conditions in Eqn.(6.59) is not satisfied), the governing algebraic equations [i.e. Eqn.(6.56)] need to be solved incrementally. The new form for the governing algebraic equations is then:

$$\left[K' \right] \cdot \left\{ d\Delta \right\} = \left\{ d\bar{F}_g \right\} \tag{6.60}$$

where $\left[K' \right]$ represents the tangent global stiffness, $\left\{ d\Delta \right\}$ is an increment of the global displacement vector and $\left\{ d\bar{F}_g \right\}$ is an increment of the corresponding total global load vector. Based on Eqn.(6.57), the governing algebraic equations in incremental form, can also be written as:

$$\left[K' \right] \cdot \left\{ d\Delta \right\} = \left[\bar{K}_s' \right] \cdot \left\{ d\Delta_g \right\} \tag{6.61}$$

where $\left[\bar{K}_s' \right]$ represents the modified tangent global stiffness of the soil restraint and $\left\{ d\Delta_g \right\}$ is an increment of the global ground displacement vector.

The initial condition of Eqn.(6.60) or Eqn.(6.61), is:

$$\left\{\Delta\right\} = 0 \qquad ; \text{for} \qquad \left\{\Delta_g\right\} = 0 \tag{6.62}$$

The tangent global stiffness, $\left[\ K'\ \right]$, is a function of $\epsilon(x)$, $\Delta u(x)$, $\Delta w(x)$, $u_{j,i}$ and $\theta_{j,i}$. On the other hand, the increment of the total global load vector, $\left\{d\bar{F}_g\right\}$ depends only on $\Delta u(x)$ and $\Delta w(x)$ along the model, and on the joint displacements and joint rotations of the two end joints, $u_{j,1}$, $\theta_{j,1}$, u_{j,n_s+1} and θ_{j,n_s+1}. More specifically, $\left[\ K'\ \right]$ and $\left\{d\bar{F}_g\right\}$ depend on all or few of the conditions in Eqn.(6.59). Since all the response parameters can be obtained from $\left\{\Delta\right\}$ and $\left\{\Delta_g\right\}$, $\left[\ K'\ \right]$ and $\left\{d\bar{F}_g\right\}$ are functions of $\left\{\Delta\right\}$ and $\left\{\Delta_g\right\}$.

The formulation of the tangent global stiffness, $\left[\ K'\ \right]$, and the increment of the total global load vector, $\left\{d\bar{F}_g\right\}$ is done in the same way as that of the global stiffness, $\left[\ K\ \right]$, and the total global load vector, $\left\{\bar{F}_g\right\}$. First, the tangent element stiffnesses of the pipe segment, soil restraint and joint, $\left[\ K_p^{e'}\ \right]$ $\left[\ K_s^{e'}\ \right]$ and $\left[\ K_j^{e'}\ \right]$, are defined. These stiffnesses relate increments of the element force vectors to the corresponding increments of the element displacement vectors. For the pipe segment and soil elements, the relation is given by:

$$\left(\left[\ K_p^{e'}\ \right] + \left[\ K_s^{e'}\ \right]\right) \cdot \left\{d\Delta^e\right\} = \left\{dF^e\right\} + \left[\ K_s^{e'}\ \right] \cdot \left\{d\Delta_g^e\right\} \tag{6.63}$$

where $\left\{d\Delta^e\right\}$, $\left\{dF^e\right\}$ and $\left\{d\Delta_g^e\right\}$ are respectively increment of the element displacement vector, increment of the element force vector and increment of the element ground displacement vector, for the pipe segment and soil system. As mentioned previously, three loading cases are considered in this study. Preliminary results show that the pipe segment strain, $\epsilon(x)$, for the first and third loading cases, which correspond respectively, pull-out of the joints, and opening of the joints by a combination of axial extension and bending rotation, is always in the elastic range (i.e. $-\epsilon^{yc} \le \epsilon(x) \le \epsilon^{yc}$). Hence, for these two loading cases, the tangent element stiffness of the pipe segment is equal to the element stiffness of the pipe segment itself. That is: $\left[\ K_p^{e'}\ \right] = \left[\ K_p^{e}\ \right]$. However, for the second loading case which corresponds to crushing of the bell, the pipe segment axial strain, $\epsilon(x)$, is expected to reach the compressive yield strain, ϵ^{yc}. In this case, the terms of $\left[\ K_p^{e'}\ \right]$ are evaluated using the integrals in Eqn.(6.30) with the constant Young's modulus, E_p, replaced by a variable tangent modulus, $E_p'(\xi)$, which is given

by:

$$E_p'(\xi) = \begin{cases} E_p & ; -\epsilon^{yc} \le \epsilon(\xi) \le \epsilon^{y} \\ E_p^{(3)} & ; \epsilon(\xi) < -\epsilon^{yc} \end{cases} \tag{6.64}$$

For example, the term in position (1,1) of $\left[K_p^{e'} \right]$ becomes equal to:

$$K_p^{e'}(1,1) = \int_{-1}^{1} E_p'(\xi) \cdot A \cdot (\frac{2}{l}) \cdot \left(\frac{dN_1^{(a)}(\xi)}{d\xi} \right)^2 \cdot d\xi \tag{6.65}$$

The same change is made to obtain the rest of the terms of $\left[K_p^{e'} \right]$.
The preliminary results, however, show that the magnitude of the relative axial displacements between the soil and the pipeline, $\Delta u(x)$ reaches the corresponding slippage value, Δu^s under high values of ground strain. The terms of $\left[K_s^{e'} \right]$ are evaluated with the integrals in Eqn.(6.31) with the initial axial soil stiffness, k_x, replaced by a tangent axial stiffness, $k_x'(\xi)$ which is given by:

$$k_x'(\xi) = \begin{cases} k_x & ; |\Delta u(\xi)| \le \Delta u^s \\ 0 & ; |\Delta u(\xi)| > \Delta u^s \end{cases} \tag{6.66}$$

Values of the relative lateral displacement, $\Delta w(x)$, are as expected much smaller in magnitude than the corresponding slippage value, Δw^s, even under high values of ground rotation. However, for completness, the initial lateral soil stiffness, k_z, is replaced by a tangent lateral soil stiffness, $k_z'(\xi)$, in the formulation of $\left[K_s^{e'} \right]$. The tangent lateral soil stiffness is given by:

$$k_z'(\xi) = \begin{cases} k_z & ; |\Delta w(\xi)| \le \Delta w^s \\ 0 & ; |\Delta w(\xi)| > \Delta w^s \end{cases} \tag{6.67}$$

For example, the terms in positions (1,1) and (2,2) of $\left[K_s^{e'} \right]$ can be obtained from the following

equations:

$$K_s^{e'}(1,1) = \int_{-1}^{1} k_x'(\xi) \cdot \left[N_1^{(a)}(\xi)\right]^2 \cdot (\frac{1}{2}) \cdot d\xi \tag{6.68}$$

$$K_s^{e'}(2,2) = \int_{-1}^{1} k_z'(\xi) \cdot \left[N_1^{(b)}(\xi)\right]^2 \cdot (\frac{1}{2}) \cdot d\xi \tag{6.69}$$

Similar changes are made to the integrals in Eqn.(6.31) in order to obtain the rest of the terms of $\left[K_s^{e'} \right]$

The relation between the increment of the joint element displacement vector, $\left\{d\Delta_j^e\right\}$, and the corresponding increment of the joint element force vector, $\left\{dF_j^e\right\}$, however, is given by:

$$\left[K_j^{e'} \right] \cdot \left\{d\Delta^e\right\} = \left\{dF_j^e\right\} \tag{6.70}$$

where $\left\{d\Delta_j^e\right\}$ and $\left\{dF_j^e\right\}$ are respectively increment of the element displacement vector and increment of the element force vector for the joint element. The terms of $\left[K_j^{e'} \right]$ are evaluated by replacing the initial axial and rotational stiffneses of any joint, AK_j and RK_j, respectively by tangent axial and rotational stiffnesses, AK_j' and RK_j', given by:

$$AK_j' = \begin{cases} AK_j^{(3)} & ; u_j \le -u_j^c \\ AK_j & ; |u_j| \le u_j^s \\ AK_j^{(2)} & ; u_j > u_j^s \text{ and } -u_j^s \le u_j \le -u_j^c \end{cases} \tag{6.71}$$

$$RK_j' = \begin{cases} RK_j & ; |\theta_j| \le \theta_j^s \\ RK_j^{(2)} & ; |\theta_j| > \theta_j^s \end{cases} \tag{6.72}$$

Note that: $AK_j^{(2)} = 0$, for rubber gasketed joints.

The terms of $\left[K_j^{e'} \right]$ are evaluated using the following equations:

$$K_j^{e'}(1,1) = -K_j^{e'}(1,3) = K_j^{e'}(3,3) = AK_j'$$

$$K_j^{e'}(2,2) = -K_j^{e'}(2,4) = K_j^{e'}(4,4) = RK_j'$$

and

$$K_j^{e'}(1,2) = K_j^{e'}(1,4) = K_j^{e'}(2,3) = K_j^{e'}(3,4) = 0 \tag{6.73}$$

Note that the tangent axial and rotational stiffnesses of the two end joints are doubled as in the elastic case.

Next, the increment of the element load vector, $\left\{ dF_g^e \right\}$ is defined. In incremental form, Eqn.(6.32) can be written as:

$$\left\{ dF_g^e \right\} = \left[K_s^{e'} \right] \cdot \left\{ d\Delta_g^e \right\} \tag{6.74}$$

The tangent global stiffness, $\left[K' \right]$, is assembled from the tangent element stiffnesses, $\left[K_p^{e'} \right]$, $\left[K_s^{e'} \right]$ and $\left[K_j^{e'} \right]$, for all the elements (i.e. pipe segments and joints) in the model. Similarly, the increment of the global load vector, $\left\{ dF_g \right\}$, is assembled from the element load increment vector, $\left\{ dF_g^e \right\}$, for all the pipe segments. In order to get the increment of the total load vector, $\left\{ d\bar{F}_g \right\}$, one needs to evaluate the increment of the boundary load vector, $\left\{ dF_g^{b.c.} \right\}$. The components of $\left\{ dF_g^{b.c.} \right\}$ are given by:

$$dF_g^{b.c.}(1) = 2 \cdot AK_{j,1}' \cdot du_{g,1}$$

$$dF_g^{b.c.}(2) = 0$$

$$dF_g^{b.c.}(3) = 2 \cdot RK_{j,1}' \cdot d\theta_{g,1}$$

$$dF_g^{b.c.}(i) = 0 \qquad \text{for: } 4 \le i \le n_{dof}-3$$

$$dF_g^{b.c.}(n_{dof}-2) = 2 \cdot AK'_{j,n_s+1} \cdot du_{g,n_n}$$

$$dF_g^{b.c.}(n_{dof}-1) = 0$$

$$dF_g^{b.c.}(n_{dof}) = 2 \cdot RK'_{j,n_s+1} \cdot d\theta_{g,n_n} \qquad (6.75)$$

Note that the modified tangent global stiffness of the soil restraint, $\left[\bar{K}_s' \right]$, can be obtained from the tangent global stiffness of the soil restraint, $\left[K_s' \right]$, in a way similar to that used to obtain $\left[\bar{K}_s \right]$ from the stiffness $\left[K_s \right]$ [i.e. Eqn.(6.58)]; the only difference being that the ends joint initial stiffnesses are replaced by the corresponding tangent stiffnesses given in Eqns.(6.71) and (6.72).

Eqn.(6.61) with the initial condition given by Eqn.(6.62), represent the governing algebraic equations used to study the response of the proposed pipeline model. The solution to those equations is obtained in a stepwise manner. That is:

$$\left[K'(I) \right] \cdot \left(\left\{ \Delta(I+1) \right\} - \left\{ \Delta(I) \right\} \right) = \left[\bar{K}_s'(I) \right] \cdot \left(\left\{ \Delta_g(I+1) \right\} - \left\{ \Delta_g(I) \right\} \right) \qquad I = 0,1,\ldots,N-1 \qquad (6.76)$$

or:

$$\left[K'(I) \right] \cdot \left\{ \Delta(I+1) \right\} = \left[K'(I) \right] \cdot \left\{ \Delta(I) \right\} + \left[\bar{K}_s'(I) \right] \cdot \left(\left\{ \Delta_g(I+1) \right\} - \left\{ \Delta_g(I) \right\} \right) \qquad I = 0,1,\ldots,N-1 \qquad (6.77)$$

in which $\left[K'(I) \right]$, $\left\{ \Delta(I) \right\}$, $\left[\bar{K}_s'(I) \right]$ and $\left\{ \Delta_g(I) \right\}$ are respectively the tangent global stiffness, the global displacement vector, the modified tangent global stiffness of the soil restraint and the global ground displacement vector at the I^{th} increment, and N is the total number of increments used to get the solution (i.e. $\left\{ \Delta_g(N) \right\} = \left\{ \Delta_g \right\}$).

The initial condition of Eqn.(6.62) corresponds to:

$$\left[K'(0) \right] = \left[K \right]$$

$$\left[\bar{K}_s'(0) \right] = \left[\bar{K}_s \right]$$

$$\left\{ \Delta(0) \right\} = 0$$

$$\left\{ \Delta_g(0) \right\} = 0 \qquad (6.78)$$

In the next section, the algorithm and numerical procedures used to get the response parameters, are presented.

6.4 Algorithm and Numerical Procedures

A computer program is written to represent the above described formulation. This computer program includes the case where the system characteristics are deterministic as well as the case where they are random. The following algorithm corresponds to the random case which uses the simplified Monte Carlo simultion technique described in Appendix A. It has nine steps which are:

- Step 1:

Supply the input parameters to the program. These parameters include:

* An indicator, I_T, which defines the type of pipeline system, as follows:

$$I_T = \begin{cases} 1 & \text{; for Cast Iron Pipes with Lead Caulked Joints} \\ 2 & \text{; for Ductile Iron Pipes with Rubber Gasketed Joints} \end{cases} \qquad (6.79)$$

* Number of pipe segments, n_s, and number of elements per pipe segment, n_e.
* Number of times the model is simulated and analysed, n_{sim}.
* Pipeline properties as specified in section 4.4.
* Soil properties as specified in section 5.4.
* Maximum ground strain, ϵ_g, and maximum groun rotation, θ_g.
* Total number of ground displacement increments, .., needed to get the solution if the pipeline model response reaches the inelastic range.

- Step 2:

The following arrays are constructed to describe the finite element setup of the model:

* $\left[\text{NOD} \right]$ is a $(2\times n_n - 1)$ matrix relating node numbers to corresponding elements. For each pipe segment element or joint element, the first row gives the left node number, while the second row gives the right node number. Note that $n_n - 1$ represents the sum of pipe segment elements and joint elements in the model.

* $\left[\text{ID} \right]$ is a $(3\times n_n)$ matrix giving the degree of freedom number corresponding to each node. It should be mentioned that the columns corresponding to the two end nodes have zero entries since they are not counted as degrees of freedom .

* $\left[\text{LM} \right]$ is a $(n_n - 1\times 6)$ matrix constructed from the matrices $\left[\text{NOD} \right]$ and $\left[\text{ID} \right]$. Each row gives the six degrees of freedom corresponding to a pipe segment element or joint element. For the interior joints, the degree of freedom corresponding to the vertical direction is repeated twice.

* $\left\{\text{ISKL}\right\}$ and $\left\{\text{IDIA}\right\}$ are two one-dimensional arrays (i.e. vectors) each having n_{dof} entries. A method referred to as "the skyline method" is used to store more efficiently the global stiffness, $\left[\text{K} \right]$ [84]. In this method, a region of the global stiffness which is delimited by the first non-zero term in each column and the diagonal terms, is stored in a one-dimensional array, $\left\{\text{SK}\right\}$. This region will be referred to as the non-zero region. The two arrays, $\left\{\text{ISKL}\right\}$ and $\left\{\text{IDIA}\right\}$, serve to establish a mapping betwwen the entries of $\left[\text{K} \right]$ and those of $\left\{\text{SK}\right\}$. The i^{th} entry of $\left\{\text{ISKL}\right\}$ gives the row number of the first non-zero term in the i^{th} column of $\left[\text{K} \right]$. On the other hand, the i^{th} entry of $\left\{\text{IDIA}\right\}$ gives the position of the diagonal term K(i,i) in the one-dimensional array $\left\{\text{SK}\right\}$. The terms of the non-zero region of $\left[\text{K} \right]$ are entered into $\left\{\text{SK}\right\}$, by columns, that is, entries in column 1, then entries of column 2 and so on. Accordingly, a term K(i,k) in the global stiffness is entered into $\left\{\text{SK}\right\}$ at the position given by:

$$\begin{aligned} &\text{IDIA}(k) - k + i && ; \text{if } k \geq i \\ &\text{IDIA}(i) - i + k && ; \text{if } k < i \end{aligned} \qquad (6.80)$$

The number of entries in $\left\{\text{SK}\right\}$ is determined after constructing the array $\left\{\text{IDIA}\right\}$. It is equal to $\text{IDIA}(n_{dof})$.

• Step 3:

First, calculate the axial coordinate, x, of each node along the model. Following, the components of the global ground displacement vector $\left\{\Delta_g\right\}$ are evaluated using Eqns.(3.5) and (3.7). Note that the array $\left[\text{ID} \right]$ is used to position the axial ground displacement, lateral ground displacement and ground rotation in $\left\{\Delta_g\right\}$, according to the order established for the degrees of freedom.

• Step 4:

First, generate randomly the parameters defining the axial force/displacement and bending moment/rotation relationships for each joint along the model, as described in section 4.4. Then, generate randomly the parameters defining the axial force per unit length/displacement and the lateral force per unit length/displacement relationships for each pipe segment along the model, as described in section 5.4.

• Step 5:

Construct the elastic global stiffness, $\left[K \right]$, and the elastic total global load, $\left\{ \bar{F}_g \right\}$. As mentioned in Step 2, $\left[K \right]$ is stored in a one-dimensional array, $\left\{ SK \right\}$. Subsequently, solve for the elastic global displacement vector denoted by $\left\{ \Delta^* \right\}$, from the global algebraic equations [i.e. Eqn.(6.56)]. The numerical procedure used to solve Eqn.(6.56), consists of factoring the elastic global stiffness into the product:

$$\left[K \right] = \left[LK \right] \cdot \left[DK \right] \cdot \left[LK \right]^T \tag{6.81}$$

where $\left[LK \right]$ is a ($n_{dof} \times n_{dof}$) lower-diagonal matrix with unit diagonal entry [i.e. LK(i,i) = 1 , for $1 \leq i \leq n_{dof}$], and $\left[DK \right]$ is a ($n_{dof} \times n_{dof}$) diagonal matrix.

Hughes[84] showed that the non-zero region of $\left[K \right]$ is identical to that of $\left[LK \right]^T$. Also, since the diagonal terms of $\left[LK \right]$ are equal to unity, there is no need to store them. Hence, in the same way $\left[K \right]$ was stored in $\left\{ SK \right\}$, both of the matrices $\left[LK \right]$ and $\left[DK \right]$ are stored in a one-dimensional array $\left\{ S\bar{K} \right\}$. Each term in the non-zero region of $\left[LK \right]$ (excluding the diagonal terms), LK(i,k) is stored in $\left\{ S\bar{K} \right\}$ at the position given by IDIA(i)−i+k, while each diagonal term DK(i,i) is stored in $\left\{ S\bar{K} \right\}$ at the position given by IDIA(i). The array $\left\{ S\bar{K} \right\}$ have the same number of entries as the array $\left\{ SK \right\}$, that is IDIA(n_{dof}).

Thus, Eqn.(6.56) becomes:

$$\left[LK \right] \cdot \left[DK \right] \cdot \left[LK \right]^T \cdot \left\{ \Delta^* \right\} = \left\{ \bar{F}_g \right\} \tag{6.82}$$

The new equation [i.e. Eqn.(6.82)] can be solved in three steps which are:

* Use "Forward Substitution" to solve for $\left\{ \Delta_1 \right\}$, from:

$$\left[LK \right] \cdot \left\{ \Delta_1 \right\} = \left\{ \bar{F}_g \right\} \tag{6.83}$$

* Then solve for the vector $\left\{\Delta_2\right\}$, from the uncoupled algebraic equations:

$$\left[\,DK\,\right]\cdot\left\{\Delta_2\right\} = \left\{\Delta_1\right\} \tag{6.84}$$

* Finally, use "Backward Substitution" to solve for $\left\{\Delta^*\right\}$. from:

$$\left[\,LK\,\right]^T\cdot\left\{\Delta\right\} = \left\{\Delta_2\right\} \tag{6.85}$$

Using the array $\left[\,LM\,\right]$, it is then possible to deduce the element displacement vectors for each pipe segment element and joint element, $\left\{\Delta^e\right\}$ and $\left\{\Delta_j^e\right\}$, from the elastic global displacement vector, $\left\{\Delta^*\right\}$.

For each pipe segment element, the axial strain $\epsilon(\xi)$, as well as the axial and lateral relative displacements between the soil and the pipeline, $\Delta u(\xi)$ and $\Delta w(\xi)$, are computed from the corresponding element displacement vector, $\left\{\Delta^e\right\}$, at selected points. The selected points are chosen to be the "Gaussian" four points. The local coordinates of these four points are respectively equal to:

$$\begin{aligned}\xi_1 &= -\ 0.861136\\ \xi_2 &= -\ 0.339981\\ \xi_3 &= +\ 0.339981\\ \xi_4 &= +\ 0.861136\end{aligned} \tag{6.86}$$

Note that the "Gaussian" four points will also be used to integrate the tangent stiffness terms in the case where the response parameters exceed the elastic limits.

For each joint, the axial displacement, u_j, and rotation, θ_j, are computed from the corresponding element displacement vector, $\left\{\Delta_j^e\right\}$.

• Step 6:

Check if the response parameters are within the elastic limits or not [i.e. Eqn.(6.59)]. For this purpose, the following procedure is used:

* Compute for each pipe segment element, the following ratios:

$$\left|\frac{\Delta u_s}{\Delta u(\xi_i)}\right| \quad \text{and} \quad \left|\frac{\Delta w^s}{\Delta w(\xi_i)}\right| \qquad ; \text{for } i=1,2,3,4$$

* The following ratio is computed only when the model is subjected to compressive ground strain (i.e. second loading case):

$$\left|\frac{\epsilon^{yc}}{\epsilon(\xi_i)}\right| \qquad ; \text{for } i=1,2,3,4$$

* Compute for each joint, the two ratios:

$$\left|\frac{u_j^s}{u_j}\right| \quad \text{and} \quad \left|\frac{\theta_j^s}{\theta_j}\right|$$

* Find the minimum value of all these ratios. This minimum value is denoted by: ELIND. That is:

$$\text{ELIND} = \text{Minimum}\left\{\left|\frac{\epsilon^{yc}}{\epsilon(\xi_i)}\right|, \left|\frac{\Delta u^s}{\Delta u(\xi_i)}\right|, \left|\frac{\Delta w^s}{\Delta w(\xi_i)}\right|, \left|\frac{u_j^s}{u_j}\right|, \left|\frac{\theta_j^s}{\theta_j)}\right|\right\} \tag{6.87}$$

* The coefficient ELIND represents the fraction of total ground displacements which will take the model response into the inelastic range. Therefore:

- If : ELIND $\geq$ 1 , then the elastic solution obtained is exact and the global displacement vector is equal to the elastic global displacement vector (i.e. $\{\Delta\} = \{\Delta^*\}$). Following, go directly to Step 8.

- If : ELIND < 1 , then the governing algebraic equations need to be solved incrementally [i.e. Eqn.(6.76)]. Step 7 describes how to solve Eqn.(6.76).

• Step 7:

The fraction of the total global ground displacement vector at which the model response starts being inelastic, is chosen to be equal to the global ground displacement vector at the first increment. In accordance with Eqn.(6.76), this vector is denoted by $\{\Delta_g(1)\}$. From Step 7, the global ground displacement vector at the first increment is equal to:

$$\left\{\Delta_g(1)\right\} = \text{ELIND} \cdot \left\{\Delta_g\right\} \tag{6.88}$$

Since the model response is elastic up to this first increment, the corresponding global displacement vector, $\left\{\Delta(1)\right\}$, is equal to:

$$\left\{\Delta(1)\right\} = \text{ELIND} \cdot \left\{\Delta^*\right\} \tag{6.89}$$

In the same way, the response parameters (i.e. $\epsilon(\xi)$, $\Delta u(\xi)$, $\Delta w(\xi)$, u_j and θ_j) corresponding to $\left\{\Delta_g(1)\right\}$ are obtained by multiplying the elatic response parameters from Step 5 by the coefficient ELIND.

To get the exact global displacement vector, $\left\{\Delta\right\}$, the remaining fraction of $\left\{\Delta_g\right\}$ is subdivided to $N-1$ equal increments. That is:

$$\left\{\Delta_g(I+1)\right\} - \left\{\Delta_g(I)\right\} = \frac{(1-\text{ELIND})}{(N-1)} \cdot \left\{\Delta_g\right\} \qquad I=1,2,...,N-1 \tag{6.90}$$

Hence, Eqn.(6.77) becomes:

$$\left[\,K'(I)\,\right] \cdot \left\{\Delta(I+1)\right\} = \left[\,K'(I)\,\right] \cdot \left\{\Delta(I)\right\} + \frac{(1-\text{ELIND})}{(N-1)} \cdot \left[\,\bar{K}_s'(I)\,\right] \cdot \left\{\Delta_g\right\} \qquad I = 1,2,...,N-1 \tag{6.91}$$

with

$$\left[\,K'(1)\,\right] = \left[\,K\,\right]$$

$$\left[\,\bar{K}_s'(1)\,\right] = \left[\,\bar{K}_s\,\right] \tag{6.92}$$

The second term in Eqn.(6.91) represents the I^{th} increment of the total global load vector. That is:

$$\left\{d\bar{F}_g(I)\right\} = \frac{(1-\text{ELIND})}{(N-1)} \cdot \left[\,\bar{K}_s'(I)\,\right] \cdot \left\{\Delta_g\right\} \tag{6.93}$$

Another form of Eqn.(6.77) is then given by:

$$\left[K'(I) \right] \cdot \left\{ \Delta(I+1) \right\} = \left[K'(I) \right] \cdot \left\{ \Delta(I) \right\} + \left\{ d\bar{F}_g(I) \right\} \qquad I = 1,2,...,N-1 \tag{6.94}$$

When the response parameters exceed the elastic limits, the integrals giving the terms of the tangent element stiffnesses of the pipe segments and the soil restraints, $K_p^e{}'(i,k)$ and $K_s^e{}'(i,k)$, are evaluated numerically using a four point "Gaussian" quadrature method. In this method, the integral of a function $fn(\xi)$ over the interval $[-1, 1]$ is approximated by:

$$\int_{-1}^{1} fn(\xi) \cdot d\xi = \sum_{i=1}^{4} fn(\xi_i) \cdot c_i \tag{6.95}$$

where ξ_i with $1 \leq i \leq 4$, are the coordinates of the "Gaussian" points [i.e. Eqn.(6.86)] and c_i are the corresponding coefficients. Values of these coefficients are given by:

$$\begin{aligned} c_1 &= 0.347855 \\ c_2 &= 0.652145 \\ c_3 &= 0.652145 \\ c_4 &= 0.347855 \end{aligned} \tag{6.96}$$

Note that the four point "Gaussian" quadrature method gives an exact value for the integral of polynomials with order less or equal to 7.

The algorithm used to evaluate $\left\{ \Delta \right\}$ has four stages which are:

1. Initialize the increment counter: $I = 1$

2. Solve for $\left\{ \Delta(I+1) \right\}$ from Eqn.(6.94). The numerical procedure to solve Eqn.(6.94) is the same as that used to solve Eqn.(6.56) (i.e. the elastic problem in Step 5).

3. Compute the response parameters corresponding to $\left\{ \Delta(I+1) \right\}$. As mentioned previously (i.e. Step 5), these response parameters include values of $\epsilon(\xi)$, $\Delta u(\xi)$ and $\Delta w(\xi)$ at the four "Gaussian" points of each pipe segment element, as well as values of u_j and θ_j at each joint along the model.

4. If these response parameters exceeded the elastic limits at the new position, then update the tangent global stiffness, $\left[K'(I) \right]$ and the increment of the total global load vector $\left\{ d\bar{F}_g(I) \right\}$.

After that, solve Eqn.(6.94) again with the updated $\left[K'(I) \right]$ and $\left\{ d\bar{F}_g'(I) \right\}$ [i.e. redo stage (2)]. If however, there is no new position along the model where the response parameters exceed the elastic limits, then set:

$$\left[K'(I+1) \right] = \left[K'(I) \right]$$

$$\left\{ d\bar{F}_g'(I+1) \right\} = \left\{ d\bar{F}_g'(I) \right\} \tag{6.97}$$

Subsequently, increase the increment counter by 1, that is: $I = I+1$.

If: $I+1 < N$, then go to stage 2 and start a new increment.

After $\left\{ \Delta(N) \right\}$ is obtained, go to Step 8 (i.e. stop when $I+1 = N$).

• Step 8:

Compute the final results which inclued:

* The average axial strain, ϵ, and the corresponding axial stress, σ, for each pipe segement element.

The value of ϵ is obtained from:

$$\epsilon = \sum_{i=1}^{4} \frac{\epsilon(\xi_i)}{4} \tag{6.98}$$

where $\epsilon(\xi_i)$ is the axial strain at the i^{th} "Gaussian" point of the pipe segment element of interest.

The value of σ can be evaluated from the (σ, ϵ) relationships established in Chapter 4.

* The average axial and lateral relative displacements between the soil and the pipeline, Δu and Δw, as well as the corresponding axial and lateral forces per unit length, f_x and f_z, for each pipe segment element.

Values of Δu and Δw are respectively equal to:

$$\Delta u = \sum_{i=1}^{4} \frac{\Delta u(\xi_i)}{4}$$

$$\Delta w = \sum_{i=1}^{4} \frac{\Delta w(\xi_i)}{4} \tag{6.99}$$

where $\Delta u(\xi_i)$ and $\Delta w(\xi_i)$ are respectively the axial and lateral relative displacements between

the soil and the pipeline at the local "Gaussian" coordinate ξ_i.

Values of the corresponding f_x and f_z for each pipe segment element, are obtained from the (f_x, Δu) and (f_z, Δw) relationships established in Chapter 5.

* The axial joint displacement and force, u_j and F_j, as well as the joint rotation and bending moment, θ_j and M_j.

Values of u_j and θ_j were already computed in Step 7.

The axial force and bending moment at the joint, F_j and M_j, are deduced using the (F_j,u_j) and (M_j,θ_j) relationships established in Chapter 4.

Step 4 through Step 8 is repeated n_{sim} times. That is, results are obtained for n_{sim} simulated models.

• Step 9:

In this Step, a statistical analysis of all the results is performed. For each of the response parameters, the corresponding mean value and coefficient of variation can be obtained. It is also possible to get the histogram corresponding to those response parameters.

In order to be applied to the deterministic case, the above described algorithm needs to be modified. In Step 1, the deterministic values of the pipeline and soil properties are supplied with the other input parameters. Steps 2 and 3 do not change, and Step 5 through Step 8 are followed only once. There is no need for Steps 4 and 9, however, since the input and response parameters are assumed to be deterministic. A listing of the computer program corresponding to the deterministic case can be found in reference [85].

7. RESULTS AND DISCUSSION

7.1 Introduction

Using the analytical model constructed in Chapter 6, results for the response of straight jointed buried pipelines to seismic waves are obtained. The cases considered include three types of ground excitation (i.e. loading cases), two pipeline systems and three pipe sizes. The first type of ground excitation corresponds to a tensile ground strain, the second is a compressive ground strain and the the third is a combination of tensile ground strain and ground rotation (see section 3.4). The pipeline systems, on the other hand, are cast iron pipe with lead caulked joint and ductile iron pipe with rubber gasketed joint. Finally, the pipe sizes are 16, 30 and 48 inch (40.64, 76.20 and 121.92 cm) nominal diameter.

First, the data describing the pipeline model for these cases are given. Second, results from a sensitivity analysis which quantifies the effects of joint and soil variability on the response parameters such as the displacement at joints, are presented. Following, a simplified Monte Carlo simulation technique is used to generate vulnerability graphs giving the probability of exceedence for various values of the response parameters as a function of ground excitation. Emphasis is placed on joint displacement and force since damage usually occurs at the joints. Results for the pipe segment axial strain, and the axial and lateral relative displacements between the soil and the pipeline are also obtained. Finally, the generated vulnerability graphs are combined with the information on leakage of lead caulked joints presented in section 4.2.2.1 to predict the damage ratio due to a joint pull-out failure mode (i.e. tensile ground strain loading case).

It should be mentioned that the data and results are given only in SI units. Conversion to the U.S. customary units can be done using the factors presented in Appendix B.

7.2 Data

The data needed to get results for the different cases considered herein, include values of the mechanical properties of the pipeline and soil restraint as well as values of certain modelling characteristics such as number of elements used to discretize a pipe segment. The mechanical properties of the pipeline are evaluated according to the procedure presented in section 4.4, while those of the soil restraint are evaluated according to the procedure presented in section 5.4. On the other hand, the modelling characteristics are selected in a manner such that they yield consistent results.

7.2.1 Pipeline Properties

7.2.1.1 Cast Iron Pipes with Lead Caulked Joints

The characteristics of the stress/strain relationship for cast iron were presented in section 4.2.1. Values of the pipe outside diameter, D, wall thickness, t, depth of cover, c, cross-sectional area, A, and transverse moment of inertia, I, as a function of the pipe nominal diameter, D_n, are given in Table 7-I. The pipe segment length, L, is taken as 6 m.

Tables 7-II and 7-III gives respectively the mean values of the characteristics of the force/displacement relationship and those of the bending moment/rotation relationship for lead caulked joints. Based on the test results presented in section 4.2.2, the coefficient of variation of each of those characteristics is taken as 30%. The joint axial stiffness after contact in compression, $AK_j^{(3)}$, is assigned a very high numerical value of 1.0×10^9 Kgf/cm. Numerical testing shows that a value of this order simulates the locking behavior of the joint after contact between the two adjoining pipe segments.

7.2.1.2 Ductile Iron Pipes with Rubber Gasketed Joints

The stress/strain relationship for ductile iron was fully defined in section 4.3.1. The geometric properties of the pipe segment for each of the pipe sizes considered are given in Table 7-IV. As with the cast iron system, the pipe segment length, L, is taken as 6 m.

Table 7-V presents values of the diameter of the "main body" of the rubber gasket before installation, A_g, for pipe sizes considered herein. The corresponding mean values of the characteristics of the axial force/displacement relationship and those of the bending moment/rotation relationship for rubber gasketed joints are given respectively in Tables 7-VI and 7-VII. As with the cast iron with lead caulked joint system, the coefficient of variation of each of those characteristics is taken as 30%. For this system, the joint axial stiffness after contact, $AK_j^{(3)}$ is taken equal to 1.7×10^9 Kgf/cm. Note that since $AK_j^{(3)}$ is a function of the pipe material stiffness, the ratio between the joint axial stiffnesses after contact for both systems is equal to the ratio between the corresponding Young's moduli of the materials.

7.2.2 Soil Properties

The mean values of the unit weight, γ, angle of shearing resistance, ϕ, relative density, D_r, and coefficient of lateral earthpressure, K_o, for the soil surrounding the model are equal to:

Table 7-I

Pipe Segment Geometric Properties for Cast Iron Pipes

(See Figure 2.1 for Nomenclature)

D_n	D	t	c	A	I
cm	cm	cm	cm	cm^2	cm^4
40.64	44.20	1.27	105.00	174.00	39.50×10^3
76.20	81.30	2.16	152.00	537.00	42.03×10^4
121.92	129.00	3.12	152.00	1251.00	24.50×10^5

Table 7-II

Mean Values of the Axial Force/Displacement Relationship Characteristics for Lead Caulked Joints

(See Figure 4.4 for Nomenclature)

D_n	F_j^s	u_j^s	u_j^c	u_j^u
cm	Kgf	cm	cm	cm
40.64	14.00×10^{3}	0.38×10^{-3}	0.25	5.10
76.20	26.00×10^{3}	0.38×10^{-3}	0.25	5.70
121.92	41.00×10^{3}	0.38×10^{-3}	0.25	6.30

Table 7-III

Mean Values of the Bending Moment/Rotation Relationship Characteristics for Lead Caulked Joints

(See Figure 4.8 for Nomenclature)

D_n	M_j^s	θ_j^s	θ_j^u
cm	Kgf.cm	rad	rad
40.64	44.60×10^{4}	5.50×10^{-3}	5.72×10^{-2}
76.20	10.30×10^{5}	5.50×10^{-3}	1.08×10^{-1}
121.92	19.40×10^{5}	5.50×10^{-3}	1.75×10^{-1}

Table 7-IV

Pipe Segment Geometric Properties for Ductile Iron Pipes

(See Figure 2.1 for Nomenclature)

D_n	D	t	c	A	I
cm	cm	cm	cm	cm^2	cm^4
40.64	44.20	0.86	105.00	119.00	27.60×10^3
76.20	81.30	1.20	152.00	300.30	24.10×10^4
121.92	129.00	1.83	152.00	730.80	14.80×10^5

Table 7-V

Values of the Diameter of the "Main Body" of the Rubber Gasket before Installation

(See Figure 4.11 for Nomenclature)

D_n	A_g
cm	cm
40.64	2.30
76.20	2.80
121.92	3.30

Table 7-VI

Mean Values of the Axial Force/Displacement Relationship Characteristics for Rubber Gasketed Joints

(See Figure 4.13 for Nomenclature)

D_n	$F_j^{s(*)}$	u_j^s	u_j^c	u_j^u
cm	Kgf	cm	cm	cm
40.64	290.00	0.34	0.76	3.05
76.20	650.00	0.24	0.76	3.80
121.92	1220.00	0.20	0.76	4.60

(*) $F_j^s = F_j^u$

Table 7-VII

Mean Values of the Bending Moment/Rotation Relationship Characteristics for Rubber Gasketed Joints

(See Figure 4.8 for Nomenclature)

D_n	M_j^s	θ_j^s	θ_j^u
cm	Kgf.cm	rad	rad
40.64	27.80×10^2	5.10×10^{-3}	7.00×10^{-2}
76.20	17.30×10^3	5.10×10^{-3}	7.00×10^{-2}
121.92	69.20×10^3	5.10×10^{-3}	7.00×10^{-2}

γ = 1.90×10^{-3} Kgf/cm^3 (119 pcf)

ϕ = 34° (0.59 rad)

D_r = 50%

K_o = 0.85

Using Eqn.(5.2), the mean value of the coefficient of friction at or near the soil/pipeline interface, μ_s = 0.9 tan(34°) = 0.6. In order to evaluate the shear modulus coefficient, K_2, one needs a value for the relative axial displacement at which the slope of the (f_x,Δu) curve starts decreasing appreciably, $\overline{\Delta u}$. Based on the results presented in sectio 5.2.2, it is taken equal to 0.05 cm (i.e. $\overline{\Delta u}$ = 0.05 cm). Table 7-VIII gives the mean values of the shear modulus coefficient, K_2, ultimate relative lateral displacement between the soil and the pipeline, Δw^u, and horizontal bearing capacity coefficient, N_{qh}, for each of the pipe sizes considered. A constant coefficient of variation is chosen for the five parameters: γ, μ_s, K_o, K_2 and N_{qh}. It is equal to 30%. Table 7-IX gives values for the axial and lateral force per unit length/displacement characteristics for the soil spring-sliders, corresponding to the mean values of γ, μ_s, K_o, K_2 and N_{qh}.

7.2.3 Modelling Characteristics

The modelling characteristics, which include the number of pipe segments in the model, n_s, number of elements per pipe segment, n_e, number of ground displacements increments used to get the solution in the inelastic range, N, and number of times the model is simulated, n_{sim}, need to be selected carefully.

The number of pipe segments in the model is taken equal to 10 (i.e. n_s = 10). This implies a model with total length, L_{pm}, equal to 60 m. Note also that the boundary conditions used, duplicate the model beyond the length considered.

The selection of the values of n_e, N and n_{sim} is, however, dictated by the requirements of desired accuracy for the results as well as by the constraints of computer storage capacity and time. In order to observe the influence of the two parameters n_e and N on the response parameters, a preliminary study is performed on the 76.20 cm diameter pipeline for both systems considered. In this study, the joint and soil properties are assumed to be deterministic and uniform along the model. These properties are equal to the corresponding mean values given in the previous sections. Table 7-X shows the results obtained under a uniform tensile ground strain equal to 5.0×10^{-3} (i.e. ϵ_g = 5.0×10^{-3} and θ_g = 0), for different values of n_e and N. It should be mentioned that for a ground strain of this magnitude, the system enters the inelastic range. The parameter I_T denotes the type of pipeline system as given by Eqn.(6.79). The terms u_j, ϵ^{max} and Δu^{max} represent respectively the joint axial displacement, maximum pipe segment axial

Table 7-VIII

Mean Values of the Shear Modulus Coefficient, K_2, the Ultimate Lateral Relative Displacement, Δw^u, and Horizontal Bearing Capacity Coefficient, N_{qh}

D_n cm	K_2	Δw^u cm	N_{qh}
40.64	7.00	6.10	6.80
76.20	11.30	9.40	6.00
121.92	15.70	11.20	5.50

Table 7-IX

Mean Values of the Characteristics of the Axial and Lateral Force per Unit Length/Displacement Relationships for the Soil Spring-Sliders

(See Figure 5.2 for Nomenclature)

D_n	f_x^u	k_x	f_z^u	k_z
cm	Kgf/cm	Kgf/cm^2	Kgf/cm	kgf/cm^2
40.64	19.00	150.00	75.00	80.00
76.20	51.20	280.00	180.00	130.00
121.92	94.00	420.00	300.00	180.00

Table 7-X

Influence of n_e and N on the Response Parameters under a Tensile Ground Strain, $\epsilon_g = 5.0 \times 10^{-3}$ (D_n = 76.20 cm)

I_T (*)	n_e	N	u_j	ϵ^{max}	Δu^{max}
			cm	%	cm
1	3	10	2.95	0.93×10^{-2}	0.98
1	5	20	2.95	0.95×10^{-2}	1.18
1	11	100	2.95	1.0×10^{-2}	1.34
1	19	100	2.95	1.0×10^{-2}	1.40
1	31	200	2.95	1.00×10^{-2}	1.43
2	3	10	2.99	0.19×10^{-2}	0.99
2	5	20	2.99	0.25×10^{-2}	1.20
2	11	100	2.99	0.28×10^{-2}	1.36
2	19	100	2.99	0.29×10^{-2}	1.41
2	31	200	2.99	0.29×10^{-2}	1.45

(*)

$I_T = 1$ → Cast Iron System

$I_T = 2$ → Ductile Iron System

strain and maximum relative axial displacement between the soil and the pipeline. Notice that values of u_j, ϵ^{max} and Δu^{max} do not change significantly when $n_e \geq 19$ and $N \geq 101$ for the cast iron pipe with lead caulked joint system. The same conclusion applies to the ductile iron pipe with rubber gasketed joint system when $n_e \geq 5$ and $N \geq 21$. Hence, under a tensile ground strain, the parameters n_e and N are selected as follows:

$$(n_e, N) = \begin{cases} (19,101) & \text{; for cast iron pipe with lead caulked joint} \\ (5,21) & \text{; for ductile iron pipe with rubber gasketed joint} \end{cases} \quad (7.1)$$

Table 7-XI, on the other hand, gives the response parameters when the model is subjected to a uniform compressive ground strain with magnitude, $\epsilon_g = 5.0 \times 10^{-3}$. Under such ground strain, contact between adjacent pipe segments occurs. The resulting locking behavior of the joints can be characterized with high values of n_e and N. Based on the results shown in Table 7-XI, the parameters n_e and N in this case (i.e. uniform compressive ground strain), are taken equal to:

$$(n_e, N) = \begin{cases} (31,201) & \text{; for cast iron pipe with lead caulked joint} \\ (11,101) & \text{; for ductile iron pipe with rubber gasketed joint} \end{cases} \quad (7.2)$$

For the third type of ground excitation which is a combination of tensile ground strain and ground rotation, similar results show that the parameters n_e and N can be selected according to Eqn.(7.1). Notice that for all three types of ground excitation, the values of n_e and N selected for the cast iron system with lead caulked joint are much larger than those selected for the ductile iron system with rubber gasketed joint. Lead caulked joints are much stiffer than rubber gasketed joints and therefore require larger number of elements and larger number of load increments to achieve convergence.

Finally, the parameter n_{sim} is taken equal to 100. Since the number of joints in the model is equal to 11, the population for each of the joint response parameters contains 1100 values. The response parameters of the pipe segments and soil spring-sliders used in the statistical analysis are limited to the maximum values along each pipe segment. Hence, the population for each of the pipe segment or soil spring-sliders response parameters has 1000 values.

Table 7-XI

Influence of n_e and N on the Response Parameters under a Compressive Ground Strain, $\epsilon_g = 5.0 \times 10^{-3}$ (D_n = 76.20 cm)

I_T (*)	n_e	N	u_j	ϵ^{max}	Δu^{max}
			cm	%	cm
1	3	10	0.38×10^{-3}	0.55	1.40
1	5	20	0.15	0.48	0.10
1	11	100	0.23	0.46	0.13
1	19	100	0.23	0.46	0.15
1	31	200	0.25	0.45	0.17
2	3	10	0.24	0.46	0.08
2	5	20	0.65	0.39	0.26
2	11	100	0.73	0.53	0.35
2	19	100	0.73	0.59	0.40
2	31	200	0.74	0.52	0.34

(*)

$I_T = 1$ ➔ Cast Iron System

$I_T = 2$ ➔ Ductile Iron System

7.3 Sensitivity Analysis

In order to have a good understanding of pipeline response to seismic waves, a sensitivity analysis is performed. In this analysis, the system characteristics (i.e. pipe segment, joint and soil properties) are assumed to be deterministic. For each of the cases considered, results are first obtained for systems in which the joint and soil properties are uniform along the model. This enables one to study the effects of different properties on the response parameters. Second, systems with non-uniform joint and soil properties are analysed. Results obtained highlight the effect of variable system characteristics upon pipeline response.

7.3.1 Tensile Ground Strain

In this section, the two pipeline systems are subjected to a range of tensile ground strain, $1.0\times10^{-4} \leq \epsilon_g \leq 7.0\times10^{-3}$. That is, the pipeline model is subjected to the axial ground displacement given by Eqn.(3.5) with the (+) sign. For a straight jointed buried pipeline subjected to seismic wave propagation, axial ground strain is accomodated by a combination of pipe segment axial strain and joint axial displacement. For a uniform system (i.e. same pipe segment, joint and soil properties along the model), the axial ground strain, ϵ_g, the joint axial displacement, u_j, and the pipe segment axial strain, ϵ, are related by:

$$\epsilon_g \cdot L = u_j + \epsilon^{ave} \cdot L \tag{7.3}$$

where ϵ^{ave} is the average axial strain along a pipe segment and L is the length of each pipe segment. Observations of actual behavior of pipelines during the 1978 Myiagi-Oki earthquake, support Eqn.(7.3) [86]. For a system with non uniform properties, Eqn.(7.3) becomes:

$$\epsilon_g \cdot L_{pm} = \sum_{i=1}^{11} u_j^i + \sum_{i=1}^{10} \epsilon^{ave,i} \cdot L \tag{7.4}$$

where u_j^i is the axial displacement of joint i and $\epsilon^{ave,i}$ is the average axial strain along pipe segment i.

First, the joint and soil properties are assumed to be uniform along the model and equal to the mean values given in section 7.2. The results are summarized in Table 7-XII for cast iron pipe with lead caulked joint and in Table 7-XIII for ductile iron pipe with rubber gasketed joint. As one might expect, the joint axial displacement, u_j, is constant for all joints along the model. The pipe segment axial strain, ϵ, varies along each pipe segment, with the maximum value occuring in the middle. The relative axial displacement between the soil and the pipeline, Δu, follows what

Table 7-XII

Results for Uniform Cast Iron System with Mean Properties under Tensile Ground Strain

D_n	ϵ_g	u_j	ϵ^{max}	Δu^{max}
cm	%	cm	%	cm
40.64	1.0×10^{-2}	0.01	0.81×10^{-2}	0.54×10^{-2}
40.64	7.0×10^{-2}	0.36	1.07×10^{-2}	0.17
40.64	1.0×10^{-1}	0.54	1.13×10^{-2}	0.25
40.64	7.0×10^{-1}	4.10	1.75×10^{-2}	1.94
76.20	1.0×10^{-2}	0.03	0.50×10^{-2}	0.01
76.20	7.0×10^{-2}	0.38	0.66×10^{-2}	0.18
76.20	1.0×10^{-1}	0.56	0.72×10^{-2}	0.26
76.20	7.0×10^{-1}	4.14	1.10×10^{-2}	1.96
121.92	1.0×10^{-2}	0.04	0.34×10^{-2}	0.02
121.92	7.0×10^{-2}	0.39	0.45×10^{-2}	0.19
121.92	1.0×10^{-1}	0.57	0.50×10^{-2}	0.27
121.92	7.0×10^{-1}	4.16	0.75×10^{-2}	1.97

Table 7-XIII

Results for Uniform Ductile Iron System with Mean Properties under Tensile Ground Strain

D_n	ϵ_g	u_j	ϵ^{max}	Δu^{max}
cm	%	cm	%	cm
40.64	1.0×10^{-2}	0.058	0.33×10^{-3}	0.02
40.64	7.0×10^{-2}	0.41	0.20×10^{-2}	0.16
40.64	1.0×10^{-1}	0.59	0.23×10^{-2}	0.24
40.64	7.0×10^{-1}	4.20	$0.21\times10^{-2(*)}$	1.70
76.20	1.0×10^{-2}	0.058	0.26×10^{-3}	0.02
76.20	7.0×10^{-2}	0.41	0.17×10^{-2}	0.16
76.20	1.0×10^{-1}	0.59	0.21×10^{-2}	0.24
76.20	7.0×10^{-1}	4.19	0.23×10^{-2}	1.70
121.92	1.0×10^{-2}	0.059	0.17×10^{-3}	0.02
121.92	7.0×10^{-2}	0.41	0.11×10^{-2}	0.16
121.92	1.0×10^{-1}	0.59	0.15×10^{-2}	0.24
121.92	7.0×10^{-1}	4.19	$0.15\times10^{-2(*)}$	1.70

(*) value increases when N is increased

appears to be a linear function along each pipe segment. The maximum value of Δu occurs near the joints (i.e. at both ends of the pipe segments). From Tables 7-XII and 7-XIII, it can be seen that except for low values of ground strain, u_j is practically independant of the pipe size for both systems studied. The same conclusion applies to Δu^{max}. Values of u_j obtained for the cast iron system are slightly smaller than those obtained for the ductile iron system. Conversely, values of Δu^{max} corresponding to the cast iron sytem are slightly larger than those corresponding to the ductile iron system. Figures 7-1, 7-2, 7-3, 7-4, 7-5 and 7-6 plot in doted line u_j versus ϵ_g for the uniform systems with mean properties. Observe that u_j is almost a linear function of ϵ_g, for the ductile iron system. For the cast iron system, the nonlinearity of u_j versus ϵ_g is somewhat more pronounced. Since in both cases the joint behavior becomes nonlinear, this suggests that the joint axial stiffness plays a more important role for the cast iron system than for the ductile iron system. It should be mentioned also that at $\epsilon_g = 5.0\times10^{-3}$, u_j reaches values which are of the same order of magnitude as the ultimate joint axial displacement, u_j^u, for both systems.

The maximum pipe segment axial strain, ϵ^{max}, remains in the elastic range for both systems (i.e. $\epsilon^{max} < \epsilon^y$). However, values of ϵ^{max} are much larger for the cast iron system than for the ductile iron system. This is due to the fact that rubber gasketed joints are more flexible than lead caulked joints. Note in Tables 7-II and 7-III that the initial axial stiffness of lead caulked joint, F_j^s/u_j^s, is roughly 4 orders of magnitude larger than the value for the same diameter rubber gasketed joint.

Notice also, that ϵ^{max} is a decreasing function of the pipe diameter. The value of ϵ^{max} is related to the joint axial force, F_j, and the axial soil retraint, f_x. However, F_j and f_x themselves do not vary significantly after slippage of both the joint and soil spring-slider occurs. Consequently, the rate of increase of ϵ^{max} is much smaller than that of ϵ_g for both sytems. It should be mentioned that at axial ground strain, $\epsilon_g \geq 7.0\times10^{-4}$, the joint axial force for the cast iron system, F_j, is roughly two times the axial soil restraint force over a half pipe segment. On the other hand, for the same range of axial ground strain (i.e. $\epsilon_g \geq 7.0\times10^{-4}$), the joint axial force for the ductile iron system, F_j, represents roughly 5% of the axial soil restraint over a half pipe segment.

Second, effects of joint and soil properties on uniform systems are considered. Results corresponding to the two systems for four different cases of a 76.20 cm diameter pipeline, are presented in Tables 7-XIV and 7-XV. In case I, the soil properties are equal to the mean values while the joint properties are taken as follows:

- For cast iron system:

$F_j^s = 34.00\times10^3$ Kgf

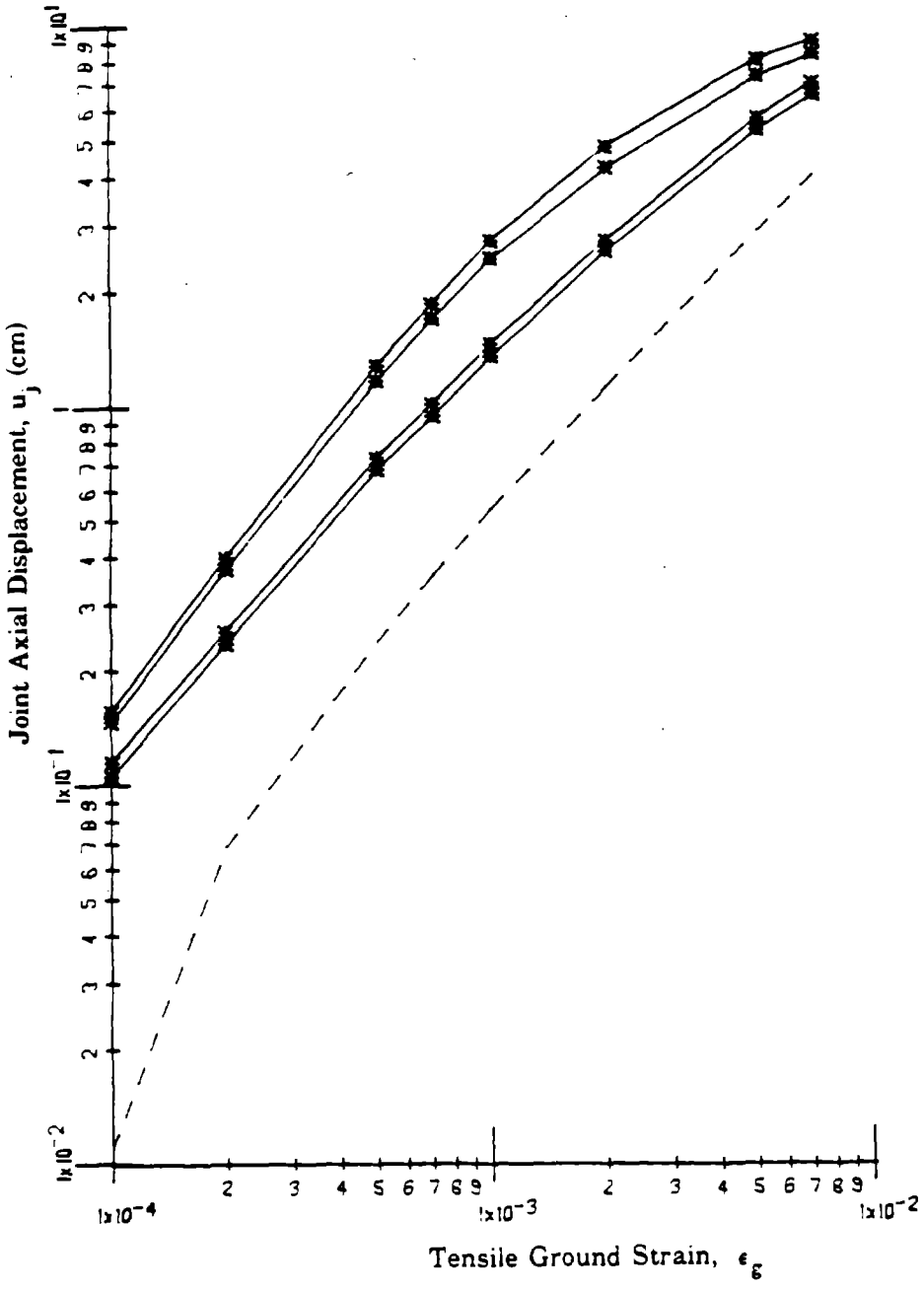

Figure 7-1. Joint Axial Displacement, u_j, for a 40.64 cm Diameter Cast Iron Pipe with Lead Caulked Joint versus Tensile Ground Strain, ϵ_g, for Various Exceedence Probabilities

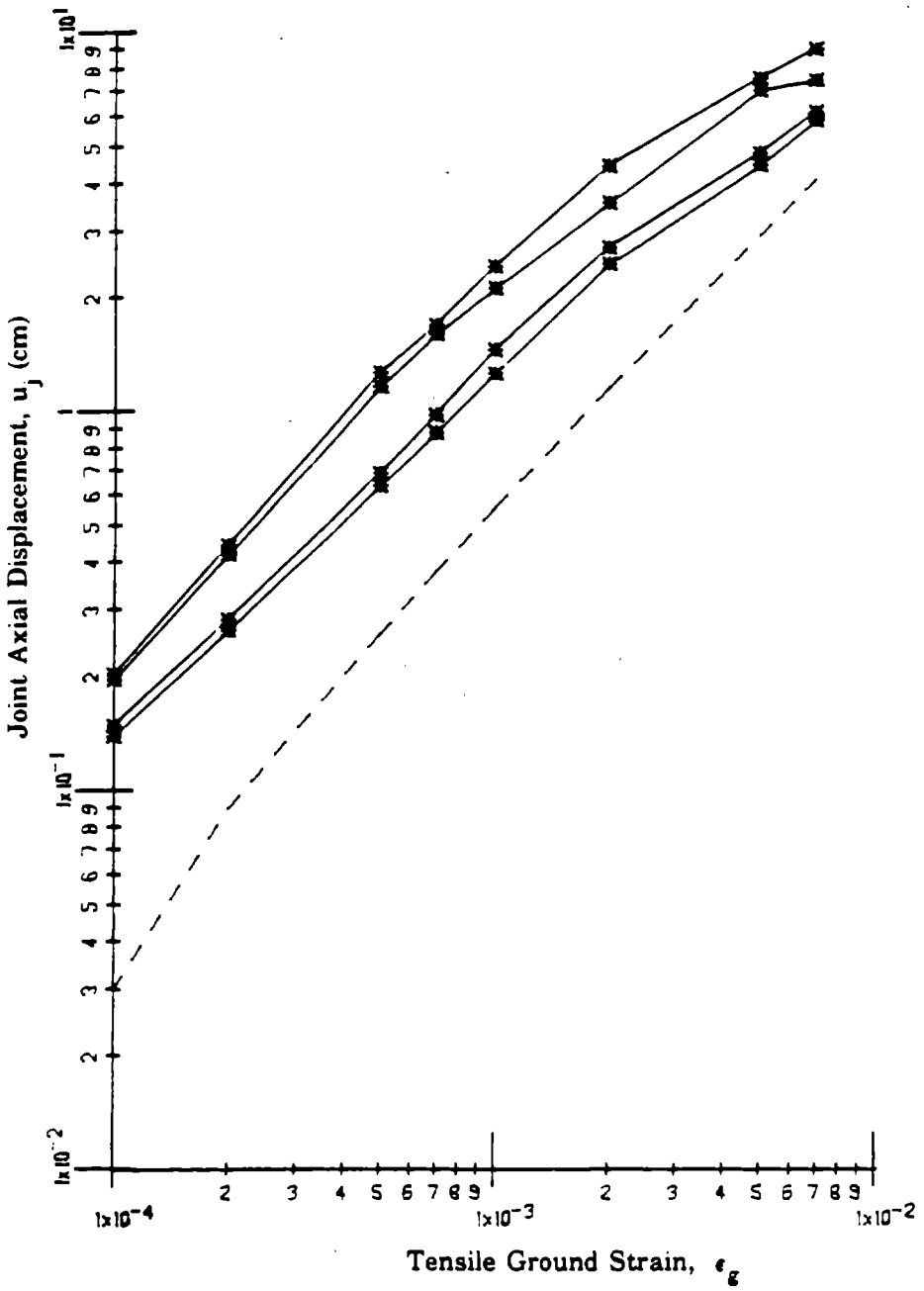

Figure 7-2. Joint Axial Displacement, u_j, for a 76.20 cm Diameter Cast Iron Pipe with Lead Caulked Joint versus the Tensile Ground Strain, ϵ_g, for Various Exceedence Probabilities

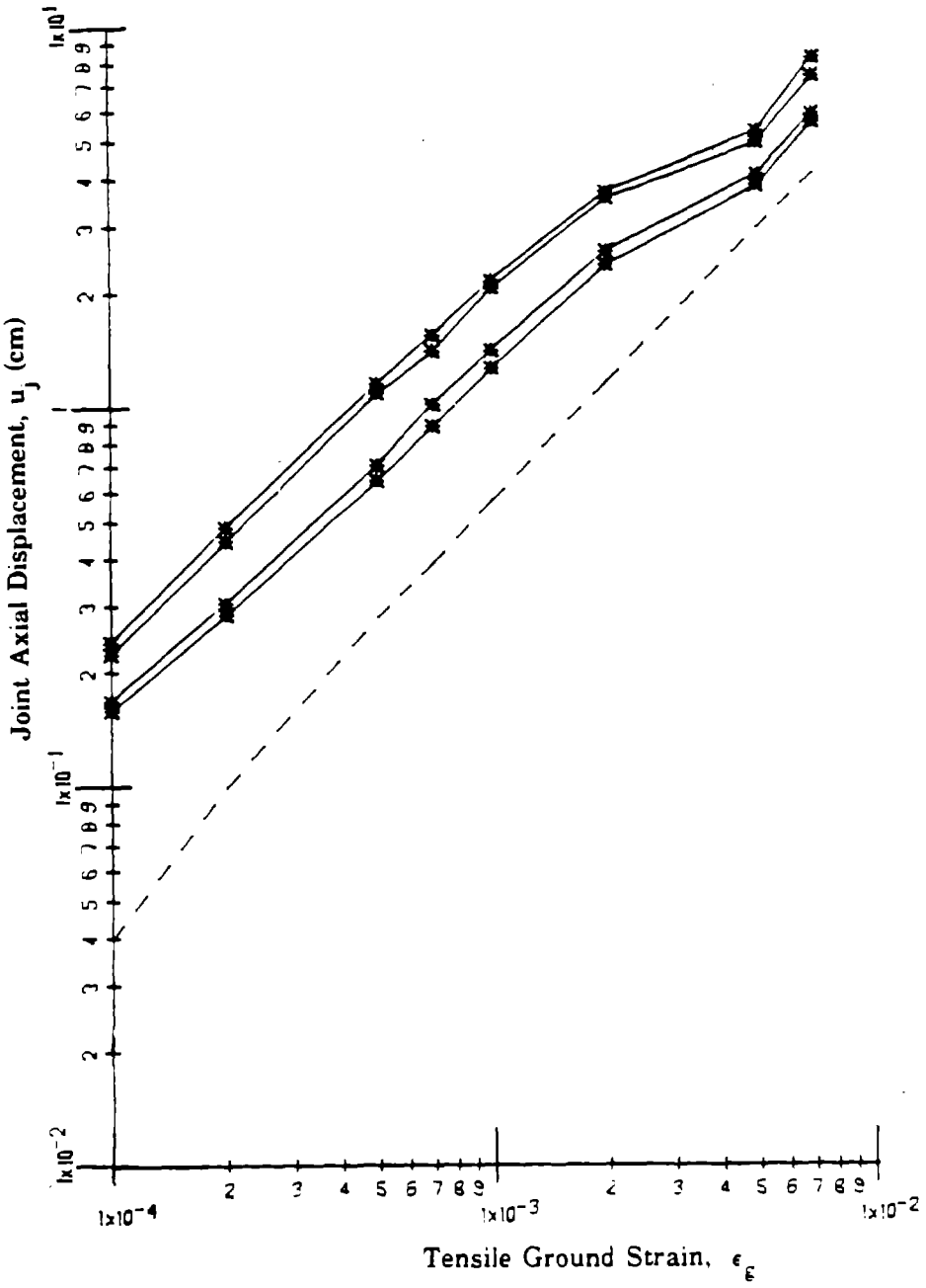

Figure 7-3. Joint Axial Displacement, u_j, for a 121.92 cm Diameter Cast Iron Pipe with Lead Caulked Joint versus Tensile Ground Strain, ϵ_g, for Various Exceedence Probabilities

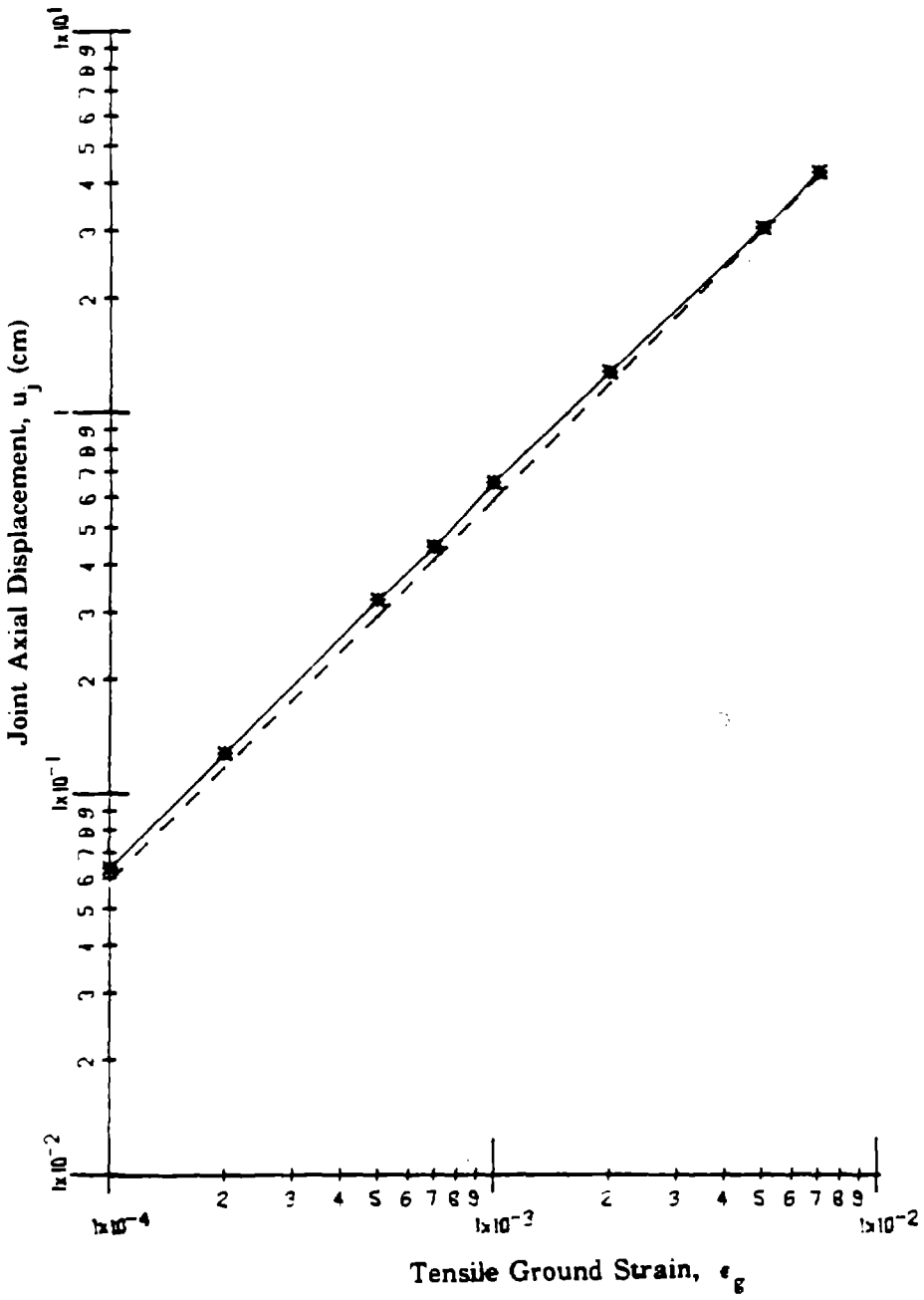

Figure 7-4. Maximum and Average Joint Axial Displacement, u_j, for a 40.64 cm Diameter Ductile Iron Pipe with Rubber Gasketed Joint versus Tensile Ground Strain, ϵ_g

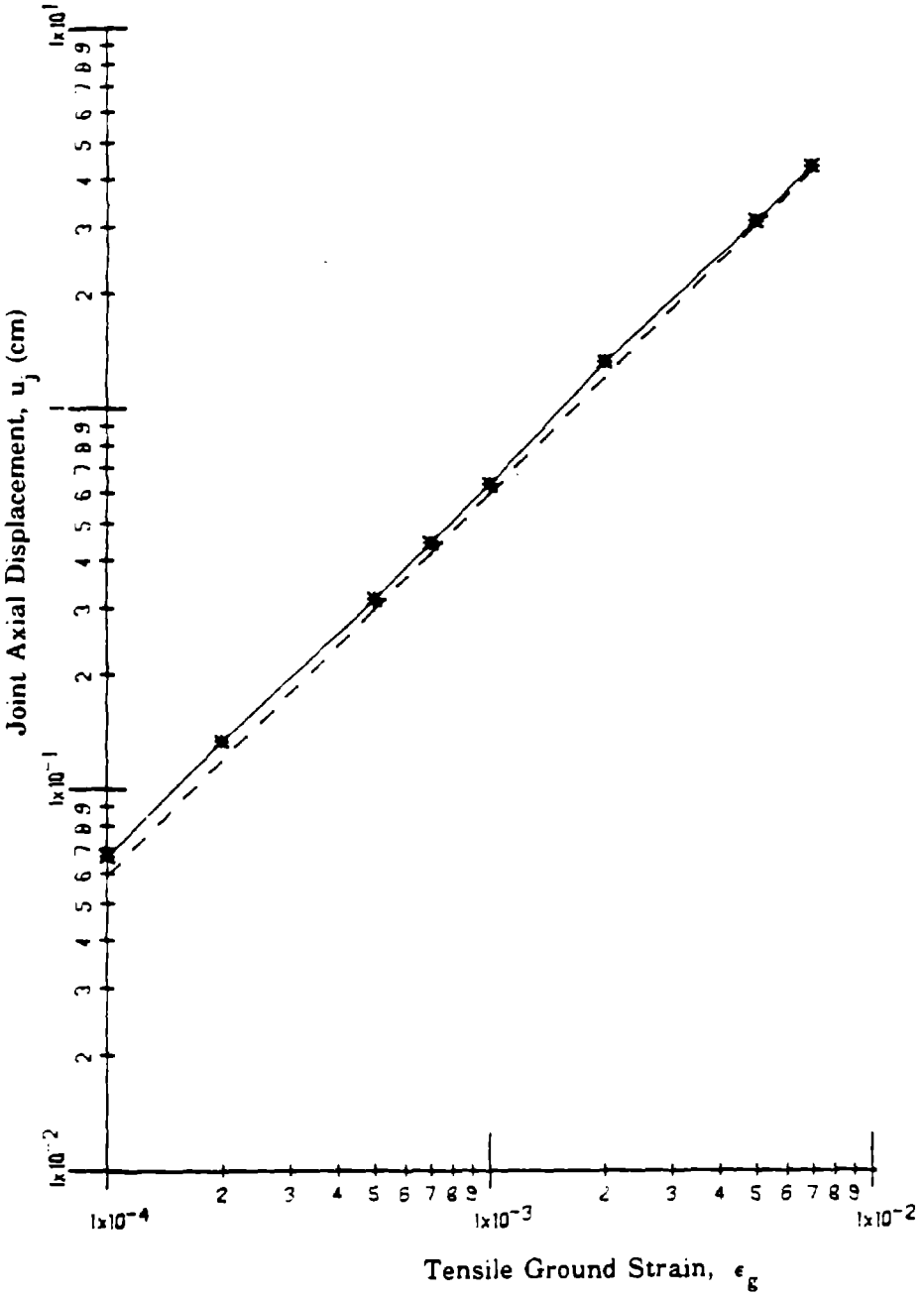

Figure 7-5. Maximum and Average Joint Axial Displacement, u_j, for a 76.20 cm Diameter Ductile Iron Pipe with Rubber Gasketed Joint versus Tensile Ground Strain, ϵ_g

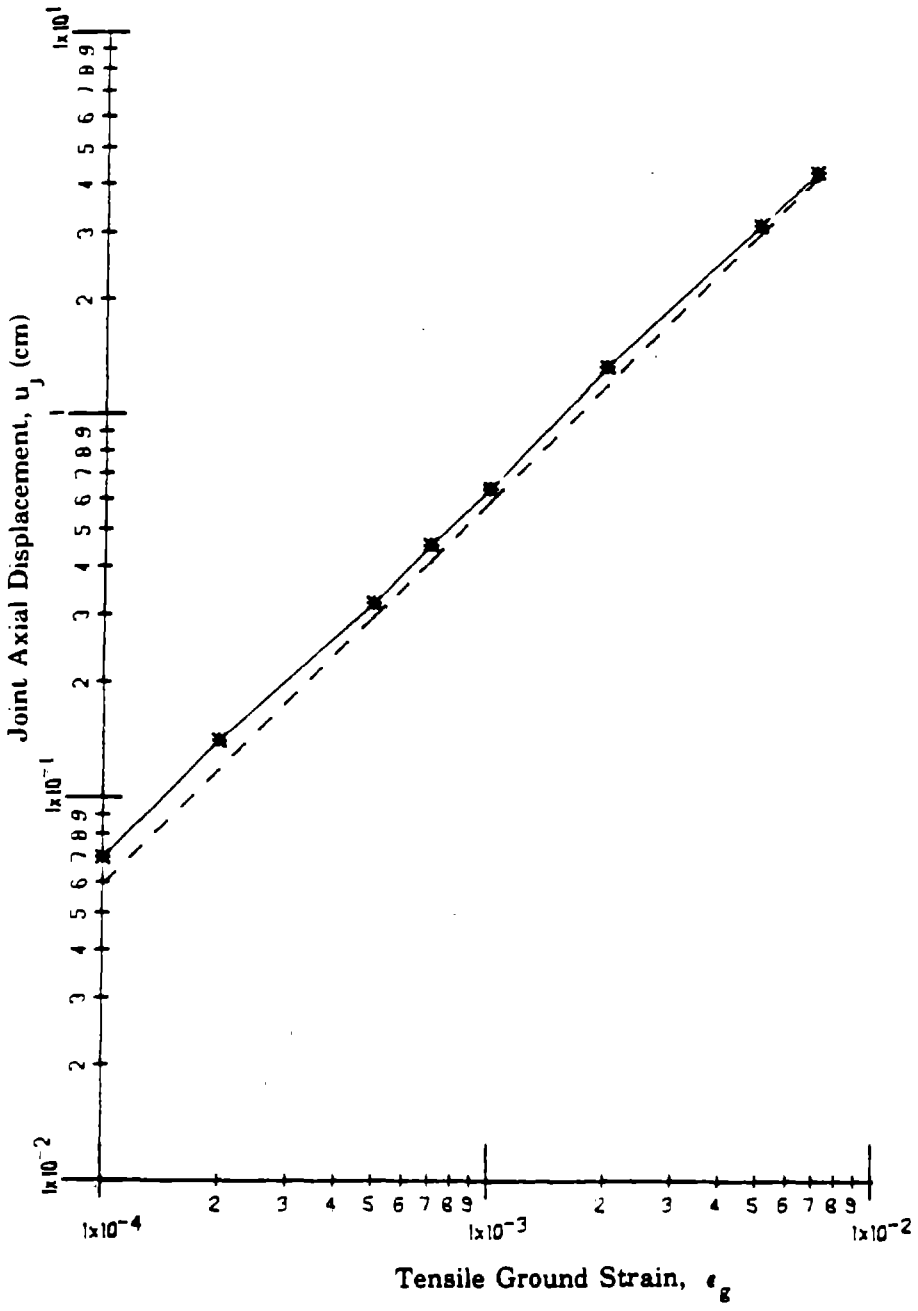

Figure 7-6. Maximum and Average Joint Axial Displacement, u_j, for a 121.92 cm Diameter Ductile Iron Pipe with Rubber Gasketed Joint versus Tensile Ground Strain, ϵ_g

Table 7-XIV

Efffects of Joint and Soil Stiffnesses on Uniform Cast Iron System under Tensile Ground Strain (D_n = 76.20 cm)

Case	ϵ_g	u_j	ϵ^{max}	Δu^{max}
	%	cm	%	cm
I-System with all Stiff Joints	1.0×10^{-2}	0.02	0.64×10^{-3}	0.01
	7.0×10^{-2}	0.37	0.82×10^{-2}	0.18
	1.0×10^{-1}	0.55	0.88×10^{-2}	0.26
	7.0×10^{-1}	4.12	1.36×10^{-2}	1.90
II-System with all Flexible Joints	1.0×10^{-2}	0.04	0.35×10^{-3}	0.02
	7.0×10^{-2}	0.39	0.51×10^{-2}	0.18
	1.0×10^{-1}	0.57	0.56×10^{-2}	0.27
	7.0×10^{-1}	4.16	0.84×10^{-2}	2.00
III-System with all Stiff Soil Spring-Sliders	1.0×10^{-2}	0.03	0.51×10^{-3}	0.01
	7.0×10^{-2}	0.38	0.80×10^{-2}	0.18
	1.0×10^{-1}	0.55	0.87×10^{-2}	0.26
	7.0×10^{-1}	4.13	1.12×10^{-2}	2.00
IV-System with all Flexible Soil Spring-Sliders	1.0×10^{-2}	0.03	0.50×10^{-3}	0.01
	7.0×10^{-2}	0.38	0.61×10^{-2}	0.18
	1.0×10^{-1}	0.56	0.66×10^{-2}	0.27
	7.0×10^{-1}	4.14	1.03×10^{-2}	2.00

Table 7-XV

Effects of Joint and Soil Stiffnesses on Uniform Ductile Iron System under Tensile Ground Strain (D_n = 76.20 cm)

Case	ϵ_g	u_j	ϵ^{max}	Δu^{max}
	%	cm	%	cm
I-System with all Stiff Joints	1.0×10^{-2}	0.058	0.29×10^{-3}	0.02
	7.0×10^{-2}	0.41	0.18×10^{-2}	0.16
	1.0×10^{-1}	0.59	0.21×10^{-2}	0.24
	7.0×10^{-1}	4.19	0.21×10^{-2}	1.70
II-System with all Flexible Joints	1.0×10^{-2}	0.059	0.25×10^{-3}	0.02
	7.0×10^{-2}	0.41	0.17×10^{-2}	0.16
	1.0×10^{-1}	0.59	0.20×10^{-2}	0.24
	7.0×10^{-1}	4.19	0.21×10^{-2}	1.70
III-System with all Stiff Soil Spring-Sliders	1.0×10^{-2}	0.058	0.52×10^{-3}	0.02
	7.0×10^{-2}	0.41	0.31×10^{-2}	0.16
	1.0×10^{-1}	0.59	0.36×10^{-2}	0.23
	7.0×10^{-1}	4.19	0.32×10^{-2}	1.70
IV-Sytem with all Flexible Soil Spring-Sliders	1.0×10^{-2}	0.059	0.17×10^{-3}	0.02
	7.0×10^{-2}	0.41	0.11×10^{-2}	0.17
	1.0×10^{-1}	0.59	0.15×10^{-2}	0.24
	7.0×10^{-1}	4.19	0.16×10^{-2}	1.70

$u_j^s = 0.27 \times 10^{-3}$ cm

- For ductile iron system:

$F_j^u = 845.00$ Kgf

$u_j^s = 0.17$ cm

These joint properties yield an initial joint axial stiffness, AK_j, which is towards the high end of the range of available tests. The resulting initial joint axial stiffness for each of the two systems is equal to 1.84 times the mean initial joint axial stiffness.

In case II, the soil properties are also equal to the mean values while the joint properties are taken as follows:

- For cast iron system:

$F_j^s = 18.00 \times 10^3$ Kgf

$u_j^s = 0.50 \times 10^{-3}$ cm

- For ductile iron system:

$F_j^u = 455.00$ Kgf

$u_j^s = 0.31$ cm

These joint properties yield an initial joint axial stiffness, AK_j, which is towards the low end of the range of available tests. The resulting joint stiffness for each of the two systems is equal to 0.54 times the mean initial joint axial stiffness.

Cases III and IV are uniform systems with mean joint properties, and soil properties corresponding respectively to high and low ends of available tests. In case III, the soil properties are given by:

$f_x^u = 80.30$ Kgf/cm

$k_x = 600.00$ Kgf/cm^2

while in case IV, they are equal to:

$f_x^u = 38.20$ Kgf/cm

$k_x = 170.00$ Kgf/cm^2

Results obtained for these four cases are compared with those obtained in the case where the joint and soil properties are all equal to their mean values. As shown in Tables 7-XIV and 7-XV, the joint axial displacement, u_j, and the maximum relative axial displacement between the soil and pipeline, Δu^{max}, are not affected by the uniform variation of the joint or soil properties. On the other hand, the pipe segment axial strain, ϵ^{max}, changes slightly. The value of ϵ^{max} is an increasing function of the initial joint axial stiffness, AK_j, and is also an increasing function of the initial axial soil spring stiffness, k_x. Notice, however, that ϵ^{max} for cast iron system is more influenced by variation in joint stiffness (cases I and II), while ϵ^{max} for ductile iron system is more sensitive to variation in soil stiffness (cases III and IV). It is clear from the above that for

tensile ground strain, the most important response parameter, u_j, is not significantly affected by the magnitude of the joint or soil properties as long as these properties are uniform over the model.

All the results obtained for uniform systems (i.e. Tables 7-XII, 7-XIII, 7-XIV and 7-XV), satisfy Eqn.(7.3). Note that, Wang et al.[15] and Wang[25] studied the effect of joint stiffness on the response of uniform systems. The conclusions of these two studies [15,25] are consistent with results of the present study. That is, Wang et al.[15] and Wang[25] found that the pipe segment axial strain is an increasing function of the joint stiffness. Also, their results show that the joint axial displacement is not sensitive to variation in the joint stiffness, for the range of joint stiffnesses considered in this study. In addition, Wang et al.[87] proposed analytical relationships for the joint axial displacement, u_j, and the maximum pipe segment axial strain, ϵ^{max}, as a function of the axial ground strain, ϵ_g, in the case where the pipe segment material, axial soil restraint and the joint axial stiffnesses are linearly elastic. As one would expect, values of u_j and ϵ^{max} obtained in the present study satisfies Wang et al.'s relationships [87] only for values of axial ground strain producing linear pipeline response.

Tables 7-XVI and 7-XVII present the results for four non-uniform cases of a 76.20 cm diameter pipeline, respectively for the cast iron and ductile iron systems. Case V is identical to the uniform system with mean properties except that the *middle* joint is assigned a high stiffness. The properties of this *middle* joint are equal to those of case I (i.e. an initial joint axial stiffness which is towards the high end of available tests). For case VI, the *middle* joint is assigned a low stiffness. The properties of the *middle* joint in this case are equal to those of case II (i.e. an initial axial joint stiffness which is towards the low end of available tests). For the cast iron system, values of u_j^{max} in both cases V and VI, are larger than those of the uniform case with mean properties. For example, under a ground strain $\epsilon_g = 1.0\times10^{-3}$, u_j is equal to 0.56 cm at all joints for the uniform case with mean properties (see Table 7-XII). In case V, u_j^{max} = 0.62 cm (see Table 7-XVI) and occurs at the two joints adjacent to the middle joint. In case VI, u_j^{max} = 0.72 cm (see Table 7-XVI) and occurs at the middle joint. Values of ϵ^{max} are slightly larger in case V than in case VI, but in both cases ϵ^{max} remains in the elastic range.

For the ductile iron system, values of u_j^{max} obtained for cases V and VI are approximately equal to values of u_j obtained for the uniform case with mean properties. Similarly, values of ϵ^{max} and Δu^{max} in cases V and VI do not change.

Two other cases in which the *soil* properties vary from pipe segment to pipe segment, are also considered. Case VII is identical to the uniform case with mean properties except that the soil spring-sliders characteristics along the middle pipe segment are equal to those of case III. That is the middle pipe segment is surrounded by stiff spring-sliders. In case VIII, the middle pipe

Table 7-XVI

Results for Non-Uniform Cast Iron System under Tensile Ground Strain (D_n = 76.20 cm)

Case	ϵ_g	u_j^{max}	ϵ^{max}	Δu^{max}
	%	cm	%	cm
V-Middle Joint	1.0×10^{-2}	0.04	0.53×10^{-2}	0.03
with High	7.0×10^{-2}	0.43	0.73×10^{-2}	0.23
Stiffness	1.0×10^{-1}	0.62	0.78×10^{-2}	0.33
	7.0×10^{-1}	4.30	1.11×10^{-2}	2.15
VI-Middle Joint	1.0×10^{-2}	0.04	0.50×10^{-2}	0.06
with Low	7.0×10^{-2}	0.49	0.65×10^{-2}	0.23
Stiffness	1.0×10^{-1}	0.71	0.71×10^{-2}	0.34
	7.0×10^{-1}	4.64	0.94×10^{-2}	2.21
VII-Middle Soil	1.0×10^{-2}	0.03	0.51×10^{-2}	0.01
Spring-Sliders	7.0×10^{-2}	0.38	0.80×10^{-2}	0.18
with High	1.0×10^{-1}	0.56	0.87×10^{-2}	0.26
Stiffness	7.0×10^{-1}	4.14	1.24×10^{-2}	1.96
VIII-Middle Soil	1.0×10^{-2}	0.03	0.50×10^{-2}	0.01
Spring-Sliders	7.0×10^{-2}	0.38	0.66×10^{-2}	0.18
with Low	1.0×10^{-1}	0.56	0.72×10^{-2}	0.27
Stiffness	7.0×10^{-1}	4.14	1.10×10^{-2}	1.96

Table 7-XVII

Results for Non-Uniform Ductile Iron System under Tensile Ground Strain

(D_n = 76.20 cm)

Case	ϵ_g	u_j^{max}	ϵ^{max}	Δu^{max}
	%	cm	%	cm
V-Middle Joint	1.0×10^{-2}	0.06	0.27×10^{-3}	0.02
with High	7.0×10^{-2}	0.41	0.18×10^{-2}	0.16
Stiffness	1.0×10^{-1}	0.59	0.21×10^{-2}	0.24
	7.0×10^{-1}	4.19	0.21×10^{-2}	1.70
VI-Middle Joint	1.0×10^{-2}	0.06	0.26×10^{-3}	0.02
with Low	7.0×10^{-2}	0.41	0.17×10^{-2}	0.17
Stiffness	1.0×10^{-1}	0.59	0.21×10^{-2}	0.24
	7.0×10^{-1}	4.19	0.23×10^{-2}	1.70
VII-Middle Soil	1.0×10^{-2}	0.058	0.51×10^{-3}	0.02
Spring-Sliders	7.0×10^{-2}	0.41	0.31×10^{-2}	0.16
with High	1.0×10^{-1}	0.59	0.36×10^{-2}	0.24
Stiffness	7.0×10^{-1}	4.19	0.32×10^{-2}	1.70
VIII-Middle Soil	1.0×10^{-2}	0.059	0.26×10^{-3}	0.02
Spring-Sliders	7.0×10^{-2}	0.41	0.17×10^{-2}	0.16
with Low	1.0×10^{-1}	0.59	0.21×10^{-2}	0.24
Stiffness	7.0×10^{-1}	4.19	0.23×10^{-2}	1.70

segment is surrounded by spring-sliders with characteristics equal to those of case IV (i.e. spring-sliders with low values of f_x^u and k_x). For both systems considered, variation of soil properties in the middle of the model does not affect the joint displacement or the relative axial displacement between the soil and the pipeline. The maximum pipe segment axial strain is more sensitive to the increase in soil spring-sliders stiffness than to its decrease. It remains however in the elastic range (i.e. $\epsilon^{max} < \epsilon^y$).

Eqn.(7.4) holds for all the results obtained for non-uniform systems (i.e. Tables 7-XVI and 7-XVII).

In summary, variations in stiffness from joint to joint result in variations in the maximum joint axial displacement of cast iron system with lead caulked joint. For ductile iron system with rubber gasketed joint, the variation in joint axial displacement is very small. This is due to the relatively low mean value of the initial joint axial stiffness, AK_j, for rubber gasketed joints. For example, a 76.20 cm rubber gasketed joint has $AK_j = 2.70\times10^3$ Kgf/cm, which is about 4 orders of magnitude lower than the value corresponding to lead caulked joint ($AK_j = 6.85\times10^7$ Kgf/cm). Results show also that the joint axial displacement is not significantly affected by variations in soil properties for both systems considered. This suggests that the joint parameter variability is more important than the soil parameter variability for cast iron pipe with lead caulked joint systems. For ductile iron pipe with rubber gasketed joint systems, both the variability of joint properties and that of the soil properties have a small influence on the results.

7.3.2 Compressive Ground Strain

This section presents the results obtained when the model is subjected to compressive ground strain [i.e. Eqn.(3.5) with the (−) sign]. For cast iron system with lead caulked joint, *contact* between pipe segments occurs at compressive ground strains between 5.0×10^{-4} and 7.0×10^{-4}. The corresponding range for ductile iron system with rubber gasketed joint is 1.0×10^{-3} to 2.0×10^{-3}. The range of "contact" ground strain is much lower for the cast iron system because the clearance distance between adjacent pipe segements, u_j^c, is smaller for lead caulked joints than for rubber gasketed joints. At compressive ground strain with magnitude less than those identified above, the system response in tension and in compression are similar. This is due to the fact that the axial force/displacement relationship in compression and in tension, are symmetric before contact between adjacent pipe segments occurs. Moreover, the pipe segment axial strain remains in the elastic range even when contact happens. After contact occurs, the response parameter of interest is the compressive force in the joint, F_j, which is related to the possibility of *crushing* at the pipe segment bell. The range of compressive ground strain

considered herein is $5.0\times10^{-4} \leq \epsilon_g \leq 7.0\times10^{-3}$ for the cast iron system, and $1.0\times10^{-3} \leq \epsilon_g \leq 7.0\times10^{-3}$ for the ductlie iron system.

Results are first obtained for the case where the joint and soil properties are uniform along the model. Table 7-XVIII shows those results for the cast iron system, while Table 7-XIX shows those results for the ductile iron system. The magnitude of the joint axial force, F_j, is larger for the cast iron system than for the ductile system. However, the rate of increase of F_j with respect to ϵ_g is higher for the ductile iron system. This is illustrated in Figures 7-7, 7-8, 7-9, 7-10, 7-11 and 7-12, which plot in doted line the value of F_j as a function of ϵ_g, for the uniform systems with mean properties. In these figures, one can identify three different regions. The first region corresponds to compressive ground strains smaller than the "contact" ground strain. That is, $\epsilon_g \leq 5.0\times10^{-4}$ for the cast iron system, and $\epsilon_g \leq 1.0\times10^{-3}$ for the ductile iron system. The second region, which starts after contact occurs, is characterized by an abrupte increase in the rate of increase of F_j with respect to ϵ_g. Finally, the third region initiates when the pipe segment material starts yielding. This yielding occurs at values of ϵ_g between 2.0×10^{-3} and 5.0×10^{-3} for both the cast iron and ductile iron systems. The maximum pipe segment axial strain, ϵ^{max}, as well as the maximum relative axial displacement between the soil and the pipeline, Δu^{max}, are nearly independent of the pipe diameter. Also, one can check that the axial stress at the pipe segment bell or spigot ends (i.e. close to the joint) given by: $\sigma = F_j/A$, is also independent of the pipe diameter. Values of σ are almost equal to the axial stress corresponding to ϵ^{max}.

Tables 7-XX and 7-XXI present results corresponding to the cases identified in section 7.3.1 as case I, case II, case III and case IV (i.e. all initial joint axial stiffnesses high values, etc), respectively for the cast iron and the ductile iron systems. Values of F_j Δu^{max} obtained for these four cases are no different from the values obtained for the uniform system with mean joint and soil properties.

Cases V, VI, VII and VIII defined in section 7.3.1 (i.e. middle joint with high initial axial stiffness, etc), are also subjected to compressive ground strain. The results are shown in Table 7-XXII for the cast iron system and in Table 7-XXIII for the ductile iron system. These results are almost equal to those obtained in the case of uniform system with mean properties.

Results obtained for compressive ground strain satisfy Eqns.(7.3) and (7.4) respectively for uniform and non-uniform sytems. These results suggest that after contact between adjacent pipe segments, variations in joint or soil properties do not lead to appreciable variation in response parameters such as the maximum joint axial force, F_j, the pipe segment axial strain, ϵ, or the relative axial displacement between the soil and the pipeline, Δu. This is due to the fact that, after contact occurs, the governing factor is the stiffness of the pipe material which is constant.

Table 7-XVIII

Results for Uniform Cast Iron System with Mean Properties under Compressive Ground Strain

D_n	ϵ_g	F_j	ϵ^{max}	Δu^{max}
cm	%	Kgf	%	cm
40.64	5.0×10^{-2}	1.47×10^{4}	1.00×10^{-2}	0.12
40.64	7.0×10^{-2}	4.75×10^{4}	2.90×10^{-2}	0.12
40.64	1.0×10^{-1}	1.00×10^{5}	5.90×10^{-2}	0.12
40.64	7.0×10^{-1}	5.61×10^{5}	0.69	0.18
76.20	5.0×10^{-2}	4.17×10^{4}	0.87×10^{-2}	0.12
76.20	7.0×10^{-2}	1.50×10^{5}	2.90×10^{-2}	0.12
76.20	1.0×10^{-1}	3.10×10^{5}	5.80×10^{-2}	0.12
76.20	7.0×10^{-1}	1.73×10^{6}	0.68	0.20
121.92	5.0×10^{-2}	1.00×10^{5}	0.81×10^{-2}	0.12
121.92	7.0×10^{-2}	3.50×10^{5}	2.86×10^{-2}	0.12
121.92	1.0×10^{-1}	7.25×10^{5}	5.90×10^{-2}	0.12
121.92	7.0×10^{-1}	4.03×10^{6}	0.66	0.21

Table 7-XIX

Results for Uniform Ductile Iron System with Mean Properties under Compressive Ground Strain

D_n	ϵ_g	F_j	ϵ^{max}	Δu^{max}
cm	%	Kgf	%	cm
40.64	2.0×10^{-1}	1.50×10^{5}	7.50×10^{-2}	0.34
40.64	5.0×10^{-1}	4.37×10^{5}	0.41	0.30(*)
40.64	7.0×10^{-1}	4.45×10^{5}	0.58	0.34
76.20	2.0×10^{-1}	3.74×10^{5}	7.50×10^{-2}	0.34
76.20	5.0×10^{-1}	1.09×10^{6}	0.53	0.30(*)
76.20	7.0×10^{-1}	1.10×10^{6}	0.58	0.34
121.92	2.0×10^{-1}	9.18×10^{5}	7.50×10^{-2}	0.34
121.92	5.0×10^{-1}	2.69×10^{6}	0.38	0.34
121.92	7.0×10^{-1}	2.69×10^{6}	0.58	0.34

(*) value increases when N is increased

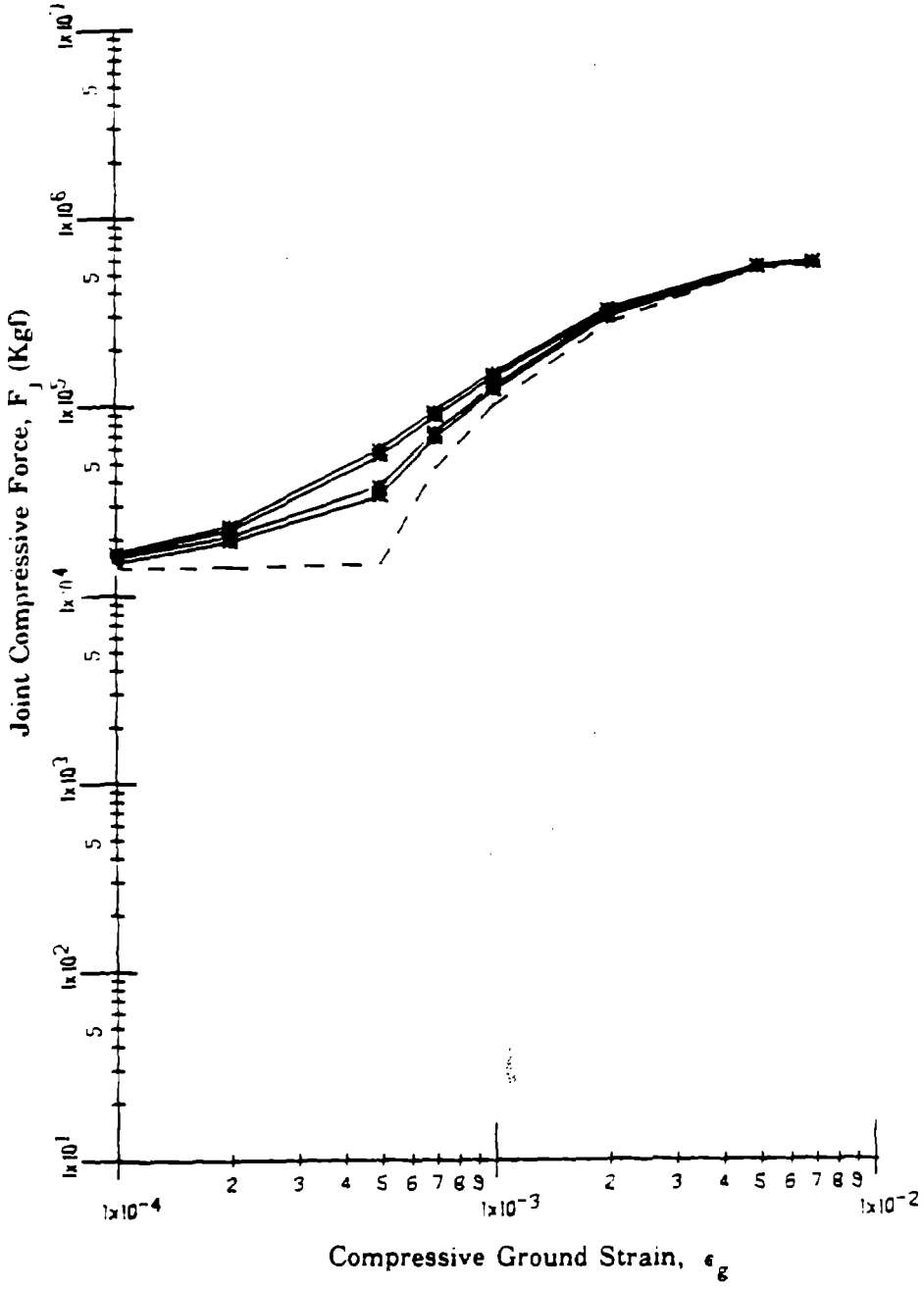

Figure 7-7. Joint Axial Force, F_j, for a 40.64 cm Diameter Cast Iron Pipe with Lead Caulked Joint versus Compressive Ground Strain, ϵ_g, for Various Exceedence Probabilities

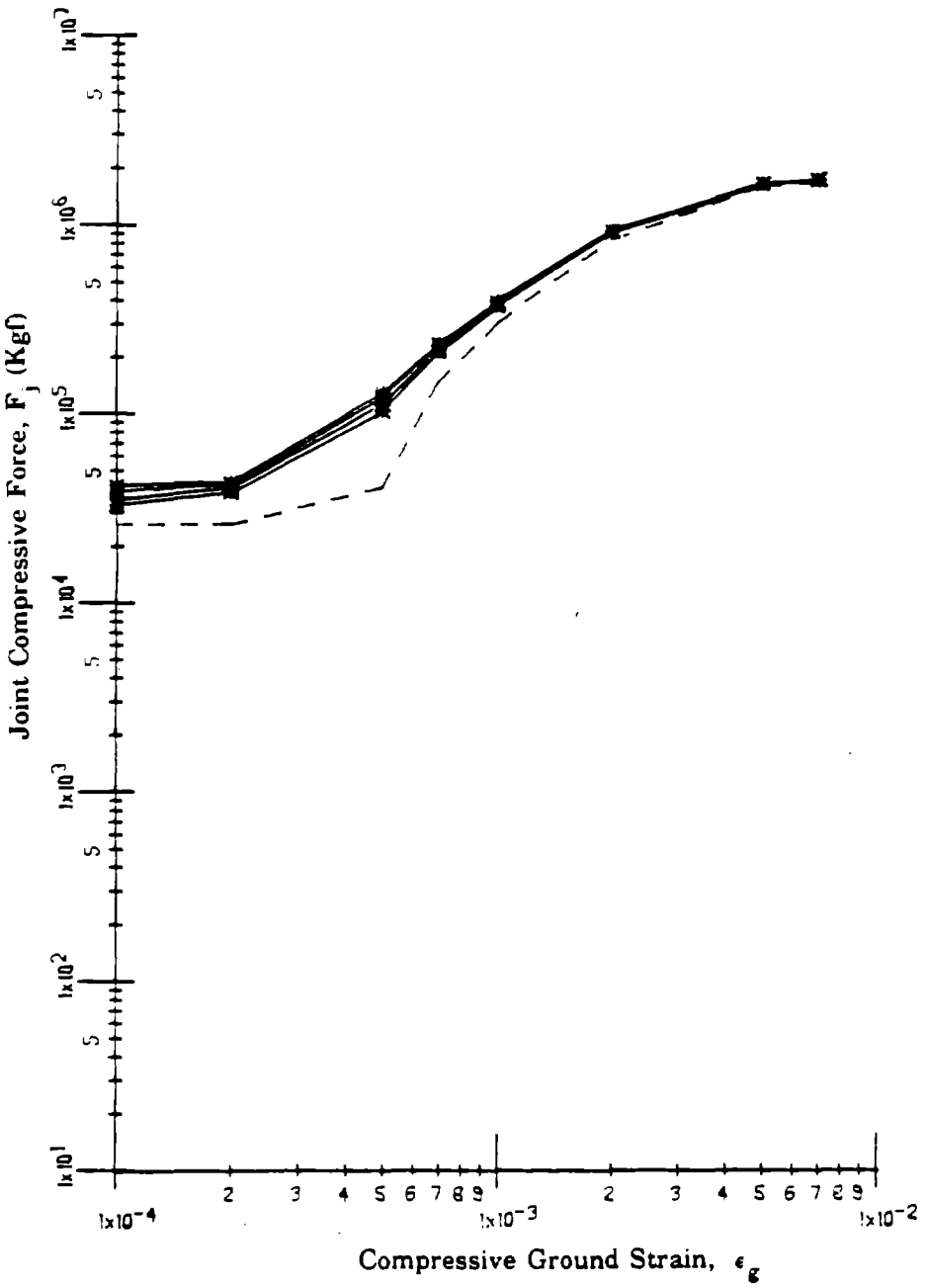

Figure 7-8. Joint Axial Force, F_j, for a 76.20 cm Diameter Cast Iron Pipe with Lead Caulked Joint versus Compressive Ground Strain, ϵ_g, for Various Exceedence Probabilities

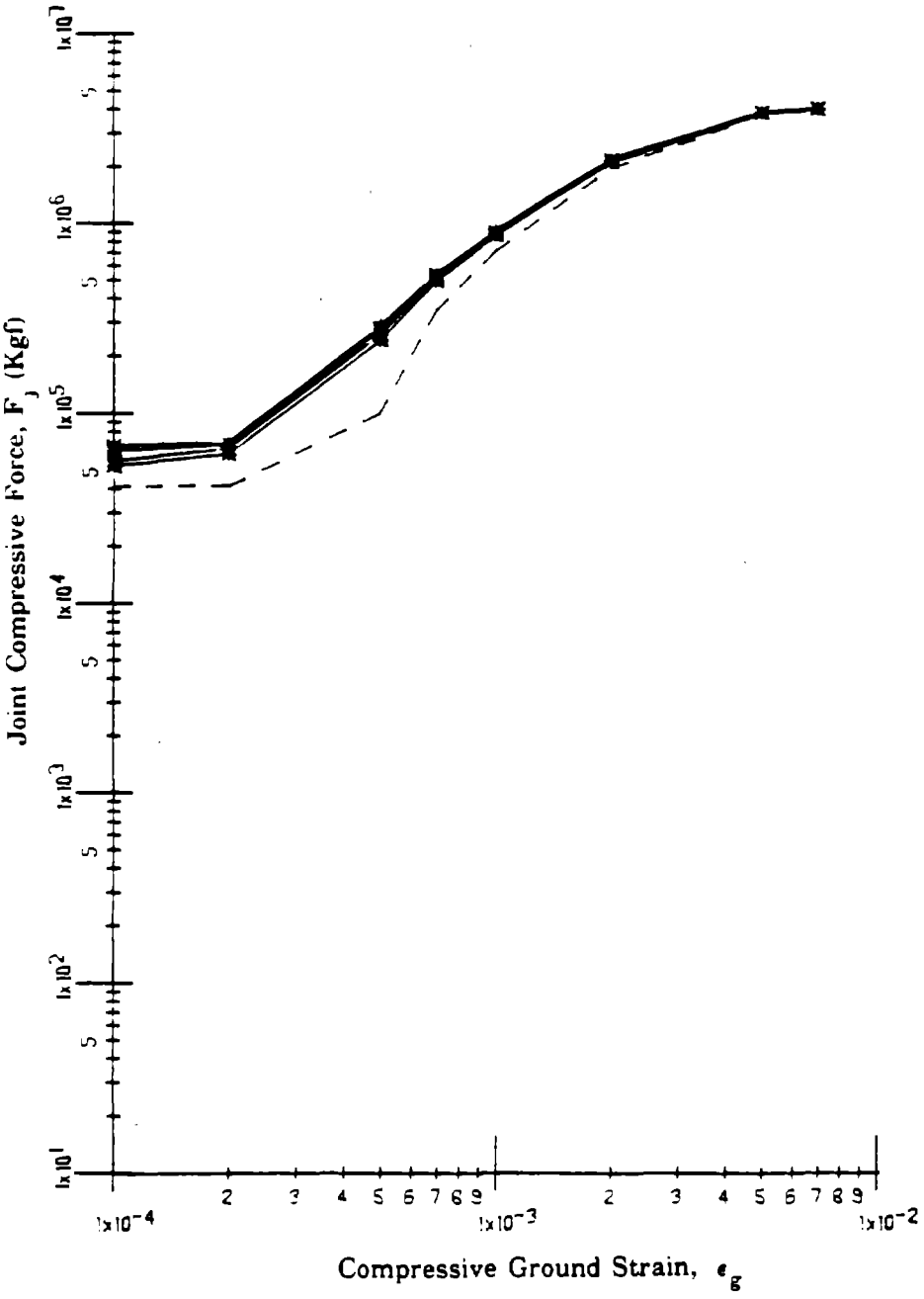

Figure 7-9. Joint Axial Force, F_j, for a 121.92 cm Diameter Cast Iron Pipe with Lead Caulked Joint versus Compressive Ground Strain, ϵ_g, for Various Exceedence Probabilities

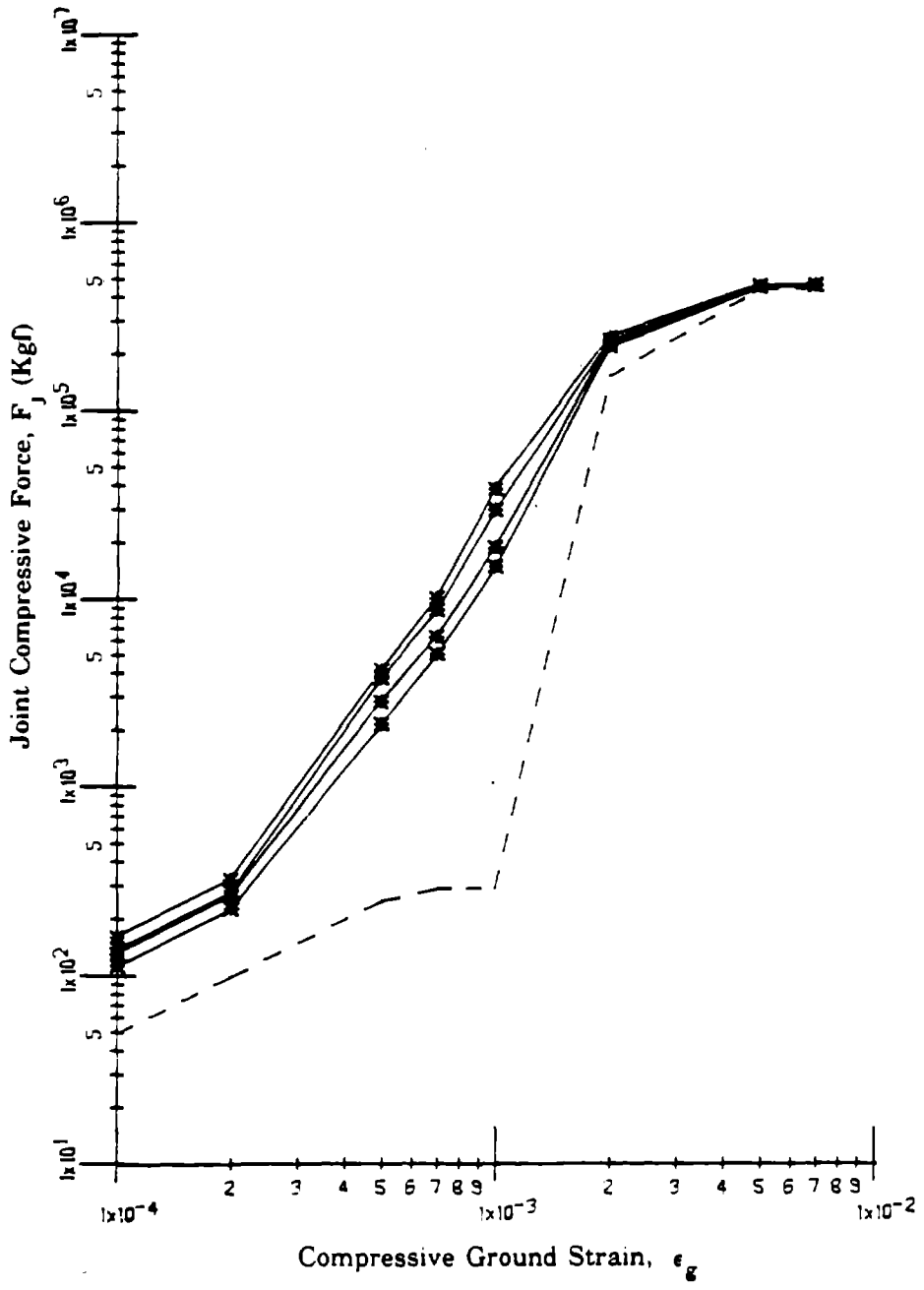

Figure 7-10. Joint Axial Force, F_j, for a 40.64 cm Diameter Ductile Iron Pipe with Rubber Gasketed Joint versus Compressive Ground Strain, ϵ_g, for Various Exceedence Probabilities

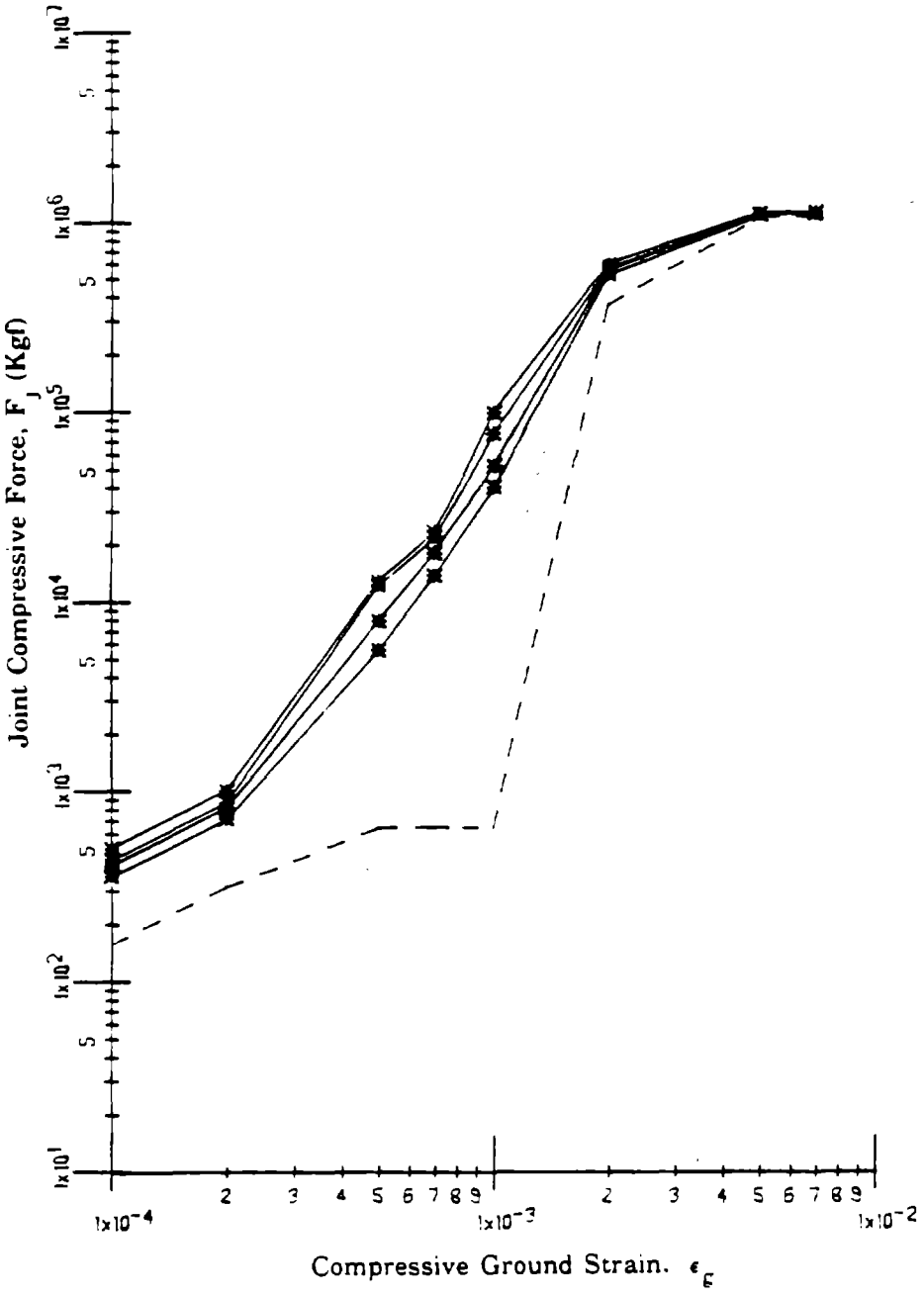

Figure 7-11. Joint Axial Force, F_j, for a 76.20 cm Diameter Ductile Iron Pipe with Rubber Gasketed Joint versus Compressive Ground Strain, ϵ_g, for Various Exceedence Probabilities

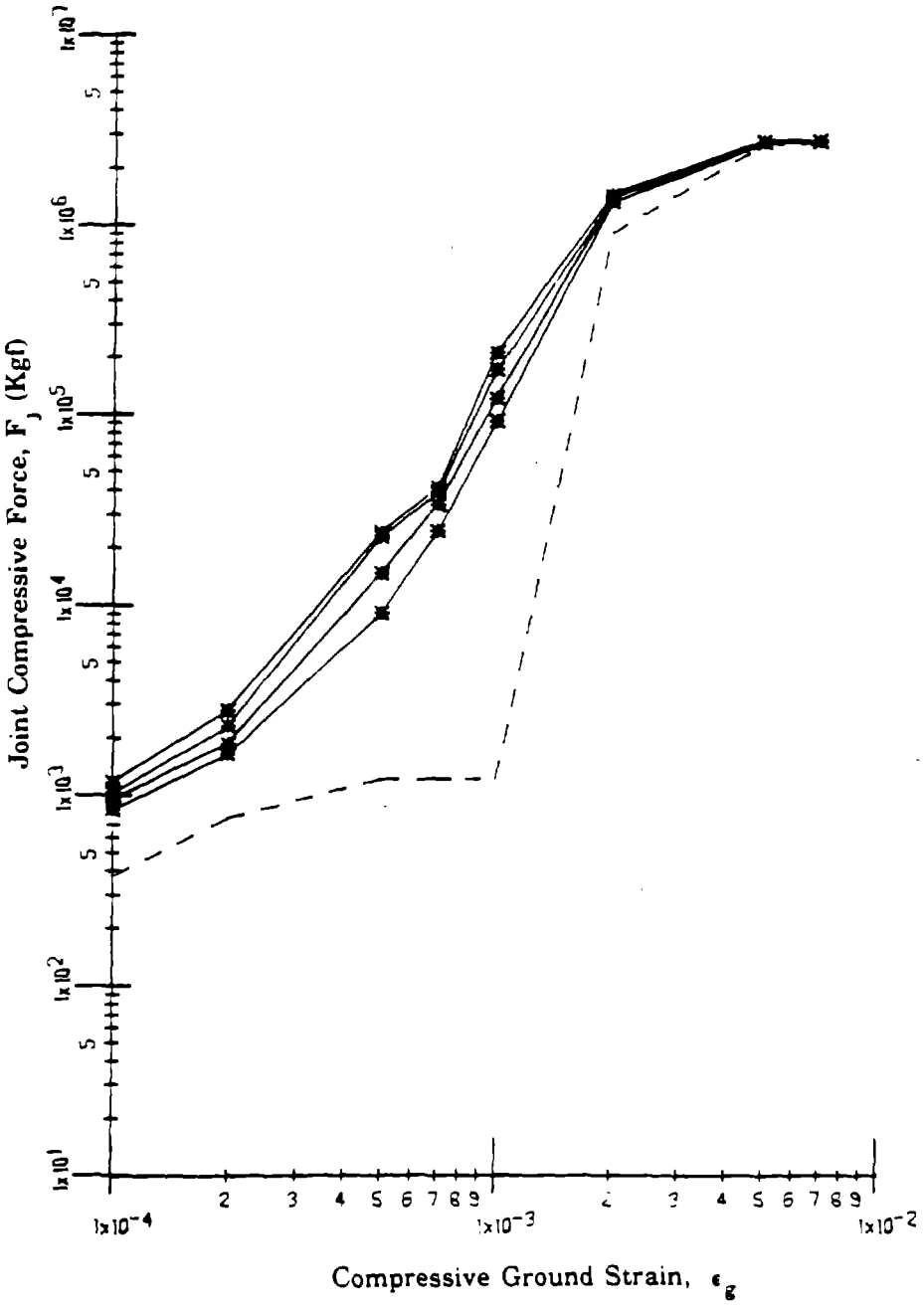

Figure 7-12. Joint Axial Force, F_j, for a 121.9 cm Diameter Ductile Iron Pipe with Rubber Gasketed Joint versus Compressive Ground Strain, ϵ_g, for Various Exceedence Probabilities

Table 7-XX

Efffects of Joint and Soil Stiffnesses on Uniform Cast Iron System under Compressive Ground Strain (D_n = 76.20 cm)

Case	ϵ_g	F_j	Δu^{max}
	%	Kgf	cm
	5.0×10^{-2}	4.25×10^{4}	0.12
I-System with	7.0×10^{-2}	1.50×10^{5}	0.12
all Stiff Joints	1.0×10^{-1}	3.12×10^{5}	0.12
	7.0×10^{-1}	1.74×10^{6}	0.20
	5.0×10^{-2}	4.25×10^{4}	0.12
II-System with	7.0×10^{-2}	1.49×10^{5}	0.12
all Flexible Joints	1.0×10^{-1}	3.12×10^{5}	0.12
	7.0×10^{-1}	1.73×10^{6}	0.15
III-System with	5.0×10^{-2}	3.80×10^{4}	0.12
all Stiff Soil	7.0×10^{-2}	1.46×10^{5}	0.12
Spring-Sliders	1.0×10^{-1}	3.08×10^{5}	0.12
	7.0×10^{-1}	1.73×10^{6}	0.14
IV-System with	5.0×10^{-2}	4.40×10^{4}	0.12
all Flexible Soil	7.0×10^{-2}	1.51×10^{5}	0.12
Spring-Sliders	1.0×10^{-1}	3.13×10^{5}	0.12
	7.0×10^{-1}	1.74×10^{6}	0.20

Table 7-XXI

Effects of Joint and Soil Stiffnesses on Uniform Ductile Iron System under Compressive Ground Strain (D_n = 76.20 cm)

Case	ϵ_g	F_j	Δu^{max}
	%	Kgf	cm
I-System with all Stiff Joints	2.0×10^{-1}	3.76×10^{5}	0.34
	5.0×10^{-1}	1.09×10^{6}	0.31
	7.0×10^{-1}	1.11×10^{6}	0.33
II-System with all Flexible Joints	2.0×10^{-1}	3.69×10^{5}	0.34
	5.0×10^{-1}	1.10×10^{6}	0.33
	7.0×10^{-1}	1.10×10^{6}	0.33
III-System with all Stiff Soil Spring-Sliders	2.0×10^{-1}	3.64×10^{5}	0.34
	5.0×10^{-1}	1.09×10^{6}	0.30
	7.0×10^{-1}	1.09×10^{6}	0.34
IV-System with all Flexible Soil Spring-Sliders	2.0×10^{-1}	3.75×10^{5}	0.34
	5.0×10^{-1}	1.10×10^{6}	0.33
	7.0×10^{-1}	1.10×10^{6}	0.32

Table 7-XXII

Results for Non-Uniform Cast Iron System under Compressive Ground Strain (D_n = 76.20 cm)

Case	ϵ_g	F_j	Δu^{max}
	%	Kgf	cm
V-Middle Joint	5.0×10^{-2}	4.27×10^{4}	0.12
with High	7.0×10^{-2}	1.51×10^{5}	0.12
Stiff	1.0×10^{-1}	3.14×10^{5}	0.12
	7.0×10^{-1}	1.74×10^{6}	0.24
VI-Middle Joint	5.0×10^{-2}	4.22×10^{4}	0.12
with Low	7.0×10^{-2}	1.51×10^{5}	0.12
Stiffness	1.0×10^{-1}	3.13×10^{5}	0.12
	7.0×10^{-1}	1.74×10^{6}	0.20
VII-Middle Soil	5.0×10^{-2}	4.17×10^{4}	0.12
Spring-Sliders	7.0×10^{-2}	1.50×10^{5}	0.12
with High	1.0×10^{-1}	3.11×10^{5}	0.12
Stiffness	7.0×10^{-1}	1.74×10^{6}	0.25
VIII-Middle Soil	5.0×10^{-2}	4.29×10^{4}	0.12
Spring-Sliders	7.0×10^{-2}	1.50×10^{5}	0.12
with Low	1.0×10^{-1}	3.11×10^{5}	0.12
Stiffness	7.0×10^{-1}	1.74×10^{6}	0.25

Table 7-XXIII

Results for Non-Uniform Ductile Iron System under Compressive Ground Strain (D_n = 76.20 cm)

Case	ϵ_g	F_j	Δu^{max}
	%	Kgf	cm
V-Middle Joint	2.0×10^{-1}	3.74×10^{5}	0.34
with High	5.0×10^{-1}	1.09×10^{6}	0.30
Stiffness	7.0×10^{-1}	1.11×10^{6}	0.33
VI-Middle Joint	2.0×10^{-1}	3.74×10^{5}	0.34
with Low	5.0×10^{-1}	1.09×10^{6}	0.34
Stiffness	7.0×10^{-1}	1.09×10^{6}	0.34
VII-Middle Soil	2.0×10^{-1}	3.74×10^{5}	0.36
Spring-Sliders with	5.0×10^{-1}	1.09×10^{6}	0.34
High Stiffness	7.0×10^{-1}	1.09×10^{6}	0.34
VIII-Middle Soil	2.0×10^{-1}	3.74×10^{5}	0.34
Spring-Sliders with	5.0×10^{-1}	1.10×10^{6}	0.34
Low Stiffness	7.0×10^{-1}	1.10×10^{6}	0.34

In a subsequent section, it will be shown that the number of joints in contact is a function of ϵ_g.

7.3.3 Tensile Ground Strain and Ground Rotation

A combination of tensile ground strain, ϵ_g, and ground rotation, θ_g, is also applied to the pipeline model [i.e. Eqn.(3.5) with the (+) sign and Eqn.(3.7)]. For a straight pipeline model, the effects of ϵ_g and θ_g are uncoupled and thus can be superimposed. Tables 7-XXIV and 7-XXV present the joint rotation, θ_j, the maximum pipe segment axial strain, ϵ^{max}, and the maximum relative lateral displacement between the soil and the pipeline, Δv^{max} under $\epsilon_g = 0.0$ and $\theta_g = 7.0\times10^{-3}$ rad, respectively for uniform cast iron systems with lead caulked joints and uniform ductile iron systems with rubber gasketed joints. Note that for this loading, $u_j = 0.0$ and $\Delta u = 0.0$.

Under ϵ_g and θ_g, the maximum joint opening (displacement), U_J, occurs at the outer fibers of the joint cross-section. The value of U_J can be obtained from the following equation:

$$U_J = u_j + |\theta_j| \cdot \frac{D}{2} \tag{7.5}$$

The first term in Eqn.(7.5) represents the joint axial displacement due to ϵ_g, while the second represents the joint axial displacement at the outer fibers due to θ_g. Observe that values obtained for θ_j, ϵ^{max} and Δv^{max} are almost null (see Tables 7-XIV and 7-XXV). Compared to the value of u_j, the product $(|\theta_j| \cdot \frac{D}{2})$ is negligible (i.e. $U_J \simeq u_j$). Hence, the effects of ground rotation on straight jointed buried pipelines are very small and can be neglected.

7.4 Simplified Monte Carlo Simulation

Simplified Monte Carlo simulation technique is applied to the two pipeline systems. This technique allows one to incorporate the variability of the system characteristics and hence models more accurately the actual conditions. In the previous section, it has been shown that ground rotation effects on straight jointed buried pipelines are negligible. Therefore, the third ground excitation type (i.e. tensile ground strain and ground curvature loading case) is not considered herein. Results are obtained when the system is subjected to tensile or compressive ground strain with magnitude ranging between 1.0×10^{-4} and 7.0×10^{-3}. Histograms for each of the response parameters as a function of the ground strain magnitude, are estabilised. Statistics corresponding to these histograms, are presented. These histograms are also used to generate the probability of exceedence for selected response parameters as a function of ground strain.

Table 7-XXIV

Results for Uniform Cast Iron System with Mean Properties under ϵ_g = 0.0 and θ_g = 7.0×10^{-3} rad

D_n	θ_j^{max}	ϵ^{max}	Δv^{max}
cm	rad		cm
40.64	0.70×10^{-14}	10^{-7}	10^{-11}
76.20	0.20×10^{-13}	0.7×10^{-8}	0.14×10^{-9}
121.92	0.55×10^{-12}	$.4\times10^{-8}$	0.80×10^{-9}

Table 7-XXV

Results for Uniform Ductile Iron System with Mean Properties under ϵ_g = 0.0 and θ_g = 7.0×10^{-3} rad

D_n	θ_j^{max}	ϵ^{max}	Δv^{max}
cm	rad		cm
40.64	0.20×10^{-14}	0.3×10^{-16}	0.15×10^{-12}
76.20	0.20×10^{-15}	0.6×10^{-17}	0.31×10^{-12}
121.92	0.13×10^{-13}	0.2×10^{-15}	0.53×10^{-11}

7.4.1 Tensile Ground Strain

Results of the simplified Monte Carlo simulation for this loading case, are first used to compute statistics of the joint axial displacement, u_j, the pipe segment axial strain, ϵ, and the relative axial displacement between the soil and the pipeline, Δu, at different levels of ground strain. Tables 7-XXVI, 7-XXVII and 7-XXVIII present the mean value and coefficient of variation, μ, corresponding to each of the response parameters, u_j, ϵ and Δu, respectively for the 40.64, 76.20 and 121.92 cm diameter cast iron pipe with lead caulked joint systems. As one might expect intuitively, the mean value of each of the response parameters is equal to the value of that response parameter obtained for uniform systems with mean joint and soil properties. That is, for the Monte Carlo simulation of the tensile ground strain loading case, the mean values of the response parameters follow Eqn.(7.3).

The variability of each of the response parameters (i.e. u_j, Δu and ϵ), quantified by the corresponding coefficient of variation, is significantly high. Notice that the coefficients of variation of u_j and Δu are decreasing functions of ϵ_g, while the coefficient of variation of ϵ is an increasing function of ϵ_g. In addition, one can see that the coefficient of variation of u_j decreases for larger pipe diameters. This appears to be due to the fact that the ratio between the initial joint axial stiffness and the axial pipe segment stiffness, $AK_j/(\frac{E_p \cdot A}{L})$, is also a decreasing function of the pipe diameter.

The mean values and coefficient of variations, μ, corresponding to u_j, ϵ and Δu, for the 40.64, 76.20 and 121.92 cm diameter ductile iron pipe with rubber gasketed joint systems, are respectively shown in Tables 7-XXIX, 7-XXX and 7-XXXI. As with the cast iron system with lead caulked joint, the mean value of each of the response parameters for the ductile iron system with rubber gasketed joint, is equal to the value of that response parameter obtained for uniform systems with mean joint and soil properties. That is, Eqn.(7.3) holds fo the mean values of the response parameters. The coefficients of variation of u_j and Δu, are very small (μ < 3%). On the other hand, the coefficient of variation of ϵ is much larger. It ranges between 50 and 76%. The maximum values of ϵ in this case are also much smaller than the ductile iron yielding strain, ϵ^y.

Hence, the variability of the system chracteristics has a stronger influence on the joint axial displacement for cast iron pipes with lead caulked joints, while it has a stronger influence on the pipe segment axial strain for ductile iron pipes with rubber gasketed joints.

Under tensile ground strain, the response parameter of interest is the joint axial displacement, u_j, which is related to the possibility of joint *pull-out*. The pipe segment axial strain, ϵ, is much smaller than the yielding material strain, ϵ^y. Histograms for u_j at different levels of tensile

Table 7-XXVI

Response Parameters Statistics for Cast Iron System under Tensile Ground Strain (D_n = 40.64 cm)

ϵ_g	u_j		ϵ^{max}		Δu^{max}	
10^{-4}	Mean cm	μ %	Mean 10^{-4}	μ %	Mean cm	μ %
1.0	0.02	150	0.67	15	0.02	85
2.0	0.07	98	0.79	18	0.04	76
5.0	0.25	72	0.94	20	0.13	65
7.0	0.36	67	1.00	23	0.20	62
10.0	0.54	64	1.10	25	0.29	60
20.0	1.14	56	1.20	28	0.58	56
50.0	2.92	39	1.33	25	1.42	45
70.0	4.12	26	1.45	23	2.00	35

Table 7-XXVII

Response Parameters Statistics for Cast Iron System under Tensile Ground Strain (D_n = 76.20 cm)

ϵ_g	u_j		ϵ^{max}		Δu^{max}	
10^{-4}	Mean cm	μ %	Mean 10^{-4}	μ %	Mean cm	μ %
1.0	0.03	123	0.43	18	0.02	78
2.0	0.09	89	0.49	19	0.05	72
5.0	0.27	61	0.59	21	0.14	58
7.0	0.39	56	0.64	23	0.20	54
10.0	0.56	54	0.70	26	0.29	53
20.0	1.16	49	0.75	33	0.58	50
50.0	2.95	24	0.84	31	1.40	29
70.0	4.15	19	0.93	29	2.00	25

Table 7-XXVIII

Response Parameters Statistics for Cast Iron System under Tensile Ground Strain (D_n = 121.92 cm)

ϵ_g	u_j		ϵ^{max}		Δu^{max}	
10^{-4}	Mean cm	μ %	Mean 10^{-4}	μ %	Mean cm	μ %
1.0	0.04	114	0.30	18	0.03	77
2.0	0.10	87	0.34	19	0.06	71
5.0	0.28	59	0.40	20	0.14	57
7.0	0.39	54	0.43	23	0.20	53
10.0	0.58	52	0.46	27	0.29	51
20.0	1.17	43	0.50	35	0.58	45
50.0	2.97	14	0.59	34	1.40	19
70.0	4.16	16	0.64	32	2.00	22

Table 7-XXIX

Response Parameters Statistics for Ductile Iron System under Tensile Ground Strain (D_n = 40.64 cm)

ϵ_g	u_j		ϵ^{max}		Δu^{max}	
10^{-4}	Mean cm	μ %	Mean 10^{-4}	μ %	Mean cm	μ %
1.0	0.06	2	0.04	51	0.02	2
2.0	0.12	2	0.07	50	0.05	2
5.0	0.29	2	0.17	52	0.12	3
7.0	0.41	2	0.22	59	0.16	3
10.0	0.59	2	0.26	65	0.24	3
20.0	1.19	2	0.27	74	0.47	3
50.0	3.00	1	0.27	74	1.20	1
70.0	4.19	1	0.27	74	1.70	1

Table 7-XXX

Response Parameters Statistics for Ductile Iron System under Tensile Ground Strain (D_n = 76.20 cm)

ϵ_g	u_j		ϵ^{max}		Δu^{max}	
10^{-4}	Mean cm	μ %	Mean 10^{-4}	μ %	Mean cm	μ %
1.0	0.06	2	0.03	50	0.02	3
2.0	0.12	2	0.06	48	0.05	3
5.0	0.29	2	0.14	50	0.12	2
7.0	0.41	2	0.19	50	0.16	2
10.0	0.59	2	0.24	62	0.23	2
20.0	1.19	2	0.29	72	0.47	3
50.0	3.00	1	0.29	76	1.20	1
70.0	4.19	1	0.29	76	1.70	1

Table 7-XXXI

Response Parameters Statistics for Ductile Iron System under Tensile Ground Strain (D_n = 121.92 cm)

ϵ_g	u_j		ϵ^{max}		Δu^{max}	
10^{-4}	Mean cm	μ %	Mean 10^{-4}	μ %	Mean cm	μ %
1.0	0.06	3	0.02	50	0.02	5
2.0	0.12	3	.04	47	0.05	5
5.0	0.29	2	0.09	50	0.12	3
7.0	0.41	2	0.12	50	0.16	2
10.0	0.59	2	0.16	56	0.24	3
20.0	1.19	3	0.21	67	0.47	3
50.0	3.00	1	0.22	77	1.20	2
70.0	4.19	1	0.22	76	1.70	1

ground strain, ϵ, were obtained. Figure 7-13 shows a histogram of u_j for the 76.20 cm diameter cast iron pipe with lead caulked joint system under $\epsilon_g = 1.0\times10^{-3}$. The same histogram for the ductile iron system with rubber gasketed joint gives a mean joint axial dislacement, u_j = 0.59 cm and a coefficient of variation, μ = 2%. For the cast iron system, these histograms are used to generate the probability of exceedence of u_j as a function of ϵ_g. Figures 7-1, 7-2 and 7-3 plot u_j versus ϵ_g for probability of exceedence equal to 0.1%, 0.2%, 1% or 2%, respectively for 40.64, 76.20 and 121.92 cm pipe diameter. In addition, these figures show in doted line the average value of u_j as a function of ϵ_g, obtained from the uniform systems with mean properties. The graphs in Figures 7-1, 7-2 and 7-3 can be used to assess the vulnerability of straight cast iron pipelines with lead caulked joints under seismic waves. If one has some information about the joint axial displacement at which leakage starts, then it is possible to estimate the probability of exceedence of this displacement for the level of seismic ground strain expected. The value of the probability of exceedence represents also an estimate of the ratio of joints that would leak. For the ductile iron system, Figures 7-4, 7-5 and 7-6 plot in solid line the maximum values of u_j and in doted line the average value of u_j obtained from the uniform systems with mean properties, as a function of ϵ_g. These figures show that the joint axial displacement is not sensitive to the system characteristics variability. Hence, Figures 7-4, 7-5 and 7-6 can be used directly for the analysis of straight ductile iron pipelines with rubber gasketed joints under the tensile ground strain loading case.

7.4.2 Compressive Ground Strain

As in the previous section, statistics of the response parameters resulting from the simplified Monte Carlo simulation are obtained when the system is subjected to compressive ground strain, ϵ_g. The response parameter of interest in this case is the joint axial force, F_j, which is related to the possibility of *crushing* of the pipe segment bell. One would also be interested in knowing the number of joints with contact, n_{jc}, as a function of ϵ_g. Tables 7-XXXII, 7-XXXIII and 7-XXXIV give the mean value and coefficient of variation, μ, corresponding to F_j and n_{jc}, respectively for the 40.64, 76.20 and 121.92 cm diameter cast iron pipe with lead caulked joint systems. Observe that more than 80% of the joints (i.e. $n_{jc} > 80\%$) are in contact for $\epsilon_g = 5.0\times10^{-4}$. At this level of ground strain, the coefficient of variation, μ, of F_j has the highest value. For compressive ground strain with magnitude higher than this level, all the joints become in contact (i.e. $n_{jc} = 100\%$) and the variability of F_j drops sharpely. Similarly, Tables 7-XXXV, 7-XXXVI and 7-XXXVII give the mean value and coefficient of variation, μ, corresponding to F_j and n_{jc} respectively, for the 40.64, 76.20 and 121.92 cm diameter ductile iron pipe with rubber gasketed joint systems. At a compressive ground strain, $\epsilon_g = 1.0\times10^{-3}$, about 30% of the joints are in

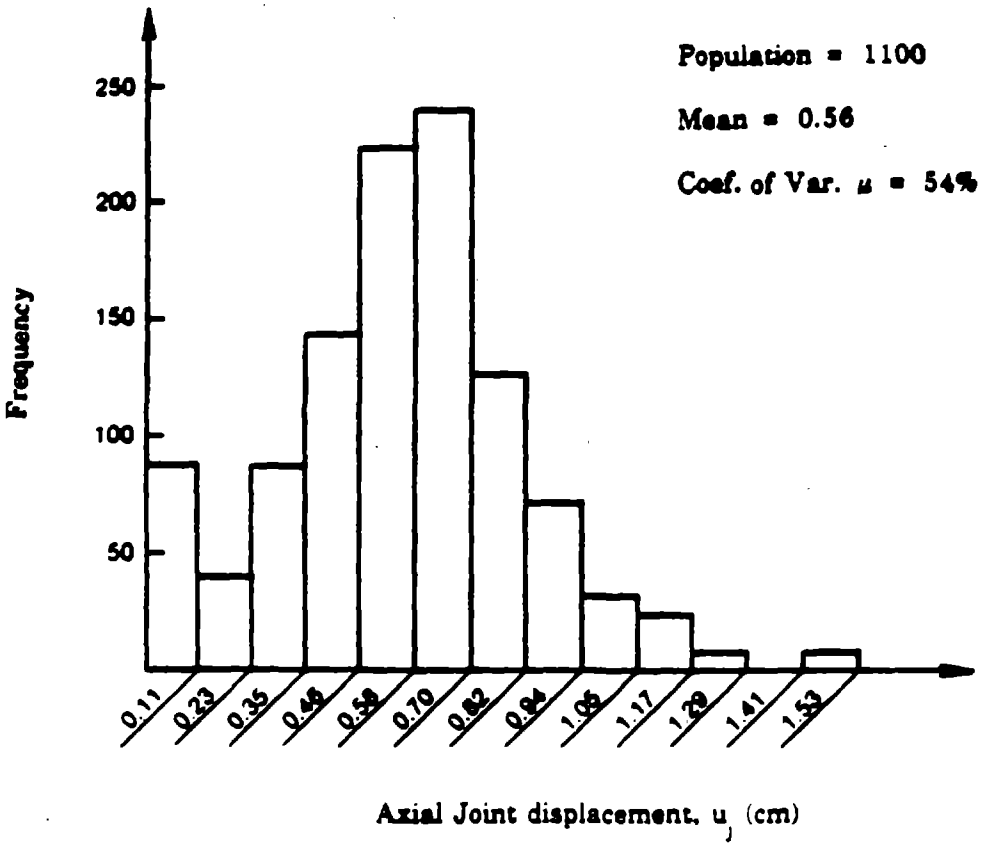

Figure 7-13. Histogram of the Joint Axial Displacement, u_j, for a 76.20 cm Diameter Cast Iron Pipe with Lead Caulked Joint ($\epsilon_g = 1.0 \times 10^{-3}$)

Table 7-XXXII

Response Parameters Statistics for Cast Iron System under Compressive Ground Strain (D_n = 40.64 cm)

ϵ_g	F_j		n_{jc}	
10^{-4}	Mean Kgf	μ %	Mean %	μ %
1.0	1.15×10^4	18	0.003	567
2.0	1.31×10^4	22	0.072	111
5.0	2.01×10^4	28	73	21
7.0	4.90×10^4	19	95	6
10.0	1.02×10^5	9	100	0
20.0	2.78×10^5	3	100	0
50.0	5.38×10^5	1	100	0
70.0	5.61×10^5	1	100	0

Table 7-XXXIII

Response Parameters Statistics for Cast Iron System under Compressive Ground Strain (D_n = 76.20 cm)

ϵ_g	F_j		n_{jc}	
10^{-4}	Mean Kgf	μ %	Mean %	μ %
1.0	2.27×10^4	22	0.01	286
2.0	2.55×10^4	24	10	91
5.0	5.41×10^4	41	82	19
7.0	1.51×10^5	18	100	0
10.0	3.15×10^5	9	100	0
20.0	8.58×10^5	3	100	0
50.0	1.66×10^6	0.6	100	0
70.0	1.73×10^6	0.8	100	0

Table 7-XXXIV

Response Parameters Statistics for Cast Iron System under Compressive Ground Strain (D_n = 121.92 cm)

ϵ_g	F_j		n_{jc}	
10^{-4}	Mean Kgf	μ %	Mean %	μ %
1.0	3.64×10^4	22	0.02	263
2.0	4.08×10^4	24	12	80
5.0	1.11×10^5	47	91	14
7.0	3.57×10^5	17	100	0
10.0	7.37×10^5	8	100	0
20.0	2.00×10^6	3	100	0
50.0	3.86×10^6	0.5	100	0
70.0	4.02×10^6	0.6	100	0

Table 7-XXXV

Response Parameters Statistics for Ductile Iron System under Compressive Ground Strain (D_n = 40.64 cm)

ϵ_g	F_j		n_{jc}	
10^{-4}	Mean Kgf	μ %	Mean %	μ %
1.0	5.47×10^{1}	42	0	-
2.0	1.09×10^{2}	41	0	-
5.0	3.22×10^{2}	129	3.70	161
7.0	3.45×10^{2}	200	1	100
10.0	1.83×10^{3}	211	29	71
20.0	1.50×10^{5}	18	100	0
50.0	4.40×10^{5}	1	100	0
70.0	4.43×10^{6}	1	100	0

Table 7-XXXVI

Response Parameters Statistics for Ductile Iron System under Compressive Ground Strain (D_n = 76.20 cm)

ϵ_g	F_j		n_{jc}	
10^{-4}	Mean Kgf	μ %	Mean %	μ %
1.0	1.74×10^2	41	0	-
2.0	3.49×10^2	41	0	-
5.0	8.32×10^2	140	3.73	161
7.0	1.36×10^3	214	1	100
10.0	4.95×10^3	214	29	72
20.0	3.76×10^5	18	100	0
50.0	1.10×10^5	1	100	0
70.0	1.10×10^6	1	100	0

Table 7-XXXVII

Response Parameters Statistics for Ductile Iron System under Compressive Ground Strain (D_n = 121.92 cm)

ϵ_g	F_j		n_{jc}	
10^{-4}	Mean Kgf	μ %	Mean %	μ %
1.0	4.15×10^{2}	40	0	-
2.0	8.25×10^{2}	40	0.3	567
5.0	1.56×10^{3}	133	4	162
7.0	2.51×10^{3}	208	1	100
10.0	1.06×10^{4}	221	31	71
20.0	9.22×10^{5}	18	100	0
50.0	2.68×10^{5}	1	100	0
70.0	2.69×10^{6}	1	100	0

contact (i.e. n_{jc} = 30%), and the coefficient of variation of μ corresponding to F_j, has the highest value ($\mu \simeq 210\%$). For higher levels of compressive ground strain, all the joints become in contact (i.e. n_{jc} = 100%) and the the coefficient of variation, μ, of F_j becomes very small. It should be mentioned that when contact starts occuring, the variability of F_j is higher for the ductile iron system. This might be due to the fact that ductile iron material is stiffer than cast iron material. However, when full contact happens (i.e. n_{jc} = 100%), the variability of F_j becomes negligible for both cast iron and ductile iron systems.

Results of the simplified Monte Carlo simulation are also used to generate graphs giving values of F_j with 0.1%, 0.2%, 1% and 2% probability of exceedence as a function of the compressive ground strain, ϵ_g. Figures 7-7, 7-8 an 7-9 give these graphs for the 40.64, 76.20 and 121.92 cm diameter cast iron pipe with lead caulked joint systems, while Figures 7-10, 7-11 and 7-12 give these graphs for the 40.64, 76.20 and 121.92 cm diameter ductile iron pipe with rubber gasketed joint systems. As mentioned before, the doted lines in these figures represent the value of F_j versus ϵ_g for the uniform systems with mean properties. Observe that the system characteristics variability has a stronger influence at smaller levels of compressive ground strain. At levels of ϵ_g corresponding to to the initiation of yielding ($\epsilon_g \simeq 2.0\times10^{-3}$), the variability of F_j becomes very small and can be neglected.

7.5 Damage Ratio of Cast Iron Pipes with Lead Caulked Joints under Tensile Ground Strain

One of the important items needed in order to evaluate the seismic vulnerability of a buried pipeline is the expected damage ratio due to seismic wave propagation. This information can be used to estimate the repair time, number of repair clamps needed, etc., for a potential earthquake. For example, the damage ratio to water systems in the Lake Zone (soft soil zone) of Metropolitan Mexico City due to the 1985 Michoacan event was about 0.45 leaks/Km [6]. Approximately one-third of these leaks occured at joints in nominally straight runs of piping while the remaining two-thirds occured at or near junctions such as tees, elbows or valve boxes.

Existing information on seismic damage to buried pipeline is based upon empirical data. Katayama et al. [3] plot damage ratios as a function of peak ground acceleration. In their figure, it appears that both permanent ground movements and wave propagation damage are included. More recently Egushi et al. [24] have developed separate plots of damage ratios for permanent ground movements and wave propagation. The wave propagation damage ratios are presented as a function of Modified Mercally Intensity (MMI).

An analytical procedure to predict seismic wave propagation damage to straight cast iron systems with lead caulked joints under tensile ground strain is presented herein. In

section 4.2.2.1, a conditional cumulative distribution function P[l | u_j/d_p] for the probability of joint leakage as a function of the normalized joint displacement u_j/d_p was developed (see Figure 4-5). On the other hand, the vulnerability graphs in Figures 7-1, 7-2 and 7-3 can be used to approximate the probability density function $\rho(u_j/d_p)$ for the normalized joint response. Using the conditional probability theorem for distributed random variables, the probability of an individual joint leaking, P_l, can be obtained from:

$$P_l = \int_0^\infty P[l \mid s] \cdot \rho(s)\, ds \tag{7.6}$$

where s stands for the normalized joint displacement u_j/d_p. The *damage ratio*, DR (number of leaks per kilometer of pipe), is then equal to P_l times the number of joints per kilometer of pipe. That is:

$$DR = \frac{1000\, P_l}{L} \tag{7.7}$$

where L equals the individual pipe segment length in meters (L = 6 m).

The procedure outlined above is applied to the cast iron systems. Table 7-XXXVIII gives the estimated values of the damage ratio, DR, as a function the pipe nominal diameter, D_n, and the tensile ground strain, ϵ_g . Notice that DR is a decreasing function of the pipe diameter. Since the average joint response is practically independent of pipe diameter, this is mainly due to the fact that the variability of joint displacement is also a decreasing function of the pipe diameter (see Tables XXVI, XXVII and XXVIII). It should be mentioned also that DR is a nonlinear function of ϵ_g.

The ground strain in parts of the Lake Zone of Mexico City during the 1985 Michoacan earthquake [6] was estimated at 2.0×10^{-3}. For this level of ground strain (i.e. $\epsilon_g = 2.0\times10^{-3}$), the damage ratio, DR, for pipes parallel to the direction of wave propagation varies between 0.06 leaks/Km for a 1291.92 cm (48 in) pipe diameter and 0.64 leaks/Km for a 40.64 cm (16 in) pipe diameter. The average damage ratio for pipes parallel to the direction of wave propagation with a diameter of 40.64 cm (16 in), 76.20 cm (30 in) or 121.92 cm (48 in) is equal to 0.32 leaks/Km. Note that this average damage ratio for straight runs of cast iron systems in the Lake Zone of Mexico City [6] is somewhat lower than the observed damage ratio for all systems which is about 0.45 leaks/Km. This is expected since leakage due to crushing at the bell and damage at elbows, tees and valve boxes are not considered in the present analysis.

Table 7-XXXVIII

Damage Ratio of Cast Iron System under Tensile Ground Strain

DR (leaks/km)	ϵ_g (10^{-4})		
	10.0	20.0	50.0
D_n = 40.64 cm (16 in)	0.02	0.64	23.80
D_n = 76.20 cm (30 in)	0.002	0.26	11.20
D_n = 121.92 cm (48 in)	0.00	0.06	5.80

The proposed procedure could be extended to include the crushing of the bell failure mode. However, this further extension awaits laboratory tests on leakage due to bell crushing.

8. SUMMARY AND CONCLUSIONS

The objective of this research is the development of new information which will facilitate the design of *straight jointed buried pipelines* for seismic wave propagation effects. An analytical model which incorporates the *nonlinear* behavior as well as the *variability* of the system characteristics is constructed and used to evaluate the system response. The inclusion of *variability* is considered a first step towards developing realistic models capable of estimating damage consistent with actual observations.

The results obtained are based upon three assumptions. It is assumed that a static formulation is appropriate for evaluating the pipeline response. Several studies have shown that inertia effects can be neglected. This is primarily due to the fact that the mass of a fluid filled pipe is typically smaller than the mass of the insitu soil it replaces. The second assumption states that the pipeline is initially strain free in the longitudinal direction. The support provided by the soil prevents the pipeline from deforming appreciably in the longitudinal direction. The last assumption limits this study to wave propagation effects. Although it is recognized that faulting, liquefaction and landsliding are potential causes of damage to pipelines, there are certain cases such as Mexico City in 1985 where damage was exclusively due to wave propagation effects. Note that two pipeline systems are considered in this study. They are *Cast Iron Pipes with Lead Caulked Joints* and *Ductile Iron Pipes with Rubber Gasketed Joints*.

In order to establish the analytical model, presently available information on the seismic environment, the mechanical behavior of pipe segments and joints, and the soil resistance to pipeline movements is reviewed and synthesized. The seismic environment due to the propagation of both body and surface waves is studied first. Simplified models are used to estimate the ground strain and ground rotation. Note that only the ground rotation in the horizontal plane (i.e. lateral direction) is considered. A range of realistic values is considered and serves to construct axial and lateral ground displacements.

After review, synthesis and integration of the existing literature, the pipeline properties for each of the two systems considered are determined. First, the mechanical behavior of the pipe segment material is characterized by established stress/strain relationships. Second, the joint behavior is studied. This behavior is characterized by a wide scatter in test results for both systems considered. The mechanical properties of the joint are described in terms of the axial force/displacement and bending moment/rotation relationships. Based on available test data, analytical and empirical expressions for mean values of the parameters defining these relationships are obtained. The test data are also used to estimate the variability of these parameters about their mean values. The probability density function for each of these

parameters is approximated by a Rayleigh density function. A step by step procedure to select the pipeline properties for each of the pipeline systems considered is also presented.

The resistance provided by the soil to axial and lateral movements of the pipeline is then quantified. Based on test data, it is shown that the soil/pipeline interaction can be modeled by axial and lateral spring-sliders distributed along the pipeline. Analytical and empirical relationships for the characteristics of these spring-sliders are given. The soil properties involved in the definition of the spring-sliders characteristics are assumed to be random variables. This is done to model their inherent variability and recognize the fact that they vary somewhat along the pipeline. A Rayleigh density function is used to approximate the variability of each of the soil properties. As with pipeline properties, a step by step procedure to select the soil properties is presented.

The proposed analytical model is based on a nonlinear static formulation. The model consists of a number of pipe segments surrounded by axial and lateral soil spring-sliders. Each pipe segment is discretized into a number of truss and beam elements. Joints exist between the pipe segments and are represented by axial and rotational nonlinear springs. The ground nodes of the soil spring-sliders as well as the two end supports of the model follow specified axial and lateral displacement functions, thus providing the input excitation. A finite element formulation is used to develop the governing algebraic equations. The variability of the system characteristics is accounted for by a simplified Monte Carlo simulation technique. Using random number generators in conjunction with the approximate probability functions (i.e. Rayleigh density functions), the joint and soil properties along the pipeline are selected. Subsequently, the model is subjected to axial and lateral ground displacements. The analysis is repeated several times and the results serve to develop histograms for the response parameters such as the joint axial displacement. A detailed algorithm representing the proposed model is given.

Results are obtained for the two pipeline systems considered, under three types of ground excitation. The first type corresponds to a tensile ground strain, the second is a compressive ground strain and the third is a combination of tensile ground strain and ground rotation. The pipe sizes studied are 16, 30 and 48 inch (40.64, 76.20 and 121.92 cm) nominal diameter. A sensitivity analysis which highlights the effect of variable system characteristics upon the pipeline response is performed first. In this analysis, the system characteristics are assumed to be deterministic.

Under tensile ground strain, it is shown that variations in joint properties along the model result in variations in the maximum joint axial displacement of cast iron systems with lead caulked joints. The variation in joint axial displacement for ductile iron systems with rubber gasketed joints is much less. This is due to the relatively low mean value of the initial joint axial stiffness

for rubber gasketed joints. Results show also that the joint axial displacement is not significantly affected by variations in soil properties for both systems considered. This suggests that the joint parameter variability is more important than the soil parameter variability for cast iron pipe with lead caulked joint systems. For ductile iron pipe with rubber gasketed joint systems, both the variability of joint properties and that of the soil properties have a small influence on the results. It should be mentioned that values of the joint axial displacement and of the axial relative displacement between the soil and the pipeline are practically independent of the pipe diameter, for both systems studied. In addition, the axial strain in the pipe segment remains in the elastic range even under high values of tensile ground strain.

For the compressive ground strain loading case, results indicate that contact between pipe segments can happen. The "contact" ground strain ranges between 5.0×10^{-4} and 7.0×10^{-4} for cast iron systems with lead caulked joints. For ductile iron systems with rubber gasketed joints, the corresponding range is 1.0×10^{-3} to 2.0×10^{-3}. The range of "contact" ground strain is much lower for the cast iron system than for the ductile iron system because the clearance distance between adjacent pipe segments is smaller for the first system. After contact between adjacent pipe segments, variations in joint or soil properties do not lead to appreciable variations in response parameters such as the maximum joint axial force or pipe segment axial strain. This is due to the fact that, after contact occurs, the governing factor is the stiffness of the pipe material which is taken as a constant. Results indicate also that after contact, the maximum pipe segment axial strain as well as the maximum axial relative displacement between the soil and the pipeline, are nearly independent of the pipe diameter.

It is found that the results obtained under ground rotation are very small when compared with the results of the tensile ground strain loading case. This suggests that, for straight jointed buried pipelines, rotation effects can be neglected.

Following, the simplified Monte Carlo simulation is applied to the two pipeline systems considered. Since ground rotation effects are found negligible, results are obtained only for tensile ground strain or compressive ground strain loading cases. For each of these two loading cases, statistics of the response parameters of interest are given. Histograms for these response parameters can also be obtained.

The response parameter of interest in the case of tensile ground strain excitation is the joint axial displacement, which is related to the possibility of *pull-out*. Results indicate in this case that the influence of the variability of the system characteristics on the joint axial displacement is much greater for the cast iron system with lead caulked joints than for the ductile iron system with rubber gasketed joints. This partially explains why caulked joints tend to experience more seismic damage than rubber gasketed joints. Note that values of the maximum axial pipe

segment strain for each of the two systems are much smaller than the corresponding yielding strain. Results for the cast iron system are used to generate graphs giving the joint axial displacement as a function of the tensile ground strain for probability of exceedence equal to 0.1%, 0.2%, 1% or 2%. These graphs can be used to assess the vulnerability of straight cast iron pipelines with lead caulked joints under seismic waves. For the ductile iron system, the joint axial displacement is not sensitive to the system characteristics variability. Figures giving the joint axial displacement as a function of the ground strain are presented.

For the compressive ground strain loading case, statistics of the joint axial force and of the number of joints at contact are given. Note that the axial joint force is related to the possibility of *crushing* of the pipe segment bell. Variability of the joint axial force and that of the number of joints at contact are high when contact starts occurring. The two variabilities are smaller for the cast iron system than for the ductile iron system. This is due to the fact that ductile iron is more rigid than cast iron. At high magnitudes of ground strain, contact between pipe segments occurs at all joints of the model, and the variability of the joint axial force becomes negligible, for both systems. Results of the simplified Monte Carlo simulation are used to generate graphs giving values of the joint axial force as a function of the compressive ground strain.

Finally, an analytical procedure to predict the damage ratio of straight cast iron pipelines with lead caulked joints due to a joint pull-out failure mode is presented. Results of the procedure are benchmarked against observed damage to water systems and is found to yield reasonable estimates. The proposed procedure can be extended to include the bell crushing failure mode. However, this extension awaits laboratory tests on leakage due to bell crushing.

This research highlights the importance of including system characteristics variability when studying the response of straight jointed buried pipelines. It is shown how the results obtained can be used to assess the seismic vulnerability of this type of pipeline. Using the model proposed, results can be obtained for other pipeline systems such as concrete pipes with rubber gasketed joints. This model can also be extended to study the response of pipeline junctions (i.e. elbows and tees) under seismic wave propagation effects.

REFERENCES

1. Lawson, A.C. et al., *The California Earthquake of April 18, 1906*, Vols 1 and 2, The State Earthquake Investigation Commission, The Carnegie Institution of Washington, Washington, D. C, 1908.

2. Youd, T.L. and Hoose, S.N., *Liquefaction during the 1906 San Francisco Earthquake*, Journal of the Geotechnical Engineering Division, ASCE, Vol. 102, No. GT5, May 1976, pp. 425-439.

3. Katayama, T., Kubo, K. and Sato, N., *Earthquake Damage to Water and Gas Distribution Systems*, Proceedings of the U.S. National Conference on Earthquake Engineering, Earthquake Engineering Research Institute, Ann Arbor, Michigan, June 1975, pp. 396-405.

4. Housner, G.W. and Jennings, P.C., *The San Fernando California Earthquake*, International Journal of Earthquake Engineering and Structural Dynamics, Vol. 1, No. 1, July-September 1972, pp. 5-31.

5. Kubo, K., *Effects of the Miyagi-Oki Japan Earthquake of June 12, 1978 on Lifeline Systems*, Proceedings of the Second U.S. National Conference on Earthquake Engineering, Earthquake Engineering Resaearch Institute, August 1979.

6. Ayala, G. and O'Rourke, M.J., *Effects of the 1985 Michoacan Earthquake on Water Systems and other Buried Lifelines in Mexico*, Technical Report NCEER-88, National Center for Earthquake Engineering Research, June 1988.

7. O'Rourke, T.D., Grigoriu, M.D. and Khater, M.M., *Seismic Response of Buried Pipelines*, Pressure Vessels and Piping Technology, A Decade of Progress, Edited by C. Sundararajan, ASME, New York, New York, 1985, pp. 281-323.

8. Trautmann, C.H., O'Rourke, T.D., Grigoriu, M.D. and Khater, M.M., *System Model for Water Supply Following Earthquakes*, Lifeline Seismic Risk Analysis-Case Studies, Proceedings of the Session sponsored by the Technical Council of Lifeline Earthquake Engineering, ASCE, Seattle, Washington, April, Edited by R.T. Egushi, 1986.

9. Newmark, N.M. and Hall, W.J., *Pipeline Design to Resist Large Fault Displacement*, Proceedings of the U.S. National Conference on Earthquake Engineering, Earthquake Engineering Research Institute, Ann Arbor, Michigan, June 1975, pp. 416-425.

10. Kennedy, R.P., Chow, A.W. and Williamson, R.A., *Fault Movement Effects on Buried Oil Pipelines*, Journal of the Transportation Engineering Division, ASCE, Vol. 103, No. TE5, May 1977, pp. 617-633.

11. O'Rourke, T.D. and Trautmann, C.H., *Earthquake Ground Rupture Effects on Jointed Pipes*, Proceedings of the Second Specialty Conference of the Technical Council on Lifeline Earthquake Engineering, ASCE, August 1981, pp. 65-80.

12. Newmark, N.M., *Problems in Wave Propagation in Soil and Rock*, Proceedings of the International Symposium on Wave Propagation and Dynamic Properties of Earth

Materials, Albuquerque, New Mexico, August 1967, pp. 7-26.

13. Sakurai, A. and Takahashi, T., *Dynamic Stresses of Underground Pipelines during Earthquakes*, Proceedings of the Fourth World Conference on Earthquake Engineering, Santiago, Chile, 1969, pp. 150-162.

14. Shah, H.H. and Chu, S.L., *Seismic Analysis of Underground Structural Elements*, Journal of the Power Division, ASCE, Vol. 100, NO. PO1, July 1974, pp. 53-62.

15. Wang, L.R., O'Rourke, M.J. and Pikul, R.R., *Seismic Vulnerability, Behavior and Design of Buried Pipelines* , Technical Report No. 9, Department of Civil Engineering, Rensselaer Polytechnic Institute, Troy, New York, March 1979.

16. Lee, L.N.H., Ariman, T. and Chen, C.C., *On Buckling of Buried Pipelines by Seismic Excitation*, Presented at the Pressure Vessel and Piping Conference, ASME, Paper No. 80-C2/PVP-75, San Francisco, California, August 1980.

17. Yun, H.D. and Kyriakides, S., *Buckling of a Heavy Beam on a Contacting Surface: A Mode for Beam Buckling of Buried Pipes*, Presented at the Pressure Vessels and Piping Conference and Exhibition, ASME, Paper No. 84-PVP-71, San Antonio, Texas, June 1984.

18. Tawfic, M.S. and O'Rourke, T.D., *Analysis of Pipelines under Large Soil Deformations*, Report No. 86-1, School of Civil Engineering and Environmental Engineering, Cornell University, Itahca, New York, March 1986.

19. Weidlinger, P. and Nelson, I., *Seismic Analysis of Pipelines with Interference Response Spectra* , Grant Report No. 7, Weidlinger Associates, Consulting Engineers, New York, New York, 1978.

20. Shinozuka, M. and Koike, T., *Estimation of Structural Strains in Underground Lifeline Pipes*, Technical Report No. NSF-PFP-78-15049-CU-4, Department of Civil Engineering and Engineering Mechanics, Columbia University, March 1979.

21. Goodling, E.C., *Buried Piping - An Analysis Procedure Update*, Proceedings of the Symposium on Lifeline Eathquake Engineering, Fourth U.S. National Conference on Pressure Vessels and Piping Technology, ASME, Vol. 77, Portland, Oregon, June 1983, pp. 225-237.

22. O'Rourke, M.J., Castro, G. and Hossain, I., *Horizontal Soil Strain due to Seismic Waves*, Journal of Geotechnical Engineering, Vol. 110, No. 9, September 1984, pp. 1173-1187.

23. Stratta, J.L., Canon, T.J., Duke, C.M. and Sehia, L.G., *Reconnaissance Report-Mindonao Philipines Earthquake, August 17, 1976*, Earthquake Engineering Research Institute, Berkeley University, California, 1977.

24. Egushi, R.T., Craig, T. and Hasselman, T.K., *Seismic Component Vulnerability Models for Lifeline Risk Analysis* , Technical Report No. 82-1396-2C, Earthquake Performance of Water and Natural Gas Supply Systems, J.H. Wiggins Company, Redondo Beach, California, 1983.

25. Wang, L.R., *Development of Lifeline Design Criteria for Incoherent Ground Motions*, Proceedings of the Third U.S. National Conference on Earthquake Engineering, Earthquake Engineering Research Institute, Charleston, North Carolina, August 1986, pp. 2293-2304.

26. Tamura, C. , *Design of Underground Structures by considering Ground Displacement during Earthquakes*, Proceedings of the U.S.-Japan Seminar on Earthquake Engineering, Research with Emphasis on Lifeline Systems, Tokyo, Japan, November 1976, pp.417-433.

27. Okamoto, S., Tamura, C. and Hamada, M., *Behavior of Submerged Tunnels during Earthquakes*, Proceedings of the Fifth World Conference on Earthquake Engineering, Rome, Italy, 1973.

28. Novak, M. and Hindy, A., *Dynamic Response of Buried Pipelines*, Presented at the Sixth European Conference on Earthquake Engineering, September 1978.

29. Tsuchida, H., Kurata, E. and Hayashi, S. (1977), *Observation of Earthquake Response of Ground with Horizontal and Vertical Seismometer Arrays*, Proceedings of the Sixth World Conference on Earthquake Engineering, New Delhi, India, January 1977.

30. Weidlinger, P. and Nelson, I., *Seismic Design of Underground Lifelines*, Journal of Technical Council, ASCE, Vol. 106, No.TC1, August 1980, pp. 185-200.

31. Newmark, N.M., *A Study of Vertical and Horizontal Earthquake Spectra*, Directorate of Licensing, U.S. Atomic Energy Commission, Washington, D.C., 1973.

32. Seed, H., Murarka, R., Lysmer, J. and Idriss, I., *Relationship between Maximum Acceleration, Maximum Velocity, Distance from Source and Local Site Conditions for Moderately Strong Earthquakes*, Report, EERC # 75-7, University of Berkeley, California, 1975.

33. Ayala, G. and Rascon, O., *Seismic Evaluation of the Aqueduct Damage during the March 19, 1979 Earthquake*, (in Spanish), Ingenieria Sismica, No. 21, 1981, pp. 17-32.

34. Idriss, I., *Characteristics of Earthquake Ground Motions*, Proceedings of the ASCE Conference on Earthquake Engineering and Soil Dynamics, Pasadena, California, 1978, pp. 1151-1265.

35. O'Rourke, M.J., Bloom, M. and Dobry, R., *Apparent Propagation Velocity of Body Waves*, International Journal of Earthquake Engineering and Structural Dynamics, Vol. 10, 1982, pp. 283-294.

36. Tamura, C., Nogushi, T. and Kato, K., *Earthquake Observations along Measuring Lines on the Surface of Alluvial Soft Ground*, Proceedings of the Sixth World Conference on Earthquake Engineering, New Delhi, 1977, pp. 2-63 to 2-68.

37. Tsuchida, H. and Kurata, E., *Observed Earthquake Ground Displacement along a 2500 Meter Line*, Proceedings of the U.S.-Japan Seminar on Earthquake Engineering, Research with Emphasis on Lifeline Systems, Tokyo, Japan, November 1976, pp.29-46.

38. Achenbach, J. and Epstein, H., *Dynamic Interaction of a Layer and a Half-space*, Journal of the Engineering Mechanics Division, ASCE, Vol. 93, No. EM5, 1967, pp. 27-42, October.

39. Mooney, H. and Bolt, B., *Dispersive Characteristics of the First Three Rayleigh Modes for a Single Surface Layer*, Bulletin of the Seismological Society of America, Vol. 56, No. 1, February 1966, pp. 43-67.

40. Shinozuka, M., Kameda, H. and Koike, T., *Ground Strain Estimation for Seismic Risk*

Analysis, Journal of Engineering Mechanics, ASCE, Vol. 109, No. 1, 1983, pp. 175-191.

41. Hanks, T., *Strong Ground Motions of the San Fernando, California Earthquake: Ground Displacements*, Bulletin of the Seismological Society of America, Vol. 65, No. 1, 1975, pp. 193-225.

42. Hanks, T., *Observations and Estimation of Long-Period Strong Ground Motion in the Los Angeles Basin*, International Journal of Eartquake Engineering and Structural Dynamics, Vol. 4, 1976, pp. 473-488.

43. Wright, J. and Takada, S., *Earthquake Relative Motions for Lifelines*, Fifth Japan Earthquake Engineering Symposium, Tokyo, 1978.

44. O'Rourke, M.J. and Elhmadi, K., *Analysis of Continuous Pipelines for Seismic Wave Effects*, International Journal of Earthquake Engineering and Structural Dynamics, Vol. 16, 1988, 917-929.

45. O'Rourke, M.J., Pikul, R.R. and Wang, L.R., *Transverse Seismic Waves at Pipeline Junctions*, Journal of the Technical Councils of ASCE, ASCE, Vol. 108, No. TC1, May 1982, pp. 173-177.

46. O'Rourke, T.D., Grigoriu, M.D. and Khater, M.M., *Risk Assessment for Pipelines subject to Earthquake Movements*, Proceedings of the Trilateral Seminar Workshop on Lifeline Earthquake Engineering, Edited by A.H-S. Ang, T. Katayama and R.Y. Tan, Taipei, Taiwan, November 1985, pp. 371-389.

47. Coffin, L.F.Jr., *Flow and Fracture of a Brittle Material*, Journal of Applied Mechanics, 1950, pp. 233-248.

48. American Society for Metals (ASM), *Metals Handbook*, Vol. 1, Properties and Selection: Iron and Steel, Nineth Edition, Metals Park, Ohio, 1978.

49. Taki, H. and O'Rourke, T.D., *Factors Affecting the Performance of Cast Iron Pipe*, Report No. 84-1, School of Civil Engineering and Environmental Engineering, Cornell University, Ithaca, New York, 1984.

50. Salvadori, M.G. and Singhal, A., *Strength characteristics of Jointed Water Pipelines*, Interim Grant Report No. IR-3, Weidlinger Associates, Consulting Engineers, New York, New York, 1977.

51. American Water Works Association (AWWA), *American National Standard for Thickness Design of Cast Iron Pipes*, AWWA C101-72, July 1972.

52. Ductile Iron Pipe Research Association (DIPRA), *Handbook of Ductile Iron Pipe*, Sixth Edition, Birmingham, Alabama, 1984.

53. Prior, J.C., *Investigation of Bell and Spigot Joints in Cast Iron Water Pipes*, Bulletin No. 87, The Engineering Experiment Station, Ohio State University Studies Engineering Series, Vol. IV, No. 1, January 1935.

54. Harris, C. and O'Rourke, T.D., *Response of Jointed Cast Iron Pipelines to Parallel Trench Construction*, Report No. 83-5, School of Civil Engineering and Environmental Engineering,

Cornell University, Ithaca, New York, March 1983.

55. O'Rourke, T.D. and Trautmann, C.H., *Analytical Modeling of Buried Pipeline Response to Permanent Earthquake Displacements*, Report No. 80-4, School of Civil Engineering and Environmental Engineering, Cornell Univeraity, Ithaca, New York, July 1980.

56. American Society for Metals (ASM), *Metals Handbook*, Vol. 1, Properties and Selection of Metals, Eighth Edition, Metals Park, Ohio, 1961.

57. American Water Works Association (AWWA) (1976), *American National Standard for Thickness Design of Ductile Iron Pipes*, AWWA C150-76, August 1976.

58. Singhal, A.C., *Behavior of Jointed Ductile Iron Pipelines*, Journal of Transportation, ASCE, Vol. 110, No. 2, 1984, pp. 235-250.

59. Lindley, P.B. (1966), *Use of Rubber in Engineering*, Edited by P.C. Allen, P.B. Lindley and A.R. Payne, Maclaren and Sons Ltd., London, 1966.

60. Singhal, A.C. and Benavides, J.C., *Pull-Out and Bending Experiments in Buried Pipes*, Proceedings of the Fourth National Congress on Pressure Vessels and Piping Technology, ASME, PVP-Vol. 77, 1983, pp. 294-303.

61. Boresi, A.P., Sidebottom, O.M. and Smith, J.O., *Advanced Mechanics of Materials*, Third Edition, John Wiley and Sons, 1978, 696 pp.

62. Singhal, A.C. and Cheng, M., *Bending Mechanism for Rubber Gasketed Pipe Joints*, Fifth ASCE Engineering Mechanics Division Specialty Conference, Engineering Mechanics in Civil Engineering, Edited by A.P. Boresi and K.P. Chong, 1-3 August 1984.

63. Committee on Gas and Liquid Fuel Lifelines, *Guidelines for the Seismic Design of Oil and Gas Pipeline Systems*, Technical Council on Lifeline Earthquake Engineering, ASCE, 1984, 473 pp.

64. Colton, J.D., Chang, P.H.P., Lindberg, H.E and Abrahamson, G.R., *Measurement of Dynamic Soil-Pipe Axial Interaction for Full-Scale Buried Pipelines under Field Conditions*, Project PYU-1434, SRI International, Menlo Park, California, November 1981.

65. Kulhawy, F.H. and Peterson,, M.S., *Behavior of Sand-Concrete Interfaces*, Proceedings of the Sixth Pan American Conference on Soil Mechanics and Foundation Engineering, Lima, Peru, Vol. 2, 1979.

66. Brumund, W.F. and Leonard, G.A., *Experimental Study of Static and Dynamic Friction between Sand and Typical Construction Materials*, Journal of Testing and Evaluation, Vol. 1, No. 2, March 1973, pp. 162-165.

67. Lambe, T.W. and Whitman, R.V., *Soil Mechanics, SI Version*, Series in Soil Engineering, John Wiley & Sons, 1979, 553 pp.

68. Ductile Iron Pipe Research Association (DIPRA), *A Guide for the Installation of Ductile Iron Pipes*, Birmingham, Alabama, 1982.

69. Perloff, W.P. and Baron, W., *Soil Mechanics: Principles and Applications*, John Wiley & Sons,

1976, 745 pp.

70. Novak, M., Nogami, T. and Abdul-Ella, F., *Dynamic Soil Reaction for Plane Strain Case*, Journal of the Engineering Mechanics Division, ASCE, Vol. 104, No. EM4, 1978, pp. 953-959.

71. O'Leary, P. and Datta, S., *Dynamics of Buried Pipelines*, International Journal of Soil Dynamics and Earthquake Engineering, Vol. 4, No. 3, 1985, pp. 151-159.

72. Shibata, A., Miwa, M., Nakano, M. and Fujihashi, K., *Site Observation of Telephone Tunnel during Earthquakes*, Development in Geotechnical Engineering 45 - Structures and Stochastic Methods, Edited by A. Cakmak, Elsevier, Amsterdam, 1987.

73. Kubota Ltd, *Earthquake-Proof Design of Buried Pipelines*, Tokyo, Japan, 1981.

74. O'Rourke, M.J. and Wang, L.R., *Earthaquake Response of Buried Pipelines*, Prceedings of the ASCE Conference on Earthquake Engineering and Soil Dynamics, Pasadena, California, June 1978.

75. Seed, H. and Idriss, I., *Soil Moduli and Damping Factors for Dynamic Response Analyses*, Report No.EERC 74-10, University of Berkeley, California, December 1970.

76. Holloway, D.M., *The Mechanics of Pile-Soil Interaction in Cohesionless Soils*, Ph.D. Thesis, Duke University, Durham, North Carolina, 1975.

77. Audibert, J.M.E. and Nyman, K.J., *Soil Restraint against Horizontal Motion of Pipes*, Journal of the Geotechnical Engineering Division, ASCE, Vol. 103, No. GT10, October 1977, pp. 1119-1142.

78. Trautmann, C.H. and O'Rourke, T.D., *Lateral Force-Displacement Response of Buried Pipes*, Journal of Geotechnical Engineering, ASCE, Vol. 111, No. 9, September 1985, pp. 1077-1092.

79. Ovesen, N.K., *Anchor Slab, Calculation Methods and Model Tests*, Bulletin 16, Danish Geotechnical Institute, Copenhagen, Denmark, 1964.

80. Ovesen, N.K. and Stromann, H., *Design Methods for Vertical Anchor Slabs in Sand*, Proceedings of the Specialty Conference on Performance of Earth and Earth-Supported Structures, ASCE, Vol. 1, Lafayette, Indiana, June 1972, pp. 1481-1500.

81. Hansen, J.B., *The Ultimate Resistance of Rigid Piles against Transversal Forces*, Bulletin 12, Danish Geotechnical Institute, Copenhagen, Denmark, 1961, pp. 1-9.

82. Thomas, H.O., *Discussion of, Soil Restraint against Horizontal Motion of Pipes, (by J.M.E. Audibert and K.J. Nyman, Journal of the Geotechnical Engineering Division)* , Vol. 10, No. GT9, September 1978, pp. 1214-1216.

83. Gallagher, R.H., *Finite Element Analyis: Fundamentals*, Prentice-Hall, Inc., Englewood Cliffs, New Jersey, 1975, 420 pp.

84. Hughes, T.J.R., *The Finite Element Method: Linear Static and Dynamic Finite Element Analysis*, Prentice-Hall, Inc., Englewood Cliffs, New Jersey, 1987, 803 pp.

85. Elhmadi, K., *Seismic Wave Propagation Effects on Straight Jointed Buried Pipelines*, Ph.D. Thesis, Rensselaer Polytechnique Institute, Troy, New York, December 1988.

86. Iwamoto, T., Yamamura, Y. and Miyamoto, H., *Observation on Behavior of Buried Pipelines and Ground Strain during Earthquakes*, Proceedings of the Ninth World Conference on Earthquake Engineering, Tokyo, Japan, August 1988.

87. Wang, L.R., Pikul, R.R. and O'Rourke, M.J., *Imposed Ground Strain and Buried Pipelines* Journal of the Technical Councils of ASCE, ASCE, Vol. 108, No. TC2, November 1982, pp. 259-263.

88. Papoulis, A., *Probability, Random Variables, and Stochastic Processes*, Second Edition, McGraw-Hill, Inc., 1984, 576 pp.

89. Kleijnen, J.P.C. (1974), *Statistical Techniques in Simulation*, Parts I and II, Statistics: Textbooks and Monographs, Volume 9, Dekker, New York, 1974.

90. Michigan Terminal System (MTS), *System Subroutine Description*, Volume 3, Update 6, University of Michigan Computing Center, Ann Arbor, Michigan, Septmber 1985.

91. SPSS-X, *User's Guide*, Third Edition, SPSS-X Inc., Chicago, Illinois, 1988.

APPENDIX A: RAYLEIGH DENSITY FUNCTION AND THE SIMPLIFIED MONTE CARLO SIMULATION TECHNIQUE

This appendix presents the Rayleigh density function and shows how it can be used in conjunction with a simplified Monte Carlo simulation technique.

The Rayleigh density function is defined as [88]:

$$f_s(s) = \frac{s}{(s_0)^2} \cdot \exp\left[\frac{-s^2}{2 \cdot (s_0)^2}\right] \cdot U(s) \qquad (A.1)$$

where s is the independent variable and s_0 is a parameter of the density function. The function U(s) is the heavyside step function, given by:

$$U(s) = \begin{cases} 0 & ; s < 0 \\ 1 & ; s > 0 \end{cases} \qquad (A.2)$$

Figure A-1 shows in solid line the Rayleigh density function, $f_s(s)$. The mean value corresponding to this density function, m_s, is related to the parameter s_0 by:

$$m_s = s_0 \cdot \sqrt{\frac{\pi}{2}} \qquad (A.3)$$

On the other hand, the corresponding coefficient of variation, μ, defined as the ratio of the mean value, m_s, to the standard deviation, σ_s, is constant and equal to 52.27% (i.e. $\mu = \frac{m_s}{\sigma_s} = 52.27\%$).

In this study, a *shifted* Rayleigh density function is used to approximate the probability density function of each of the input random variables (pipeline or soil properties). This density function is given by:

$$\bar{f}_s(s) = \frac{s - s_1}{(s_0)^2} \cdot \exp\left[\frac{-(s - s_1)^2}{2 \cdot (s_0)^2}\right] \cdot U(s - s_1) \qquad (A.4)$$

where s_1 represents the shift. The function $\bar{f}_s(s)$ is plotted in dashed line in Figure A-1. The two parameters defining the shifted Rayleigh function, s_0 and s_1, can be written as functions of the

corresponding mean value, $\bar{m}_s$, and coefficient of variation, $\bar{\mu}$. That is:

$$s_0 = \frac{\bar{\mu} \cdot \bar{m}_s}{\sqrt{2 - \frac{\pi}{2}}} \tag{A.5}$$

$$s_1 = \bar{m}_s - \frac{\bar{\mu} \cdot \bar{m}_s}{\sqrt{\frac{4}{\pi} - 1}} \tag{A.6}$$

If one knows the values of $\bar{m}_s$ and $\bar{\mu}$, Eqns.(A.5) and (A.6) can be used to evaluate respectively s_0 and s_1. Note that the condition of positiveness of s_1 (i.e. $s_1 \geq 0.0$) implies that the coefficient of variation $\bar{\mu}$ be less than or equal to 52.27%.

Integration of Eqn.(A.4) yields the cumulative probability function, $\bar{F}_s(s)$, corresponding to the shifted Rayleigh density, $\bar{f}_s(s)$. That is:

$$\bar{F}_s(s) = \int_{-\infty}^{s} \frac{\tau - s_1}{(s_0)^2} \cdot \exp\left[\frac{-(\tau - s_1)^2}{2 \cdot (s_0)^2}\right] \cdot U(\tau - s_1) \cdot d\tau \tag{A.7}$$

The integral in Eqn.(A.7) can be evaluated analytically. It is equal to:

$$\bar{F}_s(s) = 1 - \exp\left[\frac{-(s - s_1)^2}{2 \cdot (s_0)^2}\right] \cdot U(s - s_1) \tag{A.8}$$

Monte Carlo simulation is a technique which uses random numbers for the solution of a model. Using a random number generator, a sample of values for the input variables is first selected. Note that the sampling can be done in a "straight" way or by more sophisticated techniques (i.e. Variance Reduction Techniques) [89]. The relationships between the input and output variables are then applied to get to the corresponding sample of values for the output variables.

In this research, a "straight" sampling is used. Accordingly, a sequence of uniformly distributed random numbers, $r_n(I)$, is generated for each of the input random variables. This is done using a Michigan Terminal System (MTS) subroutine[90]. The size of each sequence is equal to n_{sim}. Note that n_{sim} represents also the number of times the model is simulated. Since $0.0 \leq r_n(I) \leq 1.0$, one can write:

$$r_n(I) = \bar{F}_s(s(I)) \tag{A.9}$$

Substituting Eqn.(A.9) into Eqn.(A.8) and expressing s(I) in terms of $r_n(I)$, yields:

$$s(I) = s_1 + \sqrt{-2 \cdot s_0^2 \cdot \ln[1 - r_n(I)]} \qquad I = 1,2,...,n_{sim} \tag{A.10}$$

The sequence of values s(I) generated by Eqn.(A.10) for each random input variable has a Rayleigh distribution $\bar{f}_s(s)$.

At each step I, the simulated values s(I) corresponding to the input random variables are entered into the computer program described in section 6.4. The output variables consisting of the response parameters, are then solved for. This is repeated for n_{sim} times. All the results are stored in a file. Finally, a statistical analysis on these results, is performed. For this purpose, SPSS-X[91] is used. For each of the response parameters, the corresponding histogram, as well as other statistics measures, can be obtained.

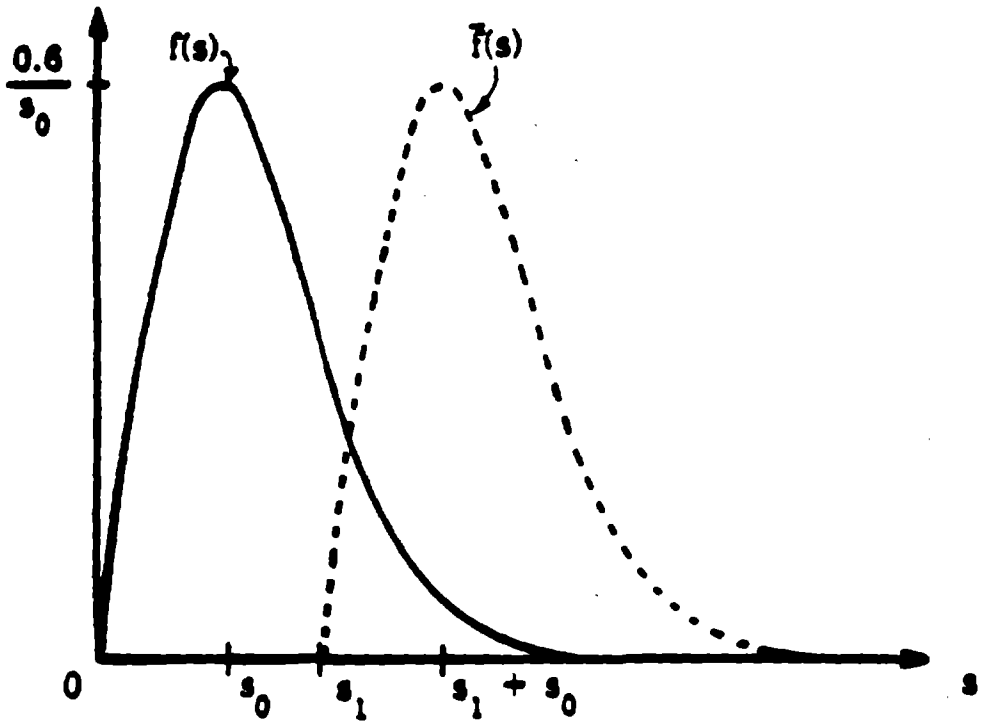

Figure A-1. Rayleigh Density function

APPENDIX B: CONVERSION FACTORS

The conversion factors of the SI units to the U.S. Customary System units for quantities used in this report, are given below:

Length	1 cm	=	0.394	inch
	m	=	3.281	ft
	km	=	0.615	mile
Area	1 cm^2	=	0.155	$inch^2$
Moment of inertia	1 cm^4	=	2.403×10^{-2}	$inch^4$
Force	1 Kgf	=	2.204	lb
Force per unit Length, Stiffness	1 Kgf/cm	=	5.599	lb/inch
Stress, Stiffness per unit length, Elastic modulus	1 Kgf/cm^2	=	14.223	psi
Unit weight	1 Kgf/cm^3	=	6.243×10^4	pcf
Moment	1 Kgf.cm	=	0.868	lb.inch

APPENDIX C: NOTATION

The following symbols are used in this report:

a = distance between left support and point of application of vertical load;

b = distance between right support and point of application of vertical load;

c = depth of earth cover;

c_p = outer diameter of joint groove;

$\{dF_g\}$ = increment of global load vector;

$\{dF_g^{b.c.}\}$ = increment of boundary load vector;

$\{d\bar{F}_g\}$ = increment of total global load vector;

$\{d\Delta\}$ = increment of global displacement vector;

$\{d\Delta_g\}$ = increment of global ground displacement vector;

d_l = depth of caulked lead;

d_p = depth of joint;

e = void ratio of soil;

e_p = inner diameter of joint groove;

f = frequency;

f_s = Rayleigh density function;

$\bar{f}_s$ = shifted Rayleigh density function;

fn = function of the variable ξ;

f_p = width of joint groove;

f_x = axial force per unit length at the soil/pipeline interface;

f_z = lateral force per unit length at the soil/pipeline interface;

g = gravitational acceleration [g = 9.80 m/s^2 (32.20 feet/s^2)];

h = thickness of soil layer;

k_x = initial axial soil spring stiffness;

k_z = initial lateral soil spring stiffness;

l = length of pipe segment element;

l_1 = distance between left support and joint;

l_2 = distance between right support and joint;

m_s = mean value of the argument s;

n_{dof} = number of degrees of freedom;

n_e = number of pipe segment elements per pipe segment;

n_{jc} = number of joints where under compressive ground strain, contact between the two adjacent pipe segments occurs;

n_n = number of nodes;

n_s = number of pipe segments;

n_{sim} = number of times the model is simulated;

p_i = pressure at inner circumference of rubber gasket;

p_o = pressure at outer circumference of rubber gasket;

r_n = random number;

s = argument of the Rayleigh density function, normalized joint displacement (u_j/d_p);

t = wall thickness of pipe;

t_l = thickness of caulked lead;

u = axial displacement of pipeline;

u_g = axial displacement of ground;

$\dot{u}_g$ = axial velocity of ground;

$\ddot{u}_g$ = axial acceleration of ground;

u_j = axial displacement of joint;

u_j^c = clearance distance between adjacent pipe segments;

u_r = radial displacement of a square cross-sectional ring;

v_j = vertical deflection of joint;

w = lateral displacement of pipeline;

w_g = lateral displacement of ground;

$\ddot{w}_g$ = lateral acceleration of ground;

x = coordinate along the pipeline axis;

y = coordinate in the vertical direction;

z = coordinate in the lateral direction;

A = cross-sectional area of pipe;

A_g = diameter of the "main body" of the rubber gasket before installation;

AK_j = initial axial stiffness of joint;

B_g = dimension of the rubber gasket before installation;

C = apparent wave propagation velocity;

C_a = adhesive strength at the pipe/lead interface;

C_g = dimension of the rubber gasket before installation;

C_{ph} = phase velocity of Rayleigh waves;

C_s = shear wave velocity of top soil layer;

C_H = shear wave velocity of halfspace;

C_L = shear wave velocity of layer;

D = outside diameter of pipe;

$[DK]$ = diagonal matrix;

D_g = dimension of the rubber gasket before installation;

D_n = nominal diameter of pipe;

D_r = relative density of soil;

E_g = dimension of the rubber gasket before installation;

E_p = Young's modulus of pipe material;

E_r = Young's modulus of rubber;

ELIND = elastic fraction of the ground displacement;

$\bar{F}_s$ = cumulative probability function corresponding to $\bar{f}_s$;

$\left\{F_g\right\}$ = global load vector;

$\left\{F_g^{b.c.}\right\}$ = boundary load vector;

$\left\{\bar{F}_g\right\}$ = total global load vector;

F_j = axial force at joint;

G_l = shear modulus of lead;

G_r = shear modulus of rubber;

G_s = shear modulus of soil;

H = depth to the pipe centerline;

H_e = depth of embedment;

I = transverse moment of inertia of pipe;

$\left[\text{ID}\right]$ = degree of freedom number/node number matrix;

$\left\{\text{IDIA}\right\}$ = vector giving the position of the diagonal terms of the global stiffness matrix in the array $\left\{\text{SK}\right\}$;

$\left\{\text{ISKL}\right\}$ = vector giving the row number of the first non-zero entry in each column of the global stiffness matrix;

I_T = type of pipeline system indicator;

$\left[K\right]$ = elastic global stiffness matrix;

$\left[K'\right]$ = tangent global stiffness matrix;

K_{sy} = system stiffness of a buried pipe;

K_o = coefficient of lateral earthpressure;

K_2 = shear modulus coefficient of soil;

L = length of pipe segment;

$\left[LK \right]$ = lower diagonal matrix;

L_{pm} = length of pipeline model;

L_s = separation distance;

M_j = bending moment at joint;

N = number of ground displacement increments;

$\left[NOD \right]$ = node number/element number matrix;

N_{qh} = horizontal bearing capacity coefficient;

$N^{(a)}$ = shape functions associated with axial degrees of freedom;

$N^{(b)}$ = shape functions associated with bending degrees of freedom;

P = applied axial force, cumulatif probability function;

P_l = probability of leakage of an individual joint;

Q = applied vertical force;

RK_j = initial rotational stiffness of joint;

$\left\{ SK \right\}$ = vector for storage of global stiffness;

$\left\{ \bar{SK} \right\}$ = vector for storage of tangent global stiffness;

U = step side function;

U_J = axial displacement at outer fibers of joint;

W = total weight of two pipe segments;

α = coefficient;

α_s = coefficient;

β = coefficient;

γ = unit weight of soil;

γ_i = angle of incidence of body waves;

ϵ = axial strain in pipe segment;

ϵ_g = maximum ground strain;

θ = rotation about y direction of pipeline;

θ_g = maximum ground rotation;

θ_j = rotation about y direction of joint;

λ = wavelength;

μ = coefficient of variation;

μ_r = coefficient of friction between rubber and pipe material;

μ_s = coefficient of friction at or near the soil/pipeline interface;

ν_r = Poisson's ratio of rubber;

ρ = probability density function for the normalized joint displacement;

σ = axial stress in pipe segment;

σ_s = standard deviation of the argument s;

ϕ = angle of shearing resistance of soil;

ξ = local axial coordinate along pipe segment elements;

$\{\Delta\}$ = global displacement vector;

$\{\Delta_g\}$ = global ground displacement vector;

Δu = relative axial displacement between the soil and the pipeline;

Δw = relative lateral displacement between the soil and the pipeline;

Γ_s = shear strain of soil at the soil/pipeline interface;

NATIONAL CENTER FOR EARTHQUAKE ENGINEERING RESEARCH
LIST OF PUBLISHED TECHNICAL REPORTS

The National Center for Earthquake Engineering Research (NCEER) publishes technical reports on a variety of subjects related to earthquake engineering written by authors funded through NCEER. These reports are available from both NCEER's Publications Department and the National Technical Information Service (NTIS). Requests for reports should be directed to the Publications Department, National Center for Earthquake Engineering Research, State University of New York at Buffalo, Red Jacket Quadrangle, Buffalo, New York 14261. Reports can also be requested through NTIS, 5285 Port Royal Road, Springfield, Virginia 22161. NTIS accession numbers are shown in parenthesis, if available.

NCEER-87-0001 "First-Year Program in Research, Education and Technology Transfer," 3/5/87, (PB88-134275/AS).

NCEER-87-0002 "Experimental Evaluation of Instantaneous Optimal Algorithms for Structural Control," by R.C. Lin, T.T. Soong and A.M. Reinhorn, 4/20/87, (PB88-134341/AS).

NCEER-87-0003 "Experimentation Using the Earthquake Simulation Facilities at University at Buffalo," by A.M. Reinhorn and R.L. Ketter, to be published.

NCEER-87-0004 "The System Characteristics and Performance of a Shaking Table," by J.S. Hwang, K.C. Chang and G.C. Lee, 6/1/87, (PB88-134259/AS).

NCEER-87-0005 "A Finite Element Formulation for Nonlinear Viscoplastic Material Using a Q Model," by O. Gyebi and G. Dasgupta, 11/2/87, (PB88-213764/AS).

NCEER-87-0006 "Symbolic Manipulation Program (SMP) - Algebraic Codes for Two and Three Dimensional Finite Element Formulations," by X. Lee and G. Dasgupta, 11/9/87, (PB88-219522/AS).

NCEER-87-0007 "Instantaneous Optimal Control Laws for Tall Buildings Under Seismic Excitations," by J.N. Yang, A. Akbarpour and P. Ghaemmaghami, 6/10/87, (PB88-134333/AS).

NCEER-87-0008 "IDARC: Inelastic Damage Analysis of Reinforced Concrete Frame - Shear-Wall Structures," by Y.J. Park, A.M. Reinhorn and S.K. Kunnath, 7/20/87, (PB88-134325/AS).

NCEER-87-0009 "Liquefaction Potential for New York State: A Preliminary Report on Sites in Manhattan and Buffalo," by M. Budhu, V. Vijayakumar, R.F. Giese and L. Baumgras, 8/31/87, (PB88-163704/AS). This report is available only through NTIS (see address given above).

NCEER-87-0010 "Vertical and Torsional Vibration of Foundations in Inhomogeneous Media," by A.S. Veletsos and K.W. Dotson, 6/1/87, (PB88-134291/AS).

NCEER-87-0011 "Seismic Probabilistic Risk Assessment and Seismic Margins Studies for Nuclear Power Plants," by Howard H.M. Hwang, 6/15/87, (PB88-134267/AS). This report is available only through NTIS (see address given above).

NCEER-87-0012 "Parametric Studies of Frequency Response of Secondary Systems Under Ground-Acceleration Excitations," by Y. Yong and Y.K. Lin, 6/10/87, (PB88-134309/AS).

NCEER-87-0013 "Frequency Response of Secondary Systems Under Seismic Excitation," by J.A. HoLung, J. Cai and Y.K. Lin, 7/31/87, (PB88-134317/AS).

NCEER-87-0014 "Modelling Earthquake Ground Motions in Seismically Active Regions Using Parametric Time Series Methods," by G.W. Ellis and A.S. Cakmak, 8/25/87, (PB88-134283/AS).

NCEER-87-0015 "Detection and Assessment of Seismic Structural Damage," by E. DiPasquale and A.S. Cakmak, 8/25/87, (PB88-163712/AS).

NCEER-87-0016 "Pipeline Experiment at Parkfield, California," by J. Isenberg and E. Richardson, 9/15/87, (PB88-163720/AS).

NCEER-87-0017 "Digital Simulation of Seismic Ground Motion," by M. Shinozuka, G. Deodatis and T. Harada, 8/31/87, (PB88-155197/AS). This report is available only through NTIS (see address given above).

NCEER-87-0018 "Practical Considerations for Structural Control: System Uncertainty, System Time Delay and Truncation of Small Control Forces," J.N. Yang and A. Akbarpour, 8/10/87, (PB88-163738/AS).

NCEER-87-0019 "Modal Analysis of Nonclassically Damped Structural Systems Using Canonical Transformation," by J.N. Yang, S. Sarkani and F.X. Long, 9/27/87, (PB88-187851/AS).

NCEER-87-0020 "A Nonstationary Solution in Random Vibration Theory," by J.R. Red-Horse and P.D. Spanos, 11/3/87, (PB88-163746/AS).

NCEER-87-0021 "Horizontal Impedances for Radially Inhomogeneous Viscoelastic Soil Layers," by A.S. Veletsos and K.W. Dotson, 10/15/87, (PB88-150859/AS).

NCEER-87-0022 "Seismic Damage Assessment of Reinforced Concrete Members," by Y.S. Chung, C. Meyer and M. Shinozuka, 10/9/87, (PB88-150867/AS). This report is available only through NTIS (see address given above).

NCEER-87-0023 "Active Structural Control in Civil Engineering," by T.T. Soong, 11/11/87, (PB88-187778/AS).

NCEER-87-0024 Vertical and Torsional Impedances for Radially Inhomogeneous Viscoelastic Soil Layers," by K.W. Dotson and A.S. Veletsos, 12/87, (PB88-187786/AS).

NCEER-87-0025 "Proceedings from the Symposium on Seismic Hazards, Ground Motions, Soil-Liquefaction and Engineering Practice in Eastern North America," October 20-22, 1987, edited by K.H. Jacob, 12/87, (PB88-188115/AS).

NCEER-87-0026 "Report on the Whittier-Narrows, California, Earthquake of October 1, 1987," by J. Pantelic and A. Reinhorn, 11/87, (PB88-187752/AS). This report is available only through NTIS (see address given above).

NCEER-87-0027 "Design of a Modular Program for Transient Nonlinear Analysis of Large 3-D Building Structures," by S. Srivastav and J.F. Abel, 12/30/87, (PB88-187950/AS).

NCEER-87-0028 "Second-Year Program in Research, Education and Technology Transfer," 3/8/88, (PB88-219480/AS).

NCEER-88-0001 "Workshop on Seismic Computer Analysis and Design of Buildings With Interactive Graphics," by W. McGuire, J.F. Abel and C.H. Conley, 1/18/88, (PB88-187760/AS).

NCEER-88-0002 "Optimal Control of Nonlinear Flexible Structures," by J.N. Yang, F.X. Long and D. Wong, 1/22/88, (PB88-213772/AS).

NCEER-88-0003 "Substructuring Techniques in the Time Domain for Primary-Secondary Structural Systems," by G.D. Manolis and G. Juhn, 2/10/88, (PB88-213780/AS).

NCEER-88-0004 "Iterative Seismic Analysis of Primary-Secondary Systems," by A. Singhal, L.D. Lutes and P.D. Spanos, 2/23/88, (PB88-213798/AS).

NCEER-88-0005 "Stochastic Finite Element Expansion for Random Media," by P.D. Spanos and R. Ghanem, 3/14/88, (PB88-213806/AS).

NCEER-88-0006 "Combining Structural Optimization and Structural Control," by F.Y. Cheng and C.P. Pantelides, 1/10/88, (PB88-213814/AS).

NCEER-88-0007 "Seismic Performance Assessment of Code-Designed Structures," by H.H-M. Hwang, J-W. Jaw and H-J. Shau, 3/20/88, (PB88-219423/AS).

NCEER-88-0008 "Reliability Analysis of Code-Designed Structures Under Natural Hazards," by H.H-M. Hwang, H. Ushiba and M. Shinozuka, 2/29/88, (PB88-229471/AS).

NCEER-88-0009 "Seismic Fragility Analysis of Shear Wall Structures," by J-W Jaw and H.H-M. Hwang, 4/30/88, (PB89-102867/AS).

NCEER-88-0010 "Base Isolation of a Multi-Story Building Under a Harmonic Ground Motion - A Comparison of Performances of Various Systems," by F-G Fan, G. Ahmadi and I.G. Tadjbakhsh, 5/18/88, (PB89-122238/AS).

NCEER-88-0011 "Seismic Floor Response Spectra for a Combined System by Green's Functions," by F.M. Lavelle, L.A. Bergman and P.D. Spanos, 5/1/88, (PB89-102875/AS).

NCEER-88-0012 "A New Solution Technique for Randomly Excited Hysteretic Structures," by G.Q. Cai and Y.K. Lin, 5/16/88, (PB89-102883/AS).

NCEER-88-0013 "A Study of Radiation Damping and Soil-Structure Interaction Effects in the Centrifuge," by K. Weissman, supervised by J.H. Prevost, 5/24/88, (PB89-144703/AS).

NCEER-88-0014 "Parameter Identification and Implementation of a Kinematic Plasticity Model for Frictional Soils," by J.H. Prevost and D.V. Griffiths, to be published.

NCEER-88-0015 "Two- and Three- Dimensional Dynamic Finite Element Analyses of the Long Valley Dam," by D.V. Griffiths and J.H. Prevost, 6/17/88, (PB89-144711/AS).

NCEER-88-0016 "Damage Assessment of Reinforced Concrete Structures in Eastern United States," by A.M. Reinhorn, M.J. Seidel, S.K. Kunnath and Y.J. Park, 6/15/88, (PB89-122220/AS).

NCEER-88-0017 "Dynamic Compliance of Vertically Loaded Strip Foundations in Multilayered Viscoelastic Soils," by S. Ahmad and A.S.M. Israil, 6/17/88, (PB89-102891/AS).

NCEER-88-0018 "An Experimental Study of Seismic Structural Response With Added Viscoelastic Dampers," by R.C. Lin, Z. Liang, T.T. Soong and R.H. Zhang, 6/30/88, (PB89-122212/AS).

NCEER-88-0019 "Experimental Investigation of Primary - Secondary System Interaction," by G.D. Manolis, G. Juhn and A.M. Reinhorn, 5/27/88, (PB89-122204/AS).

NCEER-88-0020 "A Response Spectrum Approach For Analysis of Nonclassically Damped Structures," by J.N. Yang, S. Sarkani and F.X. Long, 4/22/88, (PB89-102909/AS).

NCEER-88-0021 "Seismic Interaction of Structures and Soils: Stochastic Approach," by A.S. Veletsos and A.M. Prasad, 7/21/88, (PB89-122196/AS).

NCEER-88-0022 "Identification of the Serviceability Limit State and Detection of Seismic Structural Damage," by E. DiPasquale and A.S. Cakmak, 6/15/88, (PB89-122188/AS).

NCEER-88-0023 "Multi-Hazard Risk Analysis: Case of a Simple Offshore Structure," by B.K. Bhartia and E.H. Vanmarcke, 7/21/88, (PB89-145213/AS).

NCEER-88-0024 "Automated Seismic Design of Reinforced Concrete Buildings," by Y.S. Chung, C. Meyer and M. Shinozuka, 7/5/88, (PB89-122170/AS).

NCEER-88-0025 "Experimental Study of Active Control of MDOF Structures Under Seismic Excitations," by L.L. Chung, R.C. Lin, T.T. Soong and A.M. Reinhorn, 7/10/88, (PB89-122600/AS).

NCEER-88-0026 "Earthquake Simulation Tests of a Low-Rise Metal Structure," by J.S. Hwang, K.C. Chang, G.C. Lee and R.L. Ketter, 8/1/88, (PB89-102917/AS).

NCEER-88-0027 "Systems Study of Urban Response and Reconstruction Due to Catastrophic Earthquakes," by F. Kozin and H.K. Zhou, 9/22/88, to be published.

NCEER-88-0028 "Seismic Fragility Analysis of Plane Frame Structures," by H.H-M. Hwang and Y.K. Low, 7/31/88, (PB89-131445/AS).

NCEER-88-0029 "Response Analysis of Stochastic Structures," by A. Kardara, C. Bucher and M. Shinozuka, 9/22/88, (PB89-174429/AS).

NCEER-88-0030 "Nonnormal Accelerations Due to Yielding in a Primary Structure," by D.C.K. Chen and L.D. Lutes, 9/19/88, (PB89-131437/AS).

NCEER-88-0031 "Design Approaches for Soil-Structure Interaction," by A.S. Veletsos, A.M. Prasad and Y. Tang, 12/30/88, (PB89-174437/AS).

NCEER-88-0032 "A Re-evaluation of Design Spectra for Seismic Damage Control," by C.J. Turkstra and A.G. Tallin, 11/7/88, (PB89-145221/AS).

NCEER-88-0033 "The Behavior and Design of Noncontact Lap Splices Subjected to Repeated Inelastic Tensile Loading," by V.E. Sagan, P. Gergely and R.N. White, 12/8/88, (PB89-163737/AS).

NCEER-88-0034 "Seismic Response of Pile Foundations," by S.M. Mamoon, P.K. Banerjee and S. Ahmad, 11/1/88, (PB89-145239/AS).

NCEER-88-0035 "Modeling of R/C Building Structures With Flexible Floor Diaphragms (IDARC2)," by A.M. Reinhorn, S.K. Kunnath and N. Panahshahi, 9/7/88, (PB89-207153/AS).

NCEER-88-0036 "Solution of the Dam-Reservoir Interaction Problem Using a Combination of FEM, BEM with Particular Integrals, Modal Analysis, and Substructuring," by C-S. Tsai, G.C. Lee and R.L. Ketter, 12/31/88, (PB89-207146/AS).

NCEER-88-0037 "Optimal Placement of Actuators for Structural Control," by F.Y. Cheng and C.P. Pantelides, 8/15/88, (PB89-162846/AS).

NCEER-88-0038 "Teflon Bearings in Aseismic Base Isolation: Experimental Studies and Mathematical Modeling," by A. Mokha, M.C. Constantinou and A.M. Reinhorn, 12/5/88, (PB89-218457/AS).

NCEER-88-0039 "Seismic Behavior of Flat Slab High-Rise Buildings in the New York City Area," by P. Weidlinger and M. Ettouney, 10/15/88, to be published.

NCEER-88-0040 "Evaluation of the Earthquake Resistance of Existing Buildings in New York City," by P. Weidlinger and M. Ettouney, 10/15/88, to be published.

NCEER-88-0041 "Small-Scale Modeling Techniques for Reinforced Concrete Structures Subjected to Seismic Loads," by W. Kim, A. El-Attar and R.N. White, 11/22/88, (PB89-189625/AS).

NCEER-88-0042 "Modeling Strong Ground Motion from Multiple Event Earthquakes," by G.W. Ellis and A.S. Cakmak, 10/15/88, (PB89-174445/AS).

NCEER-88-0043 "Nonstationary Models of Seismic Ground Acceleration," by M. Grigoriu, S.E. Ruiz and E. Rosenblueth, 7/15/88, (PB89-189617/AS).

NCEER-88-0044 "SARCF User's Guide: Seismic Analysis of Reinforced Concrete Frames," by Y.S. Chung, C. Meyer and M. Shinozuka, 11/9/88, (PB89-174452/AS).

NCEER-88-0045 "First Expert Panel Meeting on Disaster Research and Planning," edited by J. Pantelic and J. Stoyle, 9/15/88, (PB89-174460/AS).

NCEER-88-0046 "Preliminary Studies of the Effect of Degrading Infill Walls on the Nonlinear Seismic Response of Steel Frames," by C.Z. Chrysostomou, P. Gergely and J.F. Abel, 12/19/88, (PB89-208383/AS).

NCEER-88-0047 "Reinforced Concrete Frame Component Testing Facility - Design, Construction, Instrumentation and Operation," by S.P. Pessiki, C. Conley, T. Bond, P. Gergely and R.N. White, 12/16/88, (PB89-174478/AS).

NCEER-89-0001 "Effects of Protective Cushion and Soil Compliancy on the Response of Equipment Within a Seismically Excited Building," by J.A. HoLung, 2/16/89, (PB89-207179/AS).

NCEER-89-0002 "Statistical Evaluation of Response Modification Factors for Reinforced Concrete Structures," by H.H-M. Hwang and J-W. Jaw, 2/17/89, (PB89-207187/AS).

NCEER-89-0003 "Hysteretic Columns Under Random Excitation," by G-Q. Cai and Y.K. Lin, 1/9/89, (PB89-196513/AS).

NCEER-89-0004 "Experimental Study of 'Elephant Foot Bulge' Instability of Thin-Walled Metal Tanks," by Z-H. Jia and R.L. Ketter, 2/22/89, (PB89-207195/AS).

NCEER-89-0005 "Experiment on Performance of Buried Pipelines Across San Andreas Fault," by J. Isenberg, E. Richardson and T.D. O'Rourke, 3/10/89, (PB89-218440/AS).

NCEER-89-0006 "A Knowledge-Based Approach to Structural Design of Earthquake-Resistant Buildings," by M. Subramani, P. Gergely, C.H. Conley, J.F. Abel and A.H. Zaghw, 1/15/89, (PB89-218465/AS).

NCEER-89-0007 "Liquefaction Hazards and Their Effects on Buried Pipelines," by T.D. O'Rourke and P.A. Lane, 2/1/89, (PB89-218481).

NCEER-89-0008 "Fundamentals of System Identification in Structural Dynamics," by H. Imai, C-B. Yun, O. Maruyama and M. Shinozuka, 1/26/89, (PB89-207211/AS).

NCEER-89-0009 "Effects of the 1985 Michoacan Earthquake on Water Systems and Other Buried Lifelines in Mexico," by A.G. Ayala and M.J. O'Rourke, 3/8/89, (PB89-207229/AS).

NCEER-89-0010 "NCEER Bibliography of Earthquake Education Materials," by K.E.K. Ross, 3/10/89, (PB89-218473/AS).

NCEER-89-0011 "Inelastic Three-Dimensional Response Analysis of Reinforced Concrete Building Structures (IDARC-3D), Part I - Modeling," by S.K. Kunnath and A.M. Reinhorn, 4/17/89.

NCEER-89-0012 "Recommended Modifications to ATC-14," by C.D. Poland and J.O. Malley, 4/12/89.

NCEER-89-0013 "Repair and Strengthening of Beam-to-Column Connections Subjected to Earthquake Loading," by M. Corazao and A.J. Durrani, 2/28/89.

NCEER-89-0014 "Program EXKAL2 for Identification of Structural Dynamic Systems," by O. Maruyama, C-B. Yun, M. Hoshiya and M. Shinozuka, 5/19/89.

NCEER-89-0015 "Response of Frames With Bolted Semi-Rigid Connections, Part I - Experimental Study and Analytical Predictions," by P.J. DiCorso, A.M. Reinhorn, J.R. Dickerson, J.B. Radziminski and W.L. Harper, 6/1/89, to be published.

NCEER-89-0016 "ARMA Monte Carlo Simulation in Probabilistic Structural Analysis," by P.D. Spanos and M.P. Mignolet, 7/10/89.

NCEER-89-0017 "Preliminary Proceedings of the Conference on Disaster Preparedness - The Place of Earthquake Education in Our Schools, July 9-11, 1989," 6/23/89.

NCEER-89-0018 "Multidimensional Models of Hysteretic Material Behavior for Vibration Analysis of Shape Memory Energy Absorbing Devices, by E.J. Graesser and F.A. Cozzarelli, 6/7/89, to be published.

NCEER-89-0019 "Nonlinear Dynamic Analysis of Three Dimensional Base Isolated Structures (3D-BASIS)," by S. Nagarajaiah, A.M. Reinhorn and M.C. Constantinou, 8/3/89, to be published.

NCEER-89-0020 "Structural Control Considering Time-Rate of Control Forces and Control Rate Constraints," by F.Y. Cheng and C.P. Pantelides, 8/3/89.

NCEER-89-0021 "Subsurface Conditions of Memphis and Shelby County," by K.W. Ng, T-S. Chang and H-H.M. Hwang, 7/26/89.

NCEER-89-0022 "Seismic Wave Propagation Effects on Straight Jointed Buried Pipelines," by K. Elhmadi and M.J. O'Rourke, 8/24/89.